

**HYDROGEL NANOPARTICLES AND ASSEMBLIES FOR
BIOAPPLICATIONS**

A Dissertation
Presented to
The Academic Faculty

by

Jeffrey Clinton Gaulding

In Partial Fulfillment
of the Requirements for the Degree
Doctor of Philosophy in the
School of Chemistry and Biochemistry

Georgia Institute of Technology
August 2013

COPYRIGHT 2013 BY JEFFREY CLINTON GAULDING

HYDROGEL NANOPARTICLES AND ASSEMBLIES FOR BIOAPPLICATIONS

Approved by:

Dr. L. Andrew Lyon, Advisor
School of Chemistry and Biochemistry
Georgia Institute of Technology

Dr. David Collard
School of Chemistry and Biochemistry
Georgia Institute of Technology

Dr. Facundo Fernandez
School of Chemistry and Biochemistry
Georgia Institute of Technology

Dr. Jiri Janata
School of Chemistry and Biochemistry
Georgia Institute of Technology

Dr. Todd McDevitt
School of Biomedical Engineering
Georgia Institute of Technology

Date Approved: April 26, 2013

For Jennifer, the highlight of each and every day.

ACKNOWLEDGEMENTS

First of all, I would not be where I am today if not for the steadfast love and support of my parents, Clint and Janice Gaulding. They encouraged my curiosity such that it has developed into a lifelong love of learning. They instilled me with a tremendous work ethic and taught me to believe in myself. I cannot imagine any two finer parents, and as I prepare myself to become a parent in turn, I am so very grateful to have them as role models.

I would like to thank the members of the Lyon group for their part in my journey. It has been a distinct pleasure and a privilege to work with such a fun, bright, and amazing group of people. All of the countless hours of work go more smoothly when you are among friends. Even now, I am amazed at how fortunate I was to have found a group where everyone is so welcoming and so willing to help one another. I especially would like to thank Dr. Toni South, who taught me how make films, which marked a turning point in my thesis research. I am also extremely grateful to Dr. Mike Smith, who was my first mentor in the lab and who served as an excellent sounding board for many, many microgel conversations. Over the last two years, I have enjoyed working closely with Shalini Saxena and Mark Spears, and I have a lot of confidence that their research is going to take them into exciting new directions. Playing softball and kickball with Ashley Brown, Kim Clarke, and Emily Herman was a lot of fun, though it did convince me that my long-term career prospects were much better in chemistry than in professional sports. I have also been fortunate enough to work with two truly wonderful undergraduates – Danielle Montanari and Akriti Singh – from whom I learned at least as much as I taught.

Last, and certainly not least, I'd like to thank Grant Hendrickson, who has been a great friend throughout this journey. His selflessness, humor, and intelligence exemplify everything about what makes the Lyon lab an incredible place to work.

Some of the work presented in this dissertation would not have been possible without the efforts of some very talented collaborators: Anh Nguyen, Andres Bratt-Leal, Denise Sullivan, John Hyatt, Apoorva Salimath, Dr. Hiro Yoshida, Dr. Todd McDevitt, Dr. Andres Garcia, and Dr. Alberto Fernandez-Nieves. I am truly grateful for all of their assistance.

I have been privileged to be a part of several amazing programs during my time at Georgia Tech. When I enrolled in 2008, I was a part of the inaugural class for the GT Biomaterials training grant. I would like to extend my thanks to Dr. Ravi Bellamkonda and Dr. Julia Babensee for their efforts in designing the program and making it a reality. I am grateful for having the opportunity to work closely with bright students (such as my peer class: Lizhi Cao, Stacie Gutowski, and Maeling Tapp) from a diverse set of backgrounds. This is truly one of the best ways to broaden one's learning and to better understand other research disciplines. In 2010, I was accepted into the Center for Drug Design, Development, and Delivery program. I have had a long-standing interest in pharmaceutical research, and Dr. Mark Prausnitz and Dr. Andy Bommarius have crafted a wonderful interdisciplinary program that captures the complexity of this intricate and important industry. Finally, since 2011 I have been a part of the Technological Innovation: Generating Economic Results (TI:GER) program. Margi Berbari, Marie Thursby, and Anne Rector work extremely hard every year to make this a valuable experience for all their students. I feel that I have greatly benefited from having a wider

perspective on the role of science and technology in the world, and that TI:GER has equipped me to be more effective both as a communicator and a scientist. I was also pleased to have the chance to work with some very talented individuals as a part of team Ancile: Josh Kimball, MBA; Shahar Sapir, JD; Lee Strasburger, JD; and Justin Welborn, MBA.

During my time at Georgia Tech, there were several other people who have played a major part in seeing me through it all. My wife's family, especially her parents Mark and Colleen Johnson and her brother and sister-in-law Dan and Janelle Johnson, have been an enormous source of support. Will Miller and our semi-regular lunches were always a great chance to get out of the lab for a change of pace. Lexi, with her personality and a wag, has a way of making every day just a little bit better.

Finally, I must sincerely thank my advisor, Dr. Andrew Lyon. Besides being an exceptional scientist and a veritable fountain of ideas, Dr. Lyon has been a truly amazing mentor. He has always been very available and approachable, so that whether I have been struggling with understanding data, designing an experiment, or just wanted some advice, he has consistently been patient, attentive, and willing to help. He is able to strike the balance between allowing each of us to follow our own interests and ideas while simultaneously ensuring that no one wanders in the wilderness for too long. I cannot be more grateful for having had the opportunity to work with such a wonderful teacher, researcher, and mentor.

TABLE OF CONTENTS

	Page
ACKNOWLEDGEMENTS	iv
LIST OF TABLES	xiv
LIST OF FIGURES	xxi
LIST OF SCHEMES	xv
LIST OF SYMBOLS AND ABBREVIATIONS	xxi
SUMMARY	xxvi
 <u>CHAPTER</u>	
1 Introduction	1
1.1. Hydrogels	1
1.1.1. Responsive Gels	2
1.1.2. Applications of Hydrogels	3
1.2. Microgels	4
1.2.1. Microgel Synthesis	5
1.2.2. Architectural Control of Microgels	7
1.2.2.1. Microgel Core-Shell Synthesis	7
1.2.2.2. Core Compression	8
1.2.3. Applications of Colloidal Hydrogels	10
1.2.3.1. Applications of Microgels	10
1.2.3.2. Applications of Core-Shell Microgels	12
1.3. Microgel Assemblies and Films	13
1.3.1. Microgels as Building Blocks	14

1.3.2. Layer-by-Layer Film Assembly	15
1.3.3. Applications of Microgel Assemblies	16
1.4. References	17
2 Hydrolytically Degradable Microgels	30
2.1. Introduction	30
2.2. Experimental	33
2.2.1. Materials	33
2.2.2. Synthesis of DMHA	34
2.2.3. Core Particle Synthesis	34
2.2.4. Shell Syntheses	35
2.2.5. Particle Characterization	35
2.2.6. Microgel Erosion	36
2.3. Results and Discussion	36
2.3.1. Particle Synthesis	36
2.3.2. Shell Erosion	42
2.4. Conclusions and Outlook	46
2.5. References	47
3 Incorporation of Disulfides into Thermo-responsive Microgels	52
3.1. Introduction	52
3.2. Experimental	55
3.2.1. Materials	55
3.2.2. Microgel Synthesis	55
3.2.2.1. BAC Cross-linked Particle Synthesis - Redox	55

3.2.2.2. BAC Cross-linked Particle Synthesis – Thermal	55
3.2.2.3. Co-Cross-linked Particle Synthesis	56
3.2.3. Particle Characterization	56
3.2.4. Fluorescent Labeling	57
3.2.5. <i>In Situ</i> Erosion	58
3.2.6. Reversible Gelation	59
3.2.7. Rheology	60
3.3. Results & Discussion	60
3.3.1. Particle Synthesis and Characterization	60
3.3.1.1. Particle Erosion	62
3.3.2. <i>In Situ</i> Erosion	65
3.3.3. Reactive Thiol Incorporation	66
3.3.4. Reversible Gelation	68
3.4. Conclusions & Outlook	71
3.5. References	72
4 Microgel Films on Colloidal Substrates	76
4.1. Introduction	76
4.2. Experimental	79
4.2.1. Materials	79
4.2.2. Microgel Synthesis	79
4.2.2.1. Sample μ gel-G	79
4.2.2.2. Sample μ gel-R	80
4.2.3. Preparation of Aminobenzophenone-functionalized Cores	80

4.2.4. Raspberry-like Particle Synthesis	81
4.2.5. Dilute Heteroaggregation for Raspberry-like Particle Synthesis	82
4.2.6. Characterization	82
4.3. Results and Discussion	83
4.3.1. Microgel Synthesis	83
4.3.2. Raspberry-Like Particles	85
4.3.3. Microgel Spreading & Surface Coverage	89
4.3.4. Expansion of Raspberry-Like Particle Synthesis	93
4.4. Conclusions and Outlook	95
4.5. References	96
5 Damage and Healing in Microgel Multilayer Films	101
5.1. Introduction	101
5.2. Experimental	103
5.2.1. Materials	103
5.2.2. Microgel Synthesis	103
5.2.3. Microgel Characterization	103
5.2.4. Substrate Preparation	104
5.2.5. Film Construction	105
5.2.6. Film Stretching	105
5.2.7. Film Characterization and Analysis	106
5.2.8. Steam Healing	107
5.2.9. Healing Driven By Relative Humidity	107
5.2.10. Film Thickness	108

5.3. Results and Discussion	108
5.3.1. Film Damage	108
5.3.2. Film Healing	112
5.3.3. Film Composition	116
5.4. Conclusions and Outlook	118
5.5. References	118
6 Cellular Adhesion Resistant Films and Microgel Film Mobility	122
6.1. Introduction	122
6.1.1. Films to Improve Biocompatibility	122
6.1.2. Microgel Films as Cellular Adhesion Resistant Interfaces	124
6.1.3. Cell-Substrate Interactions	126
6.1.4. Polyelectrolyte Multilayers	130
6.2. Experimental	134
6.2.1. Materials	134
6.2.2. Microgel Synthesis	134
6.2.3. Film Assembly	135
6.2.4. Film Stretching	136
6.2.5. Film Modulus Measurements	136
6.2.6. Protein Adsorption	137
6.2.7. In Vitro Cell Adhesion	137
6.3. Results and Discussion	138
6.3.1. Assessment of Protein Fouling	138
6.3.2. Film Assembly	140

6.3.3. Film Cross-linking and Moduli	142
6.3.4. Film Damage and Healing	144
6.3.5. Cell Adhesion	145
6.4. Conclusions and Outlook	147
6.5. Acknowledgments	148
6.6. References	148
7 Outlook and Future Directions	158
7.1. Introduction	158
7.2. Hydrolytically Degradable Microgels	158
7.2.1. Alternative Uses for DMHA	158
7.2.2. Experimental and Results	159
7.2.3. Future Perspectives	161
7.3. Disulfide Cross-linked Microgels	162
7.3.1. Introduction	162
7.3.2. Experimental	162
7.3.2.1. Materials	162
7.3.2.2. Microgel Synthesis	163
7.3.2.3. Confirmation of Multiple Reactivity Incorporation	163
7.3.2.4. Fluorescent Labeling of Carboxyls and Thiols	164
7.3.2.5. Triple Network Gel Formation and Dissolution	164
7.3.3. Results and Discussion	165
7.3.3.1. Particle Synthesis and Confirmation of Responsivity	165
7.3.3.2. Triple Gel Network Formation	168

7.3.4. Future Perspectives	169
7.4. Films on Colloidal Substrates	170
7.4.1. Introduction	170
7.4.2. Experimental and Results	171
7.4.3. Future Perspectives	172
7.5. Self-Healing Films	173
7.5.1. Introduction	173
7.5.2. Experimental	174
7.5.2.1. Film Assembly	174
7.5.2.2. Film Damage & Healing	175
7.5.3. Results and Discussion	175
7.5.4. Future Perspectives	177
7.6. Film Mobility and Cell Adhesion	179
7.7. Concluding Remarks	181
7.8. References	181
VITA	184

LIST OF TABLES

	Page
Table 2.1: Synthesis of Core-Shell Microgels with Hydrolytically Degradable Shells	37
Table 2.2: Light Scattering Characterization of Core-Shell Particles	44
Table 3.1: Size, swelling, and topology characterization for BAC-cross-linked microgels	64
Table 4.1: Microgel Compositions and Characterization	83
Table 5.1: Microgel Characterization	104

LIST OF FIGURES

	Page
Figure 2.1: Mean hydrodynamic radius as a function of temperature for pNIPAm core particles and pNIPAm/pNIPMAM-DMHA core-shell particles. Shell addition is confirmed by the increased particle size at temperatures $> 32\text{ }^{\circ}\text{C}$, indicative of the addition of pNIPMAM.	38
Figure 2.2: Distribution analysis from A4F-MALS for (a) DMHA2 and (b) DMHA4 pNIPMAM shell particles. Shell addition leads to an increase in the R_{rms} of the core-shell particles relative to the cores. Erosion of the shells leads to a further increase in R_{rms} due to the reduction in shell connectivity and concomitant core swelling.	39
Figure 2.3: AFM images and height traces of (a) Core particles, (b) DMHA2 core-shell particles, and (c) DMHA4 core-shell particles. Shell addition leads to an increase in particle stiffness, as evidenced by the increase in peak height observed in the line traces. Scan sizes in each image are $5\text{ }\mu\text{m} \times 5\text{ }\mu\text{m}$.	40
Figure 2.4: AFM images and height traces of DMHA2 (a-c) and DMHA4 (d-f) following one month of erosion in pH 7.4 buffer at $37\text{ }^{\circ}\text{C}$. Compared to particles before erosion, there is a reduction in particle height and additional particle spreading. Scan sizes in (a, d) are $5\text{ }\mu\text{m} \times 5\text{ }\mu\text{m}$. Scan sizes in (b, e) are $1\text{ }\mu\text{m} \times 1\text{ }\mu\text{m}$	45
Figure 3.1: Data and best fit model used to estimate cross-link density for disulfide cross-linked microgels. The Duracher data ³² shows reasonable agreement for pNIPMAM as well.	62
Figure 3.2: A4F-MALS separation of pNIPMAM-BAC (5%) microgels formed by the (a) thermal and (b) redox initiation methods. Incubating the particles with DTT increased retention of the thermally-initiated particles, yet led to degradation of the redox-initiated particles.	64
Figure 3.3: Nanogel erosion via cross-link scission occurs in presence of DTT (red) or cysteine (blue), monitored in situ via MALS. Error bars (black) represent one standard deviation about the mean of measurements.	66
Figure 3.4: a) Images of vials containing pNIPMAM-BAC-BIS microgel dispersions (left) before and (right) after exposure to DTT.	67

Figure 3.5: a) Fluorescence spectra ($\lambda_{\text{ex}} = 494 \text{ nm}$) of (dark green) fluorescein-labeled pNIPMAm-BAC-Bis particles, (orange) unlabeled particles, (blue) pH 7.4 HEPES buffer, and (red) the supernatant following purification by centrifugation. Particles that were not reduced and therefore retained their disulfide linkages (light green) had much lower coupling efficiency than that of the reduced particles. b) Fluorescence microscopy image (blue excitation) of pNIPMAm-BAC-BIS particles labeled with fluorescein iodoacetamide. 68

Figure 3.6: Gelation of pNIPMAm-BAC-BIS particles. Sedimented particles with intraparticle disulfides form a dense pellet, yet retain fluidity (left). Reduction by DTT leads to the production of thiol-bearing particles, a reduction in pellet density, and the retention of particle fluidity (center). Oxidation by NaIO_4 restores pellet density, but the resulting solid is a double-network of microgels cross-linked by interparticle disulfides (right). 69

Figure 3.7: Storage and loss moduli as determined by oscillatory rheology for the pNIPMAm-BAC-BIS oxidized double-network. The linearity test (a) shows G' (closed symbols) and G'' (open symbols) as a function of strain at constant frequency of 10 rad/s. (b) shows both moduli as a function of frequency at constant strain of 0.1%. The storage modulus is an order of magnitude larger than the loss modulus, indicative of the solid-like properties of the microgel double-network. Rheology experiments conducted by Mr. John Hyatt. 70

Figure 3.8: Images depicting the erosion of the pNIPMAm-BAC-BIS double-network. In response to the addition of DTT, the network dissolves leading to the reversion of the particles to their dispersed state in a matter of hours. 71

Figure 4.1: Characterization of pNIPAm/3.5% BIS/26% AAc (Sample $\mu\text{gel-R}$). a) Green excitation epifluorescence image of fluorescent particles. Scale bar is 5 μm . b) AFM image (20 x 20 μm) and c) line trace reveal the spreading behavior of $\mu\text{gel-R}$. 84

Figure 4.2: Characterization of pNIPAm/4.0% BIS (Sample $\mu\text{gel-G}$). a) Blue excitation epifluorescence image of fluorescent particles. Scale bar is 5 μm . b) AFM image (20 x 20 μm) and c) line trace reveal the spreading behavior of $\mu\text{gel-G}$. 84

Figure 4.3: Brightfield microscopy image of aminobenzophenone-functionalized 4.6- μm diameter magnetic polystyrene particles mixed in a dense colloidal phase of $\mu\text{gel-G}$. Scale bar is 10 μm . 86

Figure 4.4: (a,d) Brightfield, (b,e) Green-excitation epifluorescence, and (c,f) SEM images of isolated raspberry-like particles featuring $\mu\text{gel-R}$. Assembly of (a-c) was charge-directed using 4.6- μm diameter amino-silica particles, where (d-f) utilized 4.4- μm aminobenzophenone-functionalized polystyrene particles. The scale bar in each image is 2 μm . 87

Figure 4.5: (a,d) Brightfield, (b,e) Blue-excitation epifluorescence, and (c,f) SEM images of isolated raspberry-like particles featuring 4.6- μm diameter magnetic polystyrene particles decorated with $\mu\text{gel-B}$. (a-c) represent carboxyl-functionalized polystyrene, (d-f) represent aminobenzophenone-functionalized polystyrene. The scale bar in each image is 2 μm . 88

Figure 4.6: SEM images of raspberry-like particle assembly from dilute (2.5 mg/mL) suspensions of (a-d) $\mu\text{gel-G}$ and (e-h) $\mu\text{gel-R}$ onto 4.6- μm aminobenzophenone-functionalized magnetic polystyrene core particles. The scale bar in each image is 2 μm . 88

Figure 4.7: a) Green-excitation confocal image of 4.4- μm AB-functionalized PS decorated with $\mu\text{gel-R}$ b) blue-excitation of 4.6- μm AB-functionalized magnetic PS decorated with $\mu\text{gel-G}$. The scale bar in each image is 2 μm . Confocal imaging performed by Ms. Shalini Saxena. 93

Figure 4.8: (a) SEM image of an AB-functionalized magnetic PS particle with rough surface topology. (b) Blue-excitation epifluorescence and (c) SEM image following coverage with $\mu\text{gel-G}$. (d) Green-excitation epifluorescence and (e) SEM image following coverage with $\mu\text{gel-R}$. Scale bar in all images is 1 μm . 94

Figure 4.9: (Left) Schematic of mixed colloidal glass for raspberry coating. (Right) SEM image of 4.4- μm diameter AB-functionalized PS particles decorated with a 1:1 w:w mixture of $\mu\text{gel-R}$ and $\mu\text{gel-G}$. Scale bar is 2 μm . 95

Figure 5.1: The apparatus used to stretch microgel films on flexible substrates. The sample is clamped between glass slides and held in place by rubber washers. The left post is stationary while the right is attached to a micrometer-controlled translational stage that allows precise movement, allowing controlled strain to be applied to the films. 106

Figure 5.2: a, f, g) RMS roughness as a function of applied strain for 8-layer 30% AAC microgels/400-500 kDa PDADMAC films. Maximal strain a) 30%, f) 20%, g) 10%. b-e) Representative AFM images obtained during *in situ* stretching of the films. Film roughness remains relatively constant as the degree of strain increases (b, c), then buckling occurs as the stress is removed (c, d). Wetting of the films leads to restoration of the initial roughness (d, e). All AFM images are 40 $\mu\text{m} \times 40 \mu\text{m}$. 109

Figure 5.3: Film healed under stress. a) Film before damage displays a smooth surface with low roughness. b) Application of 30% strain does not result in a large change in surface topography. c) Film exposed to water while under strain also has a smooth surface with low roughness. d) When stress is removed from the film, the characteristic buckling behavior results. All AFM images are 40 $\mu\text{m} \times 40 \mu\text{m}$. 110

Figure 5.4: Cycles of stretching of microgel films leads to sensitivity to perpendicular compression. a) Film under 0% strain, before cycling, b) 30% strain leads to compression along the short axis, perpendicular to the applied stress, c) the film is relaxed back to 0% strain; during relaxation, the film is effectively being compressed along the long axis, d) 30% elongation is reapplied with compression again introduced along the short axis. e) This pattern persists through multiple cycles of stretching when the film is not healed. All AFM images are $40\ \mu\text{m} \times 40\ \mu\text{m}$. 111

Figure 5.5: Damage induced by scratching an 8-layer 30% AAc microgels / 400-500 kDa PDADMAC film rapidly heals in response to steam. a) Scratched film before healing b) Film exposed to steam for 5 seconds. Insets: microscopy of the scratched region before and after. Scale bars are $10\ \mu\text{m}$. 113

Figure 5.6: a – d) Damage caused by applying 20% strain to 8-layer 30% AAc microgels / 400-500 kDa PDADMAC films. Film recovery following one hour exposure to e) 55% relative humidity, f) 73% relative humidity, g) 78% relative humidity, h) 84% relative humidity. Little change is noted at 55%, while slight remnant damage is visible at 73%. Complete recovery proceeds at 78% or higher. Scale bar in all images is $10\ \mu\text{m}$. 114

Figure 5.7: Representative images used to determine film thickness for a) dry films and b) wet films. Scan sizes are $50\ \mu\text{m} \times 50\ \mu\text{m}$. The red line and two dashed red lines define the area wherein 50 scan lines are averaged, and depicted in c) and d) for a) & b), respectively. The height difference was determined between the film and glass at three points in each image. 115

Figure 5.8: a) Damage induced by pipette in an 8-layer 30% AAc/ 400-500 kDa PDADMAC film. b) After being exposed to an 83% relative humidity environment for one hour. Both AFM images are $20 \times 20\ \mu\text{m}$. c) Line traces across the two images reveal the characteristic roughness associated with damaged and healed films. 116

Figure 5.9: a, b) 8-layer 30% AAc microgel films cross-linked with 100-200 kDa PDADMAC. c, d) 10% AAc microgel films cross-linked with 100-200 kDa PDADMAC. e, f) 10% AAc microgel films cross-linked with 400-500 kDa PDADMAC. a, c, e) Films subjected to 20% strain, then relaxed. b, d, f) Films heal after being exposed to 84% relative humidity for one hour. Scale bars in all images are $10\ \mu\text{m}$. 117

Figure 6.1: a) Depiction of cell interacting with an elastic substrate. Stress fibers in the cell cytoskeleton are coupled to the surface through integrins interacting with adhesion ligands present on the surface, typically resulting from adsorbed protein. b) The range of elastic moduli characteristic of fluids and tissues in the body. 128

- Figure 6.2: Mechanical properties of the substrate direct the activities of many cell types. Cell attachment and spreading are correlated with matrix stiffness, and when possible cytotaxis favors migration towards increasing substrate stiffness. 129
- Figure 6.3: a) Numbers of adherent cells on untreated glass coverslips, monolayers of pNIPAm / 4% BIS / 30% AAc microgels, and 4-layer films of the same particles assembled with PDADMAC. b-d) Representative images of Calcein-stained films showing cell attachment. Microgel multilayers strongly inhibit cell attachment, even in the absence of PEG cross-linking. Images and analysis conducted by Ms. Apoorva Salimath. 139
- Figure 6.4: a) Epifluorescence microscopy image of a 4-layer pNIPAm / 4% BIS / 30% AAc / 400-500 kDa PDADMAC film exposed to FITC-BSA overnight. Scale bar is 10 μm . b) Exposure to monolayer and 4-layer films to fluorescently-labeled fibronectin. Multilayer films adsorb more protein than monolayers. b) is courtesy of Dr. Hiroaki Yoshida. 140
- Figure 6.5: Buildup of pNIPAm / 4% BIS / 30% AAc films with PEI. Images taken after a) one layer, b) two layers, c) three layers, and d) four layers of microgels. e) For comparison, a film of the same particles assembled with four layers of microgels and 400-500 kDa PDADMAC. All images are 20 x 20 μm . 142
- Figure 6.6: Height traces (left) and force maps (right) of 4-layer pNIPAm / 4% BIS / 30% AAc / PEI films in the before (top) and after (bottom) cross-linking with glutaraldehyde. Cross-linking of the films is determined to be successful through an increase in the elastic modulus of the films. Height traces are 25 x 25 μm , Force maps are 20 x 20 μm and concentric with the height traces. 143
- Figure 6.7: Brightfield microscopy images of pNIPAm / 4% BIS / 30% AAc films assembled with PEI deposited onto PDMS. In the absence of extrinsic cross-linking (a-c), the films undergo plastic deformation and wrinkle when strains in excess of 40% are applied (b). The wrinkles disappear upon immersion in water (c). When cross-linked with glutaraldehyde (d-f), the films undergo irreversible cracking when strained less than 20%. (e, f). The features in e) and f) appear to be cracks largely perpendicular to the axis of stretching, suggesting that the films become brittle once cross-linked. The films do not recover upon immersion in water. Scale bars in a-e) are 30 μm . Scale bar in f) is 100 μm . 145
- Figure 6.8: a) Numbers of adherent cells on glass, monolayers, and 4-layer pNIPAm / 4% BIS / 30% AAc microgels assembled with PEI. Cross-linking with glutaraldehyde leads to a five-fold increase in cell attachment. b-c) Representative images of films showing cell attachment. Images and analysis conducted by Dr. Hiroaki Yoshida. 146

- Figure 7.1: Following degradation, attempting to fluorescently label the expected amine and carboxyl groups produced by DMHA degradation leads to mixed results. Amine-targeted reactions, such as NHS-derivatized fluorescein, do not show efficient labeling, while carboxyl-targeted reactions are successful. 160
- Figure 7.2: AFM analysis of pNIPMAm / 2% BIS / 2.5% BAC / 10% AAc deposited onto solid substrates. The characteristic particle spreading (a) and height (b) in the absence of DTT is shown. Reduction by DTT leads to greater spreading (c) and a reduction in particle height (d). AFM images are 20 μm x 20 μm . 167
- Figure 7.3: Blue excitation epifluorescence microscopy demonstrates that fluorescent labeling of the thiols produced by reduction of pNIPMAm/2% BIS/2.5% BAC/10% AAc microgels with fluorescein iodoacetamide was successful. Scale bar is 10 μm . 167
- Figure 7.4: UV-excitation epifluorescence microscopy demonstrates that fluorescent labeling of pNIPMAm/2% BIS/2.5% BAC/10% AAc microgels with dansylcadaverine was successful. Scale bar is 10 μm . 168
- Figure 7.5: Gel networks formed by inter-microgel disulfide cross-link between reduced NIPMAm/2% BIS/2.5% BAC/10% AAc microgels are reinforced by the addition of PDADMAC, leading to “rescue” of the network upon reduction. The state of the gels is depicted schematically for each well (a-f). 169
- Figure 7.6: Fluorescence images of embryoid bodies mixed with microgels or microgel raspberry-like particles after eighteen hours. (a) pNIPMAm-co-AAc microgels (labeled green with chymotrypsinogen-Alexa488) alone do not sediment during centrifugally-assisted embryoid body assembly, except in the form of large, irregular aggregates. (b) Magnetic polystyrene particles decorated with microgels (labeled red with BSA-Alexa 546) show more uniform and controlled co-localization during assembly. Individual microwells in each image are 400 μm x 400 μm for scale. 172
- Figure 7.7: 8-layer films assembled from pNIPMAm-BIS-BAC-AAc microgels in the a) oxidized (SS) state and b) reduced (SH) state. Images are 20 μm x 20 μm . 175
- Figure 7.8: 8-layer films assembled from pNIPMAm-BIS-BAC-AAc microgels in the a-c) oxidized (SS) state, d-f) reduced (SH) state, and g-i) assembled in the oxidized state then reduced following film assembly. The films undergo damage when exposed to b) 80% strain, e) 20% strain, or h) 10% strain. The SS films show increases in irregular cracking following stretching, some of which seems to be reversible (c). Wrinkling damage to the SH films (e, h) in contrast, is completely reversible (f, i). Scale bar in all images is 30 μm . 177

LIST OF SCHEMES

	Page
Scheme 1.1: Synthesis of thermo-responsive microgels through precipitation polymerization.	6
Scheme 1.2: Control of particle architecture through core-shell microgel synthesis. Cores of a desired composition are heated to collapse for use as templates during further polymerization. The concentration of monomer and initiator added are sufficient to prevent new particle formation, leading to deposition on the templating core during precipitation polymerization.	8
Scheme 2.1: Shell addition leads to compression of the microgel core, as the added polymer mass and cross-linking prevents the core from re-swelling to its initial volume. Scission of cross-links in the shell enables extensive swelling of both microgel components, triggering major changes in the polymer density and mechanical flexibility of the overall core-shell microgel.	33
Scheme 2.2: Structure of core-shell microgels with pNIPAm-BIS cores and pNIPMAm-DMHA shells.	37
Scheme 2.3: Scission of DMHA cross-links in the shell leads to changes in the swelling and connectivity of both the core and shell phases of the microgel.	42
Scheme 3.1: Potential side reaction involving radical attack on the disulfide bond during particle synthesis, which leads to non-degradable thioether formation.	54
Scheme 4.1: Raspberry-like particle synthesis. A concentrated dispersion of microgels is centrifuged to form a pellet, then the supernatant is removed leaving behind a packed colloidal phase. The addition of a small volume of solvent carrying the template particles and mixing of the two leads to confinement of the cores within the packed phase. Dispersal of the microgels leads to separation of the coated, raspberry-like particles from the unincorporated microgels, which can subsequently be returned to packed colloidal phases for additional assembly.	78
Scheme 4.2: The deformable microgel approximation maximizes the contact area with the core, and thus minimizes the number of microgels on the surface. The rigid microgel approximation minimizes the contact area, and thus increases the size of the effective sphere to cover and maximizes the number of microgels on the surface.	90

Scheme 4.3: Highly deformable microgels, with large surface contact area, would on drying exhibit reductions in particle height from the surface, but minimal change in spreading. The rigid microgel approximation, leading to low surface contact area, permits isotropic de-swelling and thus an apparently sparse coating in the dry state. 91

Scheme 6.1: Comparison of PDADMAC and PEI for film assembly and cross-linking. 141

Scheme 7.1: Scission of DMHA at neutral to alkaline pH proceeds following deprotonation of the nitrogen, followed by Lossen's rearrangement to form an isocyanate intermediate which further hydrolyzes to result in amine formation. 159

LIST OF SYMBOLS AND ABBREVIATIONS

ϕ_{eff}	effective volume fraction
A4F	asymmetrical flow field-flow fractionation
AAc	acrylic acid
AB	4-aminobenzophenone
AFA	4-acrylamidofluorescein
AFM	atomic force microscopy
APS	ammonium persulfate
APTMS	(3-aminopropyl)trimethoxysilane
BAC	<i>N,N'</i> -bis(acryloyl) cystamine
BASED	bis[2-(4-azidosalicylamido)ethyl] disulfide
BIS	<i>N,N'</i> -methylenebisacrylamide
CHNS	elemental analysis of carbon, hydrogen, nitrogen, & sulfur
DHEA	(1,2-dihydroxyethylene) bisacrylamide
DI	deionized water
DLS	dynamic light scattering
DMHA	<i>N,O</i> -dimethacryloyl hydroxylamine
DMS	dimethyl suberimidate
dRI	differential refractive index
DTBP	dimethyl 3,3'-dithiobispropionimidate
EDC	1-ethyl-3-[3-dimethylaminopropyl]carbodiimide hydrochloride
FRAP	fluorescence recovery after photobleaching
FRET	fluorescence resonance energy transfer
HEPES	4-(2-hydroxyethyl)-1-piperazine ethanesulfonic acid

KPS	potassium persulfate
LbL	layer-by-layer
LCST	lower critical solution temperature
MALS	multi-angle light scattering
MERho	methacryloxyethyl thiocarbamoyl rhodamine B
MES	2-(<i>N</i> -morpholino)ethane sulfonic acid
monoM	moles of monomer unit per liter
M_w	molecular weight
NHS	<i>N</i> -hydroxysuccinimide
NIPAm	<i>N</i> -isopropylacrylamide
NIPMAm	<i>N</i> -isopropylmethacrylamide
PAH	poly(allylamine hydrochloride)
PBS	phosphate buffered saline
PDADMAC	poly(diallyldimethylammonium chloride)
PDMS	poly(dimethylsiloxane)
PEG	poly(ethylene glycol)
PEI	poly(ethyleneimine)
PLGA	poly(lactic-co-glycolic acid)
PSS	poly(styrene sulfonate)
r_h	hydrodynamic radius
r_{rms}	root-mean-square radius, radius of gyration
RH	relative humidity
RMS	root-mean-square
SDS	sodium dodecyl sulfate
TCEP	tris(2-carboxyethyl)phosphine hydrochloride

TEMED

N,N,N',N'-tetramethylethane-1,2-diamine

VPTT

volume phase transition temperature

SUMMARY

Hydrogels are cross-linked networks of highly hydrophilic polymer chains. When reduced to colloidal dimensions, particles of this sort are termed “microgels” and both discrete particles and ensembles have intriguing properties. Microgels can be made to be susceptible to numerous environmental stimuli, such as temperature and pH. The resultant changes in the network hydration lead to characteristic swelling responses which can have great impact on properties of the gel network such as the porosity, hydrophilicity, stiffness, or particle-particle packing. The multitude of responsive stimuli; the architectural versatility of discrete particles; and the variety of particle ensembles have made the study of microgels and their assemblies a very rich field. Primarily due to their physiological softness and the aforementioned versatility, responsive microgels are of great interest as a material to address the daunting challenges facing the next generation of healthcare.

This dissertation describes investigations into hydrogel nanoparticles and assemblies thereof, with the goals of expanding their utility in applications such as drug delivery and non-fouling interfaces through the development of novel materials to both extend their synthetic versatility and to probe their underlying properties. **Chapter 1** serves to introduce hydrogels, microgels, and to define the microgel assemblies of interest in this dissertation. The principles behind responsive gels, microgel synthesis by precipitation polymerization, as well as methods to control particle architecture are also presented therein. The chapter also includes some brief examples of applications of microgels and their assemblies, demonstrating the broad range of utility for these

responsive materials. **Chapter 2** describes efforts to incorporate hydrolytically degradable cross-linking localized in the shell of a core-shell microgel. Shell-localization of a degradable cross-linker serves to increase the overall density of the microgels by restricting the ability of the particle interior to swell, allowing degradation of the shell to result in dramatic changes in the mechanical properties of the microgel as a whole. Continuing the theme of physiologically-relevant degradable cross-linking, **Chapter 3** describes the synthesis of microgels cross-linked with disulfides. The resultant particles are shown to rapidly degrade under reducing conditions, and this synthesis strategy is also demonstrated to serve as a means of generating thiol-bearing microgels for conjugation and reversible particle assembly.

Microgel films have been demonstrated to have numerous desirable properties for biological applications, such as reduced cell attachment and drug delivery capabilities. **Chapter 4** is a demonstration of a technique for depositing microgel films onto colloidal substrates, allowing these properties observed on macroscopic substrates to be conferred onto smaller dimensional supports, suitable for novel applications. Another intriguing property of microgel films is that multilayered films assembled via layer-by-layer deposition of anionic microgels and linear polycation exhibit rapid self-healing upon hydration. **Chapter 5** expands on our fundamental understanding of this phenomenon by studying the origins of the characteristic wrinkling pattern observed from stretching films, demonstrating that ambient humidity is sufficient to restore film integrity following damage, and expanding the range of materials that exhibit self-healing through alterations in film connectivity. **Chapter 6** similarly expands on previous observations that microgel multilayer films strongly resist cell attachment. While initially ascribed to reduced

amounts of protein-fouling due to PEG incorporation within the microgels, this chapter demonstrates that microgels lacking PEG still strongly resist cell adhesion in multilayers. Changing the polycation used during film assembly provides a mechanism to switch the films from a mobile, self-healing, cell-resistive interface to an immobile, brittle, cell-adhesive interface. Taken together, this evidence suggests that the viscoelastic or mobile character of the films is likely the main factor that directs cell adhesion.

Finally, **Chapter 7** serves to provide some additional perspectives on each of the prior chapters and to suggest directions for future investigations. The work in this dissertation serves to both expand our toolset with regard to the functional synthesis of microgels and assemblies and to improve our fundamental understanding of phenomena of interest for a variety of potential applications. Both of these should serve to allow the enormous potential of hydrogel nanoparticles and their assemblies to be more efficiently tapped for a wide range of applications in the field of biomaterials.

CHAPTER 1

INTRODUCTION

Portion adapted from:

Gaulding, J. C., Herman, E., Lyon, L. A. Responsive Colloids with Controlled Topology. In *Responsive Membranes and Materials*. Bhattacharyya, D., Schafer, T. Eds. Wiley. Chichester, UK, 2013. pp 269-300.

Copyright 2013, John Wiley & Sons, Ltd

1.1. Hydrogels

Polymer networks that have a three-dimensional, cross-linked structure and undergo extensive swelling in water are termed hydrogels. A diverse range of constituent polymers form hydrogels, but the common theme is that all are highly hydrophilic; hydrogels are often more than 90% water by mass. The swollen structure of hydrogels results from the highly favorable interactions of water with the polymer chains, while the cross-linking serves to stabilize the gel against dissolution.¹⁻⁴ The nature of these stabilizing cross-links serves to further classify types of hydrogels. Physically cross-linked gels utilize complementary interactions such as ion-pairing, self-assembly of hydrophobic domains, crystalline polymer domains, or even protein-antigen interactions to preserve network integrity.⁵ Chemically cross-linked gels, in contrast, incorporate covalent linkages within the network, such that the gel is in effect a single molecule. Cross-linkers can be incorporated directly during polymerization (bi-functional vinylic molecules, such as *N,N'*-methylene bisacrylamide (BIS) and poly(ethylene glycol) (PEG) diacrylate are common choices), or added post-synthetically through a variety of coupling reactions.^{1,5,6}

Interest in hydrogels is primarily driven through their applications in biological-contacting materials, or biomaterials. In many ways, hydrogels represent an ideal starting point for designing materials for biological interfacing:

- Their high water content gives them an exceptional loading capacity for applications in drug delivery^{7,8}
- Hydrogels have similar hydration and mechanical properties to biological tissues, making them excellent substrates for cell culture^{9,10}
- Both natural and synthetic polymers are available, allowing gels to be tailored to a specific application^{1,4}

1.1.1. Responsive Gels

Hydrogels incorporating environmentally responsive elements are of particular interest in current research. This responsivity is due to their ability to change their hydration state in response to stimuli such as temperature, pH, light, redox potential, and even the presence of specific solutes.¹¹⁻¹⁴ Of particular interest are thermo-responsive polymers such as poly(*N*-isopropylacrylamide) (pNIPAm), which undergoes an entropically driven collapse to a globular form above its lower critical solution temperature (LCST) of approximately 32 °C.¹³ Upon collapse, water within the gel network is expelled as the pendant isopropyl groups self-associate, leading to a reduction in the total volume and permittivity of the gel. Thus there are numerous examples of interfaces, both macroscopic and colloidal, designed to exploit this attribute of pNIPAm gels or brushes to generate switchable or gated surfaces.¹⁵⁻¹⁹ Similarly, hydrogels featuring an abundance of weak acids or bases can undergo pH-responsive swelling, as the extent of chain-chain interactions and the osmotic pressure of the gel vary as a function of the network charge.⁴

Gel degradation represents a special case for responsivity, as the gel undergoes temporal changes in response to a degradation stimulus. Network degradation can

proceed either through breakdown of the polymer chains themselves, or through disruption of the cross-links that maintain gel integrity.²⁰ The most widely-used example of the former case are the polyesters poly(glycolic acid) and poly(lactic acid), copolymers of which undergo highly tunable degradation driven by hydrolysis of their ester linkages.²¹ In contrast, cross-link scission converts the gel network into individual soluble polymer chains, and the degradation can be triggered by environmental factors such as pH,^{22,23} redox state,²⁴⁻²⁶ enzymatic activity,^{27,28} or light.²⁹ Choice of the appropriate labile chemistry in the cross-linker allows the network to respond in a predictable, controlled manner to the environmental stimuli of interest.

1.1.2. Applications of Hydrogels

As previously alluded to, biomedical applications are a natural fit for hydrogels. The earliest synthetic hydrogels were developed in the 1950's for use in soft contact lenses.³⁰ A recent review by Jindrich Kopecek provides an excellent overview of the history of hydrogels in biomaterials research – from their origins in ophthalmic applications to biocompatible prostheses for nasal implants and vocal cords.³ One major avenue of exploration is drug delivery, an application investigated since the late 1960's.³

Some of the major challenges in drug delivery are the sustained and controlled release of active pharmaceuticals. Such approaches have numerous advantages, including improved patient compliance, stable dosing to avoid sub-efficacious or toxic drug levels, and long-term administration of the therapeutic.³¹ The general strategies for incorporating a drug-eluting implant within the body are to create depots – wherein the drug is isolated within a reservoir and drug release is controlled through a membrane – or matrices, wherein the drug is dispersed homogeneously within the implant.³² Hydrogels are suitable for inclusion in either approach, as their biocompatible and responsive properties make them attractive to either regulate reservoir access or to serve as the delivery matrix. Furthermore, they can offer potential advantages through formulations that gel *in situ* to

form biocompatible matrix for long-term delivery.³³ Both macromolecular and small molecule therapeutics can be entrapped within the gel network, and release can be governed by numerous factors.⁷ Typically the gels of interest for drug delivery applications incorporate some mechanism for physiologic degradation, such that there is no need to remove the delivery scaffold once it has been depleted.^{21,34} One of the key factors to regulating release is the gel's mesh size, a function of its cross-link density and the polymer-solvent interactions.^{2,7} When the loaded therapeutic is much smaller than the mesh, release is regulated by its diffusion within the network. If, on the other hand, the therapeutic is larger than the mesh, the erosion or other stimuli-responsiveness of the network may play a greater role in the release profile.^{7,21}

The softness of hydrogels tends to limit the amount of non-specific protein adsorption and cell adhesion to their surfaces, which allows for synthetic gels to serve as a “blank slate” with regard to applications in tissue engineering.⁴ Such hydrogels offer extensive control, both spatial and temporal, over the presentation and distribution of growth factors, cell binding domains, as well as the mechanical properties of the network.^{9,10,35} These capabilities allow one to apply rational design principles when creating tailored environments to regulate cell behavior. Additional discussion of cell-interacting surfaces is featured in **Chapter 6**.

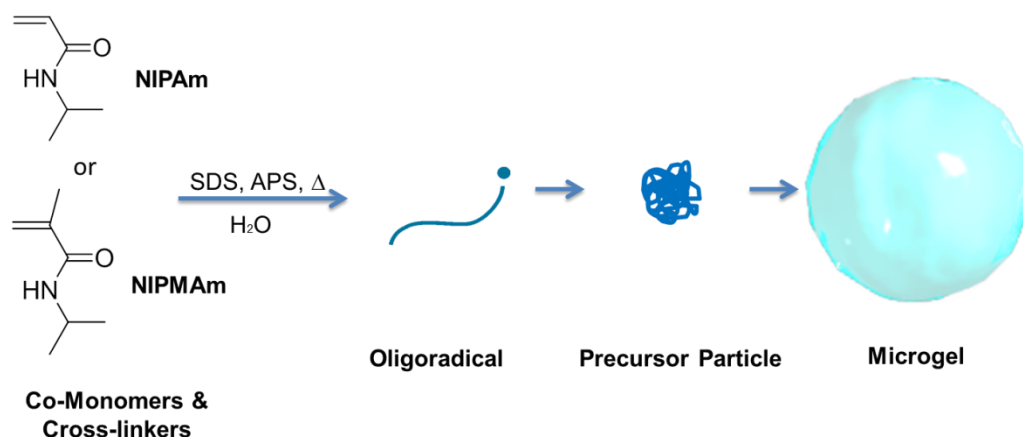
1.2. Microgels

Colloidal hydrogels, or microgels, retain the hydrophilic, cross-linked network structure of a macroscopic gel, but have dimensions on the order of micrometers. Even smaller particles with diameters measured in nanometers are sometimes dubbed, appropriately, “nanogels.”

1.2.1. Microgel Synthesis

Microgels can be synthesized through a number of methods, including mini-emulsion polymerization, self-assembly, microfluidic approaches, and controlled radical polymerizations.³⁶⁻⁴⁰ The microgels described in this thesis were all synthesized using free-radical precipitation polymerization, a technique first demonstrated for pNIPAm in 1986 by Phillip Chibante and Robert Pelton.⁴¹ For thermo-responsive polymers such as pNIPAm or poly(*N*-isopropylmethacrylamide) (pNIPMAm), precipitation polymerization provides a facile method to generate monodisperse particles in high yield using a single aqueous solvent. A depiction of the synthesis is presented in **Scheme 1.1**. Synthesis is conducted using free radical polymerization, typically with a radical source such as ammonium persulfate (APS) or potassium persulfate (KPS), which undergoes thermal decomposition, as this complements the mechanism for particle growth. As polymerization proceeds, the oligomeric chains grow until they reach a critical chain length, at which point they undergo entropically-driven collapse.⁴² The resultant “precursor particles” serve as insoluble hydrophobic nuclei for continued polymer deposition through chain addition and aggregation.⁴² Typically the particles have a net surface charge resulting from the initiating species (i.e. anionic sulfate residues from APS or KPS). The growing particles are stabilized once the surface becomes sufficiently hydrophilic as to limit continued polymer addition.⁴² Thus the concentration of an ionic surfactant, such as sodium dodecylsulfate (SDS) used during the synthesis can also strongly influence the final particle size by stabilizing the growing particles at an earlier stage.^{43,44} The concentrations of initiator and monomer used during the synthesis are also critical to controlling particle size. The total microgel yield depends on the number of precursor particles formed early in the synthesis - a function of the total radical concentration, which is itself dependent on temperature for thermally decomposing initiators such as APS. Ramping the temperature during the synthesis has been demonstrated to be a successful method of synthesizing large microgels.⁴⁵ By generating

a low number of radicals early by initiating at low temperature, there are few precursor particles initially formed. Raising the temperature over the course of the polymerization increases radical concentration to improve the overall polymer yield, while distributing the mass across a smaller number of total microgels.⁴⁵



Scheme 1.1. Synthesis of thermo-responsive microgels through precipitation polymerization.

Precipitation polymerization is exceptionally versatile, allowing a great deal of control over the final composition of thermo-responsive microgels. While pNIPAm's homopolymeric phase transition temperature is fixed by the solvent conditions or quality, acrylamide and *tert*-butylacrylamide have been demonstrated to raise and lower the phase transition, respectively, allowing even that parameter to be tuned.^{46,47} Additionally, vinyl derivatives of carboxylic acids,^{48,49} primary amines,⁵⁰⁻⁵² other weak bases,⁵³ zwitterionic moieties,⁵⁴ and even “click”-able derivatives of azide and alkyne functionalities⁵⁵ have been incorporated into pNIPAm or pNIPMAm microgels.

As with bulk hydrogels, thermo-responsive microgels synthesized through precipitation polymerization can be rendered degradable through the introduction of labile cross-linking, a subject which will be further discussed in **Chapters 2 and 3**.

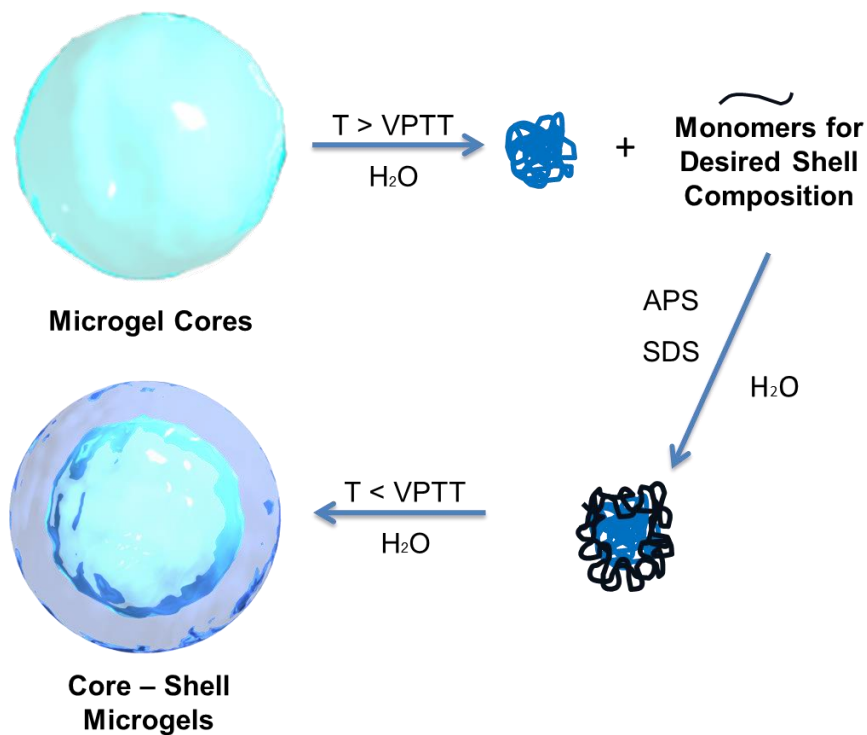
1.2.2. Architectural Control of Microgels

Controlling the presentation and distribution of functional groups in microgels can further expand their applicability, and allow a rational design approach to microgel synthesis. In some instances, the kinetics, reactivity, and/or hydrophilicity of a particular co-monomer will naturally lead to a heterogeneous distribution within the particles. Heterogeneity can take the form of microdomains distributed throughout the microgel network as is observed for microgels co-incorporating pNIPAm and pNIPMAm, similar to a ‘plum pudding’ or “dirty snowball” as Keerl et al. described them.⁵⁶ Radially variable distribution of functionality is also common – the cross-linker BIS tends to core-localize within pNIPAm microgels, leading to a particle that is best approximated as a densely cross-linked core with a loosely cross-linked, low density and highly branched corona.⁵⁷⁻⁵⁹ The distribution of carboxyl groups within a pNIPAm microgel can be controlled through the choice of the acidic co-monomer: acrylic acid tends to homogeneously incorporate, while methacrylic acid tends to core-localize while vinylacetic and fumaric acids are enriched at the particle periphery.⁶⁰ Continuous infusion of a co-monomer prone to phase segregation can aid in homogenizing its distribution, as well.^{61,62}

1.2.2.1. Microgel Core-Shell Synthesis

Core-shell syntheses provide a mechanism to control the overall architecture of a microgel. The synthesis of these particles proceeds through a “seed & feed” polymerization approach, developed in our group in 2000 for controlling the localization of acrylic acid within pNIPAm microgels.⁶³ The technique is summarized in **Scheme 1.2**. Following synthesis of the desired microgel cores, the particles are returned to conditions above their volume-phase transition temperature (VPTT). The VPTT differs from the LCST in that the collapse of polymer chains is described as transitioning at their LCST, while cross-linked gels undergo transitions at their VPTT. The monomeric constituents of

the desired shell are added, at a concentration sufficiently low to inhibit new precursor particle formation, along with optional surfactant. Initiator is then added to begin the polymerization. As shell oligomers form, they undergo collapse and deposit onto the templating cores. Once polymerization is complete, the solution is cooled, allowing the core-shell particles to re-swell.



Scheme 1.2. Control of particle architecture through core-shell microgel synthesis. Cores of a desired composition are heated to collapse for use as templates during further polymerization. The concentration of monomer and initiator added are sufficient to prevent new particle formation, leading to deposition on the templating core during precipitation polymerization.

1.2.2.2. Core Compression

The swelling relationship between core and shell is a complex one, however.⁶⁴ Studies have probed the unique nature of core/shell coupling in microgel systems. Berndt & Richtering described a system wherein two thermo-responsive polymers (pNIPAm and pNIPMAm) were used to form a core-shell microgel wherein the core and shell exhibited

different transition temperatures.⁶⁵ When the pNIPMAm phase (having the higher transition temperature, ~44 °C) was located in the shell, it tended to prevent complete deswelling of the pNIPAm core at temperatures between the two phase transitions. A collapsed pNIPAm shell exerted a compressive effect on the pNIPMAm core, preventing it from achieving its fully swollen state below its own LCST.⁶⁵ The extent to which the shell's swelling behavior dominates the core's scales with the thickness of the added shell.⁶⁵⁻⁶⁷

Shell domination of the particle swelling suggests that the addition of the shell is affecting the swollen state of the core, preventing it from completely relaxing. This phenomenon is called “core compression” and was probed by Jones et al. in our group using fluorescence resonance energy transfer, or FRET.⁶⁸ In the case where no shell has been added, the FRET efficiency was very low, as the core swelling (and hence inter-chain distance) greatly separated the donor and acceptor. Above the transition temperature, the degree of FRET increased sharply as the enhanced polymer-polymer interactions brought the dyes closer together. When considering the core-shell case below the transition temperature, the degree of FRET was less than the deswollen case, but higher than in the free core. This suggested that the ability of the polymer chains in the core to extend was inhibited by the added polymer of the shell, resisting the core's swelling ability and leading to an increased FRET signal.⁶⁸

Recently Xiaobo Hu working with our group demonstrated the first example of a core-shell microgel wherein these strong influences between the core and shell can be disrupted, leading to fully independent behavior of the core and shell.⁶⁹ These particles were synthesized using the core-shell synthesis method described previously, followed by the subsequent addition of a second shell, enabling a core-shell-shell architecture. By using the oxidation-sensitive degradable cross-linker (1,2-dihydroxyethylene) bisacrylamide (DHEA) in the first shell, the sacrificial inner shell can be degraded and

the free polymer removed from the particle. As a result, the core and outer shell are mechanically decoupled by the void volume left upon removal of the inner shell.

1.2.3. Applications of Colloidal Hydrogels

1.2.3.1. Applications of Microgels

Responsive gels make for particularly interesting micro- or nanogels, as their smaller dimensions lead to rapid equilibration compared to their bulk gel counterparts.⁷⁰ Microgels retain the solvent swollen character and biocompatible softness of bulk gels, and thus there is substantial overlap in their applications, though the colloidal nature of microgels creates new opportunities unachievable by macroscopic hydrogels. For example, microgels have been developed for use as nanoreactors, wherein catalytic metal nanoparticles or enzymes are loaded within the gel network.⁷¹⁻⁷³ The microgel support leads to a greater surface area in contact with the solution, allowing more efficient mass transport of substrate and product. Enzymatic activity can even be regulated in these nanoreactors, through enhancement via immobilization or responsive elements controlling accessibility.^{15,16,74}

When considering hydrogels in drug delivery, the same factors to govern release are in effect, but the dimensions of the particles allow them to be utilized as particulate nanocarriers.^{8,75-77} Such vehicles allow potentially immunogenic therapeutics which would otherwise have poor circulation lifetimes, such as proteins or therapeutic nucleic acids, to remain encapsulated and protected from degradation. Spatial control over therapeutics can now be exerted upon the cellular scale, through strategies such as the use of targeting ligands and triggered particle erosion or swelling sensitized to specific intracellular conditions.^{8,78,79}

Ion-pairing is an efficient means of loading microgels, as charge compensation can lead to microgel collapse to enhance retention.⁸⁰⁻⁸² Release can then be triggered by

alterations in pH or ionic strength. The properties of the loaded drug affect its uptake and distribution. For example, Bysell et al. have extensively studied the interactions of polycationic peptides with poly(acrylic acid) microgels.^{81,83,84} High molecular weight polycations have a limited ability to diffuse into the microgel, and thus their loading tends to rapidly collapse the periphery of the microgels. This creates a dense shell which inhibits further loading.^{81,83} Particles of this type have been shown to efficiently load and release peptides with antibacterial activity.^{85,86}

Going beyond charge-pairing, microgel affinity for a specific molecule can also be tuned by altering the concentration of hydrogen-bonding and hydrophobic components of the gel network.⁸⁷ From analysis of the structure of the peptide melittin, a component of bee venom, and from a screen of pNIPAm microgels co-polymerized with a range of charged, hydrophobic, and hydrophilic monomers, Hoshino et al. demonstrated that an optimized composition exhibited the ability to sequester the peptide and selectively bind it from complex media.⁸⁷ This effect is greatly enhanced when the microgels are synthesized in the presence of the peptide, leading to a molecular imprinting effect.⁸⁸ These particles were also shown to retain their efficacy when injected into a mouse model, as toxic doses of melittin are safely imbibed within the microgels.⁸⁹ More recently, this technique has been demonstrated to be effective with lysozyme, suggesting that sequestration and release of active proteins is possible as well.⁹⁰

The responsivity of microgels enables them to serve as unique sensors as well. Microgels of pNIPAm co-polymerized with a solvatochromic fluorophore underwent a broad (~ 6 °C) transition above their VPTT of ~27 °C. The accumulation of relatively hydrophobic domains within the microgels during the transition interval allowed the particle fluorescence intensity to increase accordingly.⁹¹ Thus, following calibration of their “intracellular thermometers” Gota et al. were able to observe changes in cell temperature as a function of time, and in response to cell processes and external stimuli.⁹¹ Recently, their next generation effort for intracellular thermometry was demonstrated to

have improved sensing range and spatial resolution, allowing discrimination of temperatures within different cell compartments.⁹² Several other groups have developed similar approaches for measuring the temperature or pH of regions inaccessible by other probes using nanogels.^{93,94}

1.2.3.2. Applications of Core-Shell Microgels

The core-shell architecture is enabling for numerous applications. The shell serves as a way to localize functionality on the surface of the particles. For example, a targeting ligand can be bound to the surface of the nanoparticles for drug delivery applications.^{95,96} Additionally, suitably-functionalized PEG has been incorporated into the shell of a microgel, which increases the hydrophilicity of the particle and acts to inhibit protein adsorption.⁹⁷ Taking shell-localization to an extreme, Nayak et al. in our lab confined the distribution of the degradable cross-linker DHEA into the core of a core-shell particle, such that oxidation led to dissolution of the core and the production of hollow, i.e. shell-only, microgels.⁹⁸

The shell can also serve as a barrier that restricts access to the nanoparticle core. Kleinen et al. compared a series of architectures, wherein a pNIPAm-co-methacrylic acid core particle was covered in a pNIPAm shell. Incubation of the particles with the polycation poly(diallyldimethylammonium chloride) (PDADMAC) led to interaction with the anionic microgels. However, there was a strong molecular weight dependence. Low molecular weight polymer (~15 kDa) was able to easily penetrate the shell, leading to high levels of loading within the polymer, no charge reversal (i.e. the polycation is confined to the interior), and no difference between the core-shell and the core particle behavior. However, higher molecular weight PDADMAC (~450 kDa) was unable to access the anionic sites on the particle interior as readily. As a result, the net charge of the particle surface shifted from neutral (due to the pNIPAm shell) to positive (due to excess PDADMAC adsorbed on the surface).⁹⁹ Another example from our group described by

Satish Nayak combined biotinylated core particles with a shell containing DHEA. Initially, avidin was excluded from the interior of the particles by the added shell. Upon erosion of the degradable cross-links, avidin was able to access the core and bind to the biotin contained within.¹⁰⁰

Responsive microgels with fine control over architecture can be used to develop systems containing feedback loops, enabling more advanced applications. Lapeyre et al. describe a system wherein microgels consisting of pNIPMAm cores incorporate a pNIPMAm shell co-polymerized with a phenylboronic acid derivative.¹⁰¹ Phenylboronic acids complex with glucose, and have been demonstrated to be an effective means of generating microgels whose swelling responds to glucose concentration.^{14,102} In this system, localization of the glucose-responsive elements to the surface enables a gating porosity to occur based on the external glucose concentration. The microgels were sufficiently swollen above their transition temperature to enable loading with fluorescently-labeled insulin. Increasing the temperature above the VPTT of this system (in this case, ~25 °C) collapsed the particles and retained the insulin within. Introduction of glucose led to swelling of the shell, and thus enabled insulin to diffuse out of the particles.

1.3. Microgel Assemblies and Films

There are four types of microgel assemblies that are discussed within this thesis: 1) concentrated microgel dispersions (colloidal crystals, glasses, and fluids), 2) microgels covalently bound into three dimensional gels (“gel-of-microgels”), 3) microgels interacting with macroscopic substrates (monolayer films), and 4) microgel polyelectrolyte assemblies (multilayer films). Microgels have been extensively studied with respect to their behavior in close-packed assemblies such as colloidal glasses and crystals,¹⁰³ and dense colloidal assemblies are a subject of discussion in **Chapter 4**. Gels of microgels are distinguished in that the microgels are covalently bound upon formation

of a dense assembly, as demonstrated in **Chapters 3 & 7**. The latter two types of assemblies, microgel films, will be elaborated upon in **Chapters 5 & 6**.

1.3.1. Microgels as Building Blocks

In each case, it is of interest to consider how the properties of individual microgels are influenced by their presence in an assembly. For example, pNIPAm microgels form a disordered glass when concentrated by centrifugation, but retain their thermo-responsivity; this has been demonstrated as a method to induce conversion of disordered colloidal glasses to crystalline arrays through manipulation of their volume fraction.^{104,105} Further, particle swelling is dependent upon the assembly, as concentrated particle dispersions exhibit decreases in particle size – ascribed to particle-particle contact¹⁰⁶ or to changes in the free ionic strength as a function of particle number density.¹⁰⁷ In an intriguing example of this phenomenon, the lattice spacing in colloidal crystals serves to impose a size constraint upon dopant microgels having radii greater than twice that of the constituent matrix.¹⁰⁸ Other alterations in particle packing due to responsivity to other environmental stimuli can allow colloidal crystals to function as sensors. The Asher group has demonstrated that colloidal crystalline arrays of polystyrene nanoparticles suspended in a variety of responsive hydrogels can undergo diffraction changes as an analyte of interest affects particle-particle interactions or the suspending gel network.^{109,110} Colloidal crystals of microgels have similarly been shown to exhibit color changes in response to an analyte, as changes in their swelling alter the particle-particle spacing in the colloidal crystal.¹¹¹

Surface-bound pNIPAm microgels, as in monolayers, also retain their thermo-responsivity.¹¹²⁻¹¹⁴ If these microgels are designed to be susceptible to other stimuli, that responsivity can be exploited as a sensing modality.^{115,116} Biotin-functionalized microgels bind to avidin present in solution, and the multivalency of the binding event leads to multiple chain cross-linking. This both increases the polymer density and changes its

refractive index, resulting in differences in microgel appearance discernible by visual inspection.¹¹⁵ Similarly, responsive microgel monolayers sandwiched between thin gold films form “etalons,” wherein the changes in particle swelling alter the distance between the gold films, which can lead to dramatic color changes suitable for analyte detection.^{116,117} Mixtures of microgels can also be deposited onto surfaces, allowing a mosaic-type display of particles onto a surface, which may then allow for the composition of responsive elements on the surfaces to be tuned.¹¹⁸

1.3.2. Layer-by-Layer Film Assembly

Deposition of microgels as monolayers can be achieved through passive means,¹¹⁸⁻¹²⁰ spin-coating,^{114,121,122} or centrifugal deposition.¹²³ In each case, to ensure efficient surface coverage, Coulombic interactions between charged microgels and oppositely-charged surface groups (such as amine-functionalized glass) or alternative methods to effect covalent coupling are needed. From this foundation, additional layers of microgels can be deposited using the layer-by-layer technique. First described by Decher et al., films consisting of two complementary components, such as oppositely-charged polyelectrolytes, can be readily assembled through alternating exposure (for example, dipping or spraying) to solutions of each component.^{124,125} Exposing an anionic microgel monolayer to a solution of a linear polycation, such as poly(allylamine hydrochloride) (PAH) or PDADMAC, leads to uptake within the porous oppositely charged particles. Rinsing and exposing to another microgel solution allows sequential buildup of microgel multilayered films.

First demonstrated by Serpe et al. in 2003, our group has used this technique extensively to form microgel films.¹¹⁹ As a result, the constituent particles assembled into these films necessarily have two responsivities – thermo-responsivity arising from their synthesis via precipitation polymerization, and pH-responsivity through weak acid incorporation to generate the needed anionic groups to promote interactions with an

amine-functionalized substrate. Both of these properties are conferred onto the film assembly, but microgel and polycation interactions lead to complex behaviors of the films.^{119,121} Though the films are assembled under neutral pH (corresponding to highly-charged states for both microgels and polycation) the films maintain their structure through pH excursions which result in a reduction in the overall charge of the microgels, (i.e. exposure to acidic conditions) presumably through remnant polycation interactions and entanglement of both microgel chains and the polycation. At low pH, the particles retain their thermo-responsivity in the multilayer assembly, though the response is suppressed at high pH – consistent with particle behavior in solution.¹¹⁹ The responsivity of the films is also sensitive to the last layer deposited. When the top layer is polycation, the charges within the microgels are compensated and as a result the particles are highly condensed and extensively Coulombically cross-linked at neutral pH. When microgels are the top layer under the same conditions, they remain highly swollen and act as a distinctly different phase within the films.¹²⁶

1.3.1. Applications of Microgel Assemblies

Utilizing the responsivity of numerous microgels in concert is a common theme for many of the potential sensing applications of these materials, as their hundreds of nanometer sizes allow alterations in particle spacing to lead to changes readily discerned as alterations in assembly color.^{111,116,120} The range of responses that can be introduced into microgels make sensors of this type potentially generalizable to many other stimuli.

Microgels have also been demonstrated to stabilize emulsions by forming monolayers at the oil-water interface.^{127,128} Contrary to conventional particle-stabilized, or Pickering, emulsions, electrostatics is not the primary mechanism responsible for stability. In fact, mixtures of Pickering emulsions, one stabilized by anionic microgels and the other by cationic microgels, do not coalesce under conditions where both microgels are charged – only acidic or basic pHs that neutralize one of the two sets of

microgels lead to breaking of the emulsions.¹²⁹ Instead, the deformable, amphiphilic nature of the particles seems to be the major contributor to the overall stability of the system.^{128,130} Besides being extensively studied for their rich phase behavior at these interfaces, the stimuli-responsivity of microgels allows the stability of the emulsions to be controlled by microgel composition and their coalescence triggered by stimuli such as temperature, pH, or ionic strength.^{127,129-132}

Biomedical applications of microgel assemblies and films are primarily driven by interest in drug delivery. The building block nature of the individual particles allows them to be tailored for loading and release, and film or gel assembly serves to immobilize the particles to create a delivery reservoir. *In situ* gelation of injected microgels has been demonstrated to be a method of repairing intervertebral discs¹³³ or to allow sustained release of a co-administered anesthetic.^{134,135} Others have also studied microgel multilayer films for drug delivery,¹³⁶ and even coated sutures for controlled release of anti-inflammatory agents.¹³⁷ For example, our group has demonstrated that microgel multilayers assembled using layer-by-layer film buildup can be used to deliver the small molecule drug doxorubicin¹³⁸ as well as the macromolecule insulin.^{139,140} Temperature cycling of the responsive film served to both enhance loading¹³⁸ and to allow pulsatile, sustained release from the films.¹⁴⁰ Our group has also studied microgel films as coatings for biological interfaces, and this will be detailed in **Chapter 6**.

1.4. References

- [1] Hoffman, A. S., Hydrogels for biomedical applications. *Advanced Drug Delivery Reviews* **2002**, *54*, 3-12.
- [2] Lin, C. C.; Metters, A. T., Hydrogels in controlled release formulations: Network design and mathematical modeling. *Advanced Drug Delivery Reviews* **2006**, *58*, 1379-1408.
- [3] Kopecek, J., Hydrogels: From Soft Contact Lenses and Implants to Self-Assembled Nanomaterials. *Journal of Polymer Science Part A-Polymer Chemistry* **2009**, *47*, 5929-5946.

- [4] Peppas, N. A.; Huang, Y.; Torres-Lugo, M.; Ward, J. H.; Zhang, J., Physicochemical, foundations and structural design of hydrogels in medicine and biology. *Annual Review of Biomedical Engineering* **2000**, *2*, 9-29.
- [5] Hennink, W. E.; van Nostrum, C. F., Novel crosslinking methods to design hydrogels. *Advanced Drug Delivery Reviews* **2002**, *54*, 13-36.
- [6] Yeh, P. Y.; Kopeckova, P.; Kopecek, J., Biodegradable and pH-Sensitive Hydrogels - Synthesis by Cross-Linking of N,N-Dimethylacrylamide Copolymer Precursors. *Journal of Polymer Science Part A-Polymer Chemistry* **1994**, *32*, 1627-1637.
- [7] Hoare, T. R.; Kohane, D. S., Hydrogels in drug delivery: Progress and challenges. *Polymer* **2008**, *49*, 1993-2007.
- [8] Kabanov, A. V.; Vinogradov, S. V., Nanogels as Pharmaceutical Carriers: Finite Networks of Infinite Capabilities. *Angewandte Chemie-International Edition* **2009**, *48*, 5418-5429.
- [9] Peppas, N. A.; Hilt, J. Z.; Khademhosseini, A.; Langer, R., Hydrogels in biology and medicine: From molecular principles to bionanotechnology. *Advanced Materials* **2006**, *18*, 1345-1360.
- [10] Seliktar, D., Designing Cell-Compatible Hydrogels for Biomedical Applications. *Science* **2012**, *336*, 1124-1128.
- [11] Suzuki, A.; Tanaka, T., Phase-Transition in Polymer Gels Induced by Visible-Light. *Nature* **1990**, *346*, 345-347.
- [12] Dimitrov, I.; Trzebicka, B.; Muller, A. H. E.; Dworak, A.; Tsvetanov, C. B., Thermosensitive water-soluble copolymers with doubly responsive reversibly interacting entities. *Progress in Polymer Science* **2007**, *32*, 1275-1343.
- [13] Fujishige, S.; Kubota, K.; Ando, I., Phase-Transition of Aqueous-Solutions of Poly(N-Isopropylacrylamide) and Poly(N-Isopropylmethacrylamide). *Journal of Physical Chemistry* **1989**, *93*, 3311-3313.
- [14] Hoare, T.; Pelton, R., Engineering glucose swelling responses in poly (N-isopropylacrylamide)-based microgels. *Macromolecules* **2007**, *40*, 670-678.
- [15] Lu, Y.; Mei, Y.; Ballauff, M.; Drechsler, M., Thermosensitive core-shell particles as carrier systems for metallic nanoparticles. *Journal of Physical Chemistry B* **2006**, *110*, 3930-3937.

- [16] Lu, Y.; Mei, Y.; Drechsler, M.; Ballauff, M., Thermosensitive core-shell particles as carriers for Ag nanoparticles: Modulating the catalytic activity by a phase transition in networks. *Angewandte Chemie-International Edition* **2006**, *45*, 813-816.
- [17] Cole, M. A.; Voelcker, N. H.; Thissen, H.; Griesser, H. J., Stimuli-responsive interfaces and systems for the control of protein-surface and cell-surface interactions. *Biomaterials* **2009**, *30*, 1827-1850.
- [18] Yavuz, M. S.; Cheng, Y. Y.; Chen, J. Y.; Cobley, C. M.; Zhang, Q.; Rycenga, M.; Xie, J. W.; Kim, C.; Song, K. H.; Schwartz, A. G.; Wang, L. H. V.; Xia, Y. N., Gold nanocages covered by smart polymers for controlled release with near-infrared light. *Nature Materials* **2009**, *8*, 935-939.
- [19] Ankareddi, I.; Brazel, C. S., Synthesis and characterization of grafted thermosensitive hydrogels for heating activated controlled release. *International Journal of Pharmaceutics* **2007**, *336*, 241-247.
- [20] Heller, J., Controlled Release of Biologically-Active Compounds from Bioerodible Polymers. *Biomaterials* **1980**, *1*, 51-57.
- [21] Park, K.; Shalaby, W. S. W.; Park, H. *Biodegradable hydrogels for drug delivery*; Technomic Pub.: Lancaster, PA, 1993.
- [22] Ulbrich, K.; Subr, V.; Seymour, L. W.; Duncan, R., Novel Biodegradable Hydrogels Prepared Using the Divinyllic Crosslinking Agent N,O-Dimethacryloylhydroxylamine. 1. Synthesis and Characterization of Rates of Gel Degradation, and Rate of Release of Model-Drugs, In vitro and In vivo. *Journal of Controlled Release* **1993**, *24*, 181-190.
- [23] Murthy, N.; Thng, Y. X.; Schuck, S.; Xu, M. C.; Frechet, J. M. J., A novel strategy for encapsulation and release of proteins: Hydrogels and microgels with acid-labile acetal cross-linkers. *Journal of the American Chemical Society* **2002**, *124*, 12398-12399.
- [24] Han, S. C.; He, W. D.; Li, J.; Li, L. Y.; Sun, X. L.; Zhang, B. Y.; Pan, T. T., Reducible Polyethylenimine Hydrogels with Disulfide Crosslinkers Prepared by Michael Addition Chemistry as Drug Delivery Carriers: Synthesis, Properties, and In Vitro Release. *Journal of Polymer Science Part A-Polymer Chemistry* **2009**, *47*, 4074-4082.
- [25] Aliyar, H. A.; Hamilton, P. D.; Ravi, N., Refilling of ocular lens capsule with copolymeric hydrogel containing reversible disulfide. *Biomacromolecules* **2005**, *6*, 204-211.

- [26] Lee, H.; Park, T. G., Reduction/oxidation induced cleavable/crosslinkable temperature-sensitive hydrogel network containing disulfide linkages. *Polymer Journal* **1998**, *30*, 976-980.
- [27] Ulbrich, K.; Strohalm, J.; Kopecek, J., Polymers Containing Enzymatically Degradable Bonds. VI. Hydrophilic Gels Cleavable by Chymotrypsin. *Biomaterials* **1982**, *3*, 150-154.
- [28] Shantha, K. L.; Ravichandran, P.; Rao, K. P., Azo Polymeric Hydrogels for Colon Targeted Drug-Delivery. *Biomaterials* **1995**, *16*, 1313-1318.
- [29] Kloxin, A. M.; Kasko, A. M.; Salinas, C. N.; Anseth, K. S., Photodegradable Hydrogels for Dynamic Tuning of Physical and Chemical Properties. *Science* **2009**, *324*, 59-63.
- [30] Wichterle, O.; Lim, D., Hydrophilic Gels for Biological Use. *Nature* **1960**, *185*, 117-118.
- [31] Langer, R. S.; Peppas, N. A., Present and Future Applications of Biomaterials in Controlled Drug Delivery Systems. *Biomaterials* **1981**, *2*, 201-214.
- [32] Saltzman, W. M. In *Drug Delivery: Engineering Principles for Drug Therapy*; Oxford University Press: New York, 2001, p 235-280.
- [33] Kretlow, J. D.; Klouda, L.; Mikos, A. G., Injectable matrices and scaffolds for drug delivery in tissue engineering. *Advanced Drug Delivery Reviews* **2007**, *59*, 263-273.
- [34] Dash, A. K.; Cudworth, G. C., Therapeutic applications of implantable drug delivery systems. *Journal of Pharmacological and Toxicological Methods* **1998**, *40*, 1-12.
- [35] Slaughter, B. V.; Khurshid, S. S.; Fisher, O. Z.; Khademhosseini, A.; Peppas, N. A., Hydrogels in Regenerative Medicine. *Advanced Materials* **2009**, *21*, 3307-3329.
- [36] Oh, J. K.; Drumright, R.; Siegwart, D. J.; Matyjaszewski, K., The development of microgels/nanogels for drug delivery applications. *Progress in Polymer Science* **2008**, *33*, 448-477.
- [37] Sanson, N.; Rieger, J., Synthesis of nanogels/microgels by conventional and controlled radical crosslinking copolymerization. *Polymer Chemistry* **2010**, *1*, 965-977.
- [38] Seiffert, S., Functional Microgels Tailored by Droplet-Based Microfluidics. *Macromolecular Rapid Communications* **2011**, *32*, 1600-1609.

- [39] Pelton, R.; Hoare, T. In *Microgel Suspensions: Fundamentals and Applications*; 1st ed.; Fernandez-Nieves, A., Wyss, H. M., Mattsson, J., Weitz, D. A., Eds.; Wiley: Weinheim, 2011.
- [40] Klinger, D.; Landfester, K., Stimuli-responsive microgels for the loading and release of functional compounds: Fundamental concepts and applications. *Polymer* **2012**, *53*, 5209-5231.
- [41] Pelton, R. H.; Chibante, P., Preparation of aqueous latices with N-isopropylacrylamide. *Colloids and Surfaces* **1986**, *20*, 247-256.
- [42] Pelton, R., Temperature-sensitive aqueous microgels. *Advances in Colloid and Interface Science* **2000**, *85*, 1-33.
- [43] Mcphee, W.; Tam, K. C.; Pelton, R., Poly(N-Isopropylacrylamide) Latices Prepared with Sodium Dodecyl-Sulfate. *Journal of Colloid and Interface Science* **1993**, *156*, 24-30.
- [44] Blackburn, W. H.; Lyon, L. A., Size-controlled synthesis of monodisperse core/shell nanogels. *Colloid and Polymer Science* **2008**, *286*, 563-569.
- [45] Meng, Z. Y.; Smith, M. H.; Lyon, L. A., Temperature-programmed synthesis of micron-sized multi-responsive microgels. *Colloid and Polymer Science* **2009**, *287*, 277-285.
- [46] Wang, Q.; Zhao, Y. B.; Xu, H. B.; Yang, X. L.; Yang, Y. J., Thermosensitive Phase Transition Kinetics of Poly(N-isopropylacryl amide-co-acrylamide) Microgel Aqueous Dispersions. *Journal of Applied Polymer Science* **2009**, *113*, 321-326.
- [47] Debord, J. D.; Lyon, L. A., Synthesis and characterization of pH-responsive copolymer microgels with tunable volume phase transition temperatures. *Langmuir* **2003**, *19*, 7662-7664.
- [48] Hoare, T.; Pelton, R., Functional group distributions in carboxylic acid containing poly(N-isopropylacrylamide) microgels. *Langmuir* **2004**, *20*, 2123-2133.
- [49] Hoare, T.; Pelton, R., Highly pH and temperature responsive microgels functionalized with vinylacetic acid. *Macromolecules* **2004**, *37*, 2544-2550.
- [50] Mai-ngam, K.; Boonkitpattarakul, K.; Sakulsombat, M.; Chumningan, P.; Mai-ngam, B., Synthesis and phase separation of amine-functional temperature responsive copolymers based on poly(N-isopropylacrylamide). *European Polymer Journal* **2009**, *45*, 1260-1269.

- [51] Xu, J. J.; Timmons, A. B.; Pelton, R., N-Vinylformamide as a route to amine-containing latexes and microgels. *Colloid and Polymer Science* **2004**, *282*, 256-263.
- [52] Hu, X. B.; Tong, Z.; Lyon, L. A., Synthesis and physicochemical properties of cationic microgels based on poly(N-isopropylmethacrylamide). *Colloid and Polymer Science* **2011**, *289*, 333-339.
- [53] Xu, J. J.; Pelton, R., A new route to poly(N-isopropylacrylamide) microgels supporting a polyvinylamine corona. *Journal of Colloid and Interface Science* **2004**, *276*, 113-117.
- [54] Das, M.; Sanson, N.; Kumacheva, E., Zwitterionic Poly(betaine-N-isopropylacrylamide) Microgels: Properties and Applications. *Chemistry of Materials* **2008**, *20*, 7157-7163.
- [55] Meng, Z. Y.; Hendrickson, G. R.; Lyon, L. A., Simultaneous Orthogonal Chemoligations on Multiresponsive Microgels. *Macromolecules* **2009**, *42*, 7664-7669.
- [56] Keerl, M.; Pedersen, J. S.; Richtering, W., Temperature Sensitive Copolymer Microgels with Nanophase Separated Structure. *Journal of the American Chemical Society* **2009**, *131*, 3093-3097.
- [57] Varga, I.; Gilanyi, T.; Meszaros, R.; Filipcsei, G.; Zrinyi, M., Effect of cross-link density on the internal structure of Poly(N-isopropylacrylamide) microgels. *Journal of Physical Chemistry B* **2001**, *105*, 9071-9076.
- [58] Stieger, M.; Richtering, W.; Pedersen, J. S.; Lindner, P., Small-angle neutron scattering study of structural changes in temperature sensitive microgel colloids. *Journal of Chemical Physics* **2004**, *120*, 6197-6206.
- [59] Saunders, B. R., On the structure of poly(N-isopropylacrylamide) microgel particles. *Langmuir* **2004**, *20*, 3925-3932.
- [60] Hoare, T.; McLean, D., Kinetic prediction of functional group distributions in thermosensitive microgels. *Journal of Physical Chemistry B* **2006**, *110*, 20327-20336.
- [61] Acciaro, R.; Gilanyi, T.; Varga, I., Preparation of Monodisperse Poly(N-isopropylacrylamide) Microgel Particles with Homogenous Cross-Link Density Distribution. *Langmuir* **2011**, *27*, 7917-7925.
- [62] Sheikholeslami, P.; Ewaschuk, C. M.; Ahmed, S. U.; Greenlay, B. A.; Hoare, T., Semi-batch control over functional group distributions in thermoresponsive microgels. *Colloid and Polymer Science* **2012**, *290*, 1181-1192.

- [63] Jones, C. D.; Lyon, L. A., Synthesis and characterization of multiresponsive core-shell microgels. *Macromolecules* **2000**, *33*, 8301-8306.
- [64] Richtering, W.; Pich, A., The special behaviours of responsive core-shell nanogels. *Soft Matter* **2012**, *8*, 11423-11430.
- [65] Berndt, I.; Richtering, W., Doubly temperature sensitive core-shell microgels. *Macromolecules* **2003**, *36*, 8780-8785.
- [66] Jones, C. D.; Lyon, L. A., Dependence of shell thickness on core compression in acrylic acid modified poly(N-isopropylacrylamide) core/shell microgels. *Langmuir* **2003**, *19*, 4544-4547.
- [67] Berndt, I.; Pedersen, J. S.; Richtering, W., Temperature-sensitive core-shell microgel particles with dense shell. *Angewandte Chemie-International Edition* **2006**, *45*, 1737-1741.
- [68] Jones, C. D.; McGrath, J. G.; Lyon, L. A., Characterization of cyanine dye-labeled poly(N-isopropylacrylamide) core/shell microgels using fluorescence resonance energy transfer. *Journal of Physical Chemistry B* **2004**, *108*, 12652-12657.
- [69] Hu, X. B.; Tong, Z.; Lyon, L. A., Multicompartment Core/Shell Microgels. *Journal of the American Chemical Society* **2010**, *132*, 11470-11472.
- [70] Suarez, I. J.; Fernandez-Nieves, A.; Marquez, M., Swelling kinetics of poly(N-isopropylacrylamide) minigels. *Journal of Physical Chemistry B* **2006**, *110*, 25729-25733.
- [71] Sharma, G.; Ballauff, M., Cationic spherical polyelectrolyte brushes as nanoreactors for the generation of gold particles. *Macromolecular Rapid Communications* **2004**, *25*, 547-552.
- [72] Neumann, T.; Haupt, B.; Ballauff, M., High activity of enzymes immobilized in colloidal nanoreactors. *Macromolecular Bioscience* **2004**, *4*, 13-16.
- [73] Mei, Y.; Lu, Y.; Polzer, F.; Ballauff, M.; Drechsler, M., Catalytic activity of palladium nanoparticles encapsulated in spherical polyelectrolyte brushes and core-shell microgels. *Chemistry of Materials* **2007**, *19*, 1062-1069.
- [74] Welsch, N.; Wittemann, A.; Ballauff, M., Enhanced Activity of Enzymes Immobilized in Thermoresponsive Core-Shell Microgels. *Journal of Physical Chemistry B* **2009**, *113*, 16039-16045.

- [75] Nayak, S.; Lyon, L. A., Soft nanotechnology with soft nanoparticles. *Angewandte Chemie-International Edition* **2005**, *44*, 7686-7708.
- [76] Raemdonck, K.; Demeester, J.; De Smedt, S., Advanced nanogel engineering for drug delivery. *Soft Matter* **2009**, *5*, 707-715.
- [77] Bysell, H.; Mansson, R.; Hansson, P.; Malmsten, M., Microgels and microcapsules in peptide and protein drug delivery. *Advanced Drug Delivery Reviews* **2011**, *63*, 1172-1185.
- [78] Couvreur, P.; Vauthier, C., Nanotechnology: Intelligent design to treat complex disease. *Pharmaceutical Research* **2006**, *23*, 1417-1450.
- [79] Chacko, R. T.; Ventura, J.; Zhuang, J. M.; Thayumanavan, S., Polymer nanogels: A versatile nanoscopic drug delivery platform. *Advanced Drug Delivery Reviews* **2012**, *64*, 836-851.
- [80] Eichenbaum, G. M.; Kiser, P. F.; Shah, D.; Simon, S. A.; Needham, D., Investigation of the swelling response and drug loading of ionic microgels: The dependence on functional group composition. *Macromolecules* **1999**, *32*, 8996-9006.
- [81] Bysell, H.; Malmsten, M., Visualizing the interaction between poly-L-lysine and poly(acrylic acid) microgels using microscopy techniques: Effect of electrostatics and peptide size. *Langmuir* **2006**, *22*, 5476-5484.
- [82] Smith, M. H.; Lyon, L. A., Tunable Encapsulation of Proteins within Charged Microgels. *Macromolecules* **2011**, *44*, 8154-8160.
- [83] Bysell, H.; Hansson, P.; Malmsten, M., Transport of poly-L-lysine into oppositely charged poly(acrylic acid) microgels and its effect on gel deswelling. *Journal of Colloid and Interface Science* **2008**, *323*, 60-69.
- [84] Bysell, H.; Malmsten, M., Interactions between Homopolypeptides and Lightly Cross-Linked Microgels. *Langmuir* **2009**, *25*, 522-528.
- [85] Bysell, H.; Ransson, P.; Schmidtchen, A.; Malmsten, M., Effect of Hydrophobicity on the Interaction between Antimicrobial Peptides and Poly(acrylic acid) Microgels. *Journal of Physical Chemistry B* **2010**, *114*, 1307-1313.
- [86] Bysell, H.; Schmidtchen, A.; Malmsten, M., Binding and Release of Consensus Peptides by Poly(acrylic acid) Microgels. *Biomacromolecules* **2009**, *10*, 2162-2168.

- [87] Hoshino, Y.; Urakami, T.; Kodama, T.; Koide, H.; Oku, N.; Okahata, Y.; Shea, K. J., Design of Synthetic Polymer Nanoparticles that Capture and Neutralize a Toxic Peptide. *Small* **2009**, *5*, 1562-1568.
- [88] Hoshino, Y.; Kodama, T.; Okahata, Y.; Shea, K. J., Peptide Imprinted Polymer Nanoparticles: A Plastic Antibody. *Journal of the American Chemical Society* **2008**, *130*, 15242-15243.
- [89] Hoshino, Y.; Koide, H.; Urakami, T.; Kanazawa, H.; Kodama, T.; Oku, N.; Shea, K. J., Recognition, Neutralization, and Clearance of Target Peptides in the Bloodstream of Living Mice by Molecularly Imprinted Polymer Nanoparticles: A Plastic Antibody. *Journal of the American Chemical Society* **2010**, *132*, 6644-6645.
- [90] Yoshimatsu, K.; Lesel, B. K.; Yonamine, Y.; Beierle, J. M.; Hoshino, Y.; Shea, K. J., Temperature-Responsive "Catch and Release" of Proteins by using Multifunctional Polymer-Based Nanoparticles. *Angewandte Chemie-International Edition* **2012**, *51*, 2405-2408.
- [91] Gota, C.; Okabe, K.; Funatsu, T.; Harada, Y.; Uchiyama, S., Hydrophilic Fluorescent Nanogel Thermometer for Intracellular Thermometry. *Journal of the American Chemical Society* **2009**, *131*, 2766-2767.
- [92] Okabe, K.; Inada, N.; Gota, C.; Harada, Y.; Funatsu, T.; Uchiyama, S., Intracellular temperature mapping with a fluorescent polymeric thermometer and fluorescence lifetime imaging microscopy. *Nature Communications* **2012**, *3*, 705.
- [93] Peng, H. S.; Stolwijk, J. A.; Sun, L. N.; Wegener, J.; Wolfbeis, O. S., A Nanogel for Ratiometric Fluorescent Sensing of Intracellular pH Values. *Angewandte Chemie-International Edition* **2010**, *49*, 4246-4249.
- [94] Chen, C. Y.; Chen, C. T., A PNIPAM-based fluorescent nanothermometer with ratiometric readout. *Chemical Communications* **2011**, *47*, 994-996.
- [95] Nayak, S.; Lee, H.; Chmielewski, J.; Lyon, L. A., Folate-mediated cell targeting and cytotoxicity using thermoresponsive microgels. *Journal of the American Chemical Society* **2004**, *126*, 10258-10259.
- [96] Blackburn, W. H.; Dickerson, E. B.; Smith, M. H.; McDonald, J. F.; Lyon, L. A., Peptide-Functionalized Nanogels for Targeted siRNA Delivery. *Bioconjugate Chemistry* **2009**, *20*, 960-968.
- [97] Gan, D. J.; Lyon, L. A., Synthesis and protein adsorption resistance of PEG-modified poly(N-isopropylacrylamide) core/shell microgels. *Macromolecules* **2002**, *35*, 9634-9639.

- [98] Nayak, S.; Gan, D. J.; Serpe, M. J.; Lyon, L. A., Hollow thermoresponsive microgels. *Small* **2005**, *1*, 416-421.
- [99] Kleinen, J.; Klee, A.; Richtering, W., Influence of Architecture on the Interaction of Negatively Charged Multisensitive Poly(N-isopropylacrylamide)-co-Methacrylic Acid Microgels with Oppositely Charged Polyelectrolyte: Absorption vs Adsorption. *Langmuir* **2010**, *26*, 11258-11265.
- [100] Nayak, S.; Lyon, L. A., Ligand-functionalized core/shell microgels with permselective shells. *Angewandte Chemie-International Edition* **2004**, *43*, 6706-6709.
- [101] Lapeyre, V.; Ancla, C.; Catargi, B.; Ravaine, V., Glucose-responsive microgels with a core-shell structure. *Journal of Colloid and Interface Science* **2008**, *327*, 316-323.
- [102] Zhang, Y.; Guan, Y.; Zhou, S., Synthesis and volume phase transitions of glucose-sensitive microgels. *Biomacromolecules* **2006**, *7*, 3196-3201.
- [103] Lyon, L. A.; Fernandez-Nieves, A., The Polymer/Colloid Duality of Microgel Suspensions. *Annual Review of Physical Chemistry, Vol 63* **2012**, *63*, 25-43.
- [104] Debord, J. D.; Lyon, L. A., Thermoresponsive Photonic Crystals. *The Journal of Physical Chemistry B* **2000**, *104*, 6327-6331.
- [105] St John, A. N.; Lyon, L. A., Local control over phase transitions in microgel assemblies. *Journal of Physical Chemistry B* **2008**, *112*, 11258-11263.
- [106] Romeo, G.; Imperiali, L.; Kim, J. W.; Fernandez-Nieves, A.; Weitz, D. A., Origin of de-swelling and dynamics of dense ionic microgel suspensions. *Journal of Chemical Physics* **2012**, *136*.
- [107] Holmqvist, P.; Mohanty, P. S.; Nagele, G.; Schurtenberger, P.; Heinen, M., Structure and Dynamics of Loosely Cross-Linked Ionic Microgel Dispersions in the Fluid Regime. *Physical Review Letters* **2012**, *109*.
- [108] Iyer, A. S.; Lyon, L. A., Self-Healing Colloidal Crystals. *Angewandte Chemie-International Edition* **2009**, *48*, 4562-4566.
- [109] Weissman, J. M.; Sunkara, H. B.; Tse, A. S.; Asher, S. A., Thermally switchable periodicities and diffraction from mesoscopically ordered materials. *Science* **1996**, *274*, 959-960.
- [110] Holtz, J. H.; Holtz, J. S. W.; Munro, C. H.; Asher, S. A., Intelligent polymerized crystalline colloidal arrays: Novel chemical sensor materials. *Analytical Chemistry* **1998**, *70*, 780-791.

- [111] Lapeyre, V.; Gosse, I.; Chevreux, S.; Ravaine, V., Monodispersed glucose-responsive microgels operating at physiological salinity. *Biomacromolecules* **2006**, *7*, 3356-3363.
- [112] Wiedemair, J.; Serpe, M. J.; Kim, J.; Masson, J. F.; Lyon, L. A.; Mizaikoff, B.; Kranz, C., In-situ AFM studies of the phase-transition behavior of single thermoresponsive hydrogel particles. *Langmuir* **2007**, *23*, 130-137.
- [113] Burmistrova, A.; Steitz, R.; von Klitzing, R., Temperature Response of PNIPAM Derivatives at Planar Surfaces: Comparison between Polyelectrolyte Multilayers and Adsorbed Microgels. *ChemPhysChem* **2010**, *11*, 3571-3579.
- [114] Schmidt, S.; Motschmann, H.; Hellweg, T.; von Klitzing, R., Thermoresponsive surfaces by spin-coating of PNIPAM-co-PAA microgels: A combined AFM and ellipsometry study. *Polymer* **2008**, *49*, 749-756.
- [115] Kim, J.; Nayak, S.; Lyon, L. A., Bioresponsive hydrogel microlenses. *Journal of the American Chemical Society* **2005**, *127*, 9588-9592.
- [116] Sorrell, C. D.; Serpe, M. J., Glucose sensitive poly (N-isopropylacrylamide) microgel based etalons. *Analytical and Bioanalytical Chemistry* **2012**, *402*, 2385-2393.
- [117] Sorrell, C. D.; Carter, M. C. D.; Serpe, M. J., Color Tunable Poly (N-Isopropylacrylamide)-co-Acrylic Acid Microgel-Au Hybrid Assemblies. *Advanced Functional Materials* **2011**, *21*, 425-433.
- [118] Sorrell, C. D.; Lyon, L. A., Deformation controlled assembly of binary microgel thin films. *Langmuir* **2008**, *24*, 7216-7222.
- [119] Serpe, M. J.; Jones, C. D.; Lyon, L. A., Layer-by-layer deposition of thermoresponsive microgel thin films. *Langmuir* **2003**, *19*, 8759-8764.
- [120] Tsuji, S.; Kawaguchi, H., Colored thin films prepared from hydrogel microspheres. *Langmuir* **2005**, *21*, 8439-8442.
- [121] Serpe, M. J.; Lyon, L. A., Optical and acoustic studies of pH-dependent swelling in microgel thin films. *Chemistry of Materials* **2004**, *16*, 4373-4380.
- [122] Singh, N.; Bridges, A. W.; Garcia, A. J.; Lyon, L. A., Covalent tethering of functional microgel films onto poly(ethylene terephthalate) surfaces. *Biomacromolecules* **2007**, *8*, 3271-3275.

- [123] South, A. B.; Whitmire, R. E.; Garcia, A. J.; Lyon, L. A., Centrifugal Deposition of Microgels for the Rapid Assembly of Nonfouling Thin Films. *ACS Applied Materials & Interfaces* **2009**, *1*, 2747-2754.
- [124] Decher, G.; Hong, J. D.; Schmitt, J., Buildup of Ultrathin Multilayer Films by a Self-Assembly Process .3. Consecutively Alternating Adsorption of Anionic and Cationic Polyelectrolytes on Charged Surfaces. *Thin Solid Films* **1992**, *210*, 831-835.
- [125] Decher, G., Fuzzy nanoassemblies: Toward layered polymeric multicomposites. *Science* **1997**, *277*, 1232-1237.
- [126] Sorrell, C. D.; Lyon, L. A., Bimodal swelling responses in microgel thin films. *Journal of Physical Chemistry B* **2007**, *111*, 4060-4066.
- [127] Ngai, T.; Auweter, H.; Behrens, S. H., Environmental responsiveness of microgel particles and particle-stabilized emulsions. *Macromolecules* **2006**, *39*, 8171-8177.
- [128] Richtering, W., Responsive Emulsions Stabilized by Stimuli-Sensitive Microgels: Emulsions with Special Non-Pickering Properties. *Langmuir* **2012**, *28*, 17218-17229.
- [129] Liu, T. T.; Seiffert, S.; Thiele, J.; Abate, A. R.; Weitz, D. A.; Richtering, W., Non-coalescence of oppositely charged droplets in pH-sensitive emulsions. *Proceedings of the National Academy of Sciences of the United States of America* **2012**, *109*, 384-389.
- [130] Destribats, M.; Lapeyre, V.; Wolfs, M.; Sellier, E.; Leal-Calderon, F.; Ravaine, V.; Schmitt, V., Soft microgels as Pickering emulsion stabilisers: role of particle deformability. *Soft Matter* **2011**, *7*, 7689-7698.
- [131] Brugger, B.; Rosen, B. A.; Richtering, W., Microgels as Stimuli-Responsive Stabilizers for Emulsions. *Langmuir* **2008**, *24*, 12202-12208.
- [132] Geisel, K.; Isa, L.; Richtering, W., Unraveling the 3D Localization and Deformation of Responsive Microgels at Oil/Water Interfaces: A Step Forward in Understanding Soft Emulsion Stabilizers. *Langmuir* **2012**, *28*, 15770-15776.
- [133] Milani, A. H.; Freemont, A. J.; Hoyland, J. A.; Adlam, D. J.; Saunders, B. R., Injectable Doubly Cross-Linked Microgels for Improving the Mechanical Properties of Degenerated Intervertebral Discs. *Biomacromolecules* **2012**, *13*, 2793-2801.
- [134] Sivakumaran, D.; Maitland, D.; Hoare, T., Injectable Microgel-Hydrogel Composites for Prolonged Small-Molecule Drug Delivery. *Biomacromolecules* **2011**, *12*, 4112-4120.

- [135] Hoare, T.; Young, S.; Lawlor, M. W.; Kohane, D. S., Thermoresponsive nanogels for prolonged duration local anesthesia. *Acta Biomaterialia* **2012**, *8*, 3596-3605.
- [136] Wang, X.; Zhang, L. B.; Wang, L.; Sun, J. Q.; Shen, J. C., Layer-by-Layer Assembled Polyampholyte Microgel Films for Simultaneous Release of Anionic and Cationic Molecules. *Langmuir* **2010**, *26*, 8187-8194.
- [137] Wang, L.; Chen, D. D.; Sun, J. Q., Layer-by-Layer Deposition of Polymeric Microgel Films on Surgical Sutures for Loading and Release of Ibuprofen. *Langmuir* **2009**, *25*, 7990-7994.
- [138] Serpe, M. J.; Yarmey, K. A.; Nolan, C. M.; Lyon, L. A., Doxorubicin uptake and release from microgel thin films. *Biomacromolecules* **2005**, *6*, 408-413.
- [139] Nolan, C. M.; Gelbaum, L. T.; Lyon, L. A., H-1 NMR investigation of thermally triggered insulin release from poly(N-isopropylacrylamide) microgels. *Biomacromolecules* **2006**, *7*, 2918-2922.
- [140] Nolan, C. M.; Serpe, M. J.; Lyon, L. A., Thermally modulated insulin release from microgel thin films. *Biomacromolecules* **2004**, *5*, 1940-1946.

CHAPTER 2

HYDROLYTICALLY DEGRADABLE MICROGELS

Adapted from

Gaulding, J. C., South, A. B., Lyon, L. A. Hydrolytically Degradable Shells on Thermoresponsive Microgels. *Colloid and Polymer Science*. **2013**, 221, 99.

With kind permission from Springer Science and Business Media

2.1. Introduction

The burgeoning growth in macromolecular therapeutics has driven intensive research in the realm of delivery vehicles.^{1,2} Unlike most traditional small molecule drugs, protein and nucleotide-based therapeutics are not generally suitable for oral delivery – their relative chemical fragility and functional dependence on an often-delicate folded structure make them unable to tolerate the pH extremes and digestive enzymes encountered along that delivery route. Furthermore, their hydrophilicity typically limits gastrointestinal absorption.³ Immunological responses pose additional challenges to macromolecular therapeutics that reach the bloodstream, regardless of the delivery route. Consequently, a large body of research in drug delivery vehicles has been driven by the need to provide methods to protect payloads from degradation, as well as to provide additional advantages such as targeted delivery and regulation of release.^{1,2} Countless constructs have been described in the literature with these goals in mind, with their basis on a broad range of materials including liposomes,⁴ polymeric vesicles,⁵ and metal nanoparticles.⁶ Aqueous microgels – colloidal hydrophilic, cross-linked polymer networks – offer a number of properties that make them suitable as drug delivery vehicles. Several excellent reviews highlight the advantages microgels offer as a delivery platform,⁷⁻¹¹ some of which include: 1) a high water content that gives them a high

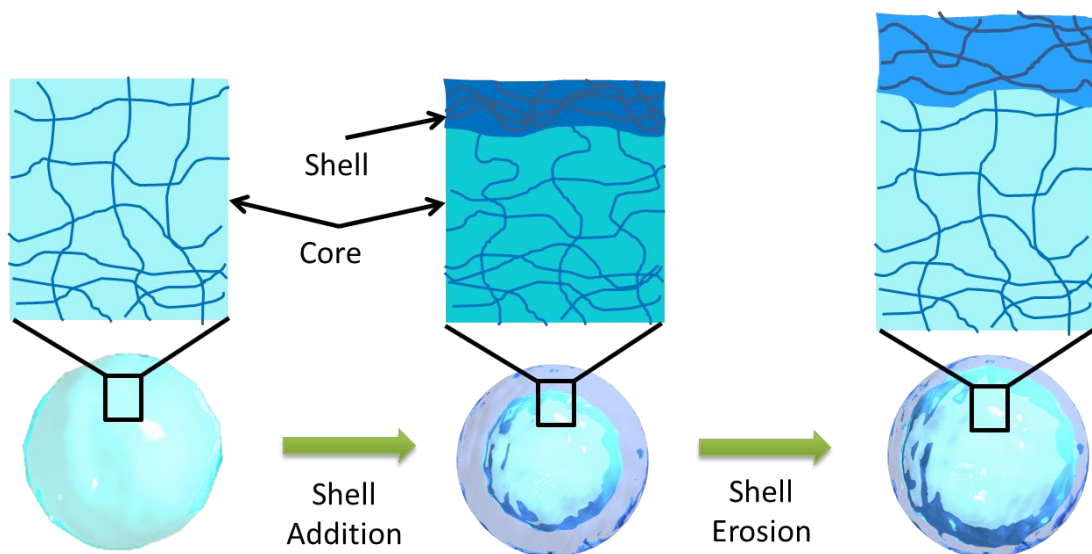
payload capacity, 2) tissue-like consistency that improves biological interfacing, 3) chemical flexibility to introduce a broad range of chemical functionalities, and 4) the potential for environmental responsiveness, such as swelling responses to triggers such as pH or temperature. Responsive microgels thus enable additional dimensions of control over the release properties of the microgel network.

Cross-link scission is one of the simplest ways to use a hydrogel network to regulate the release of an entrapped drug.¹² By incorporating labile cross-links that respond to stimuli such as light,¹³⁻¹⁵ reduction/oxidation,¹⁶⁻¹⁸ or the presence of certain enzymes,^{19,20} degradable hydrogel networks are formed, and network breakdown enables therapeutics trapped within to be released in response. A number of pH-responsive, degradable cross-links have also been described. Murthy et al. synthesized acetal-based cross-linkers that degrade under acidic conditions and thus showed strong pH-dependence on the release of protein loaded into hydrogels and microgels.^{21,22} Base-labile cross-linkers have also been described, such as those reported by Metz and Theato that are based on an activated ester moiety.²³ The cross-linker *N,O*-dimethacryloyl hydroxylamine (DMHA) occupies an intriguing niche for physiologically relevant degradation, as the cross-linker is stable under acidic conditions, yet degrades under neutral to basic conditions.²⁴ First synthesized by Ulbrich et al., hydrogels consisting of *N*-(2-hydroxypropyl) methacrylamide and DMHA were shown to erode at pH > 5, and consequently the release of both macromolecular and low molecular weight drugs was enhanced under eroding conditions.²⁴ Several groups have leveraged this characteristic of the molecule to generate physiologically-relevant, degradable particles.²⁵⁻²⁷

Achieving all of the desired attributes of a delivery vehicle – payload retention, targeted delivery, and release control – with a single material in a single phase is not always feasible. Methods to control the architecture of delivery vehicles, particularly in the form of core-shell particles, have been widely employed.²⁸⁻³⁰ Often this allows segregation of the roles of each material, such as a core that is optimized for payload

retention and therapeutic stability and a shell that is responsible for targeting and regulation of release. Sometimes this segregation arises naturally due to the properties of the vehicle (as in liposomes), but for materials such as microgels rational and intentional synthetic efforts are necessary to generate multiple particle domains. Our group pioneered the development of core-shell microgels via precipitation polymerization in 2000,³¹ and we have since demonstrated the utility of this architecture in generating microgels that are effective vehicles for targeted siRNA delivery.^{32,33} In that case, the role of the shell was to improve the efficiency of display of the targeting peptide, but other functionalities may enable the shell to play a dynamic role in such a vehicle. For example, erodible shells have been shown to serve as an effective means of regulating access to ligands localized within the microgel core.³⁴

In the work described in this chapter, we demonstrate the synthesis of thermo-responsive core-shell microgels featuring a hydrolytically degradable shell consisting of pNIPAm cross-linked with DMHA atop a non-degradable pNIPAm core. We and others have demonstrated that the interplay between core and shell in thermo-responsive microgels causes the shell to dominate the swelling properties of the entire particle.^{31,35,36} Consequently, these particles featuring a degradable shell may enable large changes in polymer density throughout both core and shell, as depicted in **Scheme 2.1**. Such a construct may be interesting for a variety of biological applications, wherein changes occurring under physiological conditions in the mechanical properties of the microgel shell may allow for *in situ* changes in release rate, display of functionalized cores, or even enhanced renal clearance.³⁷



Scheme 2.1. Shell addition leads to compression of the microgel core, as the added polymer mass and cross-linking prevents the core from re-swelling to its initial volume. Scission of cross-links in the shell enables extensive swelling of both microgel components, triggering major changes in the polymer density and mechanical flexibility of the overall core-shell microgel.

2.2. Experimental

2.2.1. Materials

All reagents were purchased from Sigma-Aldrich (St Louis, MO) and used as received, unless otherwise noted. The monomers NIPAm and NIPMAm were twice recrystallized from hexanes (VWR international, West Chester, PA) and dried in vacuo prior to use. Reagents hydroxylamine, methacryloyl chloride, pyridine, chloroform, hydrochloric acid, hexane, diethyl ether, BIS, SDS and AP) were all used as received. Water used in all reactions, particle purifications, and buffer preparations was purified to a resistance of 18 M Ω (Barnstead E-Pure system), and filtered through a 0.2 μm filter to remove particulate matter.

2.2.2. Synthesis of DMHA

DMHA synthesis was performed as described originally by Ulbrich et al.²⁴ and as performed previously within our group.^{38,39} In a typical synthesis, hydroxylamine hydrochloride (10 g, 0.14 mol) was added to a 3-neck round bottom flask, which was then sealed and purged with nitrogen for 45 min. The hydroxylamine was dissolved in pyridine (50 mL), then cooled in an ice bath. Methacryloyl chloride (24 mL, 0.24 mol) was added dropwise via syringe, while the ice bath was maintained to keep the reaction cool. After all methacryloyl chloride was added, the solution was allowed to return to room temperature while stirred for 2 hours. Conversion to DMHA was monitored via thin layer chromatography, using chloroform as a mobile phase and a UV-lamp to visualize the bands. Once converted, chloroform (100 mL) was added, and the solution cooled in an ice bath. Hydrochloric acid (12 N, 21 mL) was added dropwise while the ice bath was maintained. DMHA was isolated by 4 extractions from chloroform and DI water, keeping the organic phase each time. Magnesium sulfate was added to the cleaned solution to complete drying, then removed by filtration. The solution was evaporated to dryness, then the recovered oil was dissolved in cold diethyl ether and crystallized by the addition of hexane. The recovered solids yielded approximately 7.3 g of DMHA. The product was confirmed using a Varian Mercury Vx ¹H-NMR: (300MHz, CDCl₃): δ 2.02 [s, 3H, CH₂=C(CH₃)CO-NH-O-CO-C(CH₃)=CH₂] 2.05 [s, 3H, CH₂=C(CH₃)CO-NH-CO-C(CH₃)=CH₂] 5.52 [s, 1H, CH₂=C(CH₃)CO-NH-CO-C(CH₃)=CH₂] 5.79 [s, 1H, CH₂=C(CH₃)CO-NH-CO-C(CH₃)=CH₂] 5.87 [s, 1H, CH₂=C(CH₃)CO-NH-CO-C(CH₃)=CH₂] 6.35 [s, 1H, CH₂=C(CH₃)CO-NH-CO-C(CH₃)=CH₂] 9.20 [s, 1H, CH₂=C(CH₃)CO-NH-CO-C(CH₃)=CH₂]

2.2.3. Core Particle Synthesis

NIPAm (98 mol%) and BIS (2 mol%) were dissolved in deionized water, to a final total monomer concentration of 140 mM. The solution was filtered and SDS was

added to a concentration of 3 mM. The solution was heated to 75 °C and purged under nitrogen for 75 minutes. Polymerization was initiated by addition of an aqueous solution of 0.2 M APS (total final concentration = 3 mM). The solution was allowed to stir at 75 °C overnight, then cooled to room temperature and filtered through a #2 Whatman filter paper. Particles were purified via dialysis against deionized water prior to characterization.

2.2.4. Shell Syntheses

Shell addition was achieved via the “seed and feed” polymerization approach. NIPMAm (96 or 98 mol%) was dissolved in 43 mL of deionized water, to a final total monomer concentration of 60 mM. The monomer solution was filtered, and 5 mL of the solution of core particles was added. SDS was added to a concentration of 1 mM. The solution was heated to 75 °C and purged under nitrogen for one hour. A 1-mL solution of DMHA (60 mM or 120 mM for 2 or 4% cross-linking, respectively) in methanol was added, followed by initiation via addition of 1 mL of an aqueous solution of 26 mM APS (total concentration = 0.5 mM). The solution was allowed to stir at 75 °C for 4 hours, then was cooled to room temperature and filtered through a #2 Whatman filter paper. Particles were purified by several rounds of centrifugation and redispersal in pH 3 formate buffer.

2.2.5. Particle Characterization

The microgel hydrodynamic radii were characterized via dynamic light scattering (DLS) using a Dynapro DLS (Wyatt Technology, Santa Barbara, CA) equipped with a temperature-controlled sample chamber. Microgel sizes in **Figure 2.1** and **Table 2.2** were determined in pH 3.3 formate buffer. The microgel radii of gyration were characterized using asymmetrical flow field-flow fractionation coupled to multi-angle light scattering (A4F-MALS) using the Eclipse 1 Separation System (Wyatt) and DAWN-EOS (Wyatt) detector. For A4F analysis, the eluent was a 15 mM ionic strength pH 3.3 formate buffer

and particle separation was achieved using a constant cross-flow of 0.25 mL/min. The sizes reported are the average of three sample runs. Imaging of surface-adsorbed particles was conducted using an Asylum Research (Santa Barbara, CA) MFP-3D Atomic Force Microscope (AFM) in tapping mode using silicon Pointprobe cantilevers (NanoWorld, Neuchatel, Switzerland) with a force constant of 42 N/m. Dilute suspensions of microgels before and after degradation were incubated in pH 3.3 formate buffer above cleaned glass slides. The slides were then lightly rinsed with deionized water and imaged. The resultant images were analyzed using the MFP-3D software written in the IgorPro software environment (WaveMetrics, Inc. Lake Oswego, OR). Particle dimensions reported for each sample type are the average and standard deviation from line traces of five particles.

2.2.6. Microgel Erosion

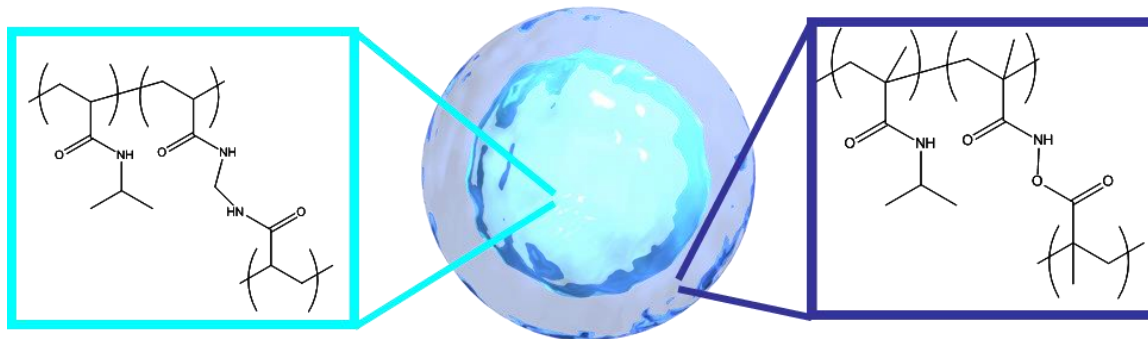
One mL of a 1.2 mg/mL solution of 2% DMHA shell particles or 1 mL of a 2.6 mg/mL solution of 4% DMHA shell particles was diluted into 4 mL of pH 7.4 HEPES buffer. The solutions were placed in a 37 °C oven with agitation and allowed to erode. The resultant particles were characterized after one month of degradation.

2.3. Results and Discussion

2.3.1. Particle Synthesis

Microgel core-shell particle synthesis has been reported by our group^{31,40} and others.^{35,41} Though one might naively anticipate shell addition to lead to a definitive increase in particle size (r_n), the interplay between the core and shell components is more complex. Because shell addition is conducted well above the LCST of pNIPAm, the core particles are collapsed and largely deswollen during shell deposition. Consequently, shell addition and the associated cross-linking at the core/shell interface can restrict the ability of the core to fully re-swell upon cooling, leading to an effect known as core-compression, which complicates the analysis of core-shell particle architecture.⁴² The use

of two different thermo-responsive polymers allows the swelling responses of the two phases to be analyzed somewhat independently by manipulating the temperature.



Scheme 2.2. Structure of core-shell microgels with pNIPAm-BIS cores and pNIPMAm-DMHA shells.

Table 2.1. Synthesis of Core-Shell Microgels with Hydrolytically Degradable Shells

Sample	Core Volume (mL)	Total volume (mL)	Total monomer conc. (mM)	Monomer Mass (g), mol%	Cross-linker Mass (g), mol%	SDS (g), conc. (mM)	APS (g), conc. (mM)
Core	--	100	140	NIPAm: 1.55, 98%	BIS: 0.044, 2%	0.086, 3	0.069, 3
DMHA2 (Shell)	5	50	60	NIPMAm: 0.374, 98%	DMHA: 0.010, 2%	0.015, 1	0.006, 0.5
DMHA4 (Shell)	5	50	60	NIPMAm: 0.368, 96%	DMHA: 0.020, 4%	0.014, 1	0.006, 0.5

For these constructs, we chose to utilize the thermo-responsive polymers, pNIPAm (LCST of ~32 °C) and pNIPMAm (LCST of ~ 43 °C), in order to provide a method of confirming shell addition. A schematic depiction of the core-shell particles is shown in **Scheme 2.2**, and the details of the synthetic conditions are given in **Table 2.1**. Particles featuring pNIPAm cores and pNIPMAm shells have previously been synthesized by Berndt, Richtering, and co-workers^{35,43,44} and for thin, lightly cross-linked

shells the characteristic volume-phase transitions for both polymers are typically observed. Thus, the addition of a pNIPAm-co-DMHA shell can be confirmed by observing the particle size as a function of temperature; the presence of the pNIPAm shell will increase the particle size relative to the core particles above pNIPAm's LCST, with a second phase transition occurring at approximately 43 °C. As shown in **Figure 2.1**, shell addition is confirmed via the presence of characteristic pNIPAm swelling behavior for both DMHA2 and DMHA4.

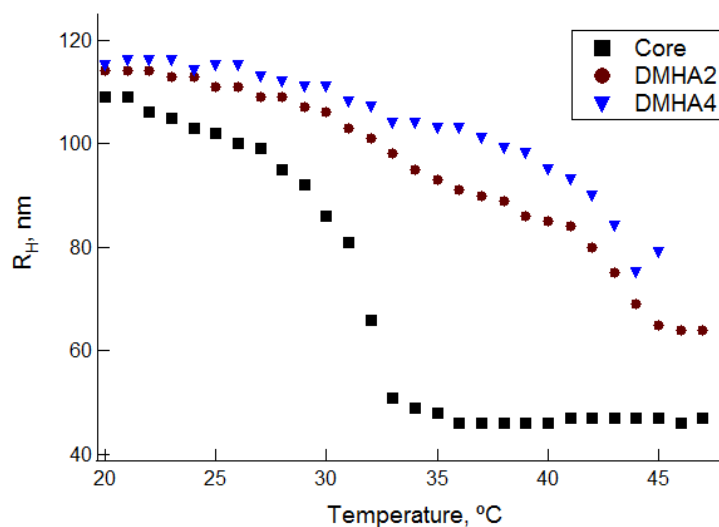


Figure 2.1. Mean hydrodynamic radius as a function of temperature for pNIPAm core particles and pNIPAm/pNIPMAM-DMHA core-shell particles. Shell addition is confirmed by the increased particle size at temperatures > 32 °C, indicative of the addition of pNIPMAM.

Shell addition leads to two competing factors that affect the particle r_{rms} (the particle radius weighted about the center of mass). Addition of polymer during shell synthesis increases the overall mass of the particles, and the surface-localization of this added mass thus increases the apparent r_{rms} . However, the addition of polymer and dense cross-linking at the core/shell interface restricts the ability of the core to re-swell. As a result, the density of the core component becomes greater after shell addition. Since the overall mass of the core is the same, but it occupies a smaller volume due to the

compressive force from the shell, the r_{rms} of the core decreases. The two factors combine to make the net change in r_{rms} associated with shell addition small. As shown in **Figure 2.2**, the addition of the 2% DMHA shell permits sufficient swelling of the core such that shell addition results in an overall r_{rms} increase of approximately 2.5 nm. In the case of the 4% DMHA shell, the two factors seemingly cancel, as the particle size distribution appears to match that of the core. Higher cross-linking, in the 4% DMHA case, despite the addition of a thicker shell, apparently leads to greater influence from the core-compression component leading to no net change in r_{rms} .

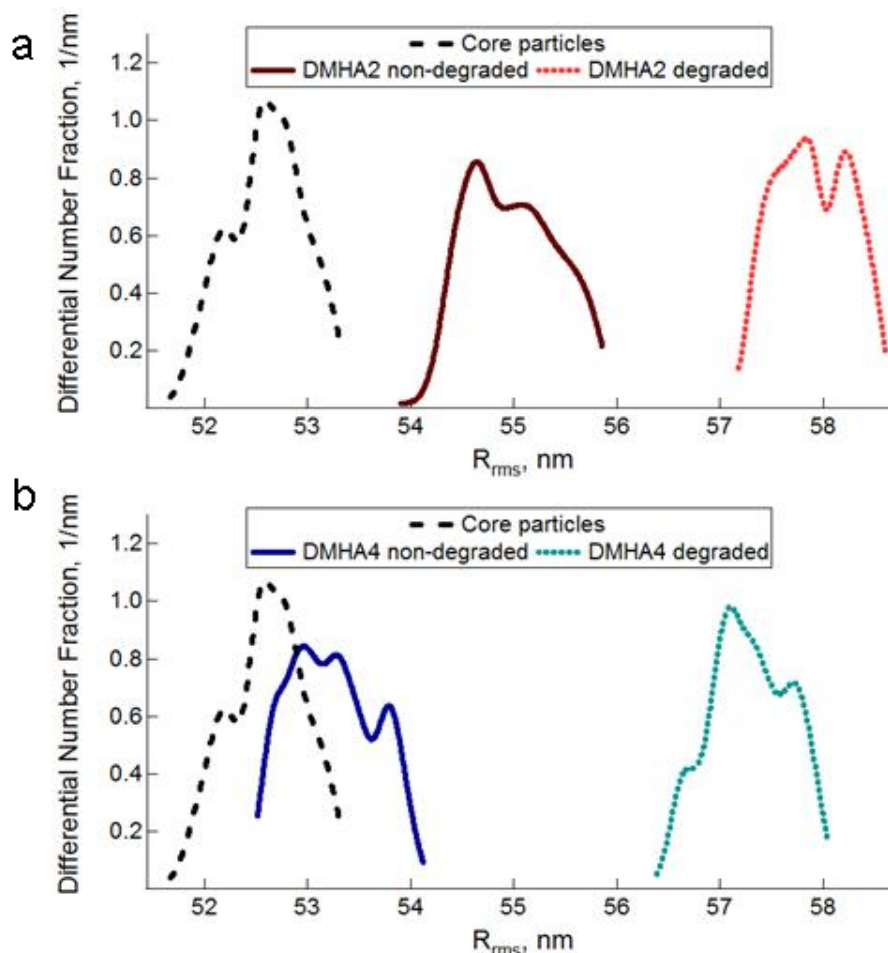


Figure 2.2. Distribution analysis from A4F-MALS for (a) DMHA2 and (b) DMHA4 pNIPMAm shell particles. Shell addition leads to an increase in the r_{rms} of the core-shell particles relative to the cores. Erosion of the shells leads to a further increase in r_{rms} due to the reduction in shell connectivity and concomitant core swelling.

Direct observation of the core-shell particles using AFM reveals several changes that accompany shell addition. The added polymer mass leads to stiffer particles, as evidenced by the particle height traces shown in **Figure 2.3**. The pNIPAm-BIS core particles spread thinly on the surface, having a diameter of 266 ± 30 nm, with accompanying particle heights of 7 ± 1 nm. However, deposition of DMHA2 & DMHA4 microgels onto a glass surface reveals a much stiffer particle. The diameter of the core-shell particles is approximately the same (259 ± 9 nm and 273 ± 18 nm for DMHA2 & DMHA4, respectively) however the particle heights are now 4-5 times taller (32 ± 5 nm for DMHA2 and 30 ± 3 nm for DMHA4). The added mass of the shell and compression of the core lead to an increase in overall particle density, contributing to a decrease in particle spreading on the surface. Additionally, the added connectivity and rigidity of the shell likely also makes the core-shell particles less deformable than the bare cores contributing to their greater height on the surface.

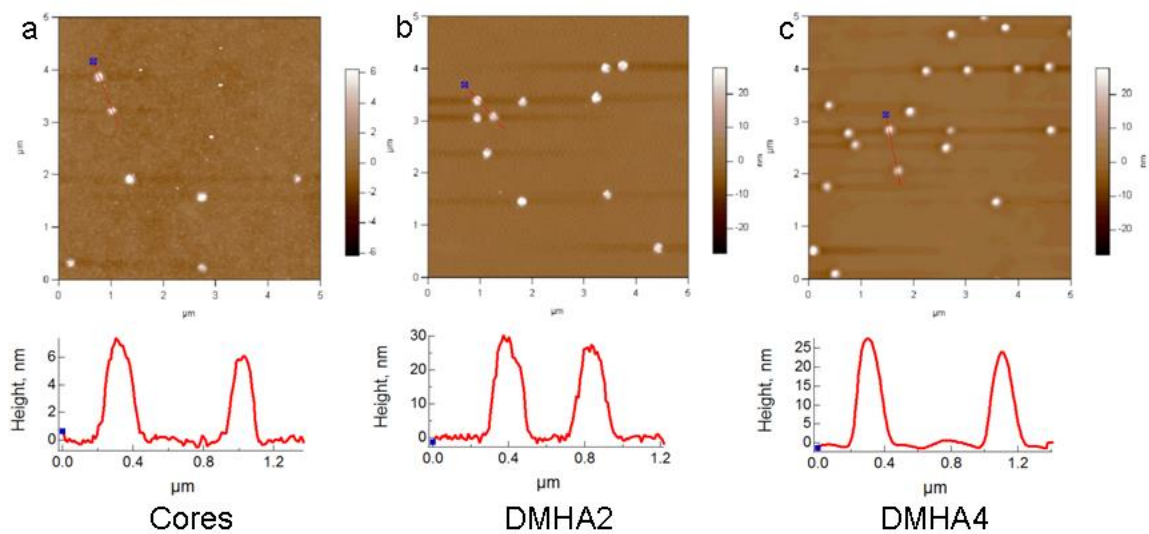


Figure 2.3. AFM images and height traces of (a) Core particles, (b) DMHA2 core-shell particles, and (c) DMHA4 core-shell particles. Shell addition leads to an increase in particle stiffness, as evidenced by the increase in peak height observed in the line traces. Scan sizes in each image are $5 \mu\text{m} \times 5 \mu\text{m}$.

As indicated previously, the two different thermo-responsive polymers in the core and shell enable characterization of the two phases separately. A simple approximation of the system would lead us to three different temperature regimes: 1) core and shell swollen; 2) core collapsed, shell swollen; 3) core and shell collapsed. While it is clear that condition 3 would occur at temperatures above the LCST of both polymers, the transition between swollen and collapsed core is not as simply defined as the LCST of pNIPAm. Mechanical coupling of the core and shell leads to the shell dominating the swelling behavior of the entire particle.^{31,35,36} Thus, a pNIPAm core may continue to be swollen above 32 °C because of its linkage to the still-swollen pNIPMAM shell. As with core compression restricting the ability of the core to re-swell, this core expansion due to shell swelling is not easily discriminated via light scattering. The behavior of the core-shell particles at temperatures between the two phase transitions is therefore difficult to predict. We can, however, estimate shell thickness based on a few factors. The shell thickness is readily determinable above the phase transition of both polymers, giving us collapsed shell thicknesses of 17 nm for DMHA2 and 28 nm for DMHA4. Similarly, the maximum shell thickness can be estimated by subtracting the collapsed core size from that of the swollen particles, giving us upper limits of 67 nm and 68 nm, respectively. By considering the particle dimensions at intermediate temperatures, we can estimate the size of the swollen shell by making the following approximations.

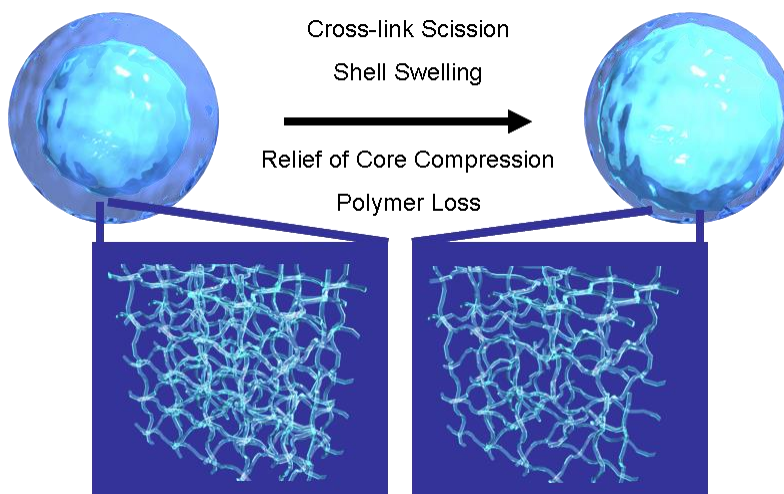
$$R_{H,shell,T<43^{\circ}C} = R_{H,core-shell,T=40^{\circ}C} - R_{H,core,T=40^{\circ}C} \quad (2.1)$$

$$R_{H,core,T<32^{\circ}C} = R_{H,core-shell,T=20^{\circ}C} - R_{H,shell} \quad (2.2)$$

This assumes that at 40 °C, the influence of core expansion by the shells has been minimized, while the pNIPMAM shell has yet to experience significant collapse. Applying this methodology to the DMHA core-shell particles, we determine shell thicknesses of 39 nm for DMHA2 and 48 nm for DMHA4.

2.3.2. Shell Erosion

Hydrolytic degradation of DMHA within the shells is expected to lead to several changes in the structure and composition of the microgels, summarized here and in **Scheme 2.3**: 1) cross-link scission in the shell should result in swelling of the shell; 2) the remnant charged residues following DMHA hydrolysis will promote counterion ingress and thus also increase shell swelling; 3) cross-link scission should relieve core-compression, enabling the core to more closely approach its initial dimensions; and 4) polymer loss from the degraded shell will decrease the shell mass. These factors are interrelated, and their relative contributions to the swelling behavior are difficult to discern. However, by comparing particle characteristics before and after erosion with a variety of analytical tools, we can gain some insight into the degraded particles as a whole.



Scheme 2.3. Scission of DMHA cross-links in the shell leads to changes in the swelling and connectivity of both the core and shell phases of the microgel.

Particle erosion was conducted at pH 7.4 and 37 °C. Our previous studies with DMHA indicated that observable changes in particle swelling and molar mass occur within a few hours under these conditions³⁹ but that complete particle erosion takes several weeks.³⁸ Characterization of the eroded core-shell particles after one month

reveals several differences between the microgels before and after erosion. As shown in **Table 2.2**, the changes in particle swelling as determined via DLS are small following cross-link scission. However, the r_h will be most sensitive to changes occurring at the particle periphery (i.e. the eroded shell). The counteracting contributions of shell polymer loss and shell swelling due to counterion ingress combine to make the apparent changes in r_h small over the course of the erosion. DLS is thus not well-suited for observing changes in network connectivity, as swelling of the core is masked by the shell effects. Significant polymer loss and softening of the remnant shell may lead to only small changes observable by DLS. For example, conversion of the pNIPAm-DMHA cross-linked shell to a remnant brush-like pNIPAm network may be expected to retain a similar r_h , while the mechanical influence the shell exerts on the core particle is weakened. The changes in polymer density accompanying such a change would reduce the scattering intensity of the particles. In this case, equivalent volumes of particles before and after degradation have their scattering intensity reduced by ~40%, suggestive of a major reduction in polymer density due to cross-link scission. Other analytical tools, such as MALS and AFM, provide a better understanding of the behavior of the pNIPAm core, where the expected changes accompanying erosion (relief of core compression) are more limited than the changes induced to the network by DMHA hydrolysis itself.

Table 2.2. Light Scattering Characterization of Core-Shell Particles

Batch	r_{rms}	r_h (20 °C) ^a	r_h (40 °C) ^a	$r_{h, Core}$ (20 °C) ^b	$r_{h, Shell}$ (20 °C) ^b
Core	52.5 ± 0.2	108	50	108	--
DMHA2 – non-degraded	55.1 ± 0.5	116	80	86	30
DMHA4 – non-degraded	53.4 ± 0.2	116	93	73	44
DMHA2 – degraded	57.9 ± 0.4	121	81	90	31
DMHA4 – degraded	57.4 ± 0.3	126	96	79	47

^a reported in pH 3.3 formate buffer, 15 mM ionic strength. ^b calculated from Equations 2.1 & 2.2

MALS is a useful tool for observing changes in mass distribution within the particles, and when coupled to A4F any oligomeric strands resulting from erosion can be separated from the microgels, eliminating their impact upon the scattering signal. Characterization of the particles before and after erosion via A4F-MALS enables changes in particle topology to be observed. For shells containing both 2% and 4% DMHA, the r_{rms} of particles shifts towards larger values following erosion, as seen in **Figure 2.2**. This shift, resulting from cross-link scission, may have contributions from the swelling of the shell, coupled with a relaxation of the core-compression. The DMHA content of the shell seems to scale with the magnitude of the change, as the 2% DMHA particles experience an increase of approximately 2.8 nm, while the 4% DMHA particles increase in radius by 4.0 nm. This is likely due to both the more significant degree of core compression in the 4% case and the greater apparent shell thickness, rendering a greater impact on the total particle size upon swelling. Comparison of the plots in **Figure 2.2** also indicates that the r_{rms} of the two batches of particles converge upon cross-link scission, which may suggest that the core is able to achieve a similar degree of swelling after erosion in the two cases.

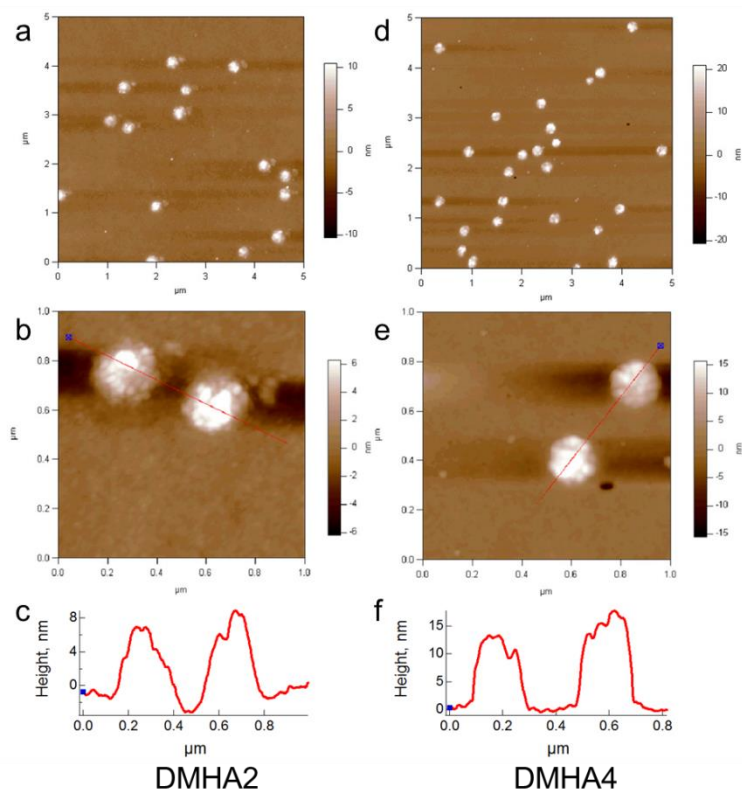


Figure 2.4. AFM images and height traces of DMHA2 (a-c) and DMHA4 (d-f) following one month of erosion in pH 7.4 buffer at 37 °C. Compared to particles before erosion, there is a reduction in particle height and additional particle spreading. Scan sizes in (a, d) are 5 μm x 5 μm . Scan sizes in (b, e) are 1 μm x 1 μm .

Direct observation of the eroded particles via AFM also enables characterization of core/shell connectivity, while permitting analysis of individual particles. Comparison of **Figure 2.3** with **Figure 2.4** reveals that the degraded core-shell particles of DMHA2 exhibit greater spreading on the surface (diameter of 353 ± 28 nm) as well as a reduction in particle height (12 ± 1 nm, 20 nm height decrease). DMHA4, in contrast, appears to undergo minimal changes in particle spreading (286 ± 18 nm) and the height reduction is less pronounced (22 ± 2 nm, 8 nm height decrease). These heights, when compared to **Figure 2.3a**, do not resemble those of the bare core particles. Thus we attribute the differences between the parent core particles and the degraded core-shell as being indicative of remnant polymer from the shell left behind following degradation. The loss

of cross-linking in the shell associated with DMHA scission would reduce the connectivity and thus rigidity of the shell, enabling the remnant shell to spread on the surface and likely contributing to the larger apparent diameters of DMHA2 on the surface. The relative resiliency of DMHA4 suggests that the thicker shell either has not eroded to the same extent as DMHA2, or that the polymer lost from the remnant shell was sufficient to reduce the apparent footprint of the particle. The additional cross-link density present in DMHA4 would tend to decrease the average polymer chain length between cross-links; the average chain length of soluble polymer liberated from the shells would be correspondingly shorter. Thus, we would anticipate that any remnant pNIPAm brushes grafted onto the pNIPAm core particles would be shorter than in the DMHA2 case.

Taken together, it is clear that localizing DMHA into the shell of thermo-responsive core-shell microgels leads to a dynamic particle wherein both chemical and physical changes occur *in situ* under physiologically-relevant conditions. The erosion of the shell of the particles leads to microgels that become mechanically softer and more porous over time. Altering the extent of cross-linking and concentration of DMHA in the shell may provide a mechanism to tune the duration and extent of these changes, and in turn the release of macromolecular payloads from the core.

2.4. Conclusions and Outlook

In the work described in this chapter, we have demonstrated the synthesis of pNIPAm core particles bearing pNIPAm shells cross-linked by the hydrolytically degradable cross-linker, DMHA. A suite of analytical tools including DLS, MALS, and AFM were used to characterize the resultant microgels. Shell addition is directly observable by analysis of particle sizes above the phase transition of pNIPAm, and suggested by changes in particle density observed by MALS and AFM. Additional polymer and cross-linking from the shell synthesis conducted above the LCST of

pNIPAm leads to compression of the pNIPAm core upon cooling, which greatly increases the density of the overall particle. Upon cross-link scission, the microgel shell undergoes a reduction in density due to polymer loss and shell swelling, and a reduction in rigidity due to losses in network connectivity. As a result, the r_h of the microgels undergoes only slight increases, suggestive of remnant low-density polymer on the surface. Increases in the r_{rms} of the microgels following scission indicate that the loss of cross-linking at the core/shell interface allows relief of core compression imposed by the pNIPAm shell. Direct observation of eroded particles deposited on glass via AFM confirms the loss of connectivity, evidenced by spreading and a reduction in particle height. Overall, these core-shell microgels provide a demonstration of particles that undergo temporal chemical and mechanical changes under physiologically-relevant conditions, which may be enabling for the rational design of drug delivery vehicles. The capability of therapeutic carriers to undergo *in situ* changes with regard to several factors of interest, including drug release rate, recognition or localization, and clearance, may allow even more sophisticated control in the next generation of healthcare.

2.5. References

- [1] Couvreur, P.; Vauthier, C., Nanotechnology: Intelligent design to treat complex disease. *Pharmaceutical Research* **2006**, *23*, 1417-1450.
- [2] Peer, D.; Karp, J. M.; Hong, S.; Farokhzad, O. C.; Margalit, R.; Langer, R., Nanocarriers as an emerging platform for cancer therapy. *Nature Nanotechnology* **2007**, *2*, 751-760.
- [3] Goldberg, M.; Gomez-Orellana, I., Challenges for the oral delivery of macromolecules. *Nature Reviews Drug Discovery* **2003**, *2*, 289-295.
- [4] Torchilin, V. P., Recent advances with liposomes as pharmaceutical carriers. *Nature Reviews Drug Discovery* **2005**, *4*, 145-160.
- [5] Yoon, H. J.; Jang, W. D., Polymeric supramolecular systems for drug delivery. *Journal of Materials Chemistry* **2010**, *20*, 211-222.

- [6] Ghosh, P.; Han, G.; De, M.; Kim, C. K.; Rotello, V. M., Gold nanoparticles in delivery applications. *Advanced Drug Delivery Reviews* **2008**, *60*, 1307-1315.
- [7] Nayak, S.; Lyon, L. A., Soft nanotechnology with soft nanoparticles. *Angewandte Chemie-International Edition* **2005**, *44*, 7686-7708.
- [8] Oh, J. K.; Drumright, R.; Siegwart, D. J.; Matyjaszewski, K., The development of microgels/nanogels for drug delivery applications. *Progress in Polymer Science* **2008**, *33*, 448-477.
- [9] Kabanov, A. V.; Vinogradov, S. V., Nanogels as Pharmaceutical Carriers: Finite Networks of Infinite Capabilities. *Angewandte Chemie-International Edition* **2009**, *48*, 5418-5429.
- [10] Raemdonck, K.; Demeester, J.; De Smedt, S., Advanced nanogel engineering for drug delivery. *Soft Matter* **2009**, *5*, 707-715.
- [11] Bysell, H.; Mansson, R.; Hansson, P.; Malmsten, M., Microgels and microcapsules in peptide and protein drug delivery. *Advanced Drug Delivery Reviews* **2011**, *63*, 1172-1185.
- [12] Park, K.; Shalaby, W. S. W.; Park, H. *Biodegradable hydrogels for drug delivery*; Technomic Pub.: Lancaster, PA, 1993.
- [13] Klinger, D.; Landfester, K., Photo-sensitive PMMA microgels: light-triggered swelling and degradation. *Soft Matter* **2011**, *7*, 1426-1440.
- [14] Klinger, D.; Landfester, K., Polymeric Photoresist Nanoparticles: Light-Induced Degradation of Hydrophobic Polymers in Aqueous Dispersion. *Macromolecular Rapid Communications* **2011**, *32*, 1979-1985.
- [15] Klinger, D.; Landfester, K., Dual Stimuli-Responsive Poly(2-hydroxyethyl methacrylate-co-methacrylic acid) Microgels Based on Photo-Cleavable Cross-Linkers: pH-Dependent Swelling and Light-Induced Degradation. *Macromolecules* **2011**, *44*, 9758-9772.
- [16] Nayak, S.; Gan, D. J.; Serpe, M. J.; Lyon, L. A., Hollow thermoresponsive microgels. *Small* **2005**, *1*, 416-421.
- [17] Smith, M. H.; Herman, E. S.; Lyon, L. A., Network Deconstruction Reveals Network Structure in Responsive Microgels. *Journal of Physical Chemistry B* **2011**, *115*, 3761-3764.
- [18] Gauding, J. C.; Smith, M. H.; Hyatt, J. S.; Fernandez-Nieves, A.; Lyon, L. A., Reversible Inter- and Intra-Microgel Cross-Linking Using Disulfides. *Macromolecules* **2012**, *45*, 39-45.

- [19] Shantha, K. L.; Ravichandran, P.; Rao, K. P., Azo Polymeric Hydrogels for Colon Targeted Drug-Delivery. *Biomaterials* **1995**, *16*, 1313-1318.
- [20] Ulbrich, K.; Strohalm, J.; Kopecek, J., Polymers Containing Enzymatically Degradable Bonds. VI. Hydrophilic Gels Cleavable by Chymotrypsin. *Biomaterials* **1982**, *3*, 150-154.
- [21] Murthy, N.; Thng, Y. X.; Schuck, S.; Xu, M. C.; Frechet, J. M. J., A novel strategy for encapsulation and release of proteins: Hydrogels and microgels with acid-labile acetal cross-linkers. *Journal of the American Chemical Society* **2002**, *124*, 12398-12399.
- [22] Murthy, N.; Xu, M. C.; Schuck, S.; Kunisawa, J.; Shastri, N.; Frechet, J. M. J., A macromolecular delivery vehicle for protein-based vaccines: Acid-degradable protein-loaded microgels. *Proceedings of the National Academy of Sciences of the United States of America* **2003**, *100*, 4995-5000.
- [23] Metz, N.; Theato, P., Synthesis and Characterization of Base Labile Poly(N-isopropylacrylamide) Networks Utilizing a Reactive Cross-Linker. *Macromolecules* **2009**, *42*, 37-39.
- [24] Ulbrich, K.; Subr, V.; Seymour, L. W.; Duncan, R., Novel Biodegradable Hydrogels Prepared Using the Divinyllic Crosslinking Agent N,O-Dimethacryloylhydroxylamine. 1. Synthesis and Characterization of Rates of Gel Degradation, and Rate of Release of Model-Drugs, In vitro and In vivo. *Journal of Controlled Release* **1993**, *24*, 181-190.
- [25] Horak, D.; Chaykivskyy, O., Poly(2-hydroxyethyl methacrylate-co-N,O-dimethacryloylhydroxylamine) particles by dispersion polymerization. *Journal of Polymer Science Part A-Polymer Chemistry* **2002**, *40*, 1625-1632.
- [26] Yin, W. S.; Akala, E. O.; Taylor, R. E., Design of naltrexone-loaded hydrolyzable crosslinked nanoparticles. *International Journal of Pharmaceutics* **2002**, *244*, 9-19.
- [27] Pradny, M.; Michalek, J.; Lesny, P.; Hejcl, A.; Vacik, J.; Slouf, M.; Sykova, E., Macroporous hydrogels based on 2-hydroxyethyl methacrylate. Part 5: Hydrolytically degradable materials. *Journal of Materials Science-Materials in Medicine* **2006**, *17*, 1357-1364.
- [28] Caruso, F., Nanoengineering of particle surfaces. *Advanced Materials* **2001**, *13*, 11-22.
- [29] Scharl, W., Current directions in core-shell nanoparticle design. *Nanoscale* **2010**, *2*, 829-843.

- [30] Cayre, O. J.; Chagneux, N.; Biggs, S., Stimulus responsive core-shell nanoparticles: synthesis and applications of polymer based aqueous systems. *Soft Matter* **2011**, *7*, 2211-2234.
- [31] Jones, C. D.; Lyon, L. A., Synthesis and characterization of multiresponsive core-shell microgels. *Macromolecules* **2000**, *33*, 8301-8306.
- [32] Blackburn, W. H.; Dickerson, E. B.; Smith, M. H.; McDonald, J. F.; Lyon, L. A., Peptide-Functionalized Nanogels for Targeted siRNA Delivery. *Bioconjugate Chemistry* **2009**, *20*, 960-968.
- [33] Smith, M. H.; Lyon, L. A., Multifunctional Nanogels for siRNA Delivery. *Accounts of Chemical Research* **2012**, *45*, 985-993.
- [34] Nayak, S.; Lyon, L. A., Ligand-functionalized core/shell microgels with permselective shells. *Angewandte Chemie-International Edition* **2004**, *43*, 6706-6709.
- [35] Berndt, I.; Richtering, W., Doubly temperature sensitive core-shell microgels. *Macromolecules* **2003**, *36*, 8780-8785.
- [36] Gan, D. J.; Lyon, L. A., Tunable swelling kinetics in core-shell hydrogel nanoparticles. *Journal of the American Chemical Society* **2001**, *123*, 7511-7517.
- [37] Hendrickson, G. R.; Lyon, L. A., Microgel Translocation through Pores under Confinement. *Angewandte Chemie-International Edition* **2010**, *49*, 2193-2197.
- [38] Smith, M. H.; South, A. B.; Gauding, J. C.; Lyon, L. A., Monitoring the Erosion of Hydrolytically-Degradable Nanogels via Multiangle Light Scattering Coupled to Asymmetrical Flow Field-Flow Fractionation. *Analytical Chemistry* **2010**, *82*, 523-530.
- [39] South, A. B.; Lyon, L. A., Direct Observation of Microgel Erosion via in-Liquid Atomic Force Microscopy. *Chemistry of Materials* **2010**, *22*, 3300-3306.
- [40] Blackburn, W. H.; Lyon, L. A., Size-controlled synthesis of monodisperse core/shell nanogels. *Colloid and Polymer Science* **2008**, *286*, 563-569.
- [41] Lapeyre, V.; Ancla, C.; Catargi, B.; Ravaine, V., Glucose-responsive microgels with a core-shell structure. *Journal of Colloid and Interface Science* **2008**, *327*, 316-323.
- [42] Jones, C. D.; Lyon, L. A., Shell-restricted swelling and core compression in poly(N-isopropylacrylamide) core-shell microgels. *Macromolecules* **2003**, *36*, 1988-1993.

- [43] Berndt, I.; Pedersen, J. S.; Lindner, P.; Richtering, W., Influence of shell thickness and cross-link density on the structure of temperature-sensitive - Poly-N-isopropylacrylamide-poly-N-isopropylmethacrylamide core-shell microgels investigated by small-angle neutron scattering. *Langmuir* **2006**, *22*, 459-468.
- [44] Berndt, I.; Popescu, C.; Wortmann, F. J.; Richtering, W., Mechanics versus thermodynamics: Swelling in multiple-temperature-sensitive core-shell microgels. *Angewandte Chemie-International Edition* **2006**, *45*, 1081-1085.

CHAPTER 3

INCORPORATION OF DISULFIDES INTO THERMO-RESPONSIVE MICROGELS

Adapted from

Gaulding, J. C., Smith, M. H., Hyatt, J. S., Fernandez-Nieves, A., Lyon, L. A. Reversible Inter-and Intra-Microgel Cross-linking Using Disulfides. *Macromolecules* **2012**, *45*, 39.

Copyright 2012 American Chemical Society

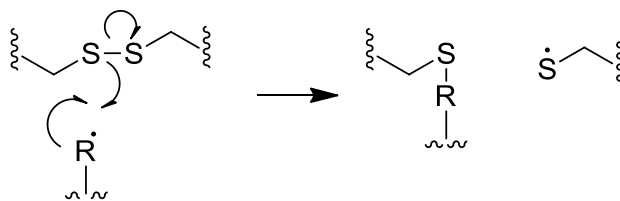
3.1. Introduction

Within the realm of biomaterials, disulfide bonds are of great interest due to their characteristic degradation in response to physiologically relevant reducing conditions.^{1,2} Polymeric drug delivery vehicles incorporating disulfide bonds as essential components of vehicular integrity are expected to undergo selective erosion upon entering the intracellular space, providing a means to trigger the delivery of payloads and improve physiologic clearance. Several groups, using a variety of architectures, have exploited this strategy.²⁻⁶ For example, Matyjaszewski et al. have used inverse mini-emulsion atom transfer polymerization to produce nanogels capable of triggered erosion for the delivery of small molecules to cancer cells.⁴ Armes and co-workers have included disulfide cross-linking in block copolymer micelles as a method to regulate the release of a payload in the micelle's interior.⁵ These examples represent only a small portion of the efforts in this domain.

Our group has worked extensively on the development of drug carriers based on poly(alkylacrylamide) nano- and micro-particles (nanogels or microgels).⁷⁻¹² However, one limiting characteristic of these vehicles is their non-degradable nature, as the polymer

is not erodible and the network is typically cross-linked covalently with non-cleavable units. Thus, the use of cross-linkers containing disulfide bonds was envisioned as a potentially useful approach, where disulfide incorporation would enable erosion of drug carrier in a triggered fashion, while also offering introduction of thiol functionalities within microgels for bioconjugation and controlled assembly. Bulk hydrogels that incorporate the reversible disulfide cross-linker *N,N'*-bis(acryloyl)cystamine (BAC) have been described in the literature,¹³⁻¹⁶ but there are few examples of microgels incorporating this functionality,^{4,17-19} and none of these syntheses utilize the aqueous precipitation polymerization method.

Precipitation polymerization has been repeatedly demonstrated to be a useful and versatile means of generating monodisperse micro- and nano-particles, and is enabling in the synthesis of particles with core/shell topologies.^{7,20,21} A notable drawback is that the method utilizes high temperatures (typically >70 °C) to promote the thermal decomposition of a radical source, such as APS. Incorporating a disulfide bond during microgel synthesis by such a process is challenging, as there are numerous side reactions that disrupt the sulfur-sulfur bond. The disulfide bond may be homolytically cleaved at high temperatures, resulting in sulfur radical formation during the synthesis.²² Additionally, the disulfide bond may enable a chain-transfer reaction, wherein radical attack at the disulfide leads to the formation of a thioether, with a second sulfur radical released as a result, as illustrated in **Scheme 3.1**.²² Finally, any conversion of the disulfide to thiols during synthesis would promote a Michael addition between the thiol and the vinyl groups of the monomers, again generating a thioether.²³⁻²⁶ Thioether formation during synthesis is still an enabling mechanism for particle formation, however the cross-links formed are no longer susceptible to reduction/cleavage.



Scheme 3.1. Potential side reaction involving radical attack on the disulfide bond during particle synthesis, which leads to non-degradable thioether formation.

For bulk hydrogel synthesis, the accelerant *N,N,N',N'*-tetramethylethylenediamine (TEMED) is commonly used to enable room temperature syntheses. When paired with APS, TEMED acts as a reducing agent, generating much higher levels of sulfate radical in solution than are achieved by thermal dissociation at the same temperature. Recently, we have shown that the use of the APS/TEMED pair is suitable for conducting microgel synthesis using microfluidic devices at lower temperatures,²⁷ and when utilized in conjunction with precipitation polymerization allows *in situ* encapsulation of proteins and the control of parasitic chain transfer reactions.²⁸ To attempt to mitigate the effects of the possible side reactions, we focused on the generation of thermo-responsive microgels containing disulfide cross-links by producing the particles at temperatures only slightly above the LCST of the thermo-responsive polymer. In this work, we demonstrate the synthesis of thermo-responsive microgels cross-linked with the commercially available disulfide cross-linker BAC, utilizing aqueous precipitation polymerization with a redox initiation pair. These particles are shown to erode in response to reducing conditions, in contrast to comparable particles synthesized using the traditional thermally-induced initiation approach. The improved control over disulfide incorporation was used in combination with the non-degradable cross-linker BIS to generate thiol-bearing microgels. These particles are shown to be suitable for iodoacetamide conjugation, and the reversible nature of the disulfide bond is exploited to form and disperse doubly cross-linked bulk gel networks of microgels, illustrating the potential utility of such particles in both bioconjugation and gel assembly.

3.2. Experimental

3.2.1. Materials

All common materials were sourced and used as described in **Chapter 2**. Additionally, reagents *N,N'*-bis(acryloyl)cystamine (BAC), *N,N,N',N'*-tetramethylethylenediamine (TEMED), dithiothreitol (DTT), cysteine, sodium periodate, fluorescein iodoacetamide, methanol, and dimethylsulfoxide (DMSO) were all used as received.

3.2.2. Microgel Synthesis

3.2.2.1. BAC Cross-linked Particle Synthesis - Redox

NIPMAm was dissolved in deionized water, to a final total monomer concentration of 140 mM. The solution was filtered, then SDS was added to a concentration of 6 mM. The solution was heated to 50 °C and purged under nitrogen for one hour. A solution of 10% (by volume) TEMED in water was added, bringing the TEMED concentration to 2 mM. Polymerization was initiated ten minutes later by addition of an aqueous solution of 0.5 M APS (total concentration = 5 mM – an excess relative to TEMED to minimize interaction with BAC), followed immediately by a 172 mM solution of BAC in methanol to achieve a final molar ratio of 5 mol% cross-linker. The solution was allowed to stir at 50 °C for six hours, then cooled to room temperature and filtered through a #2 Whatman filter paper. (CHNS: Calculated for NIPMAm/BAC/APS 61.53 C, 9.52 H, 10.54 N, 4.04 S. Found 55.19 C, 9.41 H, 9.78 N, 5.01 S)

3.2.2.2. BAC Cross-linked Particle Synthesis – Thermal

NIPMAm was dissolved in deionized water, to a final total monomer concentration of 140 mM. The solution was filtered, then SDS was added to a

concentration of 6 mM. The solution was heated to 80 °C and purged under nitrogen for one hour. Polymerization was initiated by addition of an aqueous solution of 0.1 M APS (total concentration 2 mM), followed immediately by a 172 mM solution of BAC in methanol to achieve a final molar ratio of 5 mol% cross-linker. The solution was allowed to stir at 80 °C overnight, then cooled to room temperature and filtered. (CHNS: Calculated for NIPMAm/BAC/APS 63.08 C, 9.76 H, 10.81 N, 3.07 S. Found 57.20 C, 9.80 H, 9.89 N, 3.04 S).

3.2.2.3. Co-Cross-linked Particle Synthesis

NIPMAm and BIS (2 mol%) were dissolved in deionized water, to a final total monomer concentration of 140 mM. The solution was filtered, then SDS was added to a concentration of 1 mM. The solution was heated to 50 °C and purged under nitrogen for one hour. A solution of 10% (by volume) TEMED in water was added, bringing the TEMED concentration to 2 mM. Polymerization was initiated ten minutes later by addition of an aqueous solution of 0.5 M APS (total concentration 5 mM), followed immediately by a 235 mM solution of BAC in methanol to achieve a final molar ratio of 5 mol% BAC. The solution was allowed to stir at 50 °C overnight, then cooled to room temperature and filtered through a 1.2- μ m Acrodisc filter. (CHNS: Calculated for NIPMAm/BAC/BIS/APS 61.29 C, 9.44 H, 10.70 N, 4.02 S. Found 55.95 C, 9.70 H, 9.98 N, 3.45 S).

3.2.3. Particle Characterization

The microgels were size analyzed via DLS and by A4F-MALS using the instrumentation described in **Chapter 2**. To characterize their degradation, samples with an identical particle concentration were prepared in pH 8.6 HEPES buffer. To one solution, an excess of DTT was added and allowed to incubate for 90 minutes. The two samples were analyzed using A4F-MALS using an identical procedure. The eluent was a

10 mM ionic strength (7 mM NaNO₃ + 3 mM NaN₃) aqueous buffer, and particle separation was achieved using a variable crossflow method wherein the initial crossflow rate of 1.0 mL/min was reduced over a period of 30 minutes to 0.1 mL/min. This same protocol was used to distinguish the thermally initiated particles. Particle radii (r_{rms}) values are reported as the average of three separations.

Elemental (CHNS) analysis was performed in duplicate on purified and lyophilized particles by Atlantic Microlabs, Norcross GA.

3.2.4. Fluorescent Labeling

Two (2) mL of a 4.5 mg/mL stock solution of co-cross-linked particles were suspended into two centrifuge tubes. The particles were pelleted by centrifugation at 18,000 x g for 10 min. The supernatant was removed from each tube and 1.5 mL of a 10 mM solution of DTT in pH 8.6 HEPES buffer was added to each. After four hours of reduction, the particles (now presenting reactive thiols) were purified by sequential centrifugation and the supernatant replaced with pH 7.4 HEPES buffer. Each time the particles were pelleted at 18,000 x g for 25 min, and the process was repeated five times. 200 μ L of cleaned particle stock was added to 1.1 mg of fluorescein iodoacetamide, along with 1.0 mL of pH 7.4 HEPES buffer + 200 μ L of DMSO. The microgels were allowed to react at room temperature in the dark overnight. The labeled particles were purified by sequential centrifugation and the supernatant replaced with pH 7.4 HEPES buffer. The particles were stored in the dark while redispersing, and the process was repeated ten times until the fluorescence signal from the supernatant was indistinguishable from that of buffer. Fluorescence was measured using a steady-state fluorescence spectrophotometer (Photon Technology International), equipped with a Model 814 PMT photon-counting detector. Samples were prepared by diluting labeled particles into pH 7.4 HEPES buffer. The excitation wavelength used was 494 nm, and emission spectra were collected from 500-600 nm. Unlabeled particles were diluted to a similar

concentration and spectra were collected under the same conditions. Additionally, co-cross-linked particles that were not exposed to DTT were also reacted with fluorescein iodoacetamide under the same conditions, similarly purified and spectra collected under the same conditions.

3.2.5. *In Situ* Erosion

The erosion of pNIPMAM-BAC nanogels was monitored in situ, using a previously reported light scattering method.²⁹ Using Multiangle Light Scattering (MALS) detection, the particle weight-average molar mass (M_w) was monitored in real-time during the erosion reaction. Reactants were introduced to the MALS detector using the Calypso syringe pump system (Wyatt Technology Corporation, Santa Barbara, CA). The Calypso hardware consists of a computer-controlled triplet syringe pump and a multichannel degasser, equipped with in-line filters, mixers and valves to allow rapid and automated batch measurements. MALS was performed using the DAWN-EOS (Wyatt Technology Corporation, Santa Barbara, CA) equipped with a temperature-regulated K5 flow cell with a GaAs laser light source ($\lambda = 685$ nm). Data collection and subsequent analysis was performed using the Astra software Version 5.3.4.14 (Wyatt Technology Corporation, Santa Barbara, CA). Differential refractive index (dRI) analysis was performed via composition-gradient static light scattering using the Calypso syringe pump and the OptilabrEX systems, equipped with an LED light source ($\lambda = 690$ nm).

In a typical erosion reaction, nanogels were prepared via dilution to a concentration of 3.5×10^{-2} mg/mL in 0.1 μm -filtered pH 7.0 phosphate buffer (ionic strength = 20 mM). To initiate erosion, the BAC nanogel solution and 20 mM DTT or 40 mM cysteine (prepared in the same buffer) were co-administered to the MALS flow cell via the Calypso syringe pump system. Final concentrations of particles and reducing agent were 1.74×10^{-2} mg/mL and 10 mM DTT and 20 mM cysteine, thus yielding 20 mM reactive thiolate in both cases. The particle M_w was monitored at stopped flow using

the Astra software with a determined dn/dc value of 0.158 for BAC nanogels. The dn/dc was measured in triplicate using the Calypso syringe pump system coupled with dRI detection using a five-step calibration curve for BAC particles (1.75×10^{-1} mg/mL – 3.50×10^{-2} mg/mL) suspended in filtered pH 7.0 phosphate buffer ($I = 20$ mM).

3.2.6. Reversible Gelation

Two large centrifuge tubes were filled with eight (8) mL of a 4.5 mg/mL stock solution of particles cross-linked with both BIS and BAC. The particles were purified by sequential centrifugation at $15,500 \times g$ for 25 min followed by re-dispersion in pH 7.4 HEPES buffer. After cleaning, the supernatant was replaced with 8 mL of 10 mM DTT in pH 8.6 HEPES buffer. The particles were allowed to erode with light agitation overnight. The now thiol-bearing particles were again purified using sequential centrifugation at $15,500 \times g$ for 60 min, replacing the supernatant with additional 10 mM DTT. After cleaning, the supernatant was replaced with 7 mL of 12 mM NaIO_4 in pH 7.4 HEPES. After addition, the solution was centrifuged at $15,500 \times g$ for 60 min. The resulting pellet was a solid gel, which was scraped from the bottom of the centrifuge tube and provided for rheology measurements.

The reversible nature of the double-network was demonstrated by equilibrating a large piece of the oxidized network in pH 8.6 HEPES buffer. The piece was then split into two approximately equal sized pieces and each piece placed into their own well plate. To one was added 5 mL of a solution of 22 mM DTT in pH 8.6 HEPES, while the other received only an equivalent volume of buffer. The two were allowed to shake for 24 hours until complete dissolution of the reduced network in the DTT-containing solution occurred.

3.2.7. Rheology

Oscillatory rheology was carried out using a stress-controlled rheometer (Anton-Parr Physica MCR 501) with cone-plate geometry and a roughened cone with 25 mm diameter and 2° aperture. Before measurement, the instrument was calibrated to account for different sources of instrument error: motor and air bearing noise due to imperfections in motor operation, air bearing surface, turbulence in the air bearing and the effect of the tool's inertia on stress-strain measurements without sample. All measurements were taken above the instrument's minimum torque of 0.1 μNm . Though the rheometer is stress-controlled, strain-controlled measurements can be made because of a feedback loop: stress is applied and the resulting strain is measured, and the loop enables the rheometer to adjust the applied stress to keep strain at the desired value. The time to complete the loop is on the order of milliseconds, so the accessible frequency range has an upper limit of about 100 rad/s. About 0.2 mL of the double network sample was compressed beneath the cone and plate at room temperature. A linearity test was performed at 10 rad/s between 0.1% and 1% strain; for strains below $\sim 0.3\%$, the system can be safely assumed in the linear regime, as shown in **Figure 3.7a**. The frequency measurements were done at constant strain of 0.1% and frequencies on a logarithmic scale decreasing from 100 to 0.01 rad/s with 6 points per decade.

3.3. Results & Discussion

3.3.1. Particle Synthesis and Characterization

In order to minimize interaction between TEMED and BAC, two modifications to conventional precipitation polymerization were necessary: an excess of APS relative to TEMED was utilized, and the BAC was added immediately following initiation by APS. Particle formation was confirmed by DLS, and was successful under the two synthetic protocols described, with the differences limited to the reaction temperature and hence

the method of radical generation from APS. Elemental analysis confirms sulfur incorporation for both the thermally and redox-initiated particles with BAC and APS being the two potential sources of sulfur in the monomer feed. For the redox-initiated particles, the reported sulfur values are slightly higher than expected from the feed composition. This may arise from the bi-functional reactivity of the cross-linker, which likely contributes to faster incorporation into the microgels, along with the high sulfate radical yield that is typical for redox initiation. In contrast, the thermally-initiated particles were in close agreement with their theoretical composition. This also likely represents efficient incorporation of BAC, with perhaps a lower overall degree of sulfate incorporation.

To more directly probe the cross-link density of the particles, DLS was used to determine the swelling ratio for the particles by determining the hydrodynamic radius above and below pNIPMAm's LCST. The work by Senff and Richtering, Varga et al., and Duracher et al. focused on systematically studying the effect of cross-linking density on the swelling ratio and particle topology (the ratio r_{rms}/r_h) of thermo-responsive microgels.³⁰⁻³² The data from the Varga study, which included swelling values in the regime seen for the disulfide cross-linked particles, was used to estimate the BAC particles' cross-link density. Though this data utilized pNIPAm microgels instead of the pNIPMAm used in this case, a similar study from Duracher et al.³² shows good agreement in the overlap region with the Varga data. The method of least-squares regression was used to determine a model that best fit the swelling data. An exponential function provided the best fit with a correlation coefficient of 0.9874:

$$y = 2.5752 \cdot \exp(-0.0683 \cdot x)$$

The model for estimating cross-linking, the source data, and the estimated cross-linking points are shown in **Figure 3.1**.

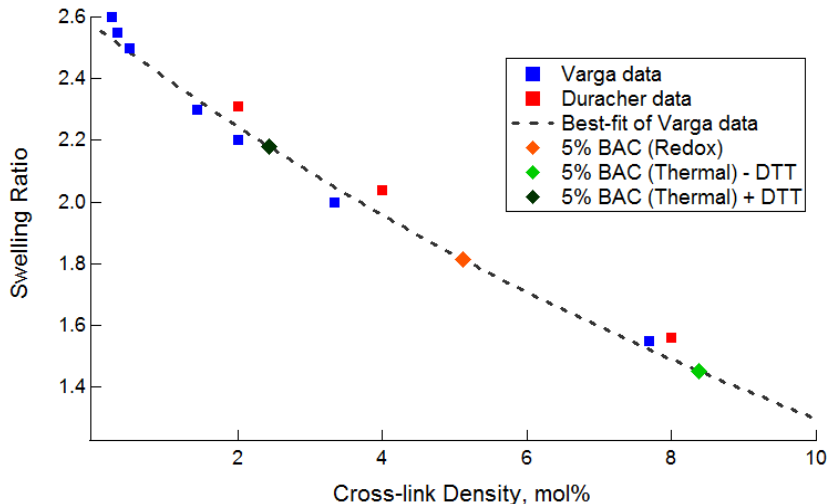


Figure 3.1. Data and best fit model used to estimate cross-link density for disulfide cross-linked microgels. The Duracher data³² shows reasonable agreement for pNIPMAm as well.

For the redox-initiated particles, the determined swelling ratio of 1.82 when mapped onto the Varga cross-link model yields an estimated cross-link density of 5.1%, in good agreement with the monomer feed composition. In contrast, the thermally-initiated particles exhibited a higher apparent cross-linking (swelling ratio = 1.45), corresponding to an estimated cross-link density of 8.4%. The higher apparent cross-linking may be a result of chain-transfer located at the disulfide bond, Michael addition, or any of the other potential cross-link forming side reactions described above.

3.3.1.1. Particle Erosion

Successful incorporation of BAC within the microgel network should lead to particles that undergo cross-link scission via disulfide reduction. Generally, a reduction in the amount of cross-linking in a particle would cause an increase in particle swelling as the network becomes more flexible. In the extreme case wherein all cross-linking points within the particle are labile, complete dissolution of the microgel should follow reduction. A comparison of the chromatograms shown in **Figure 3.2** highlights the

impact the initiation method has on particle erosion following cross-link cleavage. When the thermally-initiated particles were exposed to the reductant DTT, a small increase in the A4F retention time and a reduction in the intensity of the scattering signal were observed (**Figure 3.2a**). The increased retention time in the variable cross-flow separation is indicative of decrease in the particle diffusion coefficient, which we propose occurs due to cross-link scission and the concomitant increase in particle swelling and r_h . The accompanying reduction in scattering intensity is further indicative of particle swelling and thus a reduction in refractive index. The increase in particle r_h suggests a decrease in nanogel density as a result of cross-link scission. Offline analysis of the particles before and after erosion by DLS confirmed the expected changes accompanying cross-link scission, as shown in **Table 3.1**. Nanogel erosion resulted in an increase in the swelling ratio from 1.45 to 2.18, which correlates to a remnant cross-link density of 2.4%. A large increase in r_{rms} from 33 nm to 43 nm also resulted from scission, which was further indicative of network expansion. Interestingly, the particle mass distribution remained consistent throughout erosion reaction for thermally-initiated nanogels. The mass distribution may be inferred through the ratio of the r_{rms} (weighted-size by the mass distribution about the center of mass) and the r_h (determined from the diffusion coefficient of the particle). Monitoring changes in mass distribution following erosion is a useful way to characterize the distribution of the labile bonds within the nanogel architecture. For example, changes in mass distribution following erosion would indicate that the labile cross-links were preferentially located in a particular region of the particles. The value of r_{rms}/r_h for the thermally initiated particles (~0.56) is indicative of a radially heterogeneous segment density, with the periphery having a lower density of polymer. This value is frequently observed for nanogels prepared by precipitation polymerization, where dissimilar reactivity between the monomers results in greater polymer segment density towards the interior of spheres.³⁰ Although erosion caused a shift in the size and molar mass of the particles, there was no measureable change in

r_{rms}/r_h . This result suggests that cross-link scission from BAC featuring intact disulfide bonds occurred evenly throughout the structure. As such, the heterogeneous segment density suggests the non-labile and labile cross-link distributions are similar. However, additional work may be necessary to verify this hypothesis.

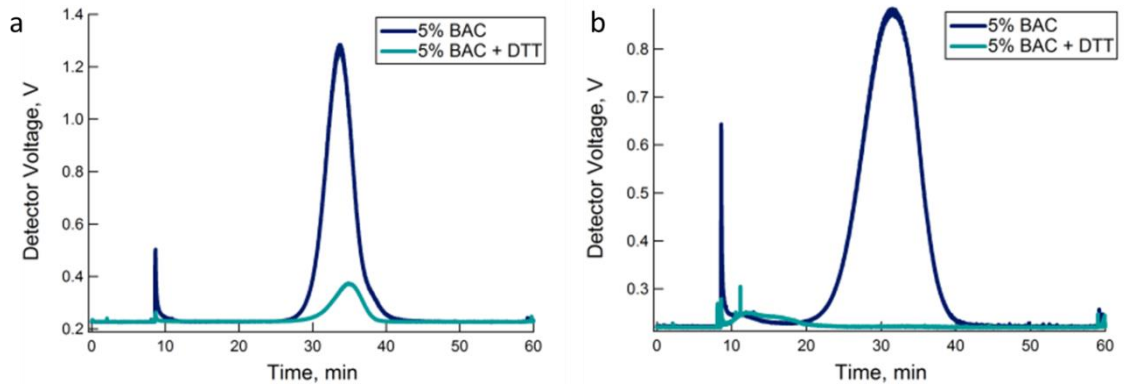


Figure 3.2. A4F-MALS separation of pNIPMAm-BAC (5%) microgels formed by the (a) thermal and (b) redox initiation methods. Incubating the particles with DTT increased retention of the thermally-initiated particles, yet led to degradation of the redox-initiated particles.

Table 3.1. Size, swelling, and topology characterization for BAC-cross-linked microgels.

	r_h , nm (20°C) ^a	r_h , nm (45°C) ^a	Swelling Ratio ^b	r_{rms} , nm ^a	r_{rms}/r_h (20°C)	Est. cross-link density ^c
5% BAC (T)	60	41	1.45	32.9 ± 0.1	0.55	8.38%
5% BAC (T) + DTT	73	34	2.18	42.4 ± 1.8	0.58	2.43%
5% BAC (R)	48	26	1.82	36.9 ± 0.6	0.78	5.12%

^aSizes reported in pH 8.6 HEPES buffer. ^bcalculated as $r_h(20\text{ °C})/r_h(45\text{ °C})$. ^ccalculated from swelling ratio using Varga model³¹

In contrast to thermally initiated nanogels, the redox-initiated particles showed complete dissolution after exposure to DTT; as evidenced by the disappearance of the peak associated with the nanogel and the emergence of a peak at very short retention times with diminished scattering signal. The loss of particle retention via A4F is indicative of a drastic decrease in the polymer diffusion coefficient, whereas the loss of

scattering signal is indicative of a significant reduction in particle density, suggesting potential mass loss from the polymer. Together, those data suggest complete dissolution of the nanogel into low molar mass, oligomeric products (**Figure 3.2b**). The differential response seen in the A4F results for the two types of particles is indicative of the difference in network structure between the two. The failure of thermally-initiated particles to completely erode into oligomeric chains reveals the presence of non-erodible residual cross-links in the structure, likely thioethers resulting from side reactions. In the redox-initiated case these parasitic reactions are limited, leading to a particle whose network integrity is completely controlled by disulfide cross-links.

3.3.2. *In Situ* Erosion

In the presence of a strong reducing agent, such as DTT, the nanogels synthesized at lower temperatures via redox initiation completely dissolved into low molar mass components. Thus, we hypothesized that those networks would be similarly sensitive to the presence of cysteine and other thiols in their environment, resulting in thiol-disulfide exchange reactions that would disrupt connectivity in the nanogel network. The timescale of erosion for thiol competition under physiologically relevant reducing conditions, such as those found in the cytoplasm, is of interest in drug delivery applications. Nanogel erosion was monitored in situ via MALS detection, using a similar method as reported previously.²⁹ Through this approach, changes in the apparent M_w of nanogels were monitored in real-time, enabling a direct comparison of erosion kinetics for particles in response to DTT and cysteine (**Figure 3.3**).

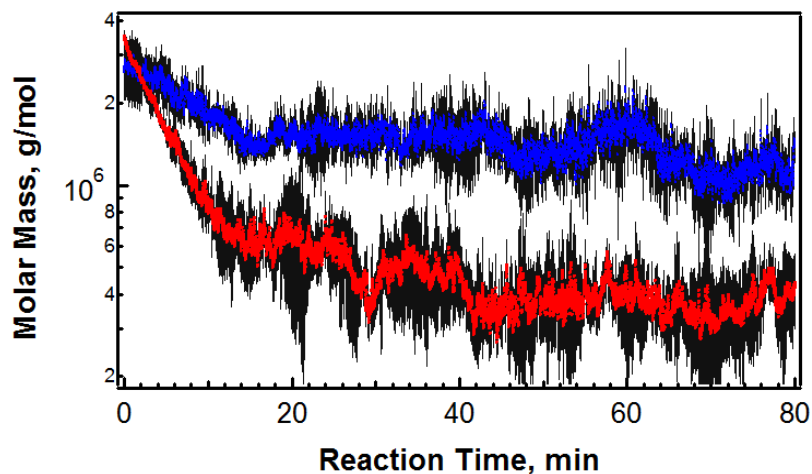


Figure 3.3. Nanogel erosion via cross-link scission occurs in presence of DTT (red) or cysteine (blue), monitored in situ via MALS. Error bars (black) represent one standard deviation about the mean of measurements.

In the presence of DTT, the M_w of nanogels decays by an order of magnitude, eventually reaching equilibrium after ~40 minutes of the reaction (**Figure 3.3.**) This indicates that swelling is accompanied by mass loss and that both effects give rise to the decrease in light scattering intensity observed via A4F analysis (**Figure 3.2.**) Erosion also proceeds in the presence of cysteine, but at a much slower rate. The higher reaction rate for DTT may result from differences in the erosion products. Following exchange DTT is released from the thiol by a cyclization reaction, reverting to an internal oxidized disulfide bond and leaving behind a pair of thiols on the microgel. In contrast, cysteine likely disrupts the BAC by participating in a single thiol-disulfide exchange reaction; the resulting product is therefore a mixed-disulfide. This leads to the possibility of reverse reactions and continued thiol-exchange reactions that are not productive towards cross-link scission.

3.3.3. Reactive Thiol Incorporation

The disulfide content imparted by BAC may enable the conjugation of thiolated molecules within the nanogel network by thiol-disulfide exchange reactions, as shown in

Figure 3.3 for cysteine. However, BAC may also be reduced to yield reactive thiols within nanogel networks, which prepares those networks for a variety of other bioconjugation chemistries. For example, reactive thiols within nanogels are of great utility due to their selective reactivity with maleimides, iodoacetamides, and other thiols under mild, aqueous conditions.³³ Yet as depicted in our results, complete reduction of BAC within the colloid results in particle decomposition. We therefore synthesized co-cross-linked particles containing both BAC and a non-degradable cross-linker, BIS. The resultant nanogels underwent a significant size increase in response to the reductant DTT, from an r_h of 183 nm to 232 nm at 20 °C and a pH of 8.6, accompanied by a large decrease in turbidity due to a decrease in the cross-link density in the network, as shown in **Figure 3.4**. The reduced form of the co-cross-linked particles presented free thiols available for conjugation with an iodoacetamide derivative of fluorescein, yielding fluorescent particles. In contrast, particles containing BAC in the oxidized form showed significantly reduced fluorescence (**Figure 3.5**).



Figure 3.4. a) Images of vials containing pNIPMAM-BAC-BIS microgel dispersions (left) before and (right) after exposure to DTT.

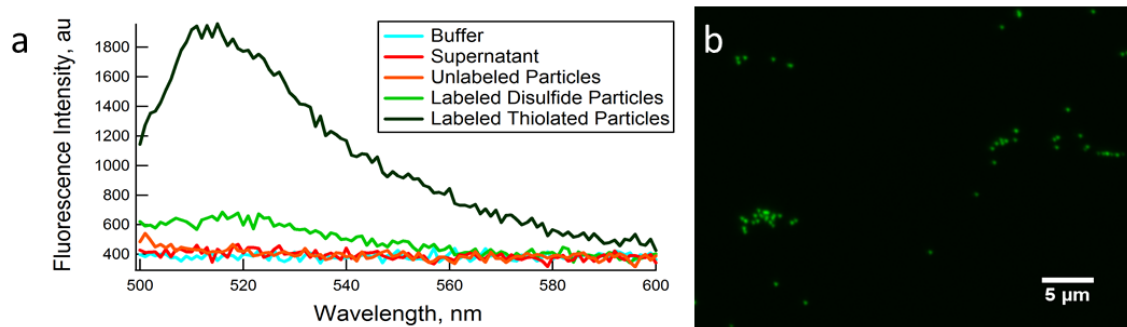


Figure 3.5. a) Fluorescence spectra ($\lambda_{\text{ex}} = 494 \text{ nm}$) of (dark green) fluorescein-labeled pNIPMAm-BAC-Bis particles, (orange) unlabeled particles, (blue) pH 7.4 HEPES buffer, and (red) the supernatant following purification by centrifugation. Particles that were not reduced and therefore retained their disulfide linkages (light green) had much lower coupling efficiency than that of the reduced particles. b) Fluorescence microscopy image (blue excitation) of pNIPMAm-BAC-BIS particles labeled with fluorescein iodoacetamide.

3.3.4. Reversible Gelation

The reversible nature of the disulfide reduction enables cross-link formation between thiols resulting from BAC reduction. Placing the thiolated particles together at high concentration, such as by centrifugation, enabled the thiols to react under oxidizing conditions and form a double network “gel of microgels”, wherein the individual microgels retain their identity through incorporation of the non-degradable BIS cross-linker, yet are tethered to one another by the resulting inter-particle disulfide linkages. Centrifugation of the co-cross-linked particles resulted in a dense pellet (**Figure 3.6-left**), whereas nanogels reacted with DTT, due to their decreased density, required a two-to-three fold increase in centrifugation time at the same relative centrifugal force to form a sediment. The resulting pellet of the reduced particles was less turbid in comparison to non-degraded particles (**Figure 3.6-center**). Despite those differences, both degraded and non-degraded nanogels were fluid in their highly concentrated, sedimented form, with water-like viscosity rendering them readily capable of being drawn up via pipette for the suspended drop images shown in **Figure 3.6**. Exposure of the thiol-bearing particles to

the oxidant sodium periodate during centrifugation dramatically increased the viscosity of the particle dispersion as a result of interparticle cross-linking. The volume and turbidity of the pellet was similar to the disulfide particles prior to reduction, indicative of the cross-link re-formation (**Figure 3.6-right**). However, the pellet did not flow when inverted, indicating the formation of a viscoelastic solid capable of being handled with tweezers, as shown in **Figure 3.6**.

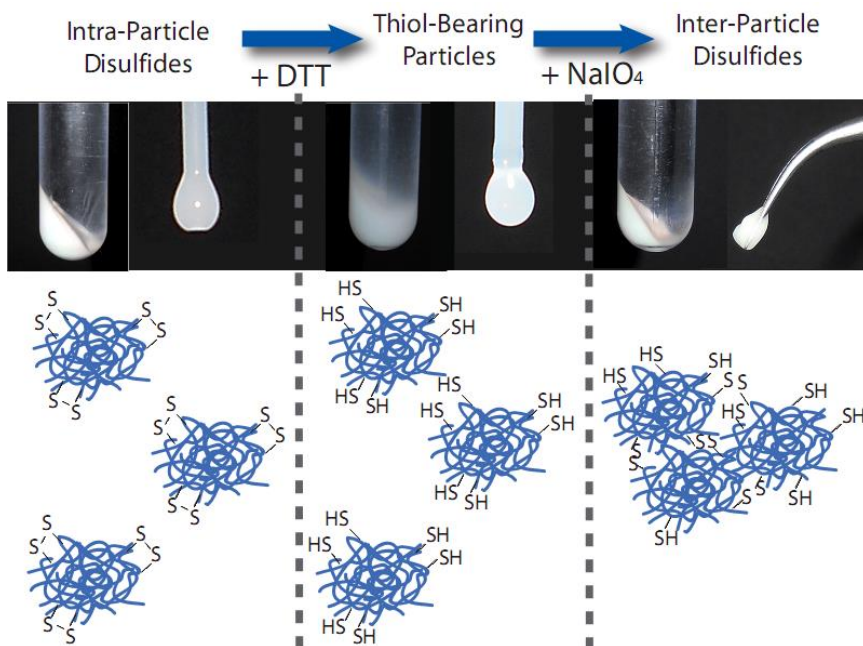


Figure 3.6. Gelation of pNIPMAm-BAC-BIS particles. Sedimented particles with intra-particle disulfides form a dense pellet, yet retain fluidity (left). Reduction by DTT leads to the production of thiol-bearing particles, a reduction in pellet density, and the retention of particle fluidity (center). Oxidation by NaIO₄ restores pellet density, but the resulting solid is a double-network of microgels cross-linked by interparticle disulfides (right).

Through rheological characterization of the resultant solids, we find that the storage modulus of our double-network is ~2000 Pa, while the loss modulus is ~100 Pa, as shown in **Figure 3.7b**. As a result, within the experimental frequency range, the complex shear modulus (G^*) is dominated by the contributions from the elastic character of the network. We note that the value of the shear modulus is comparable to that of a variety of disulfide cross-linked hydrogel networks,^{34,35} acrylamide-based hydrogels,³⁶ and densely-packed microgel assemblies.³⁷ The shear modulus is also comparable to

similar work by Hu et al.³⁸ wherein microgels composed of pNIPAm, internally cross-linked with BIS, and bearing *N*-hydroxymethacrylamide form a self-cross-linked “gel of microgels” upon drying that is analogous to the double-network discussed in this work.

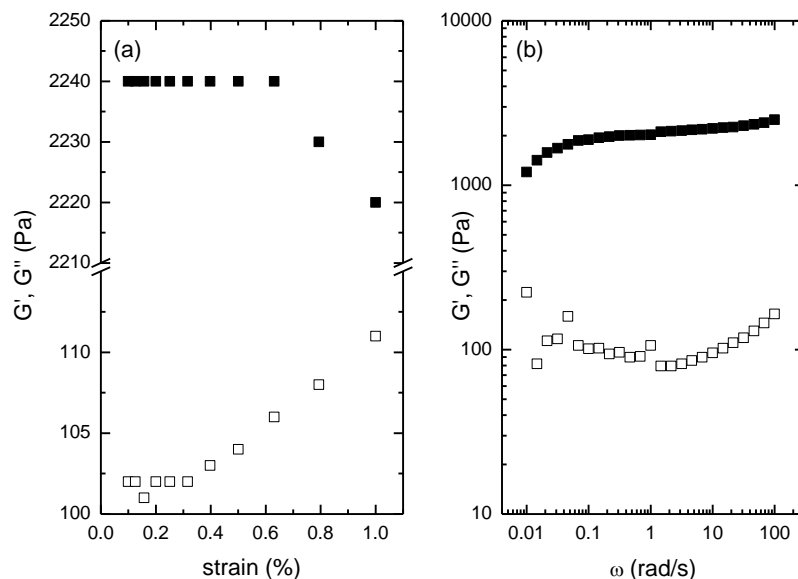


Figure 3.7. Storage and loss moduli as determined by oscillatory rheology for the pNIPAm-BAC-BIS oxidized double-network. The linearity test (a) shows G' (closed symbols) and G'' (open symbols) as a function of strain at constant frequency of 10 rad/s. (b) shows both moduli as a function of frequency at constant strain of 0.1%. The storage modulus is an order of magnitude larger than the loss modulus, indicative of the solid-like properties of the microgel double-network. Rheology experiments conducted by Mr. John Hyatt.

The inter-particle disulfide bonds that bind the microgels within the double-network can be reduced to restore the constituent thiol-bearing particles. Exposure of the double-network to DTT resulted in network dissolution. As shown in **Figure 3.8**, a significant loss in gel turbidity and a clouding of the solution occurred within 2 hours. The loss in turbidity likely resulted from a reduction in cross-link density as the inter-particle disulfides are cleaved, and the clouding was the result of dispersion of liberated microgels. The double network gel completely decomposed within 24 hours. Such a system may be enabling for numerous potential applications, such as creating erodible

gels with tunable mechanical properties, or acting as a reservoir for delivery of either a drug trapped within the matrix or for the release of microgel delivery vehicles themselves.

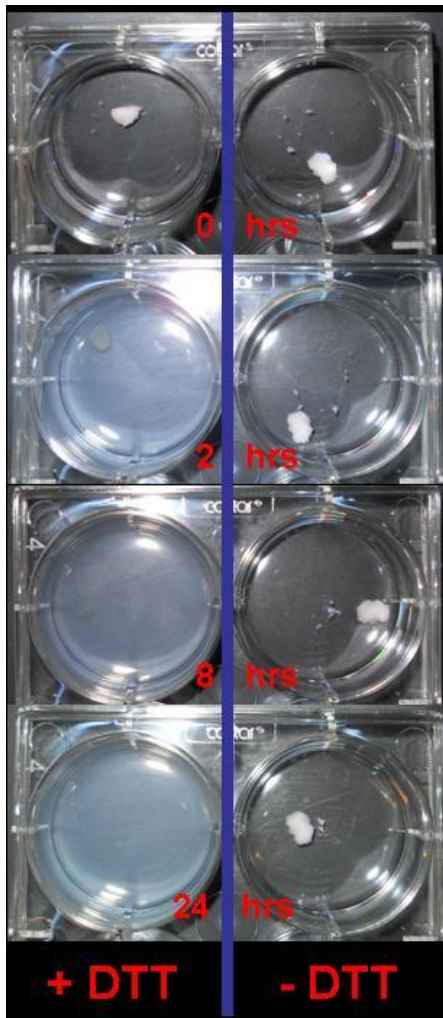


Figure 3.8. Images depicting the erosion of the pNIPMAm-BAC-BIS double-network. In response to the addition of DTT, the network dissolves leading to the reversion of the particles to their dispersed state in a matter of hours.

3.4. Conclusions & Outlook

In this work, we have demonstrated the ability to incorporate disulfide cross-links into thermo-responsive microgels using the commercially available cross-linker *N,N'*-bis(acryloyl)cystamine while utilizing aqueous precipitation polymerization. Conventional, thermally-initiated free radical precipitation polymerization leads to

uncontrolled side (self-cross-linking) reactions, leading to significant disruption of the central disulfide bond and generation of a non-degradable network. The use of a redox pair as the radical source during the polymerization leads to a reduction in the temperature needed to conduct the synthesis, while also reducing the rate of parasitic side reactions. Chemical reduction or thiol exchange of the disulfide cross-links leads to fully erodible nanogels, which may be enabling for drug delivery applications. We have demonstrated that these particles erode under mild conditions in the presence of reducing agents or a competing thiol on a timescale of minutes to hours. Furthermore, by incorporating a non-degradable second cross-linking element, intact thiol-bearing microgels can be generated through disulfide reduction, with such particles being amenable to bioconjugation and reversible double-network formation. The ability to incorporate disulfides and thiols into microgels via precipitation polymerization enables these functionalities to be used in parallel with well-characterized techniques to control particle size, topology, and functionality. We envision this additional capability to be enabling for the design of future generations of microgels for numerous applications.

3.5. References

- [1] Meng, F. H.; Hennink, W. E.; Zhong, Z., Reduction-sensitive polymers and bioconjugates for biomedical applications. *Biomaterials* **2009**, *30*, 2180-2198.
- [2] Saito, G.; Swanson, J. A.; Lee, K. D., Drug delivery strategy utilizing conjugation via reversible disulfide linkages: role and site of cellular reducing activities. *Advanced Drug Delivery Reviews* **2003**, *55*, 199-215.
- [3] Lee, H.; Mok, H.; Lee, S.; Oh, Y. K.; Park, T. G., Target-specific intracellular delivery of siRNA using degradable hyaluronic acid nanogels. *Journal of Controlled Release* **2007**, *119*, 245-252.
- [4] Oh, J. K.; Siegwart, D. J.; Lee, H. I.; Sherwood, G.; Peteanu, L.; Hollinger, J. O.; Kataoka, K.; Matyjaszewski, K., Biodegradable nanogels prepared by atom transfer radical polymerization as potential drug delivery carriers: Synthesis, biodegradation, in vitro release, and bioconjugation. *Journal of the American Chemical Society* **2007**, *129*, 5939-5945.

- [5] Li, Y. T.; Lokitz, B. S.; Armes, S. P.; McCormick, C. L., Synthesis of reversible shell cross-linked micelles for controlled release of bioactive agents. *Macromolecules* **2006**, *39*, 2726-2728.
- [6] Lin, C.; Zhong, Z. Y.; Lok, M. C.; Jiang, X. L.; Hennink, W. E.; Feijen, J.; Engbersen, J. F. J., Novel bioreducible poly(amido amine)s for highly efficient gene delivery. *Bioconjugate Chemistry* **2007**, *18*, 138-145.
- [7] Jones, C. D.; Lyon, L. A., Synthesis and characterization of multiresponsive core-shell microgels. *Macromolecules* **2000**, *33*, 8301-8306.
- [8] Nayak, S.; Gan, D. J.; Serpe, M. J.; Lyon, L. A., Hollow thermoresponsive microgels. *Small* **2005**, *1*, 416-421.
- [9] Meng, Z. Y.; Hendrickson, G. R.; Lyon, L. A., Simultaneous Orthogonal Chemoligations on Multiresponsive Microgels. *Macromolecules* **2009**, *42*, 7664-7669.
- [10] Blackburn, W. H.; Dickerson, E. B.; Smith, M. H.; McDonald, J. F.; Lyon, L. A., Peptide-Functionalized Nanogels for Targeted siRNA Delivery. *Bioconjugate Chemistry* **2009**, *20*, 960-968.
- [11] Dickerson, E. B.; Blackburn, W. H.; Smith, M. H.; Kapa, L. B.; Lyon, L. A.; McDonald, J. F., Chemosensitization of cancer cells by siRNA using targeted nanogel delivery. *BMC Cancer* **2010**, *10*, -.
- [12] Hu, X. B.; Tong, Z.; Lyon, L. A., Multicompartment Core/Shell Microgels. *Journal of the American Chemical Society* **2010**, *132*, 11470-11472.
- [13] Lee, H.; Park, T. G., Reduction/oxidation induced cleavable/crosslinkable temperature-sensitive hydrogel network containing disulfide linkages. *Polymer Journal* **1998**, *30*, 976-980.
- [14] Hiratani, H.; Alvarez-Lorenzo, C.; Chuang, J.; Guney, O.; Grosberg, A. Y.; Tanaka, T., Effect of reversible cross-linker, N,N'-bis(acryloyl)cystamine, on calcium ion adsorption by imprinted gels. *Langmuir* **2001**, *17*, 4431-4436.
- [15] Aliyar, H. A.; Hamilton, P. D.; Ravi, N., Refilling of ocular lens capsule with copolymeric hydrogel containing reversible disulfide. *Biomacromolecules* **2005**, *6*, 204-211.
- [16] Pong, F. Y.; Lee, M.; Bell, J. R.; Flynn, N. T., Thermoresponsive behavior of poly(N-isopropylacrylamide) hydrogels containing gold nanostructures. *Langmuir* **2006**, *22*, 3851-3857.

- [17] Bajomo, M.; Steinke, J. H. G.; Bismarck, A., Inducing pH responsiveness via ultralow thiol content in polyacrylamide (Micro)Gels with labile crosslinks. *Journal of Physical Chemistry B* **2007**, *111*, 8655-8662.
- [18] Plunkett, K. N.; Kraft, M. L.; Yu, Q.; Moore, J. S., Swelling kinetics of disulfide cross-linked microgels. *Macromolecules* **2003**, *36*, 3960-3966.
- [19] Oh, J. K.; Tang, C. B.; Gao, H. F.; Tsarevsky, N. V.; Matyjaszewski, K., Inverse miniemulsion ATRP: A new method for synthesis and functionalization of well-defined water-soluble/cross-linked polymeric particles. *Journal of the American Chemical Society* **2006**, *128*, 5578-5584.
- [20] Pelton, R. H.; Chibante, P., Preparation of aqueous latices with N-isopropylacrylamide. *Colloids and Surfaces* **1986**, *20*, 247-256.
- [21] Pelton, R., Temperature-sensitive aqueous microgels. *Advances in Colloid and Interface Science* **2000**, *85*, 1-33.
- [22] Kice, J. L. *Sulfur in Organic and Inorganic Chemistry*; Marcel Dekker: New York, 1971; Vol. 1.
- [23] Mather, B. D.; Viswanathan, K.; Miller, K. M.; Long, T. E., Michael addition reactions in macromolecular design for emerging technologies. *Progress in Polymer Science* **2006**, *31*, 487-531.
- [24] Torchinskii, Y. M. *Sulfhydryl and Disulfide Groups of Proteins*; Consultants Bureau: New York, 1974.
- [25] Cremllyn, R. J. *An Introduction to Organosulfur Chemistry*; Wiley: New York, 1996.
- [26] Khatik, G. L.; Kumar, R.; Chakraborti, A. K., Catalyst-free conjugated addition of thiols to alpha,beta-unsaturated carbonyl compounds in water. *Organic Letters* **2006**, *8*, 2433-2436.
- [27] Kim, J. W.; Utada, A. S.; Fernandez-Nieves, A.; Hu, Z. B.; Weitz, D. A., Fabrication of monodisperse gel shells and functional microgels in microfluidic devices. *Angewandte Chemie-International Edition* **2007**, *46*, 1819-1822.
- [28] Hu, X. B.; Tong, Z.; Lyon, L. A., Control of Poly(N-isopropylacrylamide) Microgel Network Structure by Precipitation Polymerization near the Lower Critical Solution Temperature. *Langmuir* **2011**, *27*, 4142-4148.
- [29] Smith, M. H.; Herman, E. S.; Lyon, L. A., Network Deconstruction Reveals Network Structure in Responsive Microgels. *Journal of Physical Chemistry B* **2011**, *115*, 3761-3764.

- [30] Senff, H.; Richtering, W., Influence of cross-link density on rheological properties of temperature-sensitive microgel suspensions. *Colloid and Polymer Science* **2000**, *278*, 830-840.
- [31] Varga, I.; Gilanyi, T.; Meszaros, R.; Filipcsei, G.; Zrinyi, M., Effect of cross-link density on the internal structure of Poly(N-isopropylacrylamide) microgels. *Journal of Physical Chemistry B* **2001**, *105*, 9071-9076.
- [32] Duracher, D.; Elaissari, A.; Pichot, C., Preparation of poly(N-isopropylmethacrylamide) latexes kinetic studies and characterization. *Journal of Polymer Science Part a-Polymer Chemistry* **1999**, *37*, 1823-1837.
- [33] Hermanson, G. T. *Bioconjugate Techniques*; Academic Press: San Diego, CA, 1996.
- [34] Wu, Z. M.; Zhang, X. G.; Zheng, C.; Li, C. X.; Zhang, S. M.; Dong, R. N.; Yu, D. M., Disulfide-crosslinked chitosan hydrogel for cell viability and controlled protein release. *European Journal of Pharmaceutical Sciences* **2009**, *37*, 198-206.
- [35] Van Vlierberghe, S.; Schacht, E.; Dubruel, P., Reversible gelatin-based hydrogels: Finetuning of material properties. *European Polymer Journal* **2011**, *47*, 1039-1047.
- [36] Yeung, T.; Georges, P. C.; Flanagan, L. A.; Marg, B.; Ortiz, M.; Funaki, M.; Zahir, N.; Ming, W. Y.; Weaver, V.; Janmey, P. A., Effects of substrate stiffness on cell morphology, cytoskeletal structure, and adhesion. *Cell Motility and the Cytoskeleton* **2005**, *60*, 24-34.
- [37] Senff, H.; Richtering, W., Temperature sensitive microgel suspensions: Colloidal phase behavior and rheology of soft spheres. *Journal of Chemical Physics* **1999**, *111*, 1705-1711.
- [38] Zhou, J.; Wang, G. N.; Marquez, M.; Hu, Z. B., The formation of crystalline hydrogel films by self-crosslinking microgels. *Soft Matter* **2009**, *5*, 820-826.

CHAPTER 4

MICROGEL FILMS ON COLLOIDAL SUBSTRATES

Adapted from

Gaulding, J. C., Saxena, S., Montanari, D. E. & Lyon, L. A. Packed Colloidal Phases Mediate the Synthesis of Raspberry-Structured Microgel Heteroaggregates. *ACS Macro Letters* **2013**, 2, 337.

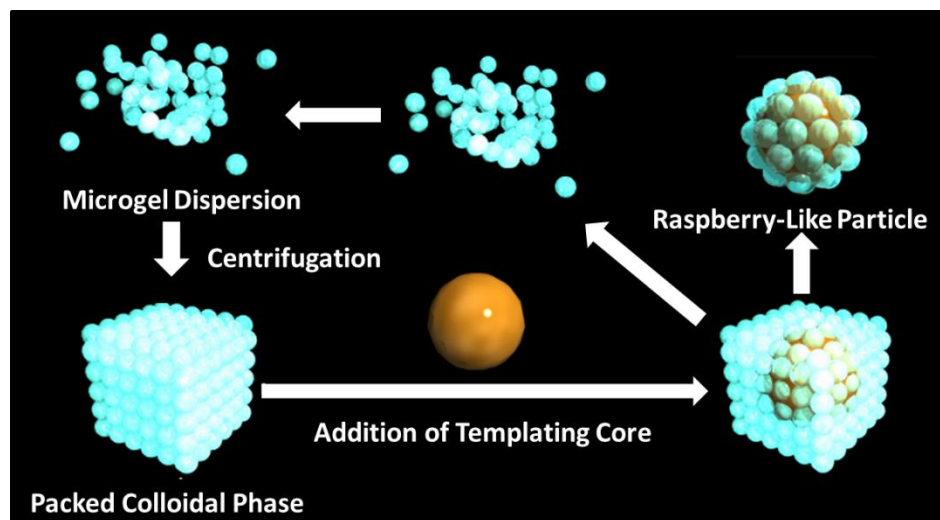
Copyright 2013 American Chemical Society

4.1. Introduction

Architectural control of nano- and microparticles is a powerful method for modulating the properties of colloidal materials.¹⁻³ In particular, hybrid colloids wherein two distinct materials form a core-shell architecture are enabling for applications such as drug delivery⁴⁻⁶ and catalysis.^{7,8} One common and versatile approach is the utilization of templates for directed assembly of heterogeneous materials, especially in the case where the surface layer itself consists of nanoparticles. Self-assembly via ion pairing has been extensively used for the formation of nanoparticle hetero-aggregates,⁹⁻¹² where solution conditions have strong impact on the surface coverage.¹³⁻¹⁵ Hydrogen bonding or other types of complementary interactions have also been utilized.^{16,17} The resultant particles consist of a shell of nanoparticles decorating the template "core", leading to a bumpy surface reminiscent of raspberries. The anisotropy and tunability in surface roughness has made particles of this nature useful in altering the hydrophobicity of surfaces, for example.^{18,19}

In the work described in this chapter, we utilize hydrogel particles (microgels) in the fabrication of hybrid colloids. Microgels are of great interest due to their applicability to a variety of fields such as sensing and drug delivery.^{20,21} In particular, thermo-

responsive microgels composed of pNIPAm have been extensively studied either as homopolymers,²² or as co-polymers with other environmentally sensitive monomers (e.g. acidic and basic monomers) to produce materials responsive to multiple stimuli.^{23,24} The responsivity of microgels has been exploited in Coulombically-directed heteroaggregation to form hybrid raspberry-like particles,²⁵⁻²⁷ and similar particles have been formed that utilize microgels as templates for colloidal shell addition.²⁸⁻³⁰ In addition, thin films of microgels coated onto solid substrates have been shown to improve the biocompatibility of the base material³¹ and allow controlled drug release from that surface.^{32,33} As such, microgels are attractive for incorporation into hybrid constructs for controlled delivery, wherein the assembly of microgels on core particles would confer soft, responsive properties to the core particle, while providing an opportunity for a multi-compartment or multi-functional vehicle. Additionally, microgels have been shown to exhibit rich phase behavior as concentrated dispersions due to their high water content and responsive nature.³⁴⁻³⁶ In this work, we exploit the soft, responsive matrix provided by packed colloidal phases of microgels (e.g. colloidal glasses or crystals) to generate hybrid particles whose surfaces are decorated with hydrogel colloids. Our method is outlined in **Scheme 4.1**.



Scheme 4.1. Raspberry-like particle synthesis. A concentrated dispersion of microgels is centrifuged to form a pellet, then the supernatant is removed leaving behind a packed colloidal phase. The addition of a small volume of solvent carrying the template particles and mixing of the two leads to confinement of the cores within the packed phase. Dispersal of the microgels leads to separation of the coated, raspberry-like particles from the unincorporated microgels, which can subsequently be returned to packed colloidal phases for additional assembly.

By introducing a variety of “core” particles to act as templates in a concentrated colloidal phase, the surfaces become decorated with a close-packed monolayer of microgels. The high volume fraction and close packing of the colloidal phase enables this method to generate decorated particles in the absence of complementary surface chemistries, which ordinarily drive heteroaggregation in dilute media. Due to the amphiphilic nature and chemical versatility of these microgels, the resultant raspberry-like particles can be stabilized on a variety of functional core particle surfaces. Upon dispersion of the colloidal phase, the remaining microgels are then easily recovered and recycled to re-form another packed colloidal phase for raspberry-like particle synthesis.

A number of “core” particles are available commercially, permitting the exploration of different surface chemistries, size ratios, and surface structures. Microgels offer a great deal of synthetic versatility, in terms of their composition, size, and architecture. In this work, we limited our investigation to particles incorporating or lacking acrylic acid (AAc) of approximately the same size. We found that concentrating

the microgels into a concentrated colloidal phase (a colloidal fluid or glass from a spatial point of view) prior to introduction of the core particles led to the coordination of the core particles' surfaces with a large number of microgels, ensuring high surface coverage. Additionally this coordination leads to assembly in the absence of complimentary surface interactions. The high viscosity of the dense colloidal phase tends to stabilize the cores against aggregation, which can be a problem in dilute solutions when assembling multiple multivalent building blocks via heteroaggregation.

4.2. Experimental

4.2.1. Materials

All common materials were sourced and used as described in **Chapter 2**. Additionally, reagents acrylic acid (AAc), *N*-hydroxysuccinimide (NHS), 1-ethyl-3-[3-dimethylaminopropyl]carbodiimide hydrochloride (EDC), 4-aminobenzophenone (AB), ethanol, and dimethylsulfoxide (DMSO) were all used as received. 4-acrylamidofluorescein (AFA) was synthesized as described previously.³⁷ Methacryloxyethyl thiocarbamoyl rhodamine B (MERho) was purchased from Polysciences, Inc. (Warrington, PA) and used as received. Amine-modified silica particles were purchased from Bangs Laboratories, Inc (Fishers, IN), carboxyl-modified polystyrene spheres were purchased from Polysciences, Inc. and carboxyl-functionalized magnetic (both smooth-surface and rough-surface) polystyrene particles were purchased from Spherotech, Inc (Lake Forest, IL).

4.2.2. Microgel Synthesis

4.2.2.1. Sample μ gel-G

NIPAm and BIS were dissolved in deionized water, to a final total monomer concentration of 100 mM. A mass of 1.0 mg of AFA was dissolved in 1 mL of DMSO,

then added to the monomer solution. The final molar composition of the particles was 96% NIPAm, 4% BIS, <0.1% AFA. The solution was filtered to remove any undissolved solids then SDS was added to a concentration of 0.2 mM. The solution was heated to 68 °C and purged under nitrogen for 60 min. Polymerization was initiated by addition of 1 mL of an aqueous solution of 25 mM APS. The solution was allowed to stir at 68 °C overnight, then cooled to room temperature, filtered, purified via centrifugation, and lyophilized for storage.

4.2.2.2. Sample µgel-R

NIPAm, and BIS (and MERho when particle fluorescence was desired) were dissolved in deionized water, to a final total monomer concentration of 124 mM. The solution was filtered to remove any undissolved solids then SDS was added to a concentration of 0.2 mM. The solution was heated to 70 °C and purged under nitrogen for 40 min. Acrylic acid was then added and the solution allowed to purge for an additional 10 min, bringing the final molar composition of the particles to 70% NIPAm, 3.5% BIS, 26% AAc, (and <0.1% MERho in fluorescent particles). Polymerization was initiated by addition of 1 mL of an aqueous solution of 35 mM APS. The solution was allowed to stir at 70 °C overnight, then cooled to room temperature, filtered, purified via centrifugation, and lyophilized for storage.

4.2.3. Preparation of Aminobenzophenone-functionalized Cores

A solution of 5 mM EDC, 8 mM NHS, and 25 mM 4-aminobenzophenone was prepared in 12 mL of DMSO. To this was added 1.2 mL of a 2.5% w/v solution of the desired carboxyl-functionalized polystyrene-based core particle, as provided in stock solution by the manufacturer. The solution was allowed to react overnight in the dark at room temperature. The resultant particles were purified by centrifugal sedimentation and

redispersal in ethanol five times. Prior to raspberry-like particle conjugation, the particles were sedimented and redispersed at a total of 0.1% w/v with pH 5.5 MES.

4.2.4. Raspberry-like Particle Synthesis

A volume of 0.5 mL of a 10 mg/mL solution of the desired microgel composition in pH 5.5 MES buffer was added to small centrifuge tubes. The tubes were centrifuged at 18,000 x g for 30 min. Pellet volumes were estimated by comparison to identical centrifuge tubes with known volumes of solvent. Effective volume fractions (ϕ_{eff}) were calculated as $k \cdot c$, where c is the microgel concentration expressed as wt / wt, and k is a shift factor. Particles previously synthesized in our group with similar compositions to $\mu\text{gel-G}$ and $\mu\text{gel-R}$ were used to estimate shift factors of 11 ($\mu\text{gel-G}$)³⁸ and 18 ($\mu\text{gel-R}$).³⁹ The supernatant was discarded, leaving a remnant pellet of approximately 75 μL for $\mu\text{gel-G}$ ($\phi_{\text{eff}} = 0.73$) and 125 μL for $\mu\text{gel-R}$ ($\phi_{\text{eff}} = 0.72$). To each pellet was added 50 μL of a 0.1% w/v solution of desired core particles was added and the pellet was vortexed to mix. The resultant ϕ_{eff} after core addition was 0.44 and 0.51 for $\mu\text{gel-G}$ and $\mu\text{gel-R}$, respectively. When UV coupling was attempted, the pellets were then exposed to longwave UV from a Blak Ray 100 W lamp for 30 minutes. If carbodiimide coupling was attempted, a solution of 50 mM EDC and 75 mM NHS in pH 5.5 MES buffer was prepared, and 50 μL was added to each tube and allowed to react for two hours. When no coupling was attempted, the glassy pellets were diluted in pH 5.5 buffer after 30 minutes and vortexed. Centrifuge tubes were combined and the resultant raspberry-like particles were isolated via sedimentation or magnetic separation. The free-microgel containing supernatants were recovered and sedimented for subsequent additional raspberry-like particle generation. The raspberry-like particles were then isolated and purified by sequential sedimentation, vortexing, sonication, and washing in ethanol to remove unincorporated microgels. Sonication served to ensure that any remnant microgels were

strongly bound to the core particles and to disperse any aggregates formed during sedimentation.

4.2.5. Dilute Heteroaggregation for Raspberry-like Particle Synthesis

A volume of 1 mL of a 10 mg/mL solution of the desired microgel composition in pH 5.5 MES buffer was diluted into 3 mL of pH 5.5 MES buffer, leading to an overall concentration of 2.5 mg/mL of microgels. To each was added 100 μ L of a 0.1% w/v solution of aminobenzophenone-functionalized smooth-surface magnetic polystyrene core particles. The vials were illuminated by longwave UV from a Blak Ray 100 W lamp for 30 min. The resultant particles were isolated by magnetic separation, and purified by sequential sedimentation, vortexing, sonication, and washing in ethanol to remove unincorporated microgels.

4.2.6. Characterization

Microgel r_h values were determined using dynamic light scattering (DLS) via a DynaPro DLS (Wyatt Technology, Santa Barbara, CA). Zeta potential was determined using a Zetasizer Nano ZS (Malvern, Worcestershire, UK) in pH 5.5 MES buffer at 20 °C. Microgel spreading was characterized by passive deposition of dilute solutions of particles in pH 7.4 buffer over amine-functionalized silica glass coverslips, which were then imaged using AFM, as described in **Chapter 2**. Brightfield and epifluorescence microscopy images of microgels and raspberry-like particles were collected using an Olympus IX-70 inverted microscope equipped with an oil-immersion 100x objective and black and white or color PixelFly CCD cameras (Cooke Corporation, Romulus, MI). Fluorescence excitation was achieved by using a mercury lamp equipped with excitation band-pass filters of 450-490 nm (blue excitation) or 510-560 nm (green excitation). Samples for confocal microscopy were prepared by placing a drop of raspberry-like particles suspended in ethanol on a microscope slide. A 22 x 22 mm coverslip was placed

over the drop, and sealed using a polymer fixative. A Zeiss LSM 510 UV Confocal Microscope (Carl Zeiss Inc.) was used with a Plan Apochromat 63X/1.4 NA Oil DIC. An Argon laser with an excitation wavelength of 488 nm was used to image AFA samples. A HeNE laser with an excitation wavelength of 543 nm was used to image MERho samples. Image analysis was carried out using ImageJ. Scanning electron microscopy (SEM) images were collected using an FEI Nova Nanolab 200 FIB/SEM. Prior to analysis, samples were dried onto copper tape, affixed to sample stubs, and gold or gold/palladium coated using a Hummer V Sputterer (Anatech USA, Union City, CA).

4.3. Results and Discussion

4.3.1. Microgel Synthesis

Table 4.1. Microgel Compositions and Characterization

	Mol % NIPAm	Mol % BIS	Mol % AAc	r_h (pH 3), nm ^a	r_h (pH 5.5), nm ^a	Zeta Potential (pH 5.5), mV	Radius on Surface, nm ^b
μgel-R	70.5	3.5	26	366	553	-23.0	475
μgel-G	96.0	4.0	0	437	448	-1.4	650

^a measured by dynamic light scattering at 20 °C and 15 mM ionic strength. ^b estimated from AFM line traces.

The microgels used in this work, μgel-R and μgel-G, were synthesized according to the compositions given in **Table 4.1**. The pH responsivity and zeta-potential are as expected for particles containing (μgel-R) or lacking (μgel-G) acrylic acid. As shown in **Figures 4.1a** and **4.2a**, incorporation of the fluorescent co-monomers was successful. Also notable is that, while the solution particle sizes appear to be similar, **Figures 4.1** and **4.2** suggest that the apparent sizes of the two particles on the surface are very different, potentially suggesting different behavior of the two microgels on contacting a surface.

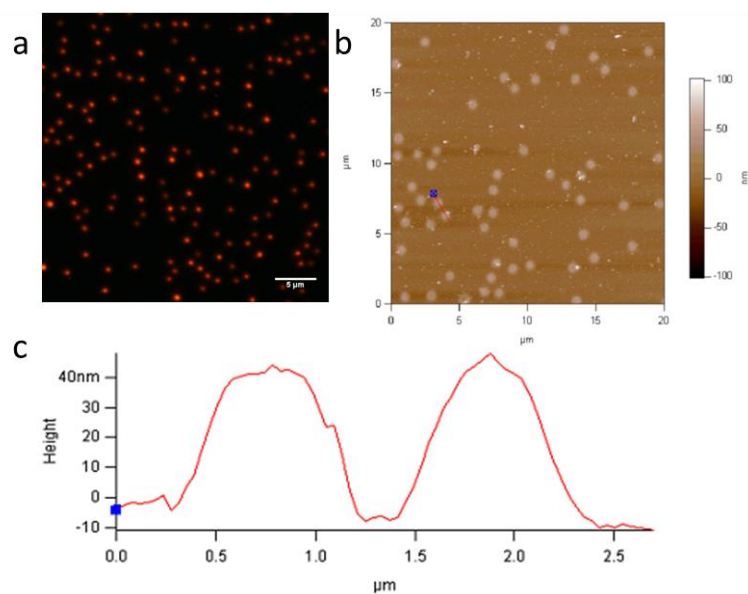


Figure 4.1. Characterization of pNIPAm/3.5% BIS/26% AAc (Sample μ gel-R). a) Green excitation epifluorescence image of fluorescent particles. Scale bar is 5 μ m. b) AFM image (20 x 20 μ m) and c) line trace reveal the spreading behavior of μ gel-R.

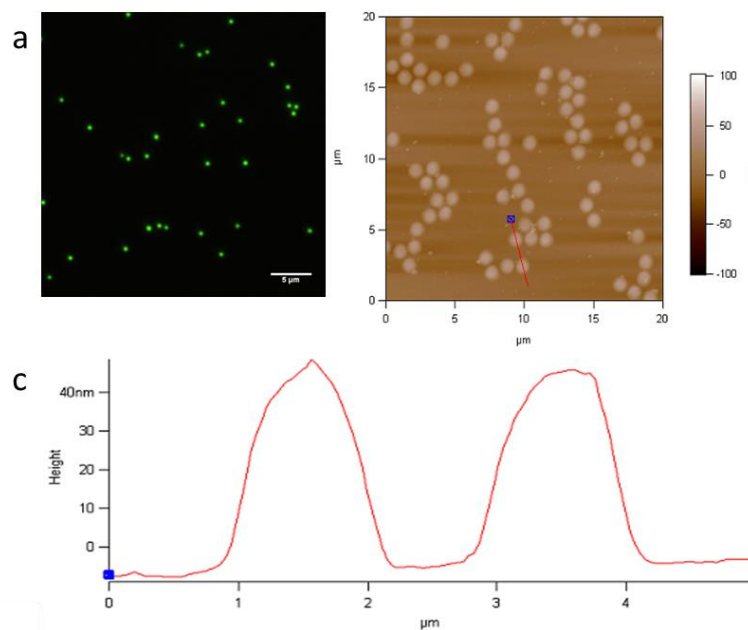


Figure 4.2. Characterization of pNIPAm/4.0% BIS (Sample μ gel-G). a) Blue excitation epifluorescence image of fluorescent particles. Scale bar is 5 μ m. b) AFM image (20 x 20 μ m) and c) line trace reveal the spreading behavior of μ gel-G.

4.3.2. Raspberry-Like Particles

Highly-packed microgel assemblies were prepared by centrifugal sedimentation, as described previously.⁴⁰ Under applied centrifugal forces, sedimentation serves to concentrate the microgels into a fraction of the available volume, until close-packing of the colloidal particles leads to pellet formation. Removal of the supernatant confines the volume available for the microgels to redisperse, thus the remnant microgels are trapped in a highly-concentrated glassy state. In all cases, the resultant pellet was viscous, turbid, and appeared homogeneous with no evidence of Bragg diffraction, as is consistent with disordered packed phases prepared by our group in previous studies.³⁴ Core particles were then introduced to the colloidal phase, and incorporated within the matrix via vortexing. As shown in **Figure 4.3**, the core particles are distributed throughout the microgel colloidal phase. Following incubation of the cores within the matrix for 30 min, isolation of stable raspberry-like particles followed dilution of the colloidal assembly. The much greater density of the core particles and subsequent raspberry-like particles led to facile isolation of the raspberry-like particles from the excess unincorporated microgels via sedimentation. The excess microgels could then be recovered and returned to a colloidal packed state for sequential rounds of raspberry-like particle assembly.

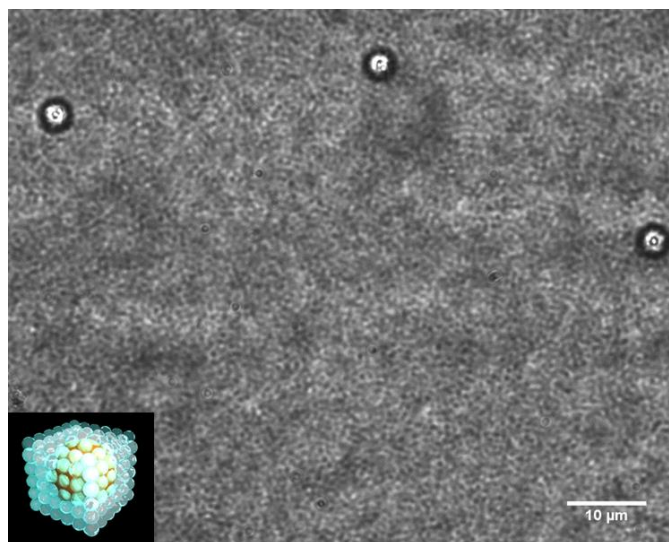


Figure 4.3. Brightfield microscopy image of aminobenzophenone-functionalized 4.6- μm diameter magnetic polystyrene particles mixed in a dense colloidal phase of $\mu\text{gel-G}$. Scale bar is 10 μm .

Upon isolation, the relative scattering intensity of the core particles and the microgels made brightfield visualization of the adsorbed microgels impossible. However, by incorporating a fluorescent monomer within the microgel network, the labeled particles are observed to co-localize with the cores, as shown in **Figures 4.4** and **4.5**, and discrimination of individual microgel particles is possible. Once the core particles have become mixed within the high volume fraction colloidal phase, a variety of interactions may lend stability to the resultant raspberry-like particles. Our initial efforts used simple ion-pairing between the anionic $\mu\text{gel-R}$ and amine-functionalized core particles, followed by carbodiimide coupling, as in **Figure 4.4a-c**. However, further investigation revealed that charge-pairing is unnecessary, as $\mu\text{gel-R}$ also readily coated carboxylated polystyrene core particles which had been conjugated to 4-aminobenzophenone (AB) (**Figure 4.4d-f**). Under UV excitation, AB forms covalent linkages with numerous organic groups, including simple aliphatic C-H bonds via hydrogen abstraction.⁴¹ We have previously demonstrated this technique to conjugate microgels to functionalized

polyethylene terephthalate surfaces.⁴² As such, AB-bearing core particles would be expected to covalently bind decorated microgels regardless of the microgel functionality. Microgels of pNIPAm lacking acrylic acid (μ gel-B) lack specific affinity for the core particles, yet also show evidence of high surface coverage on carboxyl-functionalized and AB-functionalized core particles (**Figure 4.5**). The stabilizing mechanism in these cases is less clear, but likely results from the soft and amphiphilic nature of microgels, as evidenced by their ability to stabilize Pickering-type emulsions.⁴³ Non-specific adsorption of microgels onto such cores is sufficiently tenacious to withstand isolation from the colloidal phase, along with subsequent sonication and purification from residual microgels. Such coatings may additionally be reinforced through the use of appropriate coupling chemistries, if warranted for a desired application. Importantly, the use of the packed colloidal phase-mediated technique showed improved surface coverage relative to stoichiometrically-matched controls performed under relatively dilute conditions, as shown in **Figure 4.6**.

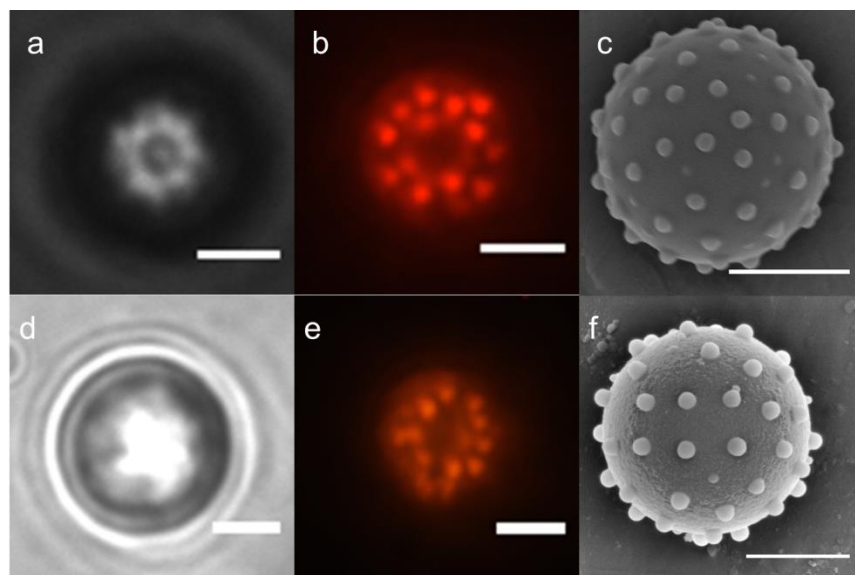


Figure 4.4. (a,d) Brightfield, (b,e) Green-excitation epifluorescence, and (c,f) SEM images of isolated raspberry-like particles featuring μ gel-R. Assembly of (a-c) was charge-directed using 4.6- μ m diameter amino-silica particles, where (d-f) utilized 4.4- μ m aminobenzophenone-functionalized polystyrene particles. The scale bar in each image is 2 μ m.

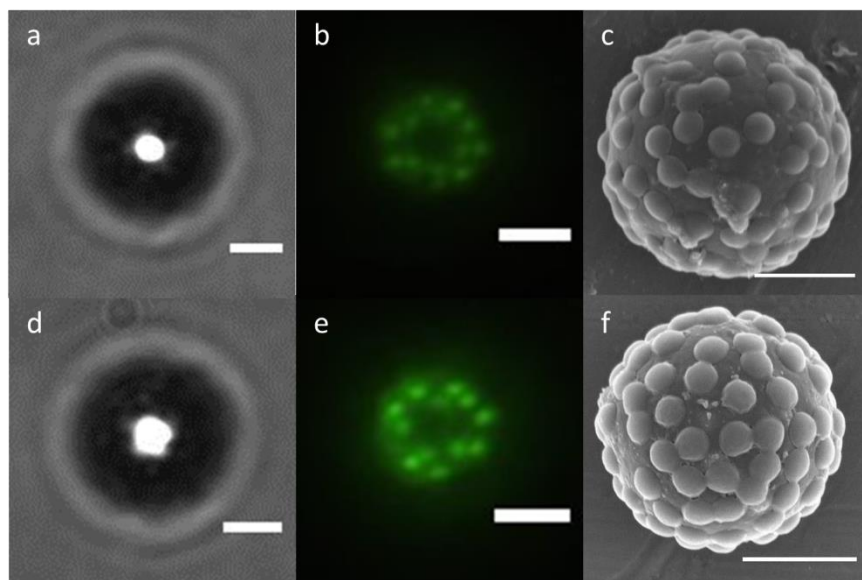


Figure 4.5. (a,d) Brightfield, (b,e) Blue-excitation epifluorescence, and (c,f) SEM images of isolated raspberry-like particles featuring 4.6- μm diameter magnetic polystyrene particles decorated with $\mu\text{gel-B}$. (a-c) represent carboxyl-functionalized polystyrene, (d-f) represent aminobenzophenone-functionalized polystyrene. The scale bar in each image is 2 μm .

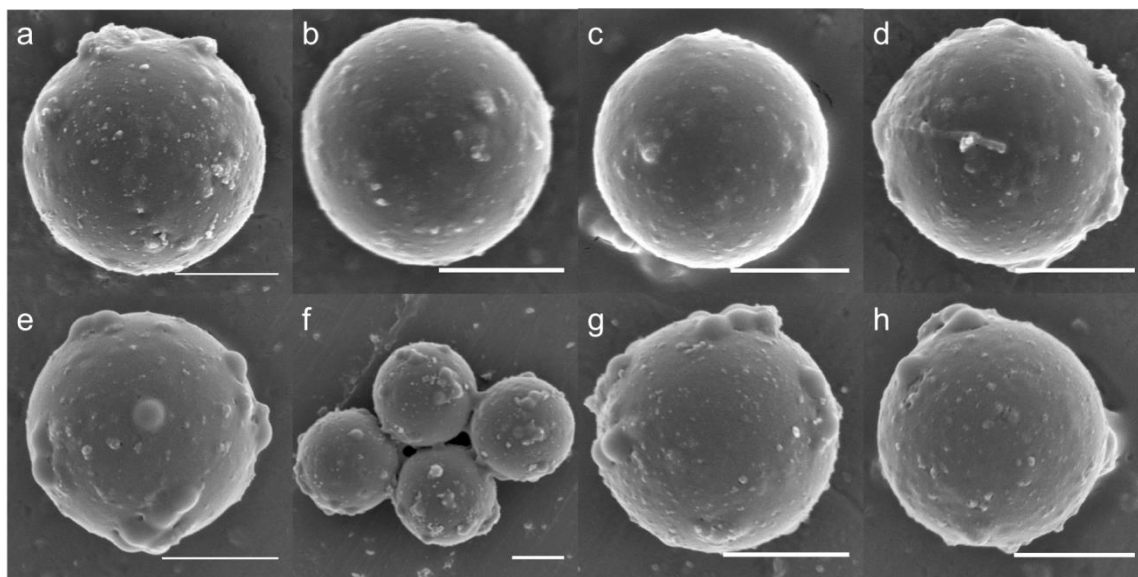


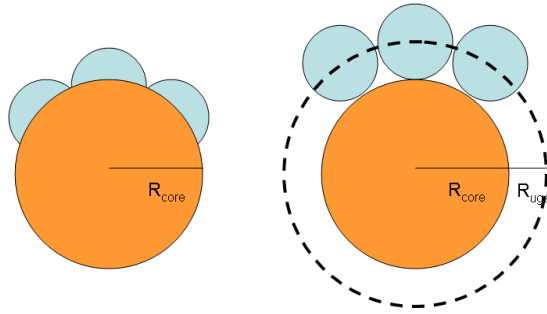
Figure 4.6. SEM images of raspberry-like particle assembly from dilute (2.5 mg/mL) suspensions of (a-d) $\mu\text{gel-G}$ and (e-h) $\mu\text{gel-R}$ onto 4.6- μm aminobenzophenone-functionalized magnetic polystyrene core particles. The scale bar in each image is 2 μm .

4.3.3. Microgel Spreading & Surface Coverage

Geometrically determining the number of microgels capable of packing onto the surface of a sphere requires that we define two characteristics: the effective footprint of the microgel, and the surface area to be covered. However, the number of microgels capable of packing onto the surface of a spherical core particle is sensitive to the swelling behavior of the microgels. Consequently, the microgel footprint (the projection of the microgel radius onto the surface) and the microgel contact area (the actual surface area interacting with the microgel) may be two different quantities. Two extreme cases can be envisioned: one wherein the microgels act as hard spheres, with minimal area contacting the surface of the core particle; and a second wherein the microgels conform to the surface, which can be estimated as hemispheres. However, in either the spherical or hemispherical approximation, the effective footprint of the microgel is the same, πR_{ugel}^2 . Consequently, the variation between the two approximations lies in the surface area of the sphere to be covered. Assuming completely deformable microgels, the microgel footprint and the contact area are the same, thus giving us a surface area of $4\pi(R_{\text{core}})^2$. The hard sphere approximation, in contrast, forces us to account for the height of the microgel above the surface of the sphere in order to determine the effective surface area to cover. The resultant area would be $4\pi(R_{\text{core}} + R_{\text{ugel}})^2$. The difference in effective sphere radius to cover due to deformable microgels is illustrated in **Scheme 4.2**. Further, the packing efficiency will limit the effective area that the microgels are able to cover. Random three dimensional close packing of spheres imposes a packing efficiency of 0.64 within the glass, but the spherical core surface is sufficiently larger than the microgels as to present a 2-dimensional surface for coverage, with a theoretical close packing limit of approximately 0.91. The ratio of the radii of the core particles and microgels will determine where within this range the packing efficiency will fall – as the ratio decreases, the greater the effect the curvature of the core particles will have on packing efficiency.

In the systems studied, the microgel radii are approximately 20-25% that of the core particles, suggesting the packing efficiency will be on the lower end of that range. Estimations of the packing efficiency based on methods described by Balmer et al.⁴⁴ and using solutions for points on a sphere available online,⁴⁵ for the case of μ gel-R and 4.4 μ m core particles suggest a theoretical maximum of 83 microgels and a packing efficiency of 0.84. Significant deviation from this value can be expected due to experimental factors such as microgel-microgel interactions, polydispersity, and the adhesion between microgel and core. These factors compound with particle softness to make particle coverage difficult to estimate numerically. Considering the theoretical maximum of 0.84 packing efficiency, the range of particles expected to cover a given core is estimated as:

$$(0.84) \cdot \frac{4R_{core}^2}{R_{ugel}^2} < \# \text{Microgels} < (0.84) \cdot \frac{4(R_{core} + R_{ugel})^2}{R_{ugel}^2}$$

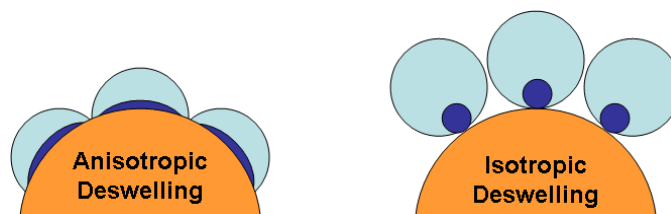


Scheme 4.2. The deformable microgel approximation maximizes the contact area with the core, and thus minimizes the number of microgels on the surface. The rigid microgel approximation minimizes the contact area, and thus increases the size of the effective sphere to cover and maximizes the number of microgels on the surface.

Comparison of the particle dimensions observed in solution and upon surface deposition via AFM (**Table 4.1**) shows the effect that particle de-swelling has on the surface morphology of the particles. When contacting a planar substrate, such as the glass slides used in AFM sample preparation, the microgels appear to have radii commensurate with what is observed in solution, as the contact with the surface leads to deformation of

the particles and thus anisotropic de-swelling. When introduced to the core particles within the colloidal matrix, if the microgels underwent significant deformation upon contacting the core surface, the resultant spreading would lead to surface pinning of the spread state and thus more anisotropic de-swelling of the microgels. However, the limited footprint observed via SEM indicates that the dried particles de-swell isotropically, and the large reduction in particle diameter thus exposes much of the underlying substrate.

Scheme 4.3 depicts the differences expected of anisotropic and isotropic microgel de-swelling on curved surfaces. In the case of μ gel-R and μ gel-G, the two particles exhibit differing degrees of anisotropy in their de-swelling behavior on the surface.



Scheme 4.3. Highly deformable microgels, with large surface contact area, would on drying exhibit reductions in particle height from the surface, but minimal change in spreading. The rigid microgel approximation, leading to low surface contact area, permits isotropic de-swelling and thus an apparently sparse coating in the dry state.

The difference in appearance between μ gel-R and μ gel-G, as well as the discrepancy in particle size with respect to characterization under dilute conditions, may also have contributions from packing-induced de-swelling, which has been observed previously for charged microgels.^{46,47} An additional possibility is that the differential appearance of the two particles is the result of differences in the polymer density distribution of the two different microgels. Microgels are well known to exhibit differences in mass distribution as a function of their composition. The addition of acrylic acid in μ gel-R may lead to a particle architecture that is more akin to a dense core with a lightly cross-linked corona. The highest density regions would be the most prominent by SEM. Analysis of Pickering emulsions stabilized by microgels have been conducted

using cryo-SEM, and the appearance of the microgels is observed to vary with regard to factors like cross-linking density and solution pH for acid-containing microgels – factors that govern the deformability of the particles.⁴⁸⁻⁵⁰ However Pickering emulsions represent a liquid/liquid interface that directs the microgel shape, whereas the shape of microgels at the solid/liquid interface, as well as the overall surface coverage of these raspberry-like particles may not be entirely directed by the same factors.

For the case of the raspberry-like particles shown in **Figure 4.4**, the average radius of μ gel-R is approximately 550 nm and the average PS core radius is approximately 2.2 μ m. This leads to a surface coverage of between 54 and 84 microgels per particle. Though quantitative measurement of the number of microgels on the surface is challenging using microscopic techniques, semi-quantitative assessment of the SEM images in **Figure 4.4** indicates that this is a reasonable approximation. **Figures 4.4** and **4.5** also provide some insight into the microgel/surface interaction. Visualization of swollen microgels, as in **Figure 4.4b**, **4.4e**, **4.5b**, and **4.5e**, seems to indicate that the microgels are densely packed on the surface, as we expect from the templating colloidal phase. Thus, for μ gel-R comparison of **Figure 4.4b & 4.4c** suggests that upon vacuum drying, the particles de-swell isotropically leading to a reduction in apparent dry particle diameter to approximately 30% of that observed via AFM. This suggests that the effective particle footprint is commensurate with that of a spherical microgel contacting a spherical core. Deformation upon contacting the core surface and the resultant spreading would lead to surface pinning of the spread state and more anisotropic de-swelling of the microgels, as is typically seen via AFM. This isotropic de-swelling in all dimensions save the points anchored to the core substrate underneath contributes to the apparent sparseness of the surface coverage. In contrast, the neutral microgels (μ gel-G) in **Figure 4.5** appear to coat the surface in a more uniform manner and undergo more spreading with a reduction in particle diameter of approximately 50% of that observed via AFM. Greater microgel-microgel interactions may also be occurring in this case as well, as the

particles appear to have more irregular spacing following de-swelling and drying, though this may simply be more prominent due to the smaller discrepancy with respect to the AFM diameter.

More detailed observation of the swelling properties of swollen microgels can be achieved using confocal microscopy. As shown in **Figure 4.7** for raspberry-like particles featuring each type of microgel, the swelling and spacing patterns observed via SEM persist. Interestingly, the microgel diameters observed by confocal are similarly smaller than the hydrodynamic and AFM diameters would suggest. This is likely due to greater fluorophore density about the center of mass of the particles, but may suggest that the particle coronas play a major role in determining their packing on the colloidal surface.

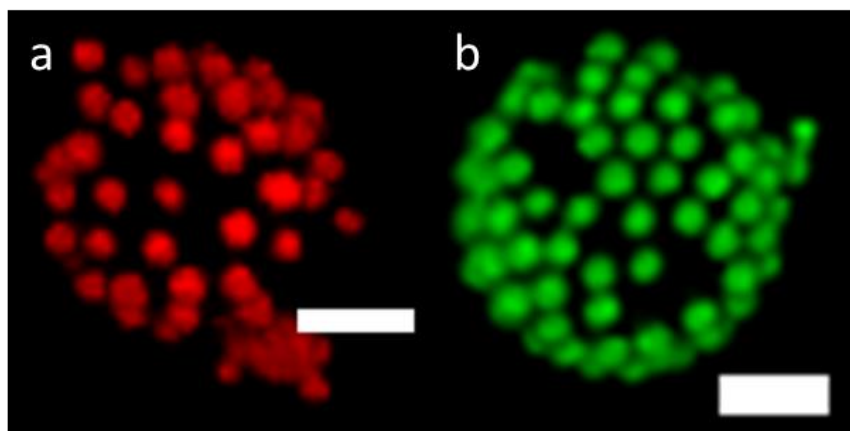


Figure 4.7. a) Green-excitation confocal image of 4.4- μm AB-functionalized PS decorated with $\mu\text{gel-R}$ b) blue-excitation of 4.6- μm AB-functionalized magnetic PS decorated with $\mu\text{gel-G}$. The scale bar in each image is 2 μm . Confocal imaging performed by Ms. Shalini Saxena.

4.3.4. Expansion of Raspberry-Like Particle Synthesis

The nature of the core particles can be used to impart additional functionality into the raspberry-like particles, such as paramagnetism. We chose rough-surface magnetic PS nanoparticles as a particularly challenging core. These particles were smaller (2.5 μm in diameter) than the cores described previously, and had a very rough surface due to the presence of surface-grown polymer brushes containing adsorbed iron oxide nanoparticles

(**Figure 4.8a**). However, these rough surface core particles were readily incorporated within the microgel colloidal phase, leading to successful raspberry-like particle synthesis and recovery (**Figure 4.8**). This case exemplifies one of the advantages of hybrid, compartmentalized vehicles such as these particles. The magnetic-functionality of the core particles is conferred upon the entire assembly, while the soft and responsive nature of microgels dominates the surface interactions. Thus, the core material and the microgel coating retain different functionalities and synergistically benefit from the raspberry-like particle assembly. Also notable in **Figure 4.8c** and **4.8e** is that the characteristic surface deformations of $\mu\text{gel-G}$ and $\mu\text{gel-R}$ are preserved on a surface with both greater curvature and greater surface roughness.

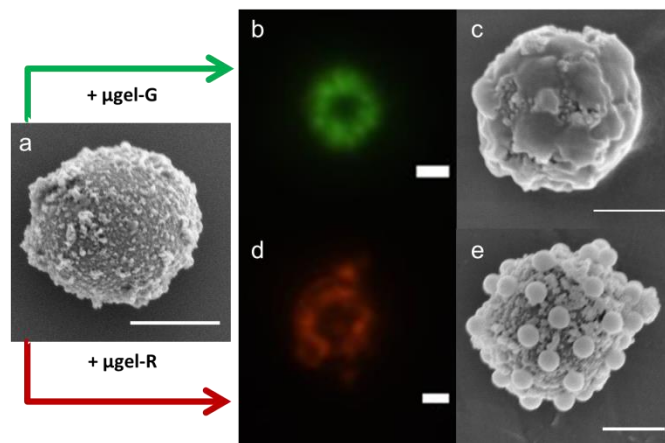


Figure 4.8. (a) SEM image of an AB-functionalized magnetic PS particle with rough surface topology. (b) Blue-excitation epifluorescence and (c) SEM image following coverage with $\mu\text{gel-G}$. (d) Green-excitation epifluorescence and (e) SEM image following coverage with $\mu\text{gel-R}$. Scale bar in all images is 1 μm .

In addition to high surface coverage and the stabilization of the core particles brought about by the high microgel packing densities, another advantage that arises from the use of jammed microgel phases is the ability to make multi-functional raspberry-like coatings, or patchy particles. Microgel colloidal crystals have been shown to be highly defect-tolerant,³⁵ which enables mixtures of compositionally distinct microgels in a single colloidal phase without extensive phase segregation. Thus we reasoned that multiple

distinct microgels should be able to form a mixed coating on the surface of the core. We demonstrated this using μ gel-R and μ gel-G. The two particles when sufficiently mixed in the glassy state by vortexing yielded a homogeneously colored pellet. Upon introduction of the AB-functionalized core particles, followed by UV excitation, raspberry-like particles were recovered with both types of microgels present on their surface, as shown in **Figure 4.9**. Comparison of the microgel morphologies via SEM in **Figure 4.9** to their respective panels in **Figures 4.4** and **4.5** show the characteristic differences in surface spreading between the two microgels.

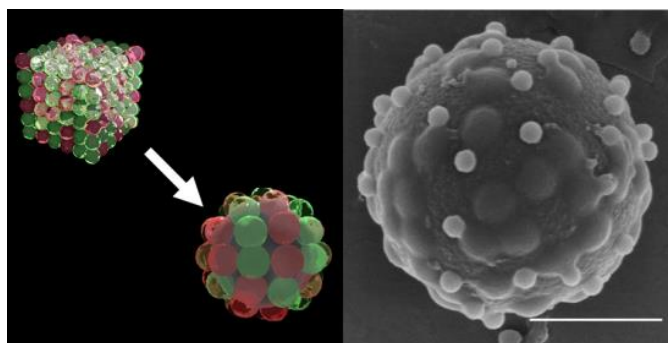


Figure 4.9. (Left) Schematic of mixed colloidal glass for raspberry coating. (Right) SEM image of 4.4- μ m diameter AB-functionalized PS particles decorated with a 1:1 w:w mixture of μ gel-R and μ gel-G. Scale bar is 2 μ m.

4.4. Conclusions and Outlook

Though this method shows a great deal of versatility, especially with regard to the absence of the necessity for complementary interactions, there are several practical limitations. The inefficiency of microgel incorporation due to the large excess of particles inherent in the technique is only somewhat ameliorated by the ability to recycle the residual microgels. While the ratio of cores to microgels within the matrix has a theoretical maximum based on monolayer coverage of microgels, the practical limit for incorporation will be lessened by factors such as the core-addition solution and core mixing within the concentrated colloidal phase.

In summary, we have demonstrated that responsive microgels can be used to coat the surface of a variety of spherical, micron-scale substrates using a packed colloidal phase-mediated approach. The use of a high-volume fraction and high-viscosity phase during assembly provides a means to enable efficient surface coverage in the absence of compatible surface chemistries to direct such assembly from dilute media. This method seems highly tolerant with regard to microgel size, composition, and core substrate size, functionality, and topography. Mixtures of compositionally dissimilar microgels were also shown to form multi-functional surfaces. Overall, this method is a versatile technique that exploits the softness of responsive microgels to form densely-packed assemblies on the surfaces of micron-scale particles, providing a flexible method to generate hybrid microgel constructs enabling for drug delivery or other applications.

4.5. References

- [1] Caruso, F., Nanoengineering of particle surfaces. *Advanced Materials* **2001**, *13*, 11-22.
- [2] Glotzer, S. C.; Solomon, M. J., Anisotropy of building blocks and their assembly into complex structures. *Nature Materials* **2007**, *6*, 557-562.
- [3] Buck, M. R.; Bondi, J. F.; Schaak, R. E., A total-synthesis framework for the construction of high-order colloidal hybrid nanoparticles. *Nature Chemistry* **2012**, *4*, 37-44.
- [4] Peyratout, C. S.; Dahne, L., Tailor-made polyelectrolyte microcapsules: From multilayers to smart containers. *Angewandte Chemie-International Edition* **2004**, *43*, 3762-3783.
- [5] Johnston, A. P. R.; Such, G. K.; Ng, S. L.; Caruso, F., Challenges facing colloidal delivery systems: From synthesis to the clinic. *Current Opinion in Colloid & Interface Science* **2011**, *16*, 171-181.
- [6] Yan, Y.; Such, G. K.; Johnston, A. P. R.; Lomas, H.; Caruso, F., Toward Therapeutic Delivery with Layer-by-Layer Engineered Particles. *ACS Nano* **2011**, *5*, 4252-4257.
- [7] Lu, Y.; Mei, Y.; Drechsler, M.; Ballauff, M., Thermosensitive core-shell particles as carriers for Ag nanoparticles: Modulating the catalytic activity by a phase

- transition in networks. *Angewandte Chemie-International Edition* **2006**, *45*, 813-816.
- [8] Mei, Y.; Lu, Y.; Polzer, F.; Ballauff, M.; Drechsler, M., Catalytic activity of palladium nanoparticles encapsulated in spherical polyelectrolyte brushes and core-shell microgels. *Chemistry of Materials* **2007**, *19*, 1062-1069.
- [9] Caruso, F.; Caruso, R. A.; Möhwald, H., Nanoengineering of inorganic and hybrid hollow spheres by colloidal templating. *Science* **1998**, *282*, 1111-1114.
- [10] Okubo, M.; Lu, Y.; Wang, Z., Analysis of stepwise heterocoagulation for the preparation of soft core hard shell composite polymer particles. *Colloid and Polymer Science* **1999**, *277*, 77-82.
- [11] Li, H.; Han, J.; Panioukhine, A.; Kumacheva, E., From heterocoagulated colloids to core-shell particles. *Journal of Colloid and Interface Science* **2002**, *255*, 119-128.
- [12] Chen, R.; Pearce, D. J. G.; Fortuna, S.; Cheung, D. L.; Bon, S. A. F., Polymer vesicles with a colloidal armor of nanoparticles. *Journal of the American Chemical Society* **2011**, *133*, 2151-2153.
- [13] Vincent, B.; Young, C. A.; Tadros, T. F., Equilibrium Aspects of Hetero-Flocculation in Mixed Sterically-Stabilized Dispersions. *Faraday Discussions* **1978**, *65*, 296-305.
- [14] Furusawa, K.; Anzai, C., Heterocoagulation Behavior of Polymer Lattices with Spherical Silica. *Colloids and Surfaces* **1992**, *63*, 103-111.
- [15] Harley, S.; Thompson, D. W.; Vincent, B., The Adsorption of Small Particles onto Larger Particles of Opposite Charge - Direct Electron-Microscope Studies. *Colloids and Surfaces* **1992**, *62*, 163-176.
- [16] Li, R.; Yang, X. L.; Li, G. L.; Li, S. N.; Huang, W. Q., Core-corona polymer composite particles by self-assembled heterocoagulation based on a hydrogen-bonding interaction. *Langmuir* **2006**, *22*, 8127-8133.
- [17] Fleming, M. S.; Mandal, T. K.; Walt, D. R., Nanosphere-microsphere assembly: Methods for core-shell materials preparation. *Chemistry of Materials* **2001**, *13*, 2210-2216.
- [18] Ming, W.; Wu, D.; van Benthem, R.; de With, G., Superhydrophobic films from raspberry-like particles. *Nano Letters* **2005**, *5*, 2298-2301.
- [19] Tsai, H. J.; Lee, Y. L., Facile method to fabricate raspberry-like particulate films for superhydrophobic surfaces. *Langmuir* **2007**, *23*, 12687-12692.

- [20] Nayak, S.; Lyon, L. A., Soft nanotechnology with soft nanoparticles. *Angewandte Chemie-International Edition* **2005**, *44*, 7686-7708.
- [21] Kabanov, A. V.; Vinogradov, S. V., Nanogels as Pharmaceutical Carriers: Finite Networks of Infinite Capabilities. *Angewandte Chemie-International Edition* **2009**, *48*, 5418-5429.
- [22] Pelton, R., Temperature-sensitive aqueous microgels. *Advances in Colloid and Interface Science* **2000**, *85*, 1-33.
- [23] Hoare, T.; Pelton, R., Functional group distributions in carboxylic acid containing poly(N-isopropylacrylamide) microgels. *Langmuir* **2004**, *20*, 2123-2133.
- [24] Xu, J. J.; Timmons, A. B.; Pelton, R., N-Vinylformamide as a route to amine-containing latexes and microgels. *Colloid and Polymer Science* **2004**, *282*, 256-263.
- [25] Islam, A. M.; Chowdhry, B. Z.; Snowden, M. J., Temperature-Induced Heteroflocculation in Particulate Colloidal Dispersions. *Journal of Physical Chemistry* **1995**, *99*, 14205-14206.
- [26] Atkin, R.; Bradley, M.; Vincent, B., Core-shell particles having silica cores and pH-responsive poly(vinylpyridine) shells. *Soft Matter* **2005**, *1*, 160-165.
- [27] Agrawal, M.; Rubio-Retama, J.; Zafeiropoulos, N. E.; Gaponik, N.; Gupta, S.; Cimrova, V.; Lesnyak, V.; Lopez-Cabarcos, E.; Tzavalas, S.; Rojas-Reyna, R.; Eychmuller, A.; Stamm, M., Switchable photoluminescence of CdTe nanocrystals by temperature-responsive microgels. *Langmuir* **2008**, *24*, 9820-9824.
- [28] Mrkic, J.; Saunders, B. R., Microgel particles as a matrix for polymerization: A study of poly(N-isopropylacrylamide)-poly(N-methylpyrrole) dispersions. *Journal of Colloid and Interface Science* **2000**, *222*, 75-82.
- [29] Kim, J.-W.; Fernandez-Nieves, A.; Dan, N.; Utada, A. S.; Marquez, M.; Weitz, D. A., Colloidal assembly route for responsive colloidosomes with tunable permeability. *Nano Letters* **2007**, *7*, 2876-2880.
- [30] Dechezelles, J. F.; Malik, V.; Crassous, J. J.; Schurtenberger, P., Hybrid raspberry microgels with tunable thermoresponsive behavior. *Soft Matter* **2013**, *9*, 2798-2802.
- [31] Bridges, A. W.; Singh, N.; Burns, K. L.; Babensee, J. E.; Lyon, L. A.; Garcia, A. J., Reduced acute inflammatory responses to microgel conformal coatings. *Biomaterials* **2008**, *29*, 4605-4615.

- [32] Nolan, C. M.; Serpe, M. J.; Lyon, L. A., Thermally modulated insulin release from microgel thin films. *Biomacromolecules* **2004**, *5*, 1940-1946.
- [33] Serpe, M. J.; Yarmey, K. A.; Nolan, C. M.; Lyon, L. A., Doxorubicin uptake and release from microgel thin films. *Biomacromolecules* **2005**, *6*, 408-413.
- [34] Lyon, L. A.; Debord, J. D.; Debord, S. B.; Jones, C. D.; McGrath, J. G.; Serpe, M. J., Microgel colloidal crystals. *Journal of Physical Chemistry B* **2004**, *108*, 19099-19108.
- [35] Iyer, A. S.; Lyon, L. A., Self-Healing Colloidal Crystals. *Angewandte Chemie-International Edition* **2009**, *48*, 4562-4566.
- [36] Meng, Z.; Cho, J. K.; Breedveld, V.; Lyon, L. A., Physical aging and phase behavior of multiresponsive microgel colloidal dispersions. *The Journal of Physical Chemistry. B* **2009**, *113*, 4590-4599.
- [37] Serpe, M. J.; Jones, C. D.; Lyon, L. A., Layer-by-layer deposition of thermoresponsive microgel thin films. *Langmuir* **2003**, *19*, 8759-8764.
- [38] St John, A. N.; Breedveld, V.; Lyon, L. A., Phase behavior in highly concentrated assemblies of microgels with soft repulsive interaction potentials. *Journal of Physical Chemistry B* **2007**, *111*, 7796-7801.
- [39] Debord, S. B. Phase Behavior of Multiresponsive Microgel Dispersions. Ph.D. Thesis, Georgia Institute of Technology, Atlanta, GA, 2006.
- [40] Debord, J. D.; Eustis, S.; Debord, S. B.; Lofye, M. T.; Lyon, L. A., Color-Tunable Colloidal Crystals from Soft Hydrogel Nanoparticles. *Advanced Materials* **2002**, *14*, 658-662.
- [41] Hermanson, G. T. *Bioconjugate Techniques*; Academic Press: San Diego, CA, 1996.
- [42] Singh, N.; Bridges, A. W.; Garcia, A. J.; Lyon, L. A., Covalent tethering of functional microgel films onto poly(ethylene terephthalate) surfaces. *Biomacromolecules* **2007**, *8*, 3271-3275.
- [43] Ngai, T.; Auweter, H.; Behrens, S. H., Environmental responsiveness of microgel particles and particle-stabilized emulsions. *Macromolecules* **2006**, *39*, 8171-8177.
- [44] Balmer, J. A.; Armes, S. P.; Fowler, P. W.; Tarnai, T.; Gaspar, Z.; Murray, K. A.; Williams, N. S. J., Packing Efficiency of Small Silica Particles on Large Latex Particles: A Facile Route to Colloidal Nanocomposites. *Langmuir* **2009**, *25*, 5339-5347.

- [45] Sloane, N. J. A.; Hardin, R. H.; Smith, W. D., Tables of Spherical Codes, published electronically at www.research.att.com/~njas/packings/.
- [46] Romeo, G.; Imperiali, L.; Kim, J. W.; Fernandez-Nieves, A.; Weitz, D. A., Origin of de-swelling and dynamics of dense ionic microgel suspensions. *Journal of Chemical Physics* **2012**, *136*, 124905.
- [47] Holmqvist, P.; Mohanty, P. S.; Nagele, G.; Schurtenberger, P.; Heinen, M., Structure and Dynamics of Loosely Cross-Linked Ionic Microgel Dispersions in the Fluid Regime. *Physical Review Letters* **2012**, *109*, 048302.
- [48] Destribats, M.; Lapeyre, V.; Wolfs, M.; Sellier, E.; Leal-Calderon, F.; Ravaine, V.; Schmitt, V., Soft microgels as Pickering emulsion stabilisers: role of particle deformability. *Soft Matter* **2011**, *7*, 7689-7698.
- [49] Geisel, K.; Isa, L.; Richtering, W., Unraveling the 3D Localization and Deformation of Responsive Microgels at Oil/Water Interfaces: A Step Forward in Understanding Soft Emulsion Stabilizers. *Langmuir* **2012**, *28*, 15770-15776.
- [50] Schmidt, S.; Liu, T. T.; Rutten, S.; Phan, K. H.; Moller, M.; Richtering, W., Influence of Microgel Architecture and Oil Polarity on Stabilization of Emulsions by Stimuli-Sensitive Core-Shell Poly(N-isopropylacrylamide-co-methacrylic acid) Microgels: Mickering versus Pickering Behavior? *Langmuir* **2011**, *27*, 9801-9806.

CHAPTER 5

DAMAGE AND HEALING IN MICROGEL MULTILAYER FILMS

Adapted from

Gaulding, J. C., Spears, M. W., and Lyon, L. A. Plastic Deformation, Wrinkling, and Recovery in Microgel Multi-layered Films. *Polymer Chemistry*. Online Ahead of Print.

DOI: 10.1039/C3PY00173C

Reproduced by permission of The Royal Society of Chemistry

5.1. Introduction

Self-healing materials are particularly desirable in applications where the integrity of a material or coating is crucial to its performance, especially if the material is to be used for long durations. Biological materials provide inspiration for design of self-healing structures because living systems have innate ability to sense and repair damage in order to restore functionality to the injured site. Accomplishing this feat with synthetic materials is a major challenge for current research, and requires thoughtful control over the underlying chemistry, configuration, and mechanical properties of the materials. Consequently, there is no “one-size-fits-all” approach to the development of self-healing materials, as different applications have very different material demands.¹⁻⁵

Several distinctions can be made between types of self-healing materials. Autonomic self-healing materials are able to self-repair in the absence of an external trigger. Some of the best known examples feature encapsulated catalysts and monomers contained within a matrix, such that damage to the matrix leads to capsule rupture, catalyst and monomer mixing, polymerization, and thus restoration of matrix integrity.⁶ Taking a step towards bio-inspiration, this concept has been more recently extended such that two-phase microvasculature serves to deliver the necessary components for healing.⁷

Materials that require the input of energy, typically in the form of heat or light, in order to begin repair are referred to as “non-autonomic.”⁴ Their self-healing capabilities originate from the dynamic (and typically non-covalent) interactions that serve to reversibly connect their substituents. The external trigger often serves to fluidize or decrease the viscosity of the system or alter the equilibrium towards reactive, unconnected species. Removal of the stimulus resets the connected, original state. Some examples of reversible chemistries that have been used in self-healing systems include Diels-Alder reactions,⁸⁻¹⁰ π - π interactions,^{11,12} disulfide linkages,^{13,14} trithiocarbonates,^{15, 16} hydrogen bonding,¹⁷⁻²⁰ metal complexes,^{21,22} ion-pairing^{23,24} and even systems using combinations of strategies.²⁵

Our group has previously described thin films composed of anionic hydrogel microparticles (microgels) cross-linked by linear polycations and assembled using layer-by-layer techniques.^{26,27} An intriguing finding is that when such films are deposited on elastomeric substrates, they undergo autonomic self-healing in aqueous media in response to damage events such as bending, stretching, or mechanical “poking”, leading to restoration of the initial film integrity.²⁸ Further investigation of such films found that their mechanical properties could be reinforced by gold nanoparticles.²⁹ The initial discovery of this self-healing behavior was a serendipitous result of studying the deposition of microgel-based films onto elastomeric substrates.²⁸ However, none of the studies so far have offered a great deal of insight into the mechanism of film damage or what drives restoration of film integrity following damaging events. In the work described in this chapter, we elucidate key factors in understanding the mechanical origins of this damage, as well as the drivers that promote rapid self-healing. In addition, we study the applicability of this healing effect to a range of film compositions.

5.2. Experimental

5.2.1. Materials

All common materials were sourced and used as described in **Chapter 2**. Additionally, reagents acrylic acid (AAc), monobasic sodium phosphate (NaH_2PO_4), sodium chloride, magnesium nitrate hexahydrate, potassium chloride, hydrochloric acid, (3-aminopropyl)trimethoxysilane (APTMS), *N*-(3-dimethylaminopropyl)-*N*'-ethylcarbodiimide hydrochloride (EDC), *N*-hydroxysuccinimide (NHS), and 2-(*N*-morpholino)ethanesulfonic acid (MES) were used as received. Solutions of 20% w/w PDADMAC in water with molecular weights of 100-200 kDa and 400-500 kDa were used as received.

5.2.2. Microgel Synthesis

Microgels were synthesized using previously described aqueous precipitation polymerization methods.³⁰ Anionic microgels were prepared by dissolving NIPAm, BIS, (100 mM total monomer concentration) and SDS (0.17 mM) in 100-mL of deionized water. The solution was filtered through a 0.2 μm syringe filter, heated to 70 °C, and purged with N_2 for one hour. AAc was added 10 minutes before initiation of the reaction, which was achieved with 1 mM APS. The reaction was carried out under a N_2 atmosphere for 4 hours with constant stirring. All syntheses were filtered through glass wool to remove coagulum and then subjected to at least 4 rounds of centrifugation and resuspension in distilled water. Finally, all syntheses were lyophilized for 72 hours before use.

5.2.3. Microgel Characterization

Microgel hydrodynamic radii (r_h) were measured using DLS, using instrumentation detailed in **Chapter 2**. All DLS measurements were carried out at 20 °C in either 10 mM PBS at pH 7.4 and 15 mM ionic strength or 10 mM formate buffer at pH

3.0 with 15 mM ionic strength to confirm pH responsivity. The composition, sizes, and pH responsivity of the recovered microgels are presented in **Table 5.1**.

Table 5.1. Microgel Characterization

NIPAm, mol %	AAc, mol %	BIS, mol%	r_h , nm (pH 3.0) ^a	r_h , nm (pH 7.4) ^a
68	30	2	337	629
88	10	2	269	413

^aSizes determined via dynamic light scattering, reported at 20 °C in buffer with 15 mM ionic strength

5.2.4. Substrate Preparation

Films were constructed using layer-by-layer techniques (LbL) previously described by our group.²⁸ Briefly, poly(dimethylsiloxane) (PDMS) was mixed in a 10:1 ratio by weight of elastomer to curing agent (Sylgard 184 Silicone Elastomer Kit, Dow Corning), degassed for 30 minutes, and cured at 50 °C overnight. Cured PDMS was cut into 9 × 18 mm pieces, equilibrated in hexane for 2 hours, and again incubated at 50 °C in an oven for 2 hours to remove hexane. Pieces were stored in individual Eppendorf tubes filled with water until further use. Prior to use, the water was removed and replaced with 1.2 M HCl for approximately sixteen hours. The pieces were then removed, washed 3 times with water, washed 2 times with absolute ethanol, and shaken in absolute ethanol for 30 minutes. Finally, the pieces were removed and placed in a separate solution of 1% APTMS in absolute ethanol for 2 hours while shaking. Once removed, the pieces were rinsed with water, at which point they were ready for LbL coating.

5.2.5. Film Construction

Films were constructed using an LbL approach described previously.^{26,28} Briefly, prepared substrates were placed in well plates and covered with a 0.1 mg/mL solution of microgels in pH 7.4 PBS. The plates were centrifuged with an Eppendorf 5804 R centrifuge in a microwell plate rotor at $2250 \times g$ for 10 minutes. The substrates were then removed and rinsed with water. The microgels were covalently coupled to the substrate using a carbodiimide coupling reaction using 2 mM EDC and 5 mM NHS in 10 mM MES pH 5.7 buffer for 2 hours. The microgel-modified substrates were then shaken in a solution of polycation for 30 min in either 100-200 kDa or 400-500 kDa Mw PDADMAC at a concentration of 0.1 monoM in PBS, and the layer-by-layer process was repeated up to 8 layers of microgels.

5.2.6. Film Stretching

Films were loaded into a homemade stretching apparatus that allowed precise mechanical control over the degree of strain applied to the substrate, as depicted in **Figure 5.1**. Coated PDMS substrates were clamped at both ends between glass plates connected to a micrometer-controlled, single-axis translation stage. The film was parallel to the floor with the coated side up. Before applying a stress, the exposed film area was wet with distilled water for at least 1 minute to heal any damage associated with handling, dried with nitrogen, and measured along the stretching axis.

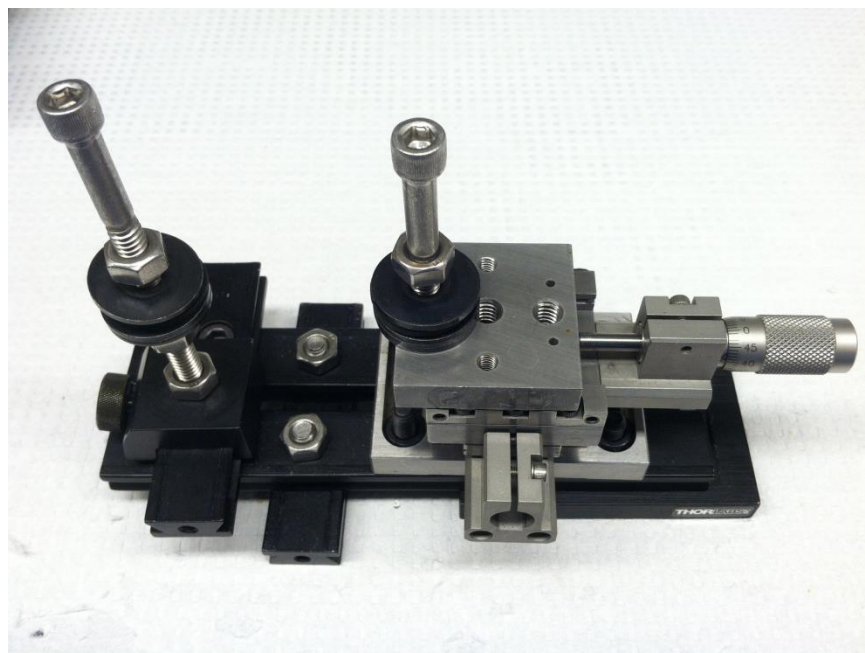


Figure 5.1. The apparatus used to stretch microgel films on flexible substrates. The sample is clamped between glass slides and held in place by rubber washers. The left post is stationary while the right is attached to a micrometer-controlled translational stage that allows precise movement, allowing controlled strain to be applied to the films.

5.2.7. Film Characterization and Analysis

Brightfield microscopy images at 40x or 100x magnification were captured on the Olympus IX-70 inverted microscope described in **Chapter 4**. Atomic force microscopy images were captured on an Asylum Research (Santa Barbara, CA) MFP-3D AFM in AC-mode. The resultant images were analyzed using the MFP-3D software written in the IgorPro software environment (WaveMetrics, Inc, Lake Oswego, OR). Cantilevers for the Asylum instrument were operated in tapping mode and were Si-SPM with Al reflex coating, 42 N/m force constant, model NCHR purchased from NANOWORLD (Neuchâtel, Switzerland). Atomic force microscopy images of films under stress were captured using a Nanosurf (Boston, MA) EasyScan 2 AFM. Cantilevers used with the Nanosurf were operated in tapping mode and were Si, N-type with Al reflex coating, 45 N/m nominal force constant, model ACLA purchased from APPNANO (Santa Clara, CA). The Nanosurf scan head was positioned on top of the stretching apparatus to

suspend the tip over a mounted sample. The scan head imaged at an angle 45 degrees relative to the axis of stretching. Collected images were analyzed using analysis tools in the Nanosurf AFM software (v. 3.0.2.4) to determine root-mean-square (RMS) roughness, with values reported as the average \pm SD of four $20 \times 20 \mu\text{m}$ regions.

5.2.8. Steam Healing

A 200-mL beaker was filled with approximately 170 mL of DI water. The water was heated until steam was visibly rising from the surface. Microgel films were damaged by pressing a plastic pipette tip against the film and gently dragging the tip across the coating, such that a mark was clearly visible. The sample was then suspended above the steaming beaker, film side down, for a period of five seconds.

5.2.9. Healing Driven By Relative Humidity

To prepare the high relative humidity environment, two petri dishes were filled with DI water, placed within slightly larger petri dishes to minimize spills, and placed within a sealed 2-gallon plastic bag. This bag was sealed within a second bag, and allowed to equilibrate. An Acu-Rite relative humidity sensor was sealed along with the petri dishes and allowed monitoring of the humidity within the inner bag. The inner bag was allowed to equilibrate until humidity measured within the bag exceeded 80%. To observe intermediate humidity states, saturated solutions were prepared by adding the following masses to approximately 80 mL of deionized water in a 100-mL beaker, such that undissolved solids coated the bottom of the beakers: 71 g magnesium nitrate hexahydrate (55% relative humidity), 30 g sodium chloride (73% relative humidity), 36 g potassium chloride (78% relative humidity). These were again sealed within two bags and allowed to equilibrate to the steady state humidity value. Films that were damaged either through controlled stretching or pipette scratching (as described above) were placed in open-topped 6-well plates, then placed within the inner bag of the humidity

chamber. Films could be monitored visually during healing, and were removed after one hour for further characterization.

5.2.10. Film Thickness

Cleaned glass coverslips were functionalized using 1% v/v APTMS in absolute ethanol, then incubated overnight. Following rinsing and incubation in PBS for 30 minutes, film assembly proceeded as described for the PDMS substrates above, creating films with identical composition. A clean razor blade was used to scratch the surface of the films, exposing the glass substrate. The region of the scratch was imaged using the Asylum MFP-3D AFM. Film thicknesses for hydrated films were determined using the iDrive accessory for the MFP3D after incubating the scratched area in deionized water for a minimum of thirty minutes. The iDrive cantilevers were silicon nitride coated with Cr/Au with nominal spring constant of 0.02 N/m (Asylum Research, Santa Barbara, CA). All images were collected at 512×512 scan resolution. The resultant images of the film scratches were analyzed by averaging the results from 150 line traces wherein the surface of the film and the glass substrate were clearly discernible, then the height difference between the substrate and film used to determine the thickness.

5.3. Results and Discussion

5.3.1. Film Damage

Stretching microgel multilayered films on elastomeric substrates had previously been shown to result in a series of parallel cracks perpendicular to the axis of applied stress. These cracks subsequently disappear upon immersion in water.^{28,29} Though these results demonstrate the reversibility of even large-scale damage, the origin of these parallel cracks was unclear, with two prevailing hypotheses being that they arose due to cracking of the microgel film under the applied stress (e.g. the films are brittle), or that the films underwent plastic deformation as the degree of strain was increased (e.g. the

films are deformable). The Nanosurf's compact scanning head allowed it to be stationed atop the stretching apparatus and thus allowed the surface topography of the films to be monitored *in situ* under applied stress in order to ascertain the origin of the cracking or wrinkling pattern.

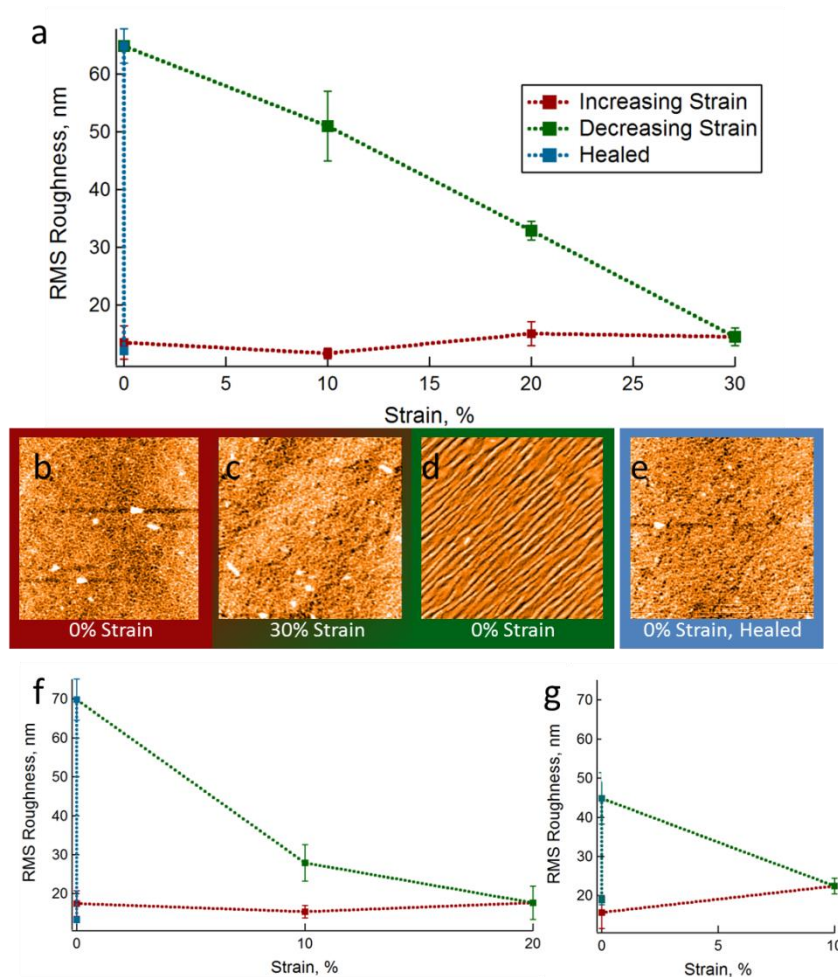


Figure 5.2. a, f, g) RMS roughness as a function of applied strain for 8-layer 30% AAc microgels/400-500 kDa PDADMAC films. Maximal strain a) 30%, f) 20%, g) 10%. b-e) Representative AFM images obtained during *in situ* stretching of the films. Film roughness remains relatively constant as the degree of strain increases (b, c), then buckling occurs as the stress is removed (c, d). Wetting of the films leads to restoration of the initial roughness (d, e). All AFM images are $40\ \mu\text{m} \times 40\ \mu\text{m}$.

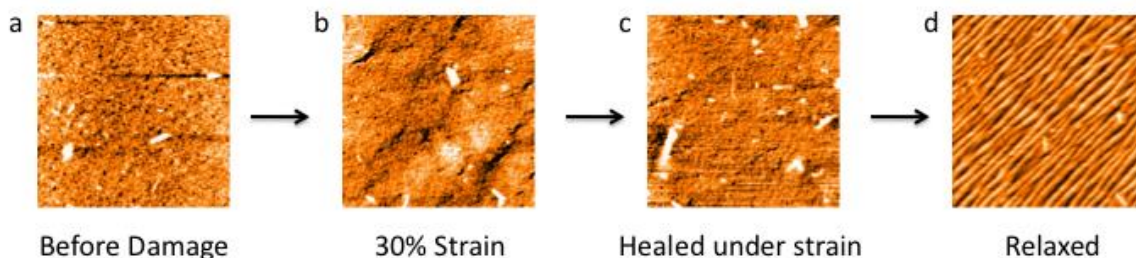


Figure 5.3. Film healed under stress. a) Film before damage displays a smooth surface with low roughness. b) Application of 30% strain does not result in a large change in surface topography. c) Film exposed to water while under strain also has a smooth surface with low roughness. d) When stress is removed from the film, the characteristic buckling behavior results. All AFM images are $40\ \mu\text{m} \times 40\ \mu\text{m}$.

As shown in **Figure 5.2**, the RMS roughness of the film as a function of applied stress remains relatively constant as the degree of strain is increased. As the stress is released, however, the parallel cracking pattern appears and results in an increase in the RMS roughness. Roughness continues to increase as stress is removed, until restoration of the zero-strain state. At that point, wetting and subsequent drying of the film leads to the characteristic healing response, and the RMS roughness returns to its baseline level as the wrinkled pattern disappears. The same pattern is observed even when lower degrees of maximal strain are applied (**Figure 5.2f, g**), as the roughness begins to increase only when the strain is removed. Additionally, stretching the film to 30% strain, then exposing to water, as shown in **Figure 5.3**, revealed minimal changes in surface topography. Relaxation of the stress from this state leads to the same wrinkling pattern as that observed without the intermediate wetting step.

Further *in situ* investigation of the stretched film revealed additional evidence that the wrinkling pattern is the result of a plastic deformation. **Figure 5.4** reveals that as an undamaged film is subjected to 30% strain and then relaxed, the characteristic buckling pattern appears. Returning that film to 30% strain without healing leaves wrinkles behind, with the wrinkling pattern lying orthogonal to the original pattern. The wrinkles seen upon initial relaxation of the film are always observed to lie on the diagonal from the bottom left of the image to the top right, due to the Nanosurf's 45 degree angle of

imaging (see **Figure 5.2**, for example). This corresponds to wrinkles that are perpendicular to the stretching direction, suggesting buckling behavior. However, when a film was re-stretched to 30% strain without a healing step, the lines were observed to lie along the opposite diagonal (**Figure 5.4d**), indicative that the wrinkles are now parallel to the axis of stretching. We attribute this change in direction to the elongation and compression forces that the film experiences during stretching on an elastomeric substrate. As PDMS is stretched, it elongates along one axis and compresses along the perpendicular axes (Poisson ratio = 0.5).³¹ Therefore, if we assume that the entire film undergoes some deformation during the initial stretching event, the in-plane film axis perpendicular to the initial stretching axis is actually under compression during a second stretching event, thereby resulting in a new wrinkling pattern perpendicular to the axis of the second stretch. As seen in **Figure 5.4e**, this pattern persists following multiple rounds of film stretching and relaxation.

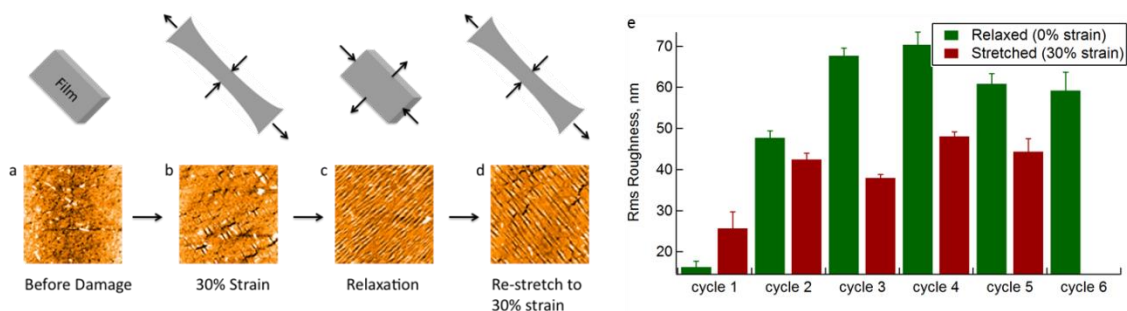


Figure 5.4. Cycles of stretching of microgel films leads to sensitivity to perpendicular compression. a) Film under 0% strain, before cycling, b) 30% strain leads to compression along the short axis, perpendicular to the applied stress, c) the film is relaxed back to 0% strain; during relaxation, the film is effectively being compressed along the long axis, d) 30% elongation is reapplied with compression again introduced along the short axis. e) This pattern persists through multiple cycles of stretching when the film is not healed. All AFM images are $40\ \mu\text{m} \times 40\ \mu\text{m}$.

The above evidence supports the conclusion that the observed damage pattern arises from plastic deformation (stretching) when the film is under linear stress, followed by film wrinkling as the stress is removed. Upon stretching, the total area of the film

increases to accommodate the stretching of the elastomeric substrate. Removing the stress reduces the effective area of the substrate, while the film lacks the elasticity needed to return to its original area, thus resulting in wrinkling. In contrast, observation of cracking in the films as stress was applied would have indicated strain-induced cracking as the origin of the observed damage pattern.

It is illustrative to think of the microparticulate structure of the films when considering the origin of the differential responses to elongation versus compression. The multilayered film consists of anionic polymer nanoparticles cross-linked Coulombically with highly-charged, linear polycation chains. Consequently, the individual particles have their own elastic properties, and connectivity to neighboring particles in the film is through a strong, though non-covalent (charge-based) interaction. As stress is applied, the Coulombic interactions between discrete acid sites on the microgels and individual monomer units of PDADMAC would seem to be the weakest link, and these interactions may be sacrificed in favor of an altered ion pairing structure that allows for an increase in film dimension along the stretching axis. Upon removal of the elongational stress, the original ion pairing arrangement does not recover, and the now elongated film simply wrinkles to accommodate the elastic recovery of the substrate. The polymer and ion mobility that occurs during hydration of the film then allows restoration of the smooth, low-energy confirmation.

5.3.2. Film Healing

The rapidity with which damage to microgel multilayered films is resolved upon immersion in water has limited our ability to observe the stages of the healing process, and thus limited our understanding what drives self-healing. In an attempt to reduce the influence of passing the film across the air/water interface during immersion, film healing was attempted by exposure to the high relative humidity above a steaming beaker of water. As can be seen in **Figure 5.5**, this too leads to the complete restoration of film

integrity following damage by a plastic pipette tip. Once again, this response is rapid, requiring less than five seconds of exposure to steam (a video depicting the rapid healing is available online: <http://www.rsc.org/suppdata/py/c3/c3py00173c/c3py00173c.m4v>). This finding suggests that immersion is unnecessary, as is the need for bulk water; surface hydration is sufficient to effect healing.

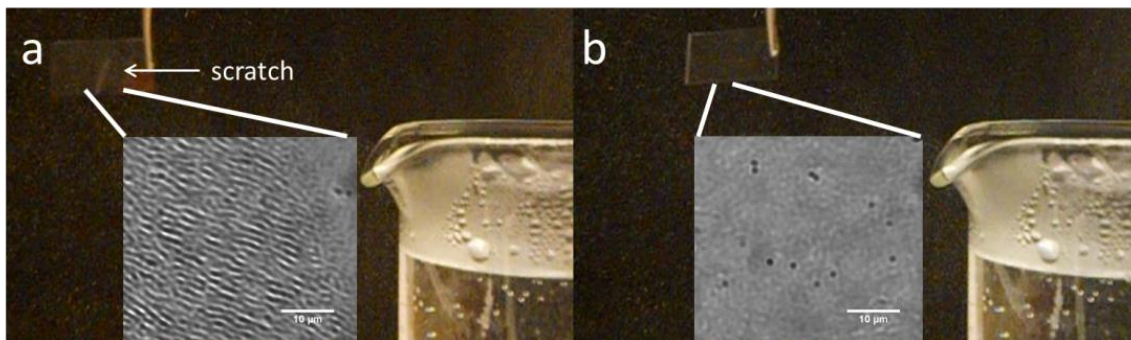


Figure 5.5. Damage induced by scratching an 8-layer 30% AAc microgels / 400-500 kDa PDADMAC film rapidly heals in response to steam. a) Scratched film before healing b) Film exposed to steam for 5 seconds. Insets: microscopy of the scratched region before and after. Scale bars are 10 μm .

Having ascertained that water vapor was sufficient to heal film damage, we next sought to determine what level of ambient humidity was necessary to drive fully autonomous film healing. We explored the effects of intermediate humidity on films that had been stretched by 20%, thereby damaging the entire film area. These films were then placed them into sealed environments with controlled relative humidity, ranging from 55-84% by RH sensor. As shown in **Figure 5.6e**, little effect is observed in films at 55% relative humidity. At 73% humidity, in **Figure 5.6f**, the films seem to have almost completely healed – the wrinkled pattern has nearly disappeared, but small parallel lines are still discernible. When exposed to higher relative humidity, as in **Figure 5.6g & h**, the films do not show any remnant wrinkling. This suggests that the films are sufficiently hygroscopic to imbibe enough ambient water under high humidity conditions to effect the requisite polymer mobility for healing to occur. This hydration of the film leads to swelling, which in and of itself necessitates a rearrangement of the microgels and

polycation in the film. The intermediate state visible in **Figure 5.6f** suggests that healing proceeds first in the dimension normal to the plane of the film, since the intensity of the wrinkles diminishes as the film progresses from a wrinkled to a smooth state, as opposed to changes in the periodicity or width of the wrinkled features. This ability to drive film healing based on ambient humidity levels suggests that these coatings may be autonomous in high humidity environments, making them “equatorial-” or “rainy-day-” autonomous.

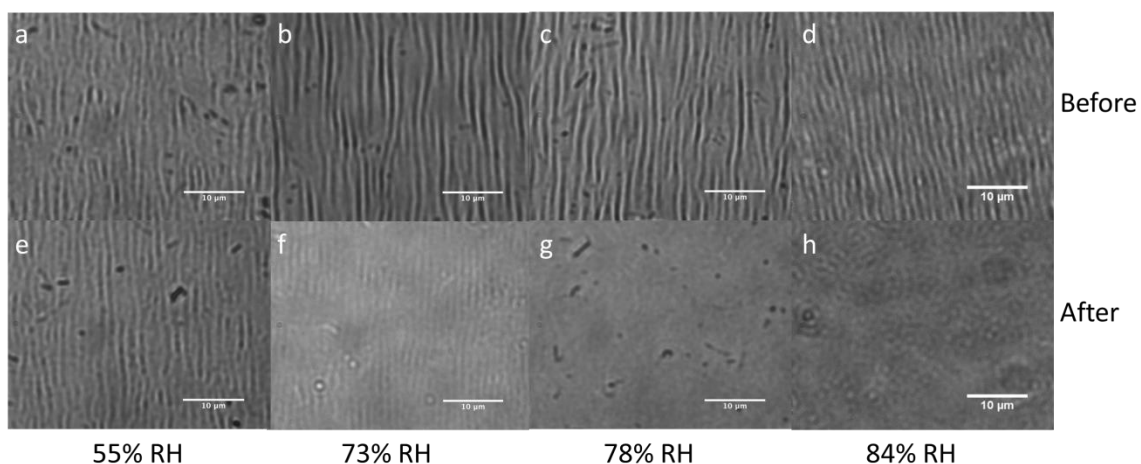


Figure 5.6. a – d) Damage caused by applying 20% strain to 8-layer 30% AAc microgels / 400-500 kDa PDADMAC films. Film recovery following one hour exposure to e) 55% relative humidity, f) 73% relative humidity, g) 78% relative humidity, h) 84% relative humidity. Little change is noted at 55%, while slight remnant damage is visible at 73%. Complete recovery proceeds at 78% or higher. Scale bar in all images is 10 μm .

Hydration and swelling of an individual microgel is very rapid because of its relatively small dimensions, occurring within fractions of a second.^{32,33} Swelling therefore may provide the driving force responsible for the rapidity with which film integrity is restored. Film thickness measurements comparing the dry and wet thickness of multilayered films are shown in **Figure 5.7**. Films composed of 30% AAc microgels cross-linked with 400-500 kDa PDADMAC (8 microgel layers) have a typical dry thickness of approximately 75 nm, while film swelling leads to a greater than four-fold

increase in film thickness to approximately 350 nm. As observed by AFM, and shown in **Figure 5.8**, wrinkling damage induced by pipette damage to the films leads to a feature size of the damage on the order of 100 nm. As a result, swelling of the film leads to a greater overall change in the film thickness than that which is introduced by damage. The rearrangement of polymer chains in the microgels and polycation within the film accompanying swelling are likely responsible for restoration of the overall film integrity.

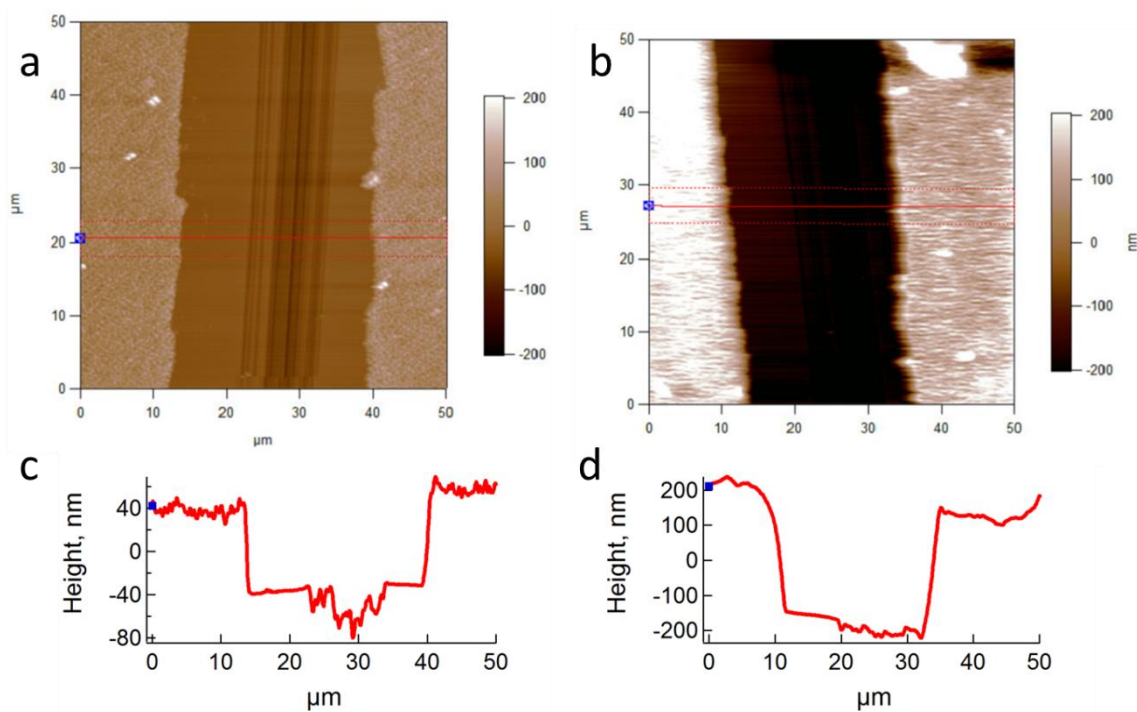


Figure 5.7. Representative images used to determine film thickness for a) dry films and b) wet films. Scan sizes are $50\ \mu\text{m} \times 50\ \mu\text{m}$. The red line and two dashed red lines define the area wherein 50 scan lines are averaged, and depicted in c) and d) for a) & b), respectively. The height difference was determined between the film and glass at three points in each image.

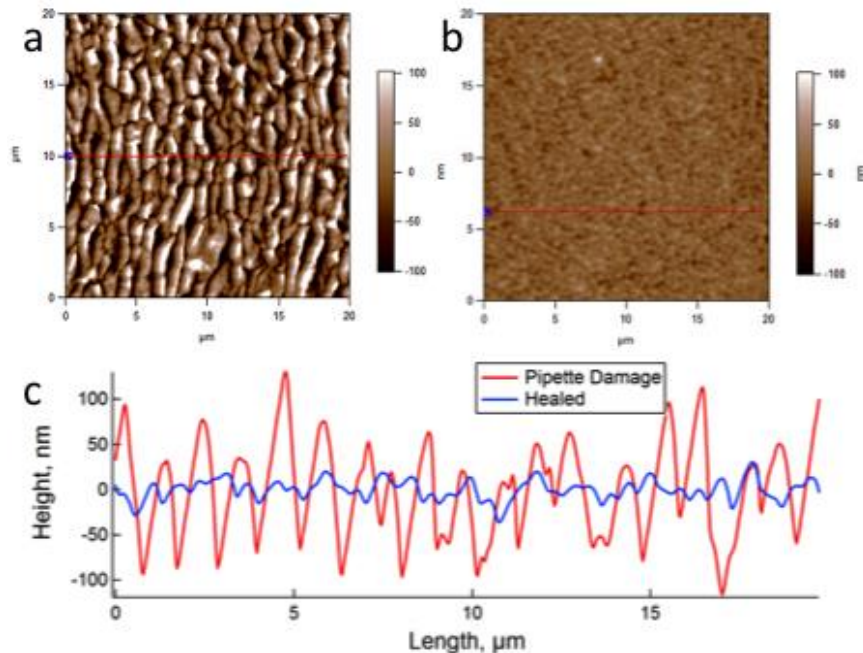


Figure 5.8. a) Damage induced by pipette in an 8-layer 30% AAc/ 400-500 kDA PDADMAC film. b) After being exposed to an 83% relative humidity environment for one hour. Both AFM images are 20 x 20 μm . c) Line traces across the two images reveal the characteristic roughness associated with damaged and healed films.

5.3.3. Film Composition

To test the generalizability of the self-healing phenomenon in microgel multilayered films, we explored changes in the charge density and distribution in the films. Recently other examples of self-healing polyelectrolyte multilayer assemblies driven by water addition have been demonstrated,^{23,24} suggesting charge pairing and ion mobility are an important component of the self-healing characteristics. We explored the effects of particle charge density by reducing the AAc content of pNIPAm-AAc microgels from 30 to 10%. Additionally, film connectivity can be manipulated by changing the length of the PDADMAC used during assembly. The longer polymer chains associated with higher molecular weight polycation results in limited penetration into the microgel network,³⁴ as well as serving to cross-link neighboring microgels. As such, one would also anticipate that higher molecular weights would tend to lead to higher levels of microgel-to-microgel cross-linking within the films; shorter chains should result in poorer

connectivity. The molecular weights of PDADMAC used in this work, 100-200 kDa and 400-500 kDa, would have estimated end-to-end distances ranging from 15 - 21 nm and 31 - 34 nm, respectively. As shown in **Figure 5.9**, using lower AAc content microgels and shorter PDADMAC still leads to the formation of self-healing microgel multilayers, as neither the reduced acid content nor the shorter polycation disrupts connectivity sufficiently for the self-healing characteristic to be suppressed.

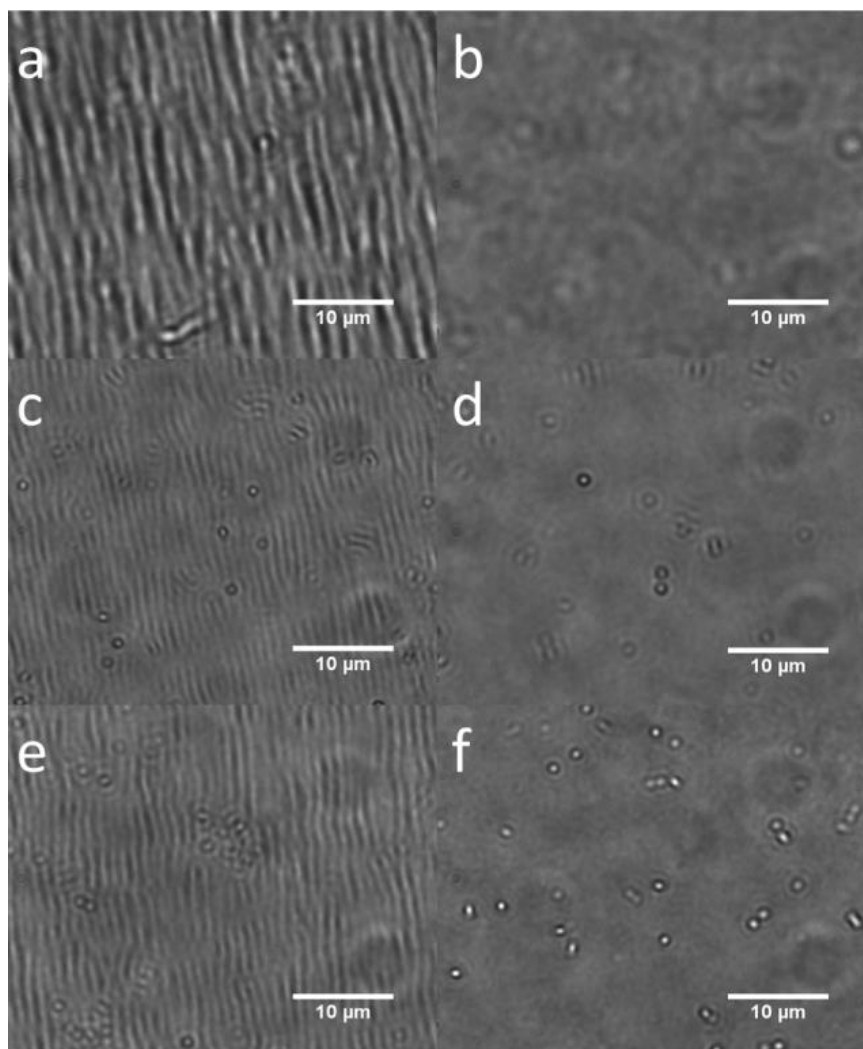


Figure 5.9. a, b) 8-layer 30% AAc microgel films cross-linked with 100-200 kDa PDADMAC. c, d) 10% AAc microgel films cross-linked with 100-200 kDa PDADMAC. e, f) 10% AAc microgel films cross-linked with 400-500 kDa PDADMAC. a, c, e) Films subjected to 20% strain, then relaxed. b, d, f) Films heal after being exposed to 84% relative humidity for one hour. Scale bars in all images are 10 μm .

5.4. Conclusions and Outlook

In this work, we have demonstrated that microgel multilayered films undergo plastic deformation in response to elongation, as evidenced by the onset of a characteristic buckling pattern upon removal of the linear stress. Additionally, the rapid healing response of the microgel films does not require immersion in water as exposure to a relative humidity greater than 75% is sufficient to promote healing. This suggests that film swelling is a key driving force in the rearrangement of polymer within the film, and hence healing. Finally, the generality of the self-healing phenomenon for microgel multilayer films has been extended to lower acid content and shorter polycation, both of which reduce film connectivity. Taken together, it is clear that microgel multilayered films represent a dynamic and intriguing approach to self-healing materials, and that better understanding of the fundamental parameters of these assemblies will aid in their future applications.

5.5. References

- [1] Bergman, S. D.; Wudl, F., Mendable polymers. *Journal of Materials Chemistry* **2008**, *18*, 41-62.
- [2] Burattini, S.; Greenland, B. W.; Chappell, D.; Colquhoun, H. M.; Hayes, W., Healable polymeric materials: a tutorial review. *Chemical Society Reviews* **2010**, *39*, 1973-1985.
- [3] Syrett, J. A.; Becer, C. R.; Haddleton, D. M., Self-healing and self-mendable polymers. *Polymer Chemistry* **2010**, *1*, 978-987.
- [4] Hager, M. D.; Greil, P.; Leyens, C.; van der Zwaag, S.; Schubert, U. S., Self-Healing Materials. *Advanced Materials* **2010**, *22*, 5424-5430.
- [5] van Gemert, G. M. L.; Peeters, J. W.; Sontjens, S. H. M.; Janssen, H. M.; Bosman, A. W., Self-Healing Supramolecular Polymers In Action. *Macromolecular Chemistry and Physics* **2012**, *213*, 234-242.
- [6] White, S. R.; Sottos, N. R.; Geubelle, P. H.; Moore, J. S.; Kessler, M. R.; Sriram, S. R.; Brown, E. N.; Viswanathan, S., Autonomic healing of polymer composites. *Nature* **2001**, *409*, 794-797.

- [7] Toohey, K. S.; Sottos, N. R.; Lewis, J. A.; Moore, J. S.; White, S. R., Self-healing materials with microvascular networks. *Nature Materials* **2007**, *6*, 581-585.
- [8] Chen, X. X.; Wudl, F.; Mal, A. K.; Shen, H. B.; Nutt, S. R., New thermally remendable highly cross-linked polymeric materials. *Macromolecules* **2003**, *36*, 1802-1807.
- [9] Reutenauer, P.; Buhler, E.; Boul, P. J.; Candau, S. J.; Lehn, J. M., Room Temperature Dynamic Polymers Based on Diels-Alder Chemistry. *Chemistry-a European Journal* **2009**, *15*, 1893-1900.
- [10] Syrett, J. A.; Mantovani, G.; Barton, W. R. S.; Price, D.; Haddleton, D. M., Self-healing polymers prepared via living radical polymerisation. *Polymer Chemistry* **2010**, *1*, 102-106.
- [11] Burattini, S.; Colquhoun, H. M.; Greenland, B. W.; Hayes, W., A novel self-healing supramolecular polymer system. *Faraday Discussions* **2009**, *143*, 251-264.
- [12] Burattini, S.; Colquhoun, H. M.; Fox, J. D.; Friedmann, D.; Greenland, B. W.; Harris, P. J. F.; Hayes, W.; Mackay, M. E.; Rowan, S. J., A self-repairing, supramolecular polymer system: healability as a consequence of donor-acceptor pi-pi stacking interactions. *Chemical Communications* **2009**, 6717-6719.
- [13] Canadell, J.; Goossens, H.; Klumperman, B., Self-Healing Materials Based on Disulfide Links. *Macromolecules* **2011**, *44*, 2536-2541.
- [14] Yoon, J. A.; Kamada, J.; Koynov, K.; Mohin, J.; Nicolay, R.; Zhang, Y. Z.; Balazs, A. C.; Kowalewski, T.; Matyjaszewski, K., Self-Healing Polymer Films Based on Thiol-Disulfide Exchange Reactions and Self-Healing Kinetics Measured Using Atomic Force Microscopy. *Macromolecules* **2012**, *45*, 142-149.
- [15] Nicolay, R.; Kamada, J.; Van Wassen, A.; Matyjaszewski, K., Responsive Gels Based on a Dynamic Covalent Trithiocarbonate Cross-Linker. *Macromolecules* **2010**, *43*, 4355-4361.
- [16] Amamoto, Y.; Kamada, J.; Otsuka, H.; Takahara, A.; Matyjaszewski, K., Repeatable Photoinduced Self-Healing of Covalently Cross-linked Polymers through Reshuffling of Trithiocarbonate Units. *Angewandte Chemie-International Edition* **2011**, *50*, 1660-1663.
- [17] Cordier, P.; Tournilhac, F.; Soulie-Ziakovic, C.; Leibler, L., Self-healing and thermoreversible rubber from supramolecular assembly. *Nature* **2008**, *451*, 977-980.

- [18] Chen, Y. L.; Kushner, A. M.; Williams, G. A.; Guan, Z. B., Multiphase design of autonomic self-healing thermoplastic elastomers. *Nature Chemistry* **2012**, *4*, 467-472.
- [19] Cui, J. X.; del Campo, A., Multivalent H-bonds for self-healing hydrogels. *Chemical Communications* **2012**, *48*, 9302-9304.
- [20] Phadke, A.; Zhang, C.; Arman, B.; Hsu, C. C.; Mashelkar, R. A.; Lele, A. K.; Tauber, M. J.; Arya, G.; Varghese, S., Rapid self-healing hydrogels. *Proceedings of the National Academy of Sciences of the United States of America* **2012**, *109*, 4383-4388.
- [21] Burnworth, M.; Tang, L. M.; Kumpfer, J. R.; Duncan, A. J.; Beyer, F. L.; Fiore, G. L.; Rowan, S. J.; Weder, C., Optically healable supramolecular polymers. *Nature* **2011**, *472*, 334-337.
- [22] Yuan, J. C.; Fang, X. L.; Zhang, L. X.; Hong, G. N.; Lin, Y. J.; Zheng, Q. F.; Xu, Y. Z.; Ruan, Y. H.; Weng, W. G.; Xia, H. P.; Chen, G. H., Multi-responsive self-healing metallo-supramolecular gels based on "click" ligand. *Journal of Materials Chemistry* **2012**, *22*, 11515-11522.
- [23] Wang, X.; Liu, F.; Zheng, X. W.; Sun, J. Q., Water-Enabled Self-Healing of Polyelectrolyte Multilayer Coatings. *Angewandte Chemie-International Edition* **2011**, *50*, 11378-11381.
- [24] Li, Y.; Chen, S. S.; Wu, M. C.; Sun, J. Q., Polyelectrolyte Multilayers Impart Healability to Highly Electrically Conductive Films. *Advanced Materials* **2012**, *24*, 4578-4582.
- [25] Deng, G. H.; Li, F. Y.; Yu, H. X.; Liu, F. Y.; Liu, C. Y.; Sun, W. X.; Jiang, H. F.; Chen, Y. M., Dynamic Hydrogels with an Environmental Adaptive Self-Healing Ability and Dual Responsive Sol-Gel Transitions. *ACS Macro Letters* **2012**, *1*, 275-279.
- [26] Serpe, M. J.; Jones, C. D.; Lyon, L. A., Layer-by-layer deposition of thermoresponsive microgel thin films. *Langmuir* **2003**, *19*, 8759-8764.
- [27] South, A. B.; Whitmire, R. E.; Garcia, A. J.; Lyon, L. A., Centrifugal Deposition of Microgels for the Rapid Assembly of Nonfouling Thin Films. *ACS Applied Materials & Interfaces* **2009**, *1*, 2747-2754.
- [28] South, A. B.; Lyon, L. A., Autonomic Self-Healing of Hydrogel Thin Films. *Angewandte Chemie-International Edition* **2010**, *49*, 767-771.

- [29] Park, C. W.; South, A. B.; Hu, X. B.; Verdes, C.; Kim, J. D.; Lyon, L. A., Gold nanoparticles reinforce self-healing microgel multilayers. *Colloid and Polymer Science* **2011**, *289*, 583-590.
- [30] Hendrickson, G. R.; Smith, M. H.; South, A. B.; Lyon, L. A., Design of Multiresponsive Hydrogel Particles and Assemblies. *Advanced Functional Materials* **2010**, *20*, 1697-1712.
- [31] Mark, J. E. *Polymer data handbook*; Oxford University Press: Oxford ; New York, 1998.
- [32] Suarez, I. J.; Fernandez-Nieves, A.; Marquez, M., Swelling kinetics of poly(N-isopropylacrylamide) minigels. *Journal of Physical Chemistry B* **2006**, *110*, 25729-25733.
- [33] Tanaka, T.; Fillmore, D. J., Kinetics of Swelling of Gels. *Journal of Chemical Physics* **1979**, *70*, 1214-1218.
- [34] Kleinen, J.; Klee, A.; Richtering, W., Influence of Architecture on the Interaction of Negatively Charged Multisensitive Poly(N-isopropylacrylamide)-co-Methacrylic Acid Microgels with Oppositely Charged Polyelectrolyte: Absorption vs Adsorption. *Langmuir* **2010**, *26*, 11258-11265.

CHAPTER 6

CELLULAR ADHESION RESISTANT FILMS AND MICROGEL

FILM MOBILITY

6.1. Introduction

6.1.1. Films to Improve Biocompatibility

One of the major challenges facing biomaterials in many applications is the host-immune, or wound-healing, response to implanted materials.¹ The presence of foreign material within a body triggers a cascade of responses that detect, break down and/or isolate the foreign body from the remainder of the host. The evolutionary benefits of such a response have been clearly demonstrated, as this strategy serves to ward off infectious organisms and improves healing from injury. However, modern medicine has progressed such that vital treatments require long-term, intimate contact with physiological fluids; these are the environments most prone to triggering a significant immune response, which for many applications may impede their performance or lead to serious complications for a patient.

Upon exposure of a foreign surface to blood or interstitial fluids, proteins present in the solution, such as albumin, fibronectin, vitronectin, IgG, fibrinogen, and von Willebrand factor, rapidly begin to adsorb.²⁻⁵ These proteins serve to “tag” the foreign material, making it detectable by the host, and triggering a cascade of inflammatory responses.⁵ These proteins mediate interactions with immunological cells, predominantly neutrophils during the acute inflammatory response, and begin the process of attempting to destroy the foreign material.⁴ Chemical signals released by these cells recruit additional cells, such as macrophages and lymphocytes, to the implantation site.^{5,6} Working in concert, the cells attempt to destroy the foreign material through

phagocytosis as well as the extracellular secretion of reactive oxygen species and other chemical degradants.⁷⁻¹⁰ Foreign objects larger than a few microns are unable to be engulfed during phagocytosis, and material that is able to withstand chemical damage does not deter this immune response. If the macrophages are unable to destroy the invading material, they merge and change phenotype to a foreign body giant cell, which eventually serves to form a fibrous capsule consisting of scar tissue, which isolates the implanted material.^{4,5} This capsule is dense and avascular, which leads to numerous complications for a range of medical devices. Some brief examples include:

- diminished pacemaker performance as the leads become electrically isolated from the heart muscle^{11,12}
- pain and discomfort associated with breast implants due to compression/contraction induced by capsule formation^{12,13}
- inaccurate measurement of glucose levels by sensors segregated from blood¹⁴⁻¹⁶

The most common strategies for preventing these responses seek to prevent the initial protein adsorption step.¹⁷ There are a range of materials that have been shown to diminish protein adsorption, including polysaccharides¹⁸⁻²¹ and zwitterionic polymers.²²⁻²⁴ Far and away the most common method used is to incorporate lengths of poly(ethylene glycol), or PEG, which tends to inhibit protein adsorption due to its hydrophilicity and high conformational flexibility.²⁵ The specific mechanisms for preventing protein adsorption for these materials are not completely understood, but contact with a surface typically leads to disruption of protein folding as residues within the structure interact with functionalities on the material surface. Thus a common theme for materials that successfully resist protein fouling are efforts to preserve the natural, aqueous solution-folded structure of serum proteins by either mimicking the protein-water interactions or preserving those interactions through their own strong hydration.²⁶

Denying cells suitable domains for adhesion through prevention of protein fouling is but one approach to attempt to prevent the host inflammatory response. Other strategies

include the incorporation of anti-inflammatory drugs,^{16,27} the release of nitric oxide,^{28,29} and biomimetic materials to promote healing interactions.³⁰ Though there are many promising candidates and strategies, long term *in vivo* use of such coatings places some very strict requirements on their performance and endurance.

6.1.2. Microgel Films as Cellular Adhesion Resistant Interfaces

Microgels represent an intriguing strategy to form interfaces with respect to cellular adhesion. In addition to their “building block” nature with regard to film assembly, their hydrophilicity and softness were expected to make them highly resistant to protein adsorption, and this capability could be further extended by the incorporation of PEG. Early studies conducted in the Lyon group by Dr. Daoji Gan first demonstrated that the extensive incorporation of PEG methacrylate (mol% 5-40%) into pNIPAm microgels served to reduce the amount of protein adsorbed by the microgels in solution.³¹ Nolan et al. were able to demonstrate that even small amounts (<2 mol%) of PEG, incorporated as a diacrylate cross-linker, adsorbed approximately 25% less protein than similar microgels cross-linked with BIS, and that increasing the molecular weight of the PEG-DA could lead to a reduction in protein adsorption by close to 75%.³² Cell studies conducted in collaboration with the lab of Dr. Andres Garcia demonstrated that this non-fouling characteristic of microgels in solution also correlated well with the ability of monolayer microgel films to resist cell attachment, as the PEG-cross-linked particles blocked cell attachment and spreading much more effectively than those cross-linked with BIS.³²

Building from this example, the Lyon and Garcia labs developed a method to coat polyethylene terephthalate disks with a monolayer of PEG-cross-linked microgels through a benzophenone-based UV-coupling reaction.³³ The disks were demonstrated to reduce fibrinogen adsorption as efficiently as self-assembled monolayers of PEG brushes, and reduced both the adhesion and spreading of macrophages *in vitro*.³⁴ Upon

implantation of these disks within mouse models, the microgel-coated samples significantly reduced the adherence of leukocytes and macrophages during the initial 48 hours associated with the acute inflammatory response, and adherent cells showed reduced expression of pro-inflammatory markers.³⁴ Longer-term studies on disks implanted for 4 weeks revealed that the microgel coating led to thinner fibrous capsule formation, suggesting that microgel monolayers were able to diminish the chronic inflammatory response to foreign materials as well.³⁵

Examination of monolayer films by microscopy, however, suggests that there may be opportunities for improving the cell-resistance capabilities by improving the surface coating. Monolayers of particles have variable polymer density (radial from the particle center), and are limited by their packing efficiency on the surface, such that one can envision cells taking advantage of defects in the coating to interact with the substrate and attach to protein found there. Microgel multilayers, of the sort described in **Chapter 5**, serve to limit the appearance of these defects by addition of multiple layers of microgels tethered to one another through Coulombic interaction with linear polycation. Using PEG cross-linked microgels and PDADMAC, microgel multilayered films could be assembled and were shown to also strongly resist macrophage adhesion.³⁶

Having demonstrated that these films were suitable for prevention of non-specific cell adhesion, my predecessor, Dr. Toni South, next sought to create films suitable for the selective binding of cells. As discussed previously, the long-term stability of implanted materials is dependent upon normalization of the surrounding tissue, and incorporating biomimetic binding domains within otherwise cell-resistant coatings can promote non-inflammatory reactions and wound healing.²⁵ She synthesized microgels featuring the peptide RGD in the particle shell, and deposited them as the top layer on these multilayer films.³⁷ However, despite RGD's widely demonstrated integrin binding affinity and its ability to greatly promote cell attachment to many substrates,³⁸⁻⁴⁰ these films did not show improved cell attachment compared to the films in the absence of the peptide.³⁷

Furthermore, additional work within the group conducted by Dr. Mike Smith revealed that highly charged microgels, as are used during multilayer film assembly, actually adsorb a great deal of protein from solution.⁴¹ Finally, the discovery of the self-healing characteristics of multilayers^{42,43} (for further discussion see **Chapter 5**) suggested that hydrated films exhibit some degree of mobility. These findings taken together suggest that our initial hypothesis that *microgel multilayer films* resist cell attachment due to a non-fouling mechanism analogous to what is observed with monolayers is incomplete, and that an alternative mechanism, based on the mobile or viscoelastic properties of these films, may in fact be the dominant factor.

6.1.3. Cell-Substrate Interactions

To assess the possibility that microgel multilayers do not reduce cell adhesion through a stealth, non-fouling mechanism (i.e. the cells remain naïve of the substrate), let us now consider how cells gather information on their substrates, and how mechanical cues influence cell behavior.

Successful cellular attachment begins when integrins on the cell surface bind to proteins in the extracellular matrix or other substrate. Typical proteins for allowing cell attachment include collagen, laminin, and fibronectin, and may be present from passive adsorption from serum or growth media, produced by the cells themselves, or otherwise integrated into the substrate directly.^{39,44,45} Cells present an array of integrins on their surfaces, each consisting of an α and β subunit, creating 24 distinctive binding domains that have been observed in mammalian cells.³⁹ Once bound, additional integrins are recruited to the site and begin to cluster and form a structure known as a focal adhesion.⁴⁶ These supramolecular structures form from integrins and proteins such as talin and vinculin, and serve to mechanically connect the extracellular environment to the cell's cytoskeleton.^{44,47}

Focal adhesions are the primary mechanism by which cells mechanically probe their external environment, and the past few decades have shown that these mechanical cues play a major role in numerous cell processes. Once a focal adhesion complex is formed, the cells exert a force on the substrate to probe its compliance. The cell seeks to equilibrate its internal tension by pulling on the substrate, and thus match its elastic modulus.^{45,47,48} This leads to a characteristic cell appearance – on substrates that are softer than the cells, the cells tend to remain in a rounded conformation, while stiff substrates lead to spreading.⁴⁷

Cellular adhesion has been studied using a variety of synthetic gels following the original demonstration by Pelham & Wang in 1997 that fibroblasts and epithelial cells showed the ability to alter their spreading and motility in response to mechanically stiffer (more highly cross-linked) polyacrylamide gels.⁴⁹ This observation has also been made for other cell types, such as muscle cells⁵⁰⁻⁵² and nerve cells,^{53,54} suggesting that environmental mechanical cues are a major governing factor for many cell activities. As the cells seek to balance their internal tension through the exertion of force on the substrate, the spreading response indicates cells have greater and more mature focal adhesions, a reduction in apoptosis rate, and greater proliferation.^{47,48} Cellular preference for stiff substrates is also shown by monitoring cellular movement. Several groups have demonstrated methods of forming substrates with patterned or gradient elastic moduli.⁵⁵⁻⁵⁸ For example, Lo et al. altered the extent of cross-linking in polyacrylamide sheets, and by forming composite gels without mixing were able to create single substrates with a step-gradient in elasticity.⁵⁵ Observation of cells approaching the soft-stiff interface showed a clear preference for either crossing from soft to stiff, or turning back to remain on stiff, depending on their original position.⁵⁵ Many groups have used arrays of micro-pillars to create a cell-adhesive substrate wherein the forces exerted by cells can be determined by monitoring the displacement of the pillars, and the dimensions of the pillars themselves provide a facile method to tune the mechanical properties of the

substrate.⁵⁸⁻⁶⁰ In these cases as well, cells are observed to exhibit a preference for stiff substrates, demonstrated by differences in migration rate on soft vs stiff substrates, greater density on stiff substrates, and depletion of cells from soft regions near a stiff interface.^{48,58}

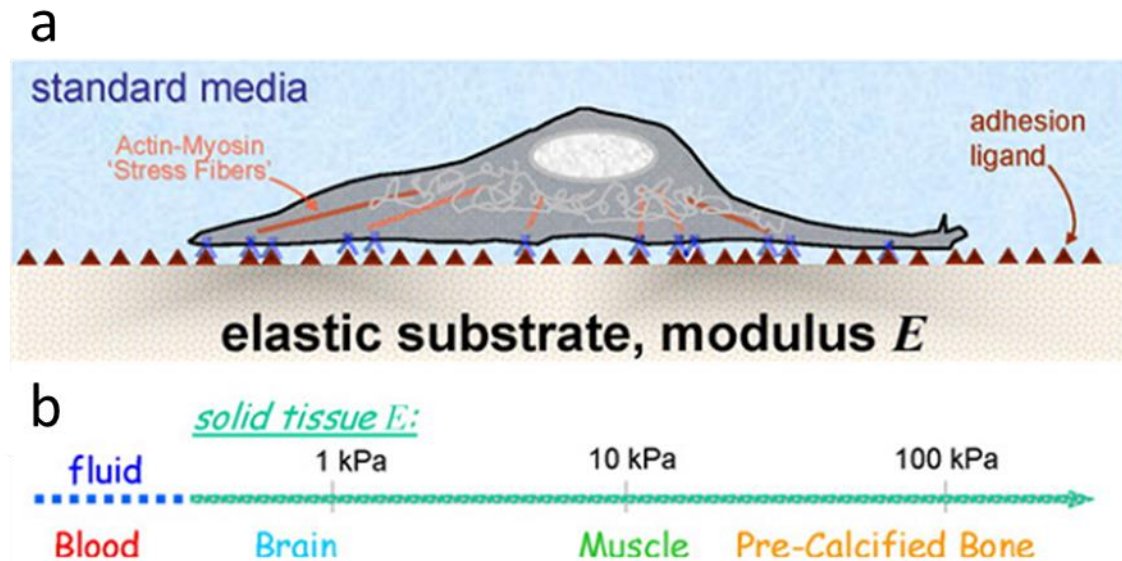


Figure 6.1. a) Depiction of cell interacting with an elastic substrate. Stress fibers in the cell cytoskeleton are coupled to the surface through integrins interacting with adhesion ligands present on the surface, typically resulting from adsorbed protein. b) The range of elastic moduli characteristic of fluids and tissues in the body. Reprinted from Rehfeldt et al. in *Advanced Drug Delivery Reviews*,⁶¹ with permission from Elsevier. Copyright 2007 Elsevier B.V.

Let us now consider the biological relevance of “soft” and “stiff”. As shown in **Figure 6.1**, the range of physiologically-relevant elastic moduli covers a range from a few Pa, such as in brain tissue, to several hundred kPa, as in cartilage or pre-calcified bone.^{61,62} As the previous studies show, cells spread well and generally show preference to being attached to substrates that are stiff. The transition from physiologically “soft” to “stiff” refers to a modulus of approximately 10kPa.^{45,63} Even far above that threshold, for materials such as glass (modulus: tens of GPa), cell behavior shows little discrimination outside of the physiologic window.^{50,51,61} Within that range, however, cells are extraordinarily sensitive to these mechanical cues. Perhaps the most striking example

comes from the work of the Discher group, as in 2006 they demonstrated that the differentiation of multipotent mesenchymal stem cells could be directed from mechanical cues from the matrix, under otherwise identical culture conditions.⁶⁴ Polyacrylamide gels with moduli ranging from 0.1 – 40 kPa were used to culture the cells, and after one week they were assayed for morphology and for characteristic markers for different differentiation pathways. Up-regulation of neurogenic markers and a highly-branched, neuron-like morphology was found on the softest gels; similar morphologic and protein expression profiles were observed for myogenic and osteogenic differentiation on intermediate (8 – 17 kPa) and stiff (> 25 kPa) substrates, respectively.⁶⁴ When compared to the characteristic tissue elasticities in **Figure 6.1**, these correspond to the local mechanical environment these cells would experience in native tissue. Beyond stem cells, the mechanical environment provides cues that regulate a variety of behaviors for many cell types: a brief summary is shown in **Figure 6.2**.

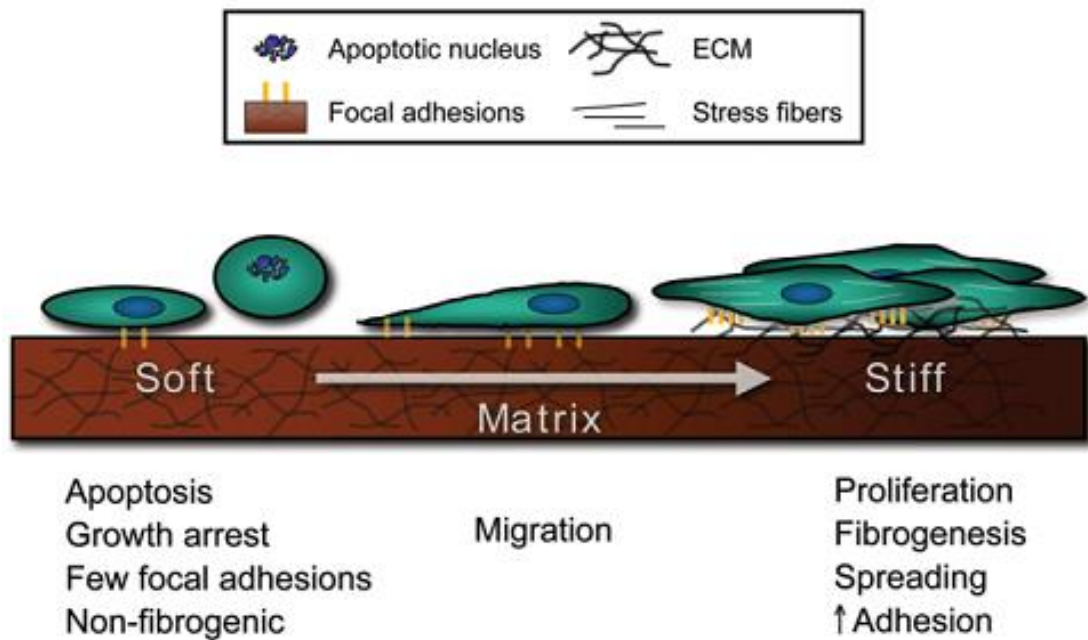


Figure 6.2. Mechanical properties of the substrate direct the activities of many cell types. Cell attachment and spreading are correlated with matrix stiffness, and when possible cytotaxis favors migration towards increasing substrate stiffness. Reproduced from Wells, R. G. in *Hepatology*,⁶⁵ with permission from Wiley. Copyright 2008 American Association for the Study of Liver Diseases.

6.1.4. Polyelectrolyte Multilayers

While there have been only limited studies on the cellular adhesion/resistance properties of microgel multilayers, the broader class of films composed of polyelectrolyte multilayers have been extensively investigated. These films are assembled from two (at minimum) complementary components, which are added in an alternating, layer-by-layer, fashion to lead to the buildup of multilayered film on a substrate of interest.^{66,67} Layer addition involves the dipping, spraying, spin coating, or other administration of one component of the film, followed by rinsing and then administration of the complementary component.^{68,69} The most common implementation utilizes a pair of highly charged cationic and anionic polymers, such as poly(allylamine hydrochloride) (PAH) and poly(styrene sulfonate) (PSS). In these cases, the surface to be coated undergoes charge reversal as each layer is added, and thus buildup is driven by Coulombic interactions between the film and the polyelectrolyte additive, as well as entropic gains from the liberation of counterions from the film.^{69,70} LbL assembly of thin polyelectrolyte films has many advantages^{68,70,71} :

- simple and inexpensive
- translatable to many surfaces (both macroscopic and colloidal)
- insensitive to substrate shape
- exquisite spatial control, both in two dimensions (patterning) and three dimensions (control overall thickness and formation of functional strata)

These advantages have driven intensive investigation in applications of these materials in fields as diverse as water purification, organic electronics, and biomaterials.⁷¹

While linear or branched polyelectrolytes are most commonly used in LbL assembly, other complementary interactions such as hydrogen bonding or click chemistry,^{72,73} have been demonstrated, and other highly charged species such as DNA and proteins,⁷⁴⁻⁷⁶ have also been successfully integrated into multilayer films through

LbL assembly. Hybrid films, wherein nanoparticles constitute one of the charged species during film incorporation, have also been demonstrated using materials such as silica, gold, and of course, microgels.⁷⁷⁻⁸⁰

The properties of films composed of polyelectrolytes are highly dependent on the individual components, the nature of their pair-wise interactions, and their assembly conditions. Certain pairings of polyelectrolytes, such as PSS and PAH have long been characterized as having very strong interactions, and this is manifested in the form of linear film growth, low elasticity, and low chain mobility.^{68,70} Many other polyelectrolyte pairs, like poly(L-lysine) and hyaluronan, exhibit exponential growth, higher in-film diffusion coefficients, and more elastic film properties.^{68,70} These factors are interrelated – for example, exponential film growth occurs when the in-film polyelectrolyte diffusion is high. During new layer deposition, the film acts as a reservoir for additional polycation or polyanion, which diffuses to the interface when the opposite polyion is present. Thus the dependence is not limited to the surface charge (as it is for linearly growing films), but scales with the overall film thickness, leading to exponential growth.^{69,70,81} There is a growing appreciation that the sensitivity of polyelectrolytes to factors such as pH (affecting polyelectrolyte charge density) and ionic strength (affecting the screening, solvation, and packing of the polymers) suggests that it is more than the polyelectrolyte pairing, but also the solution conditions of assembly that affect the final structure of the film.⁶⁹ The extent of ionic cross-linking, film water content, and the length and flexibility of the component polyelectrolytes are all factors that can govern the “strength” of the polyelectrolyte multilayer.⁷⁰

A key factor in transitioning between linear and exponential growth is the mobility of at least one phase of the polyelectrolyte. The ability of polyelectrolytes to diffuse within the films can be observed both directly, through techniques like fluorescence recovery after photobleaching (FRAP) for labeled components of the films,⁸²⁻⁸⁴ and indirectly, such as monitoring the exchange or self-exchange with

polyelectrolytes in solution,^{85,86} and demonstration of inherently mobile phenomena such as self-healing.^{87,88} Strong, linearly growing multilayers, formed from polymers such as PSS / PAH typically have very low diffusion coefficients, and additionally show very slow exchange with equivalent polymers in solution.^{83,89} Exponentially growing weaker multilayers suppress chain mobility by approximately 2 to 3 orders of magnitude relative to the solution state.⁸⁴ The mobility of chains is also anisotropic – diffusion normal to the substrate was 4 to 5 orders of magnitude slower than lateral diffusion for one exponentially growing system.⁹⁰

Multilayers that are strongly interacting will also tend to be mechanically stiffer, with Young's moduli on the order of hundreds of MPa, while weaker, more hydrated multilayers are orders of magnitude softer, on the order of tens of kPa.^{70,91-94} By reference to the cell interaction discussion previously, polyelectrolyte multilayers should appear physiologically stiff and promote cell attachment.

However, polyelectrolyte multilayers have been shown to form films capable of both resisting and promoting cell attachment – even when the film composition is kept constant. In 2003, Mendelsohn et al. explored these films and proposed a mechanism to differentiate between cell adhesive and cell resisting films.⁹⁵ Films assembled from poly(acrylic acid) (PAAc) and PAH hydrochloride demonstrated differential responses to cell adhesion as a function of their assembly pH. At intermediate pH (6.5), corresponding to highly charged states for both polymers, cell attachment was greatest, while low pH (2.0) led to highly cell resistive surfaces. No major differences in protein adsorption (fibrinogen and lysozyme) were observed between the two states, nor could differences in surface chemistry or wettability be correlated to the cellular response. The proposed mechanism instead related to the hydration of the polyelectrolytes. Under low pH conditions, when PAAc was weakly charged relative to PAH, the internal structure of the film would be expected to be very “loopy” – that is there would be internal domains that are enriched in protonated amine groups, their associated anions, and waters of hydration

for both. More highly-charged systems, on the other hand, have more intrinsic charge compensation and thus form thinner layer pairs, lacking these loop domains. Mendelsohn et al. were able to show this property explained the pH-responsivity of the cell adhesion properties of PAAc / PAH; poly(methacrylic acid) / PAH; and PSS / PAH. Even for the strong polyelectrolyte pair PSS / PDADMAC, which does not show pH sensitivity, modifying the assembly conditions by increasing the ionic strength leads to formation of the necessary loop domains. Thus even these two strong polyelectrolytes are able to switch from a cell adhesive to a cell resistive response. The characteristic that best discriminated between films was the swelling response – films whose thickness increased greater than 200% upon hydration resisted attachment, while films swelling less than that threshold allowed attachment.⁹⁵ Further expansion on this work by measuring the elastic moduli of similar films revealed that, while films that encourage cell attachment are orders of magnitude stiffer than those that prevent it, even the PAAc / PAH films assembled at pH 2.0 had a modulus on the order of 400 kPa, far stiffer than other matrices that were shown to prevent attachment through intrinsic “softness.”⁹⁴

Other than assembly conditions, other chemical modifications can be introduced into multilayers to affect their cell adhesive properties. One common strategy is carbodiimide coupling, as many polyelectrolyte pairs feature components with carboxylic acids and primary amines. Carbodiimide coupling, typically through the water-soluble EDC, serves to convert the ion-pair nature of their interaction to a covalent peptide bond.⁹⁶ The result is an increase in matrix stiffness as a function of EDC concentration,^{92,97,98} and improved cell attachment and spreading as a result. In this regard, the same trends as observed from conventional gels – that cells prefer to attach and spread on stiffer substrates – have been observed on polyelectrolyte multilayers interacting with fibroblasts,^{94,95,99} myoblasts,^{51,99-102} osteoblasts,⁹⁷ and even prokaryotes.¹⁰³ Other cross-linking modalities, such as photo-cross-linking¹⁰⁴ have also been demonstrated and show the same general pattern.

In summary, polyelectrolyte multilayers represent a rich and dynamic interface for cell attachment. Films that inhibit cell attachment do so despite adsorbing substantial amounts of serum proteins^{95,99} and being orders of magnitude stiffer than common tissue components.^{92,94} Thus it is clear that there are other mechanisms directing the resistance of these interfaces to cell attachment. Mobility of polyelectrolytes within many types of polyelectrolyte films has been demonstrated and measured, confirming that there is a viscoelastic component to these materials. Importantly, the same factors that lead to increased film stiffness and cell adhesion, such as highly coordinated poly-ion pairing, the addition of external cross-linking reagents, or a dense internal structure, would also be expected to reduce the mobility of components within the film. Therefore, when a cell begins binding to a substrate, the forces exerted by the cell on the substrate may allow the relaxation or rearrangement of the substrate in response. The resultant feedback to the cell suggests the overall substrate is too soft or compliant – or “slippery” to think of a macroscopic analogy, and thus the cells halt their attempts to adhere. Such a mechanism would reconcile the observations to date regarding the interactions of microgel films with cells, and potentially other examples in the polyelectrolyte multilayer field as well.

6.2. Experimental

6.2.1. Materials

All common materials were sourced and used as described in **Chapter 2**. Additionally, reagents AAc, sodium phosphate, PDMS, APTMS, poly(ethyleneimine) (PEI) branched, 750 kDa M_w , and glycine were used as received.

6.2.2. Microgel Synthesis

Synthesis of microgels was conducted in a manner similar to that described in **Chapter 5**. The monomer NIPAm, cross-linker BIS, and surfactant SDS were dissolved in DI water. The solution was added to a 3-neck round bottom flask and purged with

nitrogen for 50 minutes as the solution was warmed to 70 °C. Acrylic acid was added, bringing the total monomer concentration to 100mM, with a molar composition of 66% NIPAm, 30% AAc, 4% BIS. After an additional 10 minutes of nitrogen purging, the polymerization was initiated through the addition of 1 mL of a 0.1M solution of APS. The reaction was allowed to proceed at 70 °C under nitrogen for 4 hours. The resultant particles were filtered through glass wool to remove any coagulum, then purified via sequential sedimentation and redispersal in deionized water. The particles were then lyophilized for storage and resuspended in PBS buffer for use.

6.2.3. Film Assembly

Films for cell adhesion studies were built on amine-functionalized glass, prepared as described in **Chapter 5**. Films for self-healing assessment were constructed on PDMS that had been amine-functionalized, again in the same manner described in **Chapter 5**. Films were assembled from 0.1 mg/mL solutions of microgels in 10mM pH 7.4 PBS at 100mM ionic strength, and used polycation concentrations of 0.1 monoM PEI (750 kDa) or PDADMAC (400-500 kDa) in the same buffer. Films on glass substrates were assembled to four microgel layers, while those on PDMS were assembled to eight layers as this enabled clearer visualization of the damage and recovery features. Analysis of films during buildup was conducted using the Asylum Research MFP-3D with 42 N/m silicon nitride cantilevers, as in **Chapter 5**.

Films that were cross-linked were first equilibrated in the appropriate buffer, detailed as follows, for thirty minutes. For glutaraldehyde cross-linking, a 25% stock solution (Alfa Aesar) was diluted to 2% in deionized water.. The films were allowed to shake at room temperature for two hours to complete cross-linking. The films were then rinsed and any residual cross-linking reagents were quenched using a 40 mM solution of glycine overnight.

6.2.4. Film Stretching

The damage and healing responses of films were assessed using a similar approach to that outlined in **Chapter 5**. Using the same stretching apparatus, films were mounted and strain applied in the same manner. To determine the onset of damage for films in each state, strain was applied in 10% intervals, then the films examined by brightfield microscopy to assess the damage response. Healing was attempted by immersion of the films in deionized water for a period of at least fifteen seconds, followed by drying with nitrogen.

6.2.5. Film Modulus Measurements

The elastic moduli of the multilayers were measured through the nanoindentation technique using an Asylum Research (Santa Barbara, CA) MFP-3D AFM equipped with an iDrive cantilever holder for in-liquid measurements. The tips used for imaging and modulus determination were silicon nitride with a nominal spring constant of 0.02 N/m (Asylum Research, BL-TR400PB). All images were collected in AC-mode, while all force curves were collected in contact mode. Image analysis, spring constant determination, force curve analysis, and elastic modulus determination were all conducted using the MFP-3D software written in the IgorPro software environment (WaveMetrics, Inc, Lake Oswego, OR).

Films assembled on glass coverslips were scratched in order to expose the glass for cantilever calibration and mounted onto glass slides using silver paint. The samples were allowed to equilibrate under the appropriate buffer conditions for a minimum of 30 minutes in the sealed AFM chamber prior to imaging. Images were collected in the vicinity of the scratched region, such that exposed glass was visible. Force curves collected on the glass and a thermal spectrum collected far from the surface were used to determine the spring constant via the equipartition theorem using methods included in the MFP-3D software. The imaging window was then adjusted to an area not including the

scratch, and the film imaged. Force mapping then proceeded by reducing the scan size (25 μm \rightarrow 20 μm , such that all points collected on the force map are visible in the corresponding image) and collecting force curves in a 32 x 32 array. The trigger point was set to be < 50 nm for all measurements. The elastic modulus of the films was calculated for each point in the force map using the Hertz model, via modules available in the MFP-3D software, and assuming a Poisson's ratio of 0.5 for the films.

6.2.6. Protein Adsorption

Qualitative assessment of the protein-fouling characteristics of pNIPAm / 4% BIS / 30% AAc cross-linked with 400 – 500 kDa PDADMAC was conducted by incubating the film in 0.25 mg/mL of fluorescently labeled BSA overnight. The film was then rinsed and imaged via epifluorescence under blue excitation, as described in **Chapter 3**.

Quantitative assessment of the amount of fibronectin loading achieved in pNIPAm/30% AAc microgels cross-linked with either BIS or PEGDA was conducted by Dr. Hiroaki Yoshida. Films were immersed in a solution of 0.005 mg/mL fibronectin labeled with AlexaFluor-488 in PBS for 24 hours at 37 $^{\circ}\text{C}$. The films were then rinsed three times with PBS and the fluorescence measured using a multi-plate reader.

6.2.7. In Vitro Cell Adhesion

Initial cell studies on PDADMAC cross-linked multilayers were conducted by Ms. Apoorva Salimath in the lab of Dr. Andres Garcia. Murine NIH3T3 fibroblasts were cultured in standard serum-containing growth media (DMEM (Gibco), 10% fetal bovine serum (Gibco), 100 U/mL penicillin G sodium (Sigma), 100 $\mu\text{g}/\text{mL}$ streptomycin sulfate (Sigma), 1% non-essential amino acids, 1% sodium pyruvate). Each sample was washed with 70% ethanol and rinsed with sterile DPBS three times prior to cell addition. Trypsinized cells were seeded at 2500 cells/ cm^2 onto 2.2 x 2.2 cm cover slips, and placed in sterile 6 well plates. Cells were allowed to attach in an incubator at 37 $^{\circ}\text{C}$ overnight.

Cell attachment was determined through live/dead staining performed using Calcein AM and Ethidium Homodimer-1 and subsequent film imaging. The number of adherent cells was calculated based on the number of stained nuclei in the field of view for 15-20 images taken at 20x, 40x, or 60x magnification. The reported values are mean +/- standard deviation for these measurements. Cell studies on PEI cross-linked multilayers were conducted by Dr. Hiroaki Yoshida, with assistance from the Garcia lab. The methods were similar to that described above, but cell attachment was calculated following staining for actin, vinculin, and nuclei.

6.3. Results and Discussion

6.3.1. Assessment of Protein Fouling

As described in the introduction, the initial studies on cell attachment to microgel films were directed towards limiting protein fouling on the substrate, and utilizing this non-fouling characteristic to reduce cell attachment. Subsequent work with multilayered films showed strong inhibition of attachment, but did not directly assess the protein-fouling of the films. To that end, we first hypothesized that if non-fouling was not the primary mechanism responsible for the resistance to cell adhesion, then multilayered films lacking PEG should also inhibit cell attachment. Microgels were synthesized that were BIS cross-linked analogues to the published study by South et al.,³⁶ and built into multilayers in the same manner. These films were then subjected to cell attachment studies conducted by Ms. Apoorva Salimath of the Garcia group. As shown in **Figure 6.3**, fibroblast attachment was strongly inhibited relative to both uncoated glass and monolayers of the same microgels.

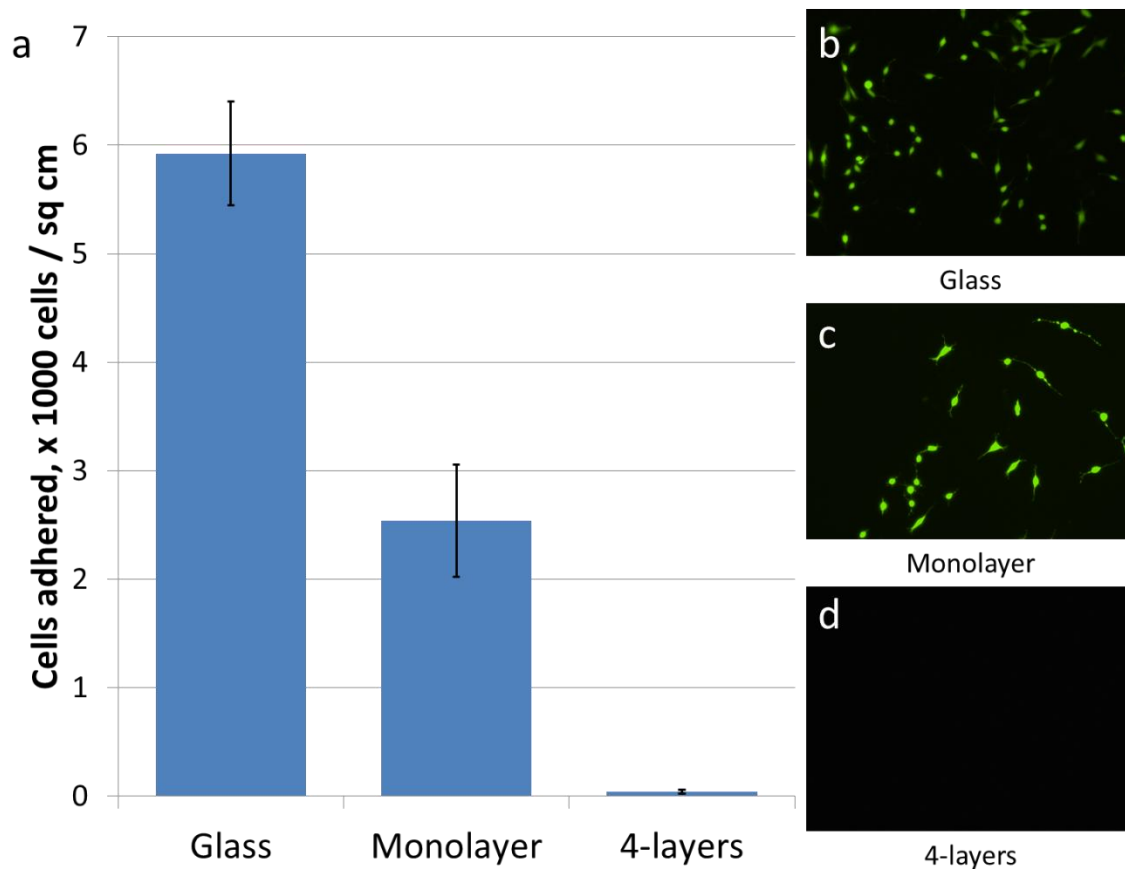


Figure 6.3. a) Numbers of adherent cells on untreated glass coverslips, monolayers of pNIPAm / 4% BIS / 30% AAc microgels, and 4-layer films of the same particles assembled with PDADMAC. b-d) Representative images of Calcein-stained films showing cell attachment. Microgel multilayers strongly inhibit cell attachment, even in the absence of PEG cross-linking. Images and analysis conducted by Ms. Apoorva Salimath.

The protein-fouling characteristics of the films were qualitatively assessed by exposure to FITC-labeled BSA, a common serum protein. **Figure 6.4a** shows strong fluorescence, indicative of high-levels of non-specific protein adsorption to the highly charged films. A more quantitative assessment using fibronectin, another serum protein important for enabling cell attachment, was conducted on these films by Dr. Hiroaki Yoshida. Also in **Figure 6.4**, this data reveals that the protein content of the multilayers is higher than in the monolayers, even for PEG-cross-linked microgels – a result that is antithetical to protein-fouling as the driving force behind cell attachment. The

combination of greater total film volume and the higher charge density of the multilayer assembly likely lead to the differential protein loading.

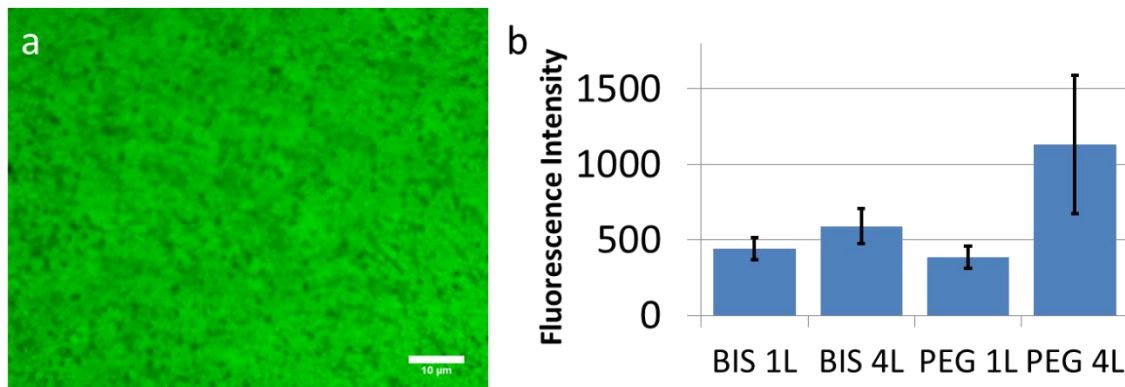
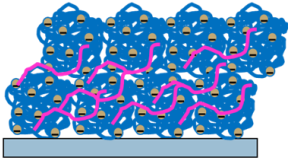
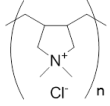
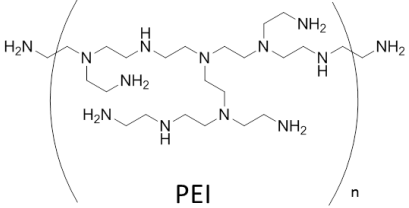


Figure 6.4. a) Epifluorescence microscopy image of a 4-layer pNIPAm / 4% BIS / 30% AAc / 400-500 kDa PDADMAC film exposed to FITC-BSA overnight. Scale bar is 10 μm . b) Exposure to monolayer and 4-layer films to fluorescently-labeled fibronectin. Multilayer films adsorb more protein than monolayers. b) is courtesy of Dr. Hiroaki Yoshida.

6.3.2. Film Assembly

Since inhibition of protein fouling does not seem to be the major factor affecting the ability of microgel films to prevent cell attachment, we next sought a way to alter the viscoelasticity, or mobility, of the microgels. Chemical cross-linking of the films is an attractive approach, however PDADMAC does not have any reactive groups amenable gentle cross-linking reactions. Alternatively, PEI is a highly branched polycation featuring numerous free amine groups suitable for cross-linking. It is also commercially available with high molecular weight, which should ensure a sufficient degree of particle-particle bridging in order to effect charge reversal and allow film buildup. The structures and relevant attributes of the polycations are summarized in **Scheme 6.1**. It was first attempted to discern whether PEI could be incorporated into multilayer films.



	 PDADMAC	 PEI
Reactive Functionality	None	Amine
Available Mw	~450 kDa	~750 kDa

Scheme 6.1. Comparison of PDADMAC and PEI for film assembly and cross-linking.

Film buildup can be directly monitored using AFM. As shown in **Figure 6.5** PEI films build up in a manner that is quite consistent with PDADMAC films that are also assembled via centrifugal deposition. Following the fourth layer of microgel deposition, the films appear uniform with no substrate visible, and individual microgels become difficult to discern, as is characteristic of well-formed multilayers.

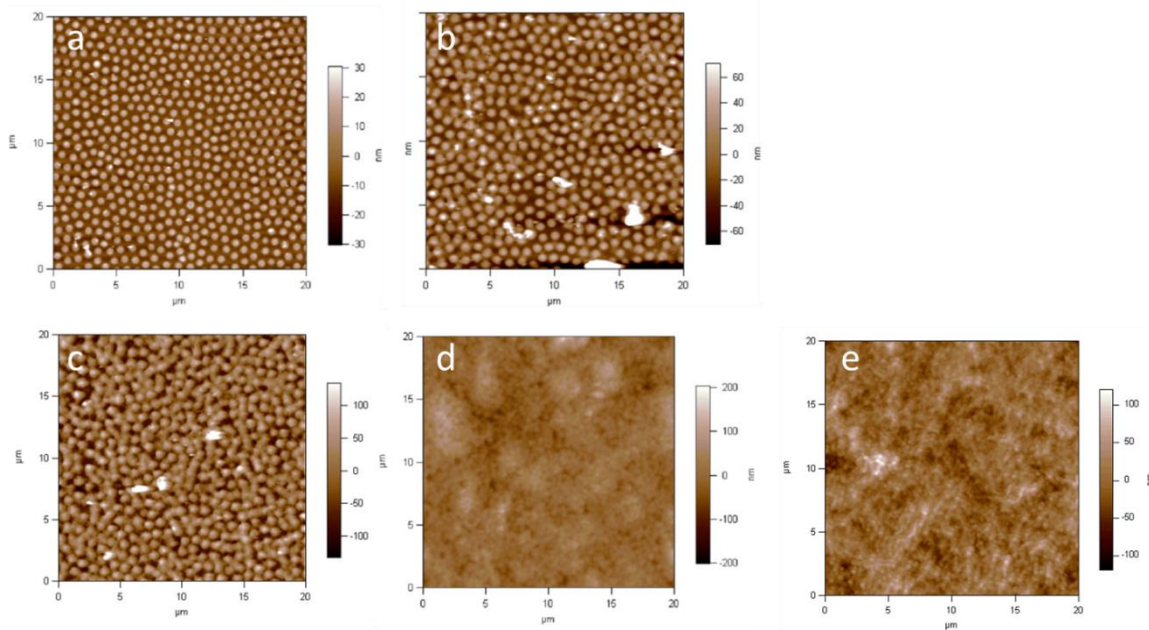


Figure 6.5. Buildup of pNIPAm / 4% BIS / 30% AAc films with PEI. Images taken after a) one layer, b) two layers, c) three layers, and d) four layers of microgels. e) For comparison, a film of the same particles assembled with four layers of microgels and 400-500 kDa PDADMAC. All images are 20 x 20 μm .

6.3.3. Film Cross-linking and Moduli

Once the PEI films are assembled, there are a number of reactions which can be used to covalently reinforce the cross-linking, and thus limit the mobile characteristics of the films. Glutaraldehyde is one such common reagent,⁹⁶ and in this context should serve to cross-link the primary amines of PEI, which will convert the Coulombically assembled multilayer into a gel that is more akin to an interpenetrating double network – the PEI forming one largely immobile phase, and the cross-linking points serving to entangle the microgels and thus restrict particle movement.

Cross-linking will also lead to changes in the mechanical properties of the films, however. Therefore we sought to use nanoindentation techniques on the films to determine their elastic moduli, which will both confirm the efficacy of the cross-linking reaction and to provide physiological context to the stiffness of the two states. Since the

films are composed of particulate gels and polycation, there is likely a great deal of heterogeneity in the plane normal to the surface, particularly when sampling with a small area such as an AFM tip (the ones in this case having a radius of ~ 42 nm). Therefore force mapping, which correlates force curves with spatial positions, was seen as an attractive method to minimize such effects. As is shown in **Figure 6.6**, film stiffness does indeed show significant heterogeneity. However, when considering the elastic moduli of the films in deionized water, the modulus of the non-cross-linked films (mean: ~ 600 kPa, median ~ 500 kPa) is approximately an order of magnitude lower than the films cross-linked with glutaraldehyde (mean: ~ 10 MPa, median ~ 4 MPa).

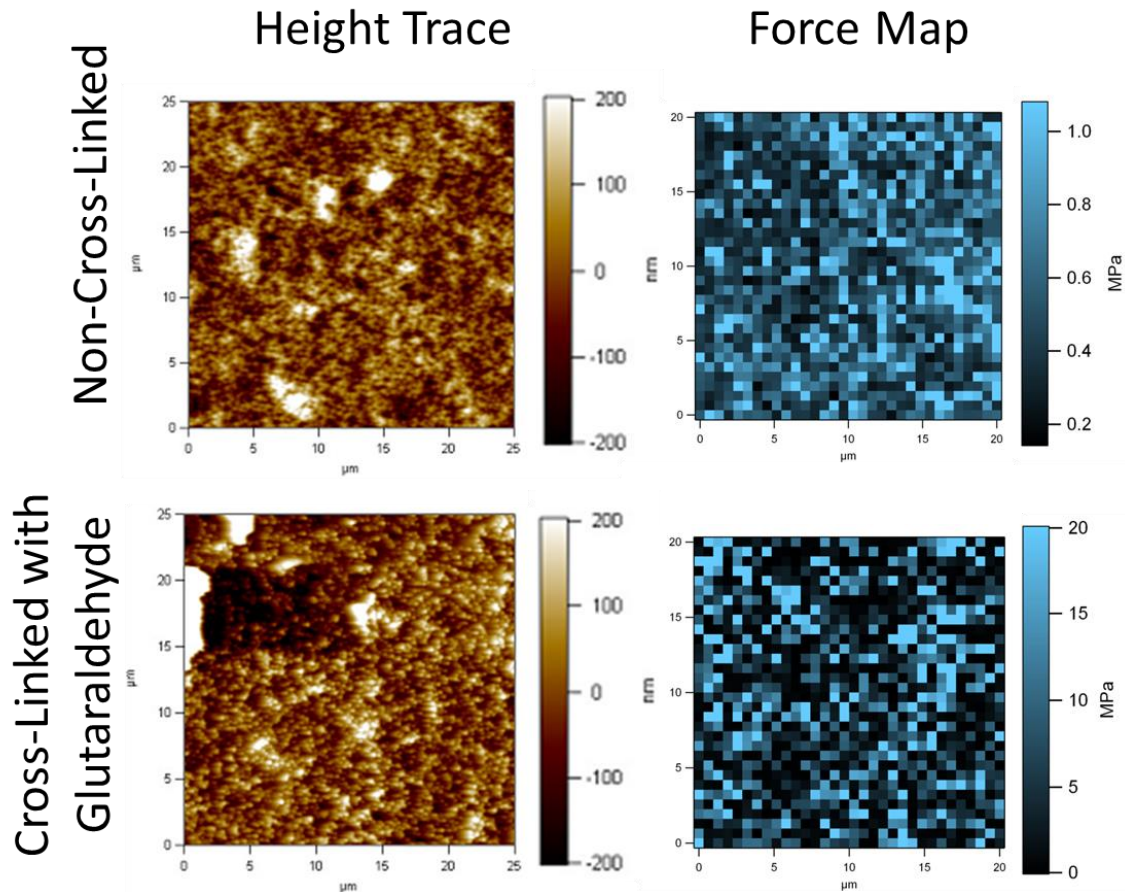


Figure 6.6. Height traces (left) and force maps (right) of 4-layer pNIPAm / 4% BIS / 30% AAc / PEI films in the before (top) and after (bottom) cross-linking with glutaraldehyde. Cross-linking of the films is determined to be successful through an increase in the elastic modulus of the films. Height traces are $25 \times 25 \mu\text{m}$, Force maps are $20 \times 20 \mu\text{m}$ and concentric with the height traces.

6.3.4. Film Damage and Healing

Having ascertained that glutaraldehyde was a suitable way to cross-link the films, we sought to evaluate the effect of cross-linking on microgel mobility. Observation of self-healing of multilayers on flexible substrates remains our best method for determining whether or not microgels are mobile. Films were assembled for that purpose, akin to what was described in **Chapter 5**. Applied strain to the films did not lead to an observable change in the films until a strain of at least 40% was applied. At that point, a characteristic wrinkling pattern appeared in the films perpendicular to the axis of stretching (see **Figure 6.7a-c**), as is consistent with the previously observed damage events for films assembled with PDADMAC. The higher onset of damage for PEI films relative to PDADMAC suggests that these films may have a lower modulus, likely arising from the differential amounts of particle-particle cross-linking that is possible due to the PEI's higher molecular weight and extent of branching. Once damaged, the films readily healed upon immersion in water and drying with nitrogen, confirming that self-healing in microgel multilayers is not confined to PDADMAC. After cross-linking the films with glutaraldehyde, application of even 20% strain causes the film to exhibit cracking. These features, shown in **Figure 6.7e-f**, are not consistent with the plastic deformation characteristic of damage that self-heals. The cracks are more irregular, though they are generally parallel to the axis of stretching. This suggests that cross-linking makes the films brittle, causing this damage to occur upon stretching. Immersion of the films in water and subsequent drying fails to restore the film's integrity. Consequently, these results demonstrate that PEI films can undergo a switch from a self-healing, mobile state to a brittle, immobile one simply through the addition of an exogenous cross-linker like glutaraldehyde.

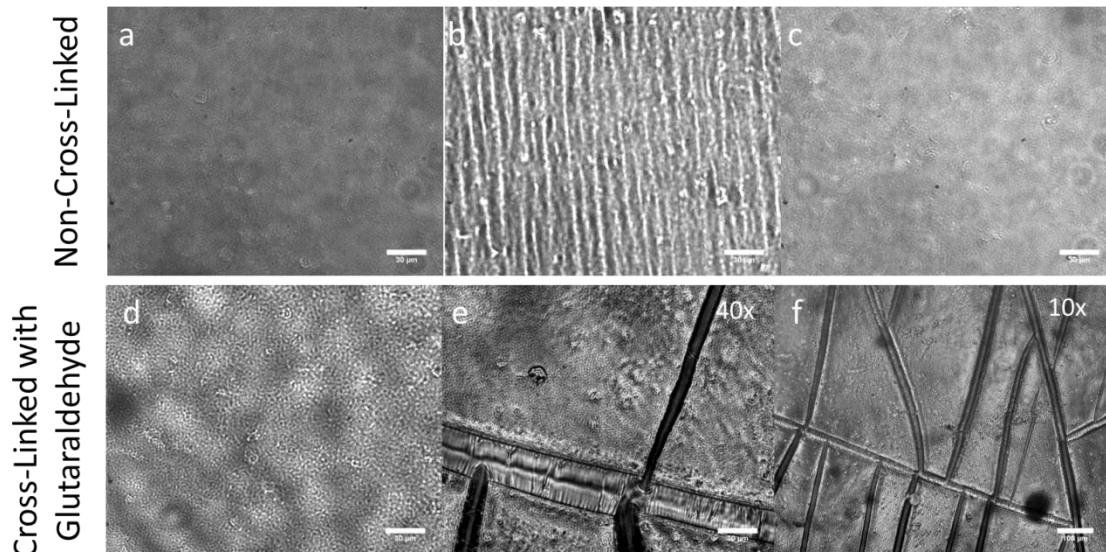


Figure 6.7. Brightfield microscopy images of pNIPAm / 4% BIS / 30 % AAc films assembled with PEI deposited onto PDMS. In the absence of extrinsic cross-linking (a-c), the films undergo plastic deformation and wrinkle when strains in excess of 40% are applied (b). The wrinkles disappear upon immersion in water (c). When cross-linked with glutaraldehyde (d-f), the films undergo irreversible cracking when strained less than 20%. (e, f). The features in e) and f) appear to be cracks largely perpendicular to the axis of stretching, suggesting that the films become brittle once cross-linked. The films do not recover upon immersion in water. Scale bars in a-e) are 30 μm . Scale bar in f) is 100 μm .

6.3.5. Cell Adhesion

The switchable nature of PEI assembled films make them an attractive substrate to use to test the importance of film mobility on the cell adhesive properties of microgel multilayers. Films were assembled in the same manner as described previously for PDADMAC films, and the ability of murine fibroblasts to adhere was investigated by Dr. Hiroaki Yoshida. As revealed in **Figure 6.8**, non-cross-linked PEI films also strongly resisted cell attachment, which coupled with their self-healing characteristics suggests that the mechanism is similar to that of PDADMAC multilayers. Cross-linking with glutaraldehyde leads to a five-fold increase in fibroblast attachment to the films, which is similar to the attachment observed with immobile monolayers. Though the stiffness of

the films increased as well, the moduli measurements described previously suggest that both states represent physiologically “stiff” surfaces. Consequently, these studies provide further evidence for a viscoelastic or mobile component to the cell-resistance properties of microgel multilayer films.

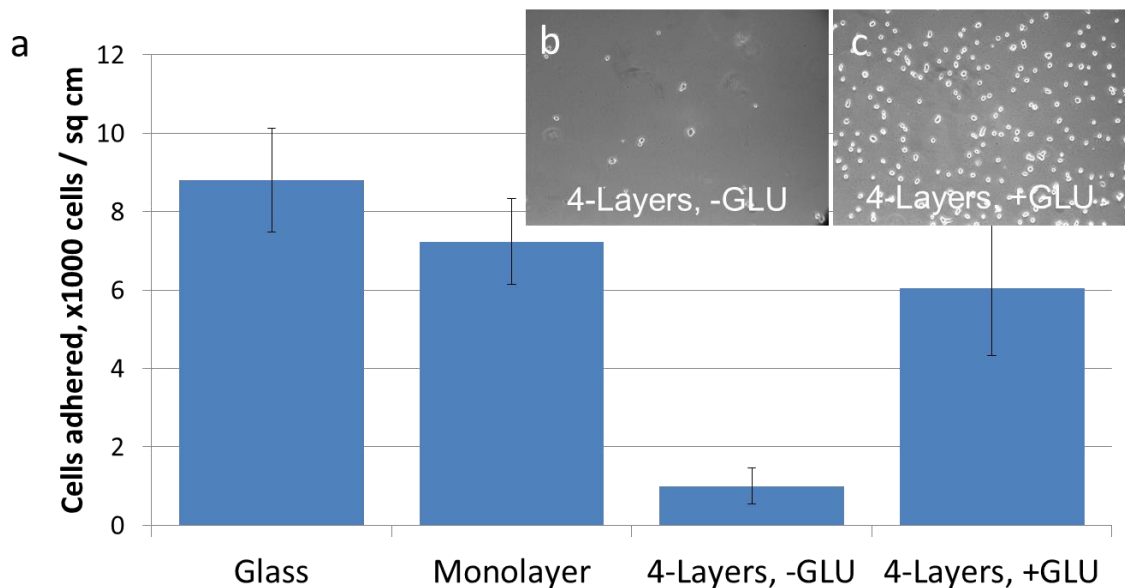


Figure 6.8. a) Numbers of adherent cells on glass, monolayers, and 4-layer pNIPAm / 4% BIS / 30% AAC microgels assembled with PEI. Cross-linking with glutaraldehyde leads to a five-fold increase in cell attachment. b-c) Representative images of films showing cell attachment. Images and analysis conducted by Dr. Hiroaki Yoshida.

While there is clear evidence that microgel multilayers behave in a manner similar to the polyelectrolyte multilayer systems described previously, there are certain differences when considering microgel assemblies which may strongly affect the cell resistance of these materials:

- high molecular weight and spatial dimensionality relative to other single molecule polyanions
- a lower charge density on the microgels than is typical for linear or branched polyanions
- a network structure defined by covalent cross-linking within the microgels that is independent of the polycation

- variable polymer density defined by each microgel

These factors may lead to greater mobility of the polycation in the films, as both the charge density and the defined mesh size of the microgels should lead to the formation of channels for which polycation passage can be relatively unhindered. The more densely cross-linked cores, which should limit polycation accessibility, may actually represent “islands” of relatively anionic polymer. Charge density for single particles within the film would then decrease radially out to the interstitial regions of the films: areas enriched with the polycation. Such structural effects may thus represent numerous domains for serum proteins and integrins to experience, as well as contributing to the overall mobility and viscoelasticity of the film. Modifications to the multilayers, such as cross-linking, may not have substantial impact on these protein-binding domains, but would serve to limit the diffusivity of the polycation in the film and convert the material to a type more akin to a conventional, stiff hydrogel.

6.4. Conclusions and Outlook

When considering their interactions with cells, microgel multilayer films are difficult to compare to the precedents in the field. The major components of the film, the microgels, are colloidal derivatives of the bulk hydrogel systems widely studied. However, by creating multilayer formations of these particles, driven by electrostatic assembly, a second polymeric phase is introduced, as well as dynamic properties common to polyelectrolyte multilayers. The key factors that govern cell attachment in these two classes of materials are quite different, and thus it is difficult to ascribe the resistance of microgel multilayers to cell attachment to a single mechanism without detailed investigation. From previous studies with microgel *monolayers*, it seems clear that the hydrogel factors (elimination of protein fouling) are most important (which is unsurprising since a monolayer by definition lacks multiple layers). Multilayer buildup leads to the emphasis on polyelectrolyte factors – as this chapter demonstrates, the

mechanical properties and protein adsorption of these films are more akin to this class of materials. Further studies may shed more light on this transition, or potentially reveal novel mechanistic origins for the properties of these films derived from their gel / polyelectrolyte duality.

6.5. Acknowledgments

I am very grateful to Ms. Apoorva Salimath and Dr. Hiroaki Yoshida for performing the cell studies described in this chapter, and also to Dr. Andres Garcia for consultation and for allowing the use of his lab space and resources for these investigations.

6.6. References

- [1] Ratner, B. D.; Bryant, S. J., Biomaterials: Where we have been and where we are going. *Annual Review of Biomedical Engineering* **2004**, *6*, 41-75.
- [2] Jenney, C. R.; Anderson, J. M., Adsorbed serum proteins responsible for surface dependent human macrophage behavior. *Journal of Biomedical Materials Research* **1999**, *49*, 435-447.
- [3] Hu, W. J.; Eaton, J. W.; Tang, L. P., Molecular basis of biomaterial-mediated foreign body reactions. *Blood* **2001**, *98*, 1231-1238.
- [4] Anderson, J. M., Biological responses to materials. *Annual Review of Materials Research* **2001**, *31*, 81-110.
- [5] Franz, S.; Rammelt, S.; Scharnweber, D.; Simon, J. C., Immune responses to implants - A review of the implications for the design of immunomodulatory biomaterials. *Biomaterials* **2011**, *32*, 6692-6709.
- [6] Kobayashi, S. D.; Voyich, J. M.; Burlak, C.; DeLeo, F. R., Neutrophils in the innate immune response. *Archivum Immunologiae et Therapiae Experimentalis* **2005**, *53*, 505-517.
- [7] Labow, R. S.; Meek, E.; Santerre, J. P., Hydrolytic degradation of poly(carbonate)-urethanes by monocyte-derived macrophages. *Biomaterials* **2001**, *22*, 3025-3033.

- [8] Labow, R. S.; Meek, E.; Matheson, L. A.; Santerre, J. P., Human macrophage-mediated biodegradation of polyurethanes: assessment of candidate enzyme activities. *Biomaterials* **2002**, *23*, 3969-3975.
- [9] Christenson, E. M.; Anderson, J. M.; Hiltner, A., Oxidative mechanisms of poly(carbonate urethane) and poly(ether urethane) biodegradation: In vivo and in vitro correlations. *Journal of Biomedical Materials Research Part A* **2004**, *70A*, 245-255.
- [10] Santerre, J. P.; Woodhouse, K.; Laroche, G.; Labow, R. S., Understanding the biodegradation of polyurethanes: From classical implants to tissue engineering materials. *Biomaterials* **2005**, *26*, 7457-7470.
- [11] Epstein, A. E.; Kay, G. N.; Plumb, V. J.; Dailey, S. M.; Anderson, P. G., Gross and microscopic pathological changes associated with nonthoracotomy implantable defibrillator leads. *Circulation* **1998**, *98*, 1517-1524.
- [12] Williams, D. F., On the mechanisms of biocompatibility. *Biomaterials* **2008**, *29*, 2941-2953.
- [13] Poepl, N.; Schreml, S.; Lichtenegger, F.; Lenich, A.; Eisenmann-Klein, M.; Prantl, L., Does the surface structure of implants have an impact on the formation of a capsular contracture? *Aesthetic Plastic Surgery* **2007**, *31*, 133-139.
- [14] Service, R. F., Can sensors make a home in the body? *Science* **2002**, *297*, 962-963.
- [15] Onuki, Y.; Bhardwaj, U.; Papadimitrakopoulos, F.; Burgess, D. J., A Review of the Biocompatibility of Implantable Devices: Current Challenges to Overcome Foreign Body Response. *Journal of Diabetes Science and Technology* **2008**, *2*, 1003-1015.
- [16] Morais, J. M.; Papadimitrakopoulos, F.; Burgess, D. J., Biomaterials/Tissue Interactions: Possible Solutions to Overcome Foreign Body Response. *AAPS Journal* **2010**, *12*, 188-196.
- [17] Blaszykowski, C.; Sheikh, S.; Thompson, M., Surface chemistry to minimize fouling from blood-based fluids. *Chemical Society Reviews* **2012**, *41*, 5599-5612.
- [18] Holland, N. B.; Qiu, Y. X.; Ruegsegger, M.; Marchant, R. E., Biomimetic engineering of non-adhesive glycocalyx-like surfaces using oligosaccharide surfactant polymers. *Nature* **1998**, *392*, 799-801.
- [19] Morra, M.; Cassineli, C., Non-fouling properties of polysaccharide-coated surfaces. *Journal of Biomaterials Science-Polymer Edition* **1999**, *10*, 1107-1124.

- [20] Luk, Y. Y.; Kato, M.; Mrksich, M., Self-assembled monolayers of alkanethiolates presenting mannitol groups are inert to protein adsorption and cell attachment. *Langmuir* **2000**, *16*, 9604-9608.
- [21] Huang, B.; Wu, H. K.; Kim, S.; Zare, R. N., Coating of poly(dimethylsiloxane) with n-dodecyl-beta-D-maltoside to minimize nonspecific protein adsorption. *Lab on a Chip* **2005**, *5*, 1005-1007.
- [22] Ishihara, K.; Fukumoto, K.; Iwasaki, Y.; Nakabayashi, N., Modification of polysulfone with phospholipid polymer for improvement of the blood compatibility. Part 2. Protein adsorption and platelet adhesion. *Biomaterials* **1999**, *20*, 1553-1559.
- [23] Goreish, H. H.; Lewis, A. L.; Rose, S.; Lloyd, A. W., The effect of phosphorylcholine-coated materials on the inflammatory response and fibrous capsule formation: *in vitro* and *in vivo* observations. *Journal of Biomedical Materials Research Part A* **2003**, *68A*, 1-9.
- [24] Huang, C. J.; Li, Y. T.; Krause, J. B.; Brault, N. D.; Jiang, S. Y., Internal Architecture of Zwitterionic Polymer Brushes Regulates Nonfouling Properties. *Macromolecular Rapid Communications* **2012**, *33*, 1003-1007.
- [25] Meyers, S. R.; Grinstaff, M. W., Biocompatible and Bioactive Surface Modifications for Prolonged In Vivo Efficacy. *Chemical Reviews* **2012**, *112*, 1615-1632.
- [26] Kane, R. S.; Deschatelets, P.; Whitesides, G. M., Kosmotropes form the basis of protein-resistant surfaces. *Langmuir* **2003**, *19*, 2388-2391.
- [27] Patil, S. D.; Papadimitrakopoulos, F.; Burgess, D. J., Concurrent delivery of dexamethasone and VEGF for localized inflammation control and angiogenesis. *Journal of Controlled Release* **2007**, *117*, 68-79.
- [28] Hetrick, E. M.; Prichard, H. L.; Klitzman, B.; Schoenfisch, M. H., Reduced foreign body response at nitric oxide-releasing subcutaneous implants. *Biomaterials* **2007**, *28*, 4571-4580.
- [29] Nichols, S. P.; Koh, A.; Brown, N. L.; Rose, M. B.; Sun, B.; Slomberg, D. L.; Riccio, D. A.; Klitzman, B.; Schoenfisch, M. H., The effect of nitric oxide surface flux on the foreign body response to subcutaneous implants. *Biomaterials* **2012**, *33*, 6305-6312.
- [30] Lutolf, M. P.; Hubbell, J. A., Synthetic biomaterials as instructive extracellular microenvironments for morphogenesis in tissue engineering. *Nature Biotechnology* **2005**, *23*, 47-55.

- [31] Gan, D. J.; Lyon, L. A., Synthesis and protein adsorption resistance of PEG-modified poly(N-isopropylacrylamide) core/shell microgels. *Macromolecules* **2002**, *35*, 9634-9639.
- [32] Nolan, C. M.; Reyes, C. D.; Debord, J. D.; Garcia, A. J.; Lyon, L. A., Phase transition behavior, protein adsorption, and cell adhesion resistance of poly(ethylene glycol) cross-linked microgel particles. *Biomacromolecules* **2005**, *6*, 2032-2039.
- [33] Singh, N.; Bridges, A. W.; Garcia, A. J.; Lyon, L. A., Covalent tethering of functional microgel films onto poly(ethylene terephthalate) surfaces. *Biomacromolecules* **2007**, *8*, 3271-3275.
- [34] Bridges, A. W.; Singh, N.; Burns, K. L.; Babensee, J. E.; Lyon, L. A.; Garcia, A. J., Reduced acute inflammatory responses to microgel conformal coatings. *Biomaterials* **2008**, *29*, 4605-4615.
- [35] Bridges, A. W.; Whitmire, R. E.; Singh, N.; Templeman, K. L.; Babensee, J. E.; Lyon, L. A.; Garcia, A. J., Chronic inflammatory responses to microgel-based implant coatings. *Journal of Biomedical Materials Research Part A* **2010**, *94A*, 252-258.
- [36] South, A. B.; Whitmire, R. E.; Garcia, A. J.; Lyon, L. A., Centrifugal Deposition of Microgels for the Rapid Assembly of Nonfouling Thin Films. *ACS Applied Materials & Interfaces* **2009**, *1*, 2747-2754.
- [37] South, A. B. Assembly and Dynamic Behavior of Microgel Thin Films and their Application to Biointerfaces. Ph.D. Thesis, Georgia Institute of Technology, Atlanta, GA, 2010.
- [38] Ruoslahti, E., RGD and other recognition sequences for integrins. *Annual Review of Cell and Developmental Biology* **1996**, *12*, 697-715.
- [39] Hynes, R. O., Integrins: Bidirectional, allosteric signaling machines. *Cell* **2002**, *110*, 673-687.
- [40] Hersel, U.; Dahmen, C.; Kessler, H., RGD modified polymers: biomaterials for stimulated cell adhesion and beyond. *Biomaterials* **2003**, *24*, 4385-4415.
- [41] Smith, M. H.; Lyon, L. A., Tunable Encapsulation of Proteins within Charged Microgels. *Macromolecules* **2011**, *44*, 8154-8160.
- [42] South, A. B.; Lyon, L. A., Autonomic Self-Healing of Hydrogel Thin Films. *Angewandte Chemie-International Edition* **2010**, *49*, 767-771.

- [43] Park, C. W.; South, A. B.; Hu, X. B.; Verdes, C.; Kim, J. D.; Lyon, L. A., Gold nanoparticles reinforce self-healing microgel multilayers. *Colloid and Polymer Science* **2011**, *289*, 583-590.
- [44] Michael, K. E.; Garcia, A. J., Cell adhesion strengthening: Measurement and analysis. *Cell Mechanics* **2007**, *83*, 329-346.
- [45] Discher, D. E.; Janmey, P.; Wang, Y. L., Tissue cells feel and respond to the stiffness of their substrate. *Science* **2005**, *310*, 1139-1143.
- [46] Liu, W. F.; Chen, C. S., Engineering biomaterials to control cell function. *Materials Today* **2005**, *8*, 28-35.
- [47] Chicurel, M. E.; Chen, C. S.; Ingber, D. E., Cellular control lies in the balance of forces. *Current Opinion in Cell Biology* **1998**, *10*, 232-239.
- [48] Nemir, S.; West, J. L., Synthetic Materials in the Study of Cell Response to Substrate Rigidity. *Annals of Biomedical Engineering* **2010**, *38*, 2-20.
- [49] Pelham, R. J.; Wang, Y. L., Cell locomotion and focal adhesions are regulated by substrate flexibility. *Proceedings of the National Academy of Sciences of the United States of America* **1997**, *94*, 13661-13665.
- [50] Engler, A.; Bacakova, L.; Newman, C.; Hategan, A.; Griffin, M.; Discher, D., Substrate compliance versus ligand density in cell on gel responses. *Biophysical Journal* **2004**, *86*, 617-628.
- [51] Engler, A. J.; Richert, L.; Wong, J. Y.; Picart, C.; Discher, D. E., Surface probe measurements of the elasticity of sectioned tissue, thin gels and polyelectrolyte multilayer films: Correlations between substrate stiffness and cell adhesion. *Surface Science* **2004**, *570*, 142-154.
- [52] Boontheekul, T.; Hill, E. E.; Kong, H. J.; Mooney, D. J., Regulating myoblast phenotype through controlled gel stiffness and degradation. *Tissue Engineering* **2007**, *13*, 1431-1442.
- [53] Georges, P. C.; Miller, W. J.; Meaney, D. F.; Sawyer, E. S.; Janmey, P. A., Matrices with compliance comparable to that of brain tissue select neuronal over glial growth in mixed cortical cultures. *Biophysical Journal* **2006**, *90*, 3012-3018.
- [54] Yeung, T.; Georges, P. C.; Flanagan, L. A.; Marg, B.; Ortiz, M.; Funaki, M.; Zahir, N.; Ming, W. Y.; Weaver, V.; Janmey, P. A., Effects of substrate stiffness on cell morphology, cytoskeletal structure, and adhesion. *Cell Motility and the Cytoskeleton* **2005**, *60*, 24-34.

- [55] Lo, C. M.; Wang, H. B.; Dembo, M.; Wang, Y. L., Cell movement is guided by the rigidity of the substrate. *Biophysical Journal* **2000**, *79*, 144-152.
- [56] Chou, S. Y.; Cheng, C. M.; Leduc, P. R., Composite polymer systems with control of local substrate elasticity and their effect on cytoskeletal and morphological characteristics of adherent cells. *Biomaterials* **2009**, *30*, 3136-3142.
- [57] Ghibaudo, M.; Saez, A.; Trichet, L.; Xayaphoummine, A.; Browaeys, J.; Silberzan, P.; Buguin, A.; Ladoux, B., Traction forces and rigidity sensing regulate cell functions. *Soft Matter* **2008**, *4*, 1836-1843.
- [58] Trichet, L.; Le Digabel, J.; Hawkins, R. J.; Vedula, R. K.; Gupta, M.; Ribault, C.; Hersen, P.; Voituriez, R.; Ladoux, B., Evidence of a large-scale mechanosensing mechanism for cellular adaptation to substrate stiffness. *Proceedings of the National Academy of Sciences of the United States of America* **2012**, *109*, 6933-6938.
- [59] Tan, J. L.; Tien, J.; Pirone, D. M.; Gray, D. S.; Bhadriraju, K.; Chen, C. S., Cells lying on a bed of microneedles: An approach to isolate mechanical force. *Proceedings of the National Academy of Sciences of the United States of America* **2003**, *100*, 1484-1489.
- [60] Saez, A.; Ghibaudo, M.; Buguin, A.; Silberzan, P.; Ladoux, B., Rigidity-driven growth and migration of epithelial cells on microstructured anisotropic substrates. *Proceedings of the National Academy of Sciences of the United States of America* **2007**, *104*, 8281-8286.
- [61] Rehfeldt, F.; Engler, A. J.; Eckhardt, A.; Ahmed, F.; Discher, D. E., Cell responses to the mechanochemical microenvironment - Implications for regenerative medicine and drug delivery. *Advanced Drug Delivery Reviews* **2007**, *59*, 1329-1339.
- [62] Levental, I.; Georges, P. C.; Janmey, P. A., Soft biological materials and their impact on cell function. *Soft Matter* **2007**, *3*, 299-306.
- [63] Schwarz, U., Soft matters in cell adhesion: rigidity sensing on soft elastic substrates. *Soft Matter* **2007**, *3*, 263-266.
- [64] Engler, A. J.; Sen, S.; Sweeney, H. L.; Discher, D. E., Matrix elasticity directs stem cell lineage specification. *Cell* **2006**, *126*, 677-689.
- [65] Wells, R. G., The role of matrix stiffness in regulating cell behavior. *Hepatology* **2008**, *47*, 1394-1400.

- [66] Decher, G.; Hong, J. D.; Schmitt, J., Buildup of Ultrathin Multilayer Films by a Self-Assembly Process .3. Consecutively Alternating Adsorption of Anionic and Cationic Polyelectrolytes on Charged Surfaces. *Thin Solid Films* **1992**, *210*, 831-835.
- [67] Decher, G., Fuzzy nanoassemblies: Toward layered polymeric multicomposites. *Science* **1997**, *277*, 1232-1237.
- [68] Boudou, T.; Crouzier, T.; Ren, K. F.; Blin, G.; Picart, C., Multiple Functionalities of Polyelectrolyte Multilayer Films: New Biomedical Applications. *Advanced Materials* **2010**, *22*, 441-467.
- [69] Lavalle, P.; Voegel, J. C.; Vautier, D.; Senger, B.; Schaaf, P.; Ball, V., Dynamic Aspects of Films Prepared by a Sequential Deposition of Species: Perspectives for Smart and Responsive Materials. *Advanced Materials* **2011**, *23*, 1191-1221.
- [70] Klitzing, R. v., Internal structure of polyelectrolyte multilayer assemblies. *Physical Chemistry Chemical Physics* **2006**, *8*, 5012-5033.
- [71] Hammond, P. T., Form and function in multilayer assembly: New applications at the nanoscale. *Advanced Materials* **2004**, *16*, 1271-1293.
- [72] Quinn, J. F.; Johnston, A. P. R.; Such, G. K.; Zelikin, A. N.; Caruso, F., Next generation, sequentially assembled ultrathin films: beyond electrostatics. *Chemical Society Reviews* **2007**, *36*, 707-718.
- [73] Kozlovskaya, V.; Kharlampieva, E.; Erel, I.; Sukhishvili, S. A., Multilayer-derived, ultrathin, stimuli-responsive hydrogels. *Soft Matter* **2009**, *5*, 4077-4087.
- [74] Caruso, F.; Mohwald, H., Protein multilayer formation on colloids through a stepwise self-assembly technique. *Journal of the American Chemical Society* **1999**, *121*, 6039-6046.
- [75] Schuler, C.; Caruso, F., Preparation of enzyme multilayers on colloids for biocatalysis. *Macromolecular Rapid Communications* **2000**, *21*, 750-753.
- [76] Johnston, A. P. R.; Read, E. S.; Caruso, F., DNA multilayer films on planar and colloidal supports: Sequential assembly of like-charged polyelectrolytes. *Nano Letters* **2005**, *5*, 953-956.
- [77] Lu, C. H.; Donch, I.; Nolte, M.; Fery, A., Au nanoparticle-based multilayer ultrathin films with covalently linked nanostructures: Spraying layer-by-layer assembly and mechanical property characterization. *Chemistry of Materials* **2006**, *18*, 6204-6210.

- [78] Caruso, F.; Lichtenfeld, H.; Giersig, M.; Mohwald, H., Electrostatic self-assembly of silica nanoparticle - Polyelectrolyte multilayers on polystyrene latex particles. *Journal of the American Chemical Society* **1998**, *120*, 8523-8524.
- [79] Serpe, M. J.; Jones, C. D.; Lyon, L. A., Layer-by-layer deposition of thermoresponsive microgel thin films. *Langmuir* **2003**, *19*, 8759-8764.
- [80] Tian, S. J.; Liu, J. Y.; Zhu, T.; Knoll, W., Polyaniline/gold nanoparticle multilayer films: Assembly, properties, and biological applications. *Chemistry of Materials* **2004**, *16*, 4103-4108.
- [81] Picart, C.; Mutterer, J.; Richert, L.; Luo, Y.; Prestwich, G. D.; Schaaf, P.; Voegel, J. C.; Lavalle, P., Molecular basis for the explanation of the exponential growth of polyelectrolyte multilayers. *Proceedings of the National Academy of Sciences of the United States of America* **2002**, *99*, 12531-12535.
- [82] Picart, C.; Mutterer, J.; Arntz, Y.; Voegel, J. C.; Schaaf, P.; Senger, B., Application of fluorescence recovery after photobleaching to diffusion of a polyelectrolyte in a multilayer film. *Microscopy Research and Technique* **2005**, *66*, 43-57.
- [83] Nazaran, P.; Bosio, V.; Jaeger, W.; Anghel, D. F.; von Klitzing, R., Lateral mobility of polyelectrolyte chains in multilayers. *Journal of Physical Chemistry B* **2007**, *111*, 8572-8581.
- [84] Jourdainne, L.; Lecuyer, S.; Arntz, Y.; Picart, C.; Schaaf, P.; Senger, B.; Voegel, J. C.; Lavalle, P.; Charitat, T., Dynamics of poly(L-lysine) in hyaluronic acid/poly(L-lysine)multilayer films studied by fluorescence recovery after pattern photobleaching. *Langmuir* **2008**, *24*, 7842-7847.
- [85] Zacharia, N. S.; Modestino, M.; Hammond, P. T., Factors influencing the interdiffusion of weak polycations in multilayers. *Macromolecules* **2007**, *40*, 9523-9528.
- [86] Zacharia, N. S.; DeLongchamp, D. M.; Modestino, M.; Hammond, P. T., Controlling diffusion and exchange in layer-by-layer assemblies. *Macromolecules* **2007**, *40*, 1598-1603.
- [87] Wang, X.; Liu, F.; Zheng, X. W.; Sun, J. Q., Water-Enabled Self-Healing of Polyelectrolyte Multilayer Coatings. *Angewandte Chemie-International Edition* **2011**, *50*, 11378-11381.
- [88] Li, Y.; Chen, S. S.; Wu, M. C.; Sun, J. Q., Polyelectrolyte Multilayers Impart Healability to Highly Electrically Conductive Films. *Advanced Materials* **2012**, *24*, 4578-4582.

- [89] Jomaa, H. W.; Schlenoff, J. B., Accelerated exchange in polyelectrolyte multilayers by "catalytic" polyvalent ion pairing. *Langmuir* **2005**, *21*, 8081-8084.
- [90] Xu, L.; Kozlovskaya, V.; Kharlampieva, E.; Ankner, J. F.; Sukhishvili, S. A., Anisotropic Diffusion of Polyelectrolyte Chains within Multilayer Films. *ACS Macro Letters* **2012**, *1*, 127-130.
- [91] Collin, D.; Lavalle, P.; Garza, J. M.; Voegel, J. C.; Schaaf, P.; Martinoty, P., Mechanical properties of cross-linked hyaluronic acid/poly-(L-lysine) multilayer films. *Macromolecules* **2004**, *37*, 10195-10198.
- [92] Richert, L.; Engler, A. J.; Discher, D. E.; Picart, C., Elasticity of native and cross-linked polyelectrolyte multilayer films. *Biomacromolecules* **2004**, *5*, 1908-1916.
- [93] Nolte, A. J.; Rubner, M. F.; Cohen, R. E., Determining the young's modulus of polyelectrolyte multilayer films via stress-induced mechanical buckling instabilities. *Macromolecules* **2005**, *38*, 5367-5370.
- [94] Thompson, M. T.; Berg, M. C.; Tobias, I. S.; Rubner, M. F.; Van Vliet, K. J., Tuning compliance of nanoscale polyelectrolyte multilayers to modulate cell adhesion. *Biomaterials* **2005**, *26*, 6836-6845.
- [95] Mendelsohn, J. D.; Yang, S. Y.; Hiller, J.; Hochbaum, A. I.; Rubner, M. F., Rational design of cytophilic and cytophobic polyelectrolyte multilayer thin films. *Biomacromolecules* **2003**, *4*, 96-106.
- [96] Hermanson, G. T. *Bioconjugate Techniques*; Academic Press: San Diego, CA, 1996.
- [97] Picart, C.; Elkaim, R.; Richert, L.; Audoin, T.; Arntz, Y.; Cardoso, M. D.; Schaaf, P.; Voegel, J. C.; Frisch, B., Primary cell adhesion on RGD-functionalized and covalently crosslinked thin polyelectrolyte multilayer films. *Advanced Functional Materials* **2005**, *15*, 83-94.
- [98] Schneider, A.; Francius, G.; Obeid, R.; Schwinte, P.; Hemmerle, J.; Frisch, B.; Schaaf, P.; Voegel, J. C.; Senger, B.; Picart, C., Polyelectrolyte multilayers with a tunable Young's modulus: Influence of film stiffness on cell adhesion. *Langmuir* **2006**, *22*, 1193-1200.
- [99] Boudou, T.; Crouzier, T.; Nicolas, C.; Ren, K.; Picart, C., Polyelectrolyte Multilayer Nanofilms Used as Thin Materials for Cell Mechano-Sensitivity Studies. *Macromolecular Bioscience* **2011**, *11*, 77-89.
- [100] Ren, K. F.; Crouzier, T.; Roy, C.; Picart, C., Polyelectrolyte multilayer films of controlled stiffness modulate myoblast cell differentiation. *Advanced Functional Materials* **2008**, *18*, 1378-1389.

- [101] Ren, K. F.; Fourel, L.; Rouviere, C. G.; Albiges-Rizo, C.; Picart, C., Manipulation of the adhesive behaviour of skeletal muscle cells on soft and stiff polyelectrolyte multilayers. *Acta Biomaterialia* **2010**, *6*, 4238-4248.
- [102] Monge, C.; Ren, K. F.; Berton, K.; Guillot, R.; Peyrade, D.; Picart, C., Engineering Muscle Tissues on Microstructured Polyelectrolyte Multilayer Films. *Tissue Engineering Part A* **2012**, *18*, 1664-1676.
- [103] Lichter, J. A.; Thompson, M. T.; Delgadillo, M.; Nishikawa, T.; Rubner, M. F.; Van Vliet, K. J., Substrata mechanical stiffness can regulate adhesion of viable bacteria. *Biomacromolecules* **2008**, *9*, 1571-1578.
- [104] Vazquez, C. P.; Boudou, T.; Dulong, V.; Nicolas, C.; Picart, C.; Glinel, K., Variation of Polyelectrolyte Film Stiffness by Photo-Cross-Linking: A New Way To Control Cell Adhesion. *Langmuir* **2009**, *25*, 3556-3563.

CHAPTER 7

OUTLOOK AND FUTURE DIRECTIONS

7.1. Introduction

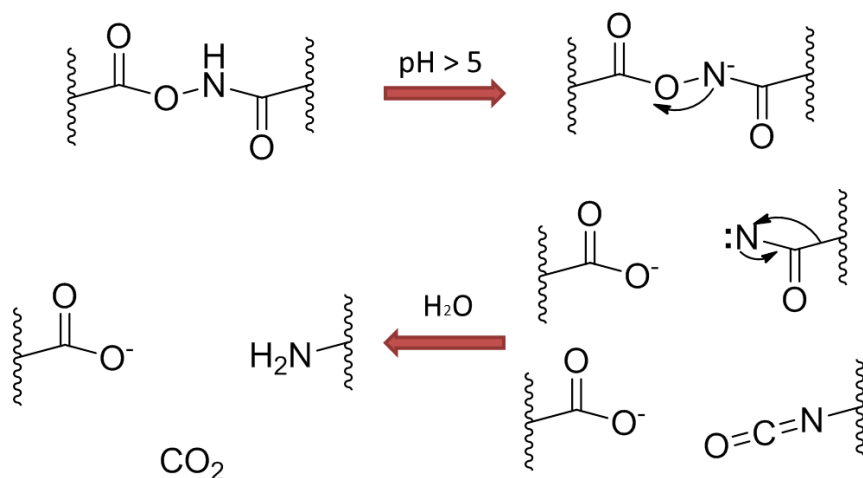
The preceding chapters have described numerous innovations in microgel synthesis and microgel assemblies, along with fundamental studies to better understand each system. Individual chapters presented one avenue of inquiry on a variety of subjects with regard to microgels and their assemblies. The goal of this chapter is to provide some additional context for the work, and suggest future research directions that may enable the translation of these materials into functional and beneficial technologies for use in solving the major challenges facing drug delivery and healthcare.

7.2. Hydrolytically Degradable Microgels

7.2.1. Alternative Uses for DMHA

While the initial interest in pursuing DMHA for cross-linking of microgels was motivated by the pH regime of its hydrolytic degradation, it also presents an opportunity for particle functionalization. In the original synthesis of the cross-linker by Ulbrich et al., the degradation products of the erosion were identified as carboxyl groups and amines.¹ Thus the cross-link scission occurs upon hydrolysis, followed by Lossen's rearrangement to an isocyanate, whereupon further hydrolysis results in amine formation and the release of carbon dioxide. The degradation mechanism is shown in **Scheme 7.1**. If DMHA cross-linking were combined with the non-degradable cross-linker BIS, in a manner similar to the production of thiolated microgels in **Chapter 3**, the erosion products would lead to a stoichiometrically zwitterionic microgel, featuring two reactive functional groups capable of orthogonal chemoligation. Synthesis of particles of this type

via conventional precipitation polymerization is quite challenging due to the inherent difficulties in multi-component synthesis, such as differences in polymerization kinetics and hydrophilicity between different monomers. Achieving incorporation of both functionalities in the form of a single, protected co-monomer may therefore provide a simple synthetic route.



Scheme 7.1. Scission of DMHA at neutral to alkaline pH proceeds following deprotonation of the nitrogen, followed by Lossen's rearrangement to form an isocyanate intermediate which further hydrolyzes to result in amine formation.

7.2.2. Experimental and Results

Investigating this approach proved to be quite challenging, however. While the synthesis of co-cross-linked microgels requires only the addition of BIS to the initial monomer solution and results in successful particle formation, following degradation the characterization of resultant particles proved quite challenging. Assessing the particle size changes and responsivity using dynamic light scattering is significantly more challenging for zwitterionic particles. Das and Kumacheva demonstrated for poly(NIPAm-co-vinyl imidazole-co-acrylic acid) microgels that the weak nature of the acidic and basic functional groups results in complex swelling behavior, with hydrodynamic radii being minimized at the isoelectric point of the microgels.² Characterization of degraded DMHA particles in this manner is challenging due to 1) the low overall incorporation of the cross-linker (≤ 4 mol %), 2) ongoing particle degradation

presenting a “moving target”, and 3) oligomeric loss from degradation making the exact stoichiometric composition of the respective groups indeterminable. Therefore, reactive labeling techniques were employed to demonstrate the presence and availability of the two functional groups. However, despite successful labeling of carboxyls with fluorescein-amine, the amine-reactive fluorophores fluorescein-isothiocyanate and fluorescein-N-hydroxysuccinimide were unsuccessful in conjugating to any remnant amines. Vial images of fluorescent conjugation attempts are shown in **Figure 7.1**.

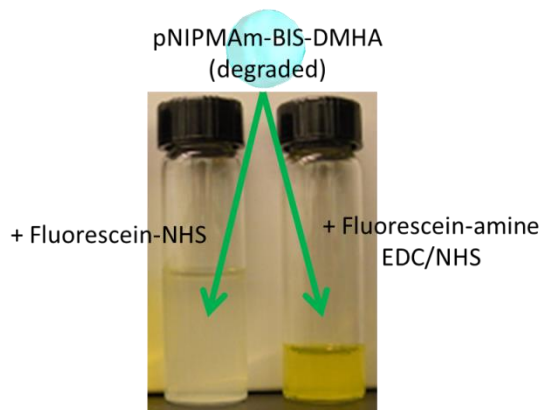


Figure 7.1. Following degradation, attempting to fluorescently label the expected amine and carboxyl groups produced by DMHA degradation leads to mixed results. Amine-targeted reactions, such as NHS-derivatized fluorescein, do not show efficient labeling, while carboxyl-targeted reactions are successful.

The inability to demonstrate incorporation of reactive amines may suggest that the primary degradation mechanism for DMHA in these microgels is hydrolysis of the cross-linker, leading to carboxyl release, and resulting in a stable isocyanate, a stable hydroxamic acid, or a second hydrolysis occurs on the hydroxamic acid leading to the production of two carboxyls. Ascertaining the degradation products is not only key for determining DMHA’s suitability for multi-functional zwitterionic particles as described above, but also is critical for any future drug delivery applications.

7.2.3. Future Perspectives

Introducing physiologically-relevant degradation motifs within microgels will continue to be a key part of translating the great potential of these materials as therapeutic carriers into impactful technologies. Thus far, our group's interests in DMHA have been limited to fundamental studies of its erosion properties: in solution,³ supported by surfaces,⁴ or localized into microgels with complex architectures,⁵ as in **Chapter 2**. However, we have yet to investigate the potential utility of DMHA-bearing microgels in drug delivery applications. One basic distinction to consider is whether DMHA is suitable for release profile modification, or simply as a mechanism to ensure long-term degradation and clearance. While degradable cross-linking as means to regulate solute release is widely demonstrated for many materials, there are reasonable concerns as to why DMHA microgels may not work well in this capacity. For macromolecular therapeutics the loading and release is primarily governed by the polymer mesh size, and if DMHA exhibits heterogeneous incorporation within microgels, the resultant particles would have domains enriched in DMHA, which would likely have smaller mesh sizes than other portions of the particles. Thus, macromolecular loading would be highest in regions with lowest DMHA content, which may mitigate its effect on the release properties. In addition, for DMHA-shell particles the added polymer density may limit the ability of therapeutics to diffuse during loading, which would require alternative strategies such as complementary interactions with other microgel components to ensure efficient loading and retention.

For these reasons, DMHA's utility in microgel delivery vehicles is unclear. In the twenty years since the original description of the synthesis, there have been only a few published efforts to incorporate the cross-linker within colloidal gels to assess properties relevant for drug delivery. PEG-based microgels cross-linked with DMHA have been investigated both for their ability to regulate release of a small molecule therapeutic,⁶ and their ability to be taken in by cells.⁷ Bartlett and Panitch recently demonstrated that

pNIPAm-based microgels could use combinations of DMHA and BIS cross-linking to regulate release of an anti-inflammatory peptide.⁸ These limited examples suggest that the potential of DMHA-based microgels has yet to be fully tapped.

7.3. Disulfide Cross-linked Microgels

7.3.1. Introduction

Chapter 3 discussed the incorporation of disulfides into thermo-responsive microgels via precipitation polymerization, and thus provided a means to incorporate responsive sulfur chemistries. To fully exploit this capability, however, these disulfide linkages need to be incorporated into more complex microgel architectures, such as the core-shell particles used for drug delivery⁹ or incorporated in conjunction with additional orthogonal chemical functionalities, as this would enable simultaneous chemoligation of targeting moieties, fluorophores, or payloads of interest.¹⁰ Expansion of the synthetic space around microgels further extends our ability to approach potential applications with a rational design perspective. Preliminary efforts in this area have focused on the incorporation of acrylic acid within microgels co-cross-linked with BIS and BAC. The resultant particles would be temperature, pH, and redox-responsive, and upon thiol conversion would present two orthogonal functional groups suitable for post-synthetic modification of the microgels.

7.3.2. Experimental

7.3.2.1. Materials

All materials and reagents were sourced and used in a manner consistent with their description in **Chapter 3**. Additionally, the reagents Tris(2-carboxyethyl)phosphine hydrochloride (TCEP) (Pierce) and dansylcadaverine hydrochloride (Sigma Aldrich) were used as received.

7.3.2.2. Microgel Synthesis

The target molar composition for these particles was: NIPMAm: 85.5%, BAC: 2.5%, BIS: 2%, AAc: 10%. The monomers NIPMAm and BIS were dissolved in deionized water, then filtered through a 0.2- μm Acrodisc filter into a 3-neck round bottom flask. SDS was added to the solution to a total final concentration of 0.17 mM. The solution was heated to 68 °C and stirred under nitrogen for seventy minutes. The acrylic acid was then added while heat and stirring were maintained. Polymerization was initiated by the addition of a 500 μL of a 0.1 M solution of APS. BAC was dissolved in methanol, to a final concentration of 0.25 M, and added immediately following initiation, bringing the total volume of the synthesis to 50 mL. The reaction was allowed to proceed for approximately 18 hours, then the resultant solution was cooled and filtered through glass wool. The recovered particles were purified by sequential sedimentation and redispersal in deionized water, and lyophilized for storage.

7.3.2.3. Confirmation of Multiple Reactivity Incorporation

The pH-responsivity of the particles was confirmed using in a manner similar to that of the anionic particles described in **Chapter 5**, by using dynamic light scattering and measuring particle sizes in pH 3.0 formate buffer and pH 7.4 HEPES buffer. The responsivity of the particles to reduction was demonstrated by adding 1 mL of a 7 mg/mL solution of cleaned particles to 9 mL of a solution of 10 mM dithiothreitol (DTT) or to 9 mL of pH 7.4 HEPES buffer, and allowing to microgels to react for a minimum of two hours. The particles were allowed to passively deposit onto APTMS-functionalized glass coverslips, then the particle heights and spreading were compared for the reduced vs. non-reduced particles using AFM, in a manner similar to that described in **Chapter 2**.

7.3.2.4. Fluorescent Labeling of Carboxyls and Thiols

Approximately 4 mg of the co-cross-linked microgels were dispersed in a 5 mM solution of TCEP in pH 3.3 formate buffer and allowed to react for eighteen hours. The thiol-bearing particles were purified by sedimentation and redispersal in formate buffer, before finally being dispersed into pH 7.4 HEPES buffer. A solution of fluorescein iodoacetamide was prepared by dissolving 0.8 mg into 200 μ L of DMSO. This solution was added to 1 mL of the particle solution in pH 7.4 HEPES buffer. A similar solution was prepared by dispersal of the co-cross-linked particles into 1 mL of pH 5.5 MES buffer. A solution of 0.85 mg of dansylcadaverine hydrochloride, 0.6 mg of EDC, and 1.4 mg of NHS in 200 μ L of DMSO was prepared and added to the MES suspension of particles. The two conjugations were allowed to proceed with shaking overnight at room temperature in the dark. Excess fluorophore was removed by sedimentation and redispersal, repeated until the fluorescence intensity (using the steady-state fluorescence spectrophotometer described in **Chapter 3**) of the supernatant was indistinguishable from buffer. Labeled particles were imaged using the microscopy setup described in **Chapter 4** Fluorescence excitation was achieved by using a mercury lamp equipped with excitation band-pass filters of 450-490 nm (blue excitation) for fluorescein iodoacetamide, or 350-370 nm (UV excitation) for dansylcadaverine.

7.3.2.5. Triple Network Gel Formation and Dissolution

To form the initial, disulfide cross-linked gel, an adapted method of that described in **Chapter 3** is presented here. Approximately 32 mg of co-cross-linked particles were dispersed into 8 mL of a 5 mM TCEP solution in pH 3.3 formate buffer, split into two centrifuge tubes. After 90 minutes, the solutions were sedimented at 8,228 x g for 10 min. No difference in pellet density was observed, so the particles were allowed to continue react for an additional fifteen hours to ensure complete conversion to thiols. At that point, the particles were pelleted as before, and the supernatant replaced with pH 3.3 formate

buffer to remove any liberated oligomers. The resuspended particles were pelleted once more, the supernatants removed and replaced with 4 mL of a 10 mM solution of sodium periodate in pH 3.3 formate buffer. Immediately following periodate addition, the samples were centrifuged at 8,228 x g for 10 min. The resultant pellets were solid gels that remained intact upon washing with formate buffer within the tube.

The disulfide cross-linked gels were transferred to a 6-well plate. For the double-network gel, a solution of 4 mL of pH 7.4 PBS buffer (100 mM ionic strength) was added to the well. For triple-network gel formation, 4 mL of a solution of 0.1 monoM 400-500 kDa PDADMAC in PBS was added, and the samples allowed to equilibrate for approximately twenty hours. The gels were then carefully transferred to fresh wells and equilibrated in fresh PBS, then allowed to remain there for 24 hours. No changes in gel morphology were observed in that time, so the PBS was removed and 4 mL of a 5 mM solution of TCEP in PBS was added to each well. Gel degradation was then monitored visually.

7.3.3. Results and Discussion

7.3.3.1. Particle Synthesis and Confirmation of Responsivity

Adding acrylic acid to the co-cross-linked particles described in **Chapter 3** necessitated a reversal of the TEMED-assisted redox initiation. In the absence of TEMED, a strong base, thermally initiated syntheses tend to be highly acidic (pH < 2). This is well below the pKa of acrylic acid (~ 4.5), and thus normally acrylic acid incorporates readily as it is not ionized during the synthesis. It is for this same reason that incorporating primary amines during precipitation polymerization is a significant challenge – these are highly charged under conventional polymerization conditions and have a tendency to phase separate or prematurely stabilize the precursor particles, thus leading to poor incorporation in the desired microgels. Altering the synthetic methods by

changing the radical source or ionic strength can counteract these effects.¹¹ Maintaining conventional thermal initiation using ammonium persulfate alone, as shown for the thermally-initiated BAC particles in **Figure 3.1**, resulted in remnant cross-linking. However, there is still a substantial response to the added DTT, indicative that this is still a viable strategy for thiol incorporation. The added BIS cross-linking should serve to further stabilize the particle against mass loss associated with reduction. The advantages in remaining in a thermally-initiated initiation are thus the incorporation of an additional, orthogonally-responsive functionality within the microgels, as well as greater compatibility with other conventional synthetic design strategies, such as core-shell syntheses.

Disulfide incorporation is confirmed by observing the redox-responsivity of the resultant particles. Deposition of the particles onto solid substrates, as shown in **Figure 7.2**, confirms the monodisperse nature of the recovered particles, with radii on the surface of 461 +/- 30 nm. The height of particles on the surface is 166 +/- 7 nm, which is somewhat taller than expected for conventional microgels. However, the total cross-linking in these particles (contributions from BIS, BAC, and any chain-transfer reactions) is quite high, leading to the apparent stiffness on the surface. Exposure of the particles to the reductant DTT leads to scission of the disulfides of BAC, and subsequent surface deposition leads to particles that exhibit greater spreading (radius of 682 +/- 30 nm) and a marked reduction in particle height (to 69 +/- 4 nm), as shown in **Figure 7.2**. These factors combine to suggest that much of the BAC incorporated remains in its active, disulfide form. This is further demonstrated by the ability to fluorescently label the resultant thiols, as shown in **Figure 7.3**.

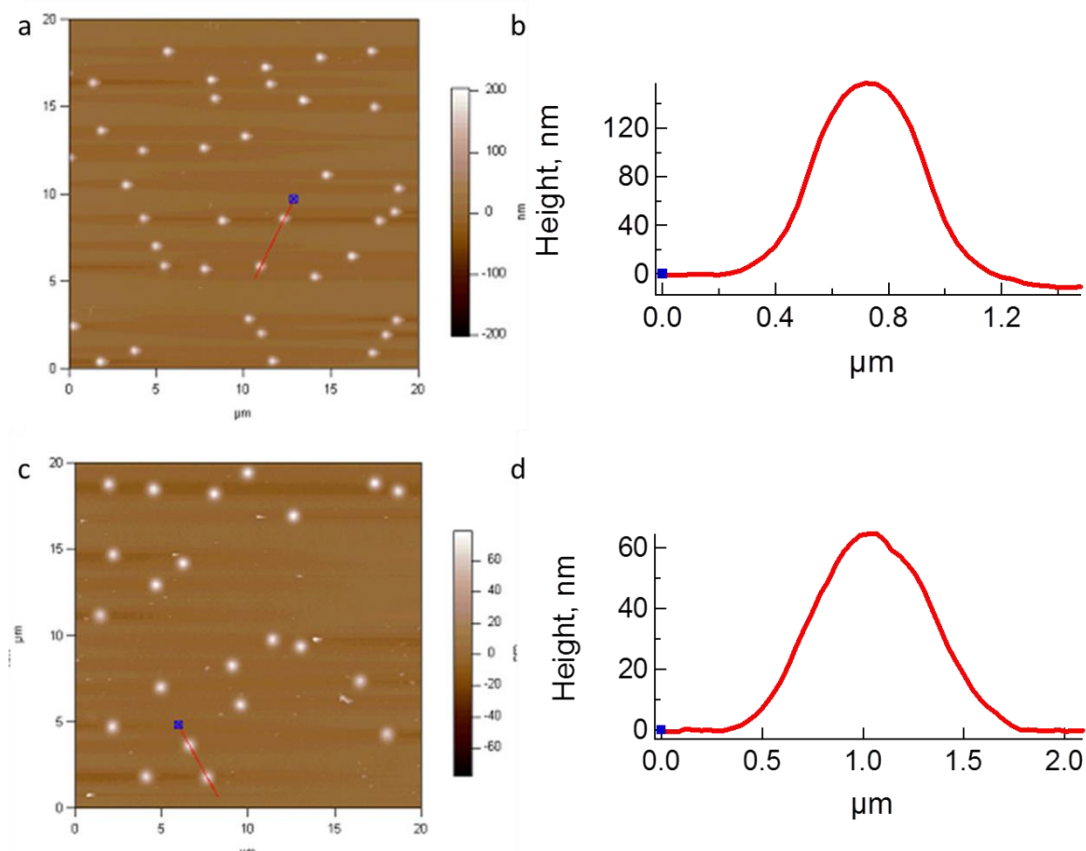


Figure 7.2. AFM analysis of pNIPMAm / 2% BIS / 2.5% BAC / 10% AAc deposited onto solid substrates. The characteristic particle spreading (a) and height (b) in the absence of DTT is shown. Reduction by DTT leads to greater spreading (c) and a reduction in particle height (d). AFM images are 20 μm x 20 μm.

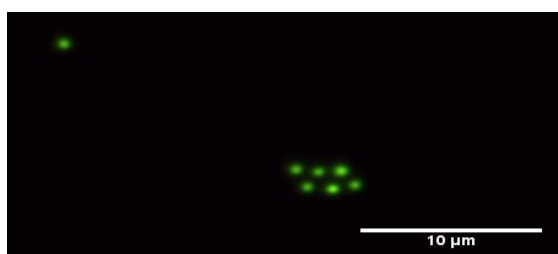


Figure 7.3. Blue excitation epifluorescence microscopy demonstrates that fluorescent labeling of the thiols produced by reduction of pNIPMAm/2% BIS/2.5% BAC/10% AAc microgels with fluorescein iodoacetamide was successful. Scale bar is 10 μm.

Acid incorporation within these particles is readily confirmed by considering the pH responsivity of the microgels. At pH 3.3, the particles have a hydrodynamic radius of 471 nm, and swell to 690 nm at pH 7.4. Further, the acid groups are available for

fluorescent conjugation to the amine-bearing fluorophore dansylcadaverine, as shown in **Figure 7.4**.



Figure 7.4. UV-excitation epifluorescence microscopy demonstrates that fluorescent labeling of pNIPMAm/2% BIS/2.5% BAC/10% AAc microgels with dansylcadaverine was successful. Scale bar is 10 μm .

7.3.3.2. Triple Gel Network Formation

The orthogonal nature of the thiol and carboxyl functionalities allows additional control over the assembly and disassembly of microgel networks. The presence of acrylic acid does not disrupt the ability of these particles to form a double network of the type demonstrated in **Chapter 3**, at least at low pH, which minimizes repulsive particle-particle interactions. Following oxidation, the gels do not dissolve when the carboxyl groups are ionized at pH 7.4 (**Figure 7.5a & b**). The addition of a linear polycation such as PDADMAC serves to Coulombically cross-link the gels. PDADMAC is able to penetrate within the gel network and reinforce the interparticle disulfide linkages within the gel network. Consequently, when the two gels are reduced through the addition of TCEP, the gel lacking PDADMAC dissolves readily within a few hours (**Figure 7.5e**). In contrast, the gel incubated with PDADMAC is stabilized, undergoing only a swelling response over the same time interval (**Figure 7.5f**).

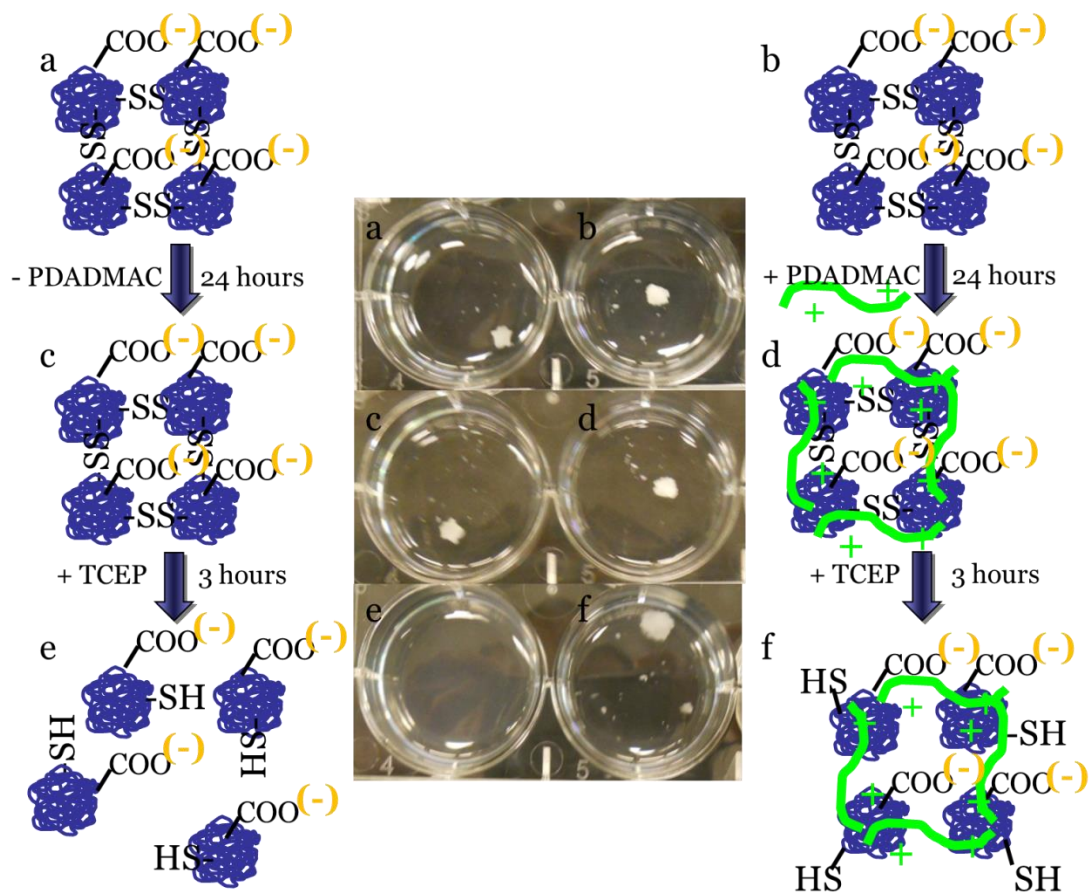


Figure 7.5. Gel networks formed by inter-microgel disulfide cross-link between reduced NIPAm/2% BIS/2.5% BAC/10% AAc microgels are reinforced by the addition of PDADMAC, leading to “rescue” of the network upon reduction. The state of the gels is depicted schematically for each well (a-f).

7.3.4. Future Perspectives

The reversible nature of the thiol-disulfide relationship creates the opportunity for reversible formation of ‘gels of microgels’, as demonstrated above and in **Chapter 3**. Recently, the group of Brian Saunders at the University of Manchester has extensively studied their own ‘gels of microgels’ or ‘DX’ gels, referring to the doubly-cross-linked nature of their assembly. The earliest examples were achieved by conjugation of glycidial methacrylate into methacrylic acid-bearing microgels.^{12,13} The post-synthetic modification of the particles with vinyl groups enabled concentrated dispersions of the particles to be converted to a DX gel through free radical polymerization. Subsequent

demonstrations exploit the reversibility of disulfides, as well.^{14,15} The Saunders group's interests include creating biocompatible gel networks suitable for *in situ* gelation to repair intervertebral disc wear or injury, an application which requires sufficient mechanical stability to withstand load under physiologic conditions. These DX networks have been shown to be promising candidates,¹⁶ and further integration of drug-delivery or responsive elements would further serve to translate these innovative technologies into needed treatments.

The Saunders group's efforts are an elegant demonstration of the potential utility of microgel assemblies for future biomaterials applications. Leveraging the reversible and orthogonal nature of the disulfide bond in a biomaterial application such as described above, whether through directing assembly or regulating release or degradation, enables further refinement and synthetic control over such double network gels.

7.4. Films on Colloidal Substrates

7.4.1. Introduction

The original motivation for making particles of this nature was to support a new collaboration with Dr. Todd McDevitt's lab. Their interest is in regulating the differentiation of stem cells. Pluripotent stem cells tend to form aggregates called embryoid bodies, which are hundreds of microns in diameter. Cells form tight junctions on the surface of these bodies, and consequently limit the ability of soluble growth factors to homogeneously penetrate to the interior of the body.¹⁷ The McDevitt lab has had great success incorporating a variety of microparticles within embryoid bodies by co-assembling them during embryoid body formation. Once distributed, these microparticles form loci for the release of soluble growth factors, which provides a more uniform internal environment to direct the differentiation of the stem cells.¹⁸ Microspheres of poly(lactic-co-glycolic acid) (PLGA) approximately 8 microns in diameter led to facile

incorporation within growing embryoid bodies, and delivered payloads throughout a period of at least ten days to the differentiating cells. Observation of inter-embryoid body diffusion of a small molecule fluorophore confirmed that the concentration of fluorophore homogenized over that interval, and delivery of the growth factor retinoic acid led to differentiation of cells in the embryoid body interior into an epithelial phenotype, demonstrating the availability and sensitivity of the stem cells to factors released from incorporated microspheres.¹⁸

7.4.2. Experimental and Results

As originally conceived, our strategy was to synthesize large (micron-sized) pNIPMAm microgels bearing reactive amines or carboxyls and a fluorescent co-monomer. These were to allow ligand coupling and visualization upon internalization. Microgels of 85% pNIPMAm / 10 % AAc / 5% Bis / < 0.1% MERho were synthesized with a diameter of approximately 1.4 μm . Ms. Anh Nguyen of the McDevitt group sought to incorporate these microgels into embryoid bodies. However, fluorescent labels such as AFA or MERho capable of incorporation during synthesis were not bright, stable, or concentrated enough to allow visualization under the experimental conditions, which necessitated post-synthetic labeling of the microgels with other fluorescent species. Through visualization of these incorporation attempts, it became readily apparent that the significant density mismatch between the cells and the microgels limited their ability to co-assemble, as shown in **Figure 7.6a**. The McDevitt lab uses a centrifugally-assisted method to drive embryoid body formation, and the microgels could not sediment under centrifugal forces that were physiologically viable.

The solution was to seek raspberry-like particle formation, of the sort described in **Chapter 4**, whereupon the biocompatible and solute-release properties of microgels would be conferred upon a solid core particle to provide the density match needed for efficient co-assembly. To validate this strategy, raspberry-like particles were synthesized

according to the methods described in **Chapter 4**. The microgels used had a composition of 88% pNIPMAm / 2% BIS / 10% AAc / < 0.1% AFA and were conjugated via EDC coupling to 2.5- μm diameter amine-functionalized rough-surface magnetic polystyrene core particles. In studies conducted by Ms. Anh Nguyen of the McDevitt lab, these particles were shown to co-assemble within embryoid bodies, as shown in **Figure 7.6b**. After demonstrating that in principle such constructs solve the density mismatch issues, continuing work on this collaboration is based on these raspberry-like particles utilizing a variety of core particles and microgel compositions in order to optimize the loading and release of selected growth factors to regulate stem cell differentiation.

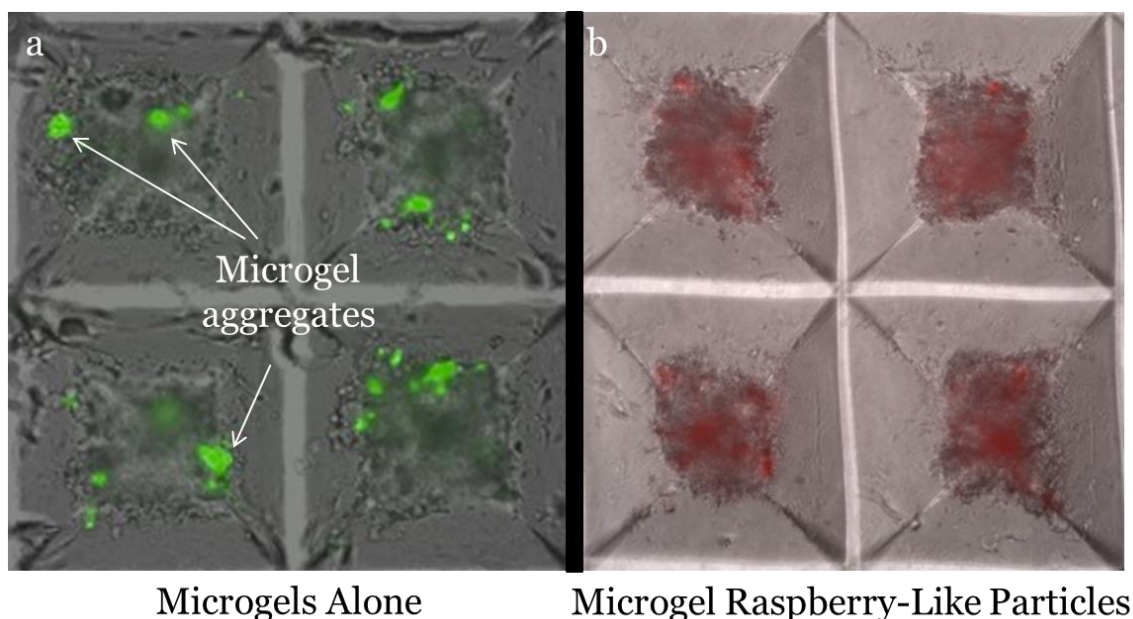


Figure 7.6. Fluorescence images of embryoid bodies mixed with microgels or microgel raspberry-like particles after eighteen hours. (a) pNIPMAm-co-AAc microgels (labeled green with chymotrypsinogen-Alexa488) alone do not sediment during centrifugally-assisted embryoid body assembly, except in the form of large, irregular aggregates. (b) Magnetic polystyrene particles decorated with microgels (labeled red with BSA-Alexa 546) show more uniform and controlled co-localization during assembly. Individual microwells in each image are 400 μm x 400 μm for scale. Courtesy of Ms. Anh Nguyen.

7.4.3. Future Perspectives

As discussed in **Chapters 1, 5, and 6**, microgel films represent a rich toolset for surface modification. The work described in **Chapter 4** is merely the first step in

translating these extensive possibilities. For example, the thermo-responsivity and drug delivery capabilities of the particles remain untapped. In principle, the raspberry-like particles could even be used to support the assembly of multilayers of microgels, which may open up even more possibilities, or reveal as yet unexpected new phenomena. Another intriguing approach would be to consider cores that are themselves functional or responsive (in a more meaningful way than simply being embedded with magnetic nanoparticles – for example, highly porous particles capable of slow solute release) and to consider how the interplay between the core and microgel shells could further extend the applications of such constructs.

To support the ongoing collaboration with the McDevitt lab, Ms. Shalini Saxena has begun working with these materials. She has already shown promising results with creating raspberry-like particles intended for “sampling” – that is, that are mixed with a growing embryoid body which can undergo thermally-driven collapse to imbibe soluble growth factors and other signals, which would enable unprecedented assay of the spatio-temporal distribution of the chemical markers of stem cell differentiation. Translating well-understood behaviors of microgels in free solution or bound to macroscopic substrates to colloidal domains will likely continue to be a fruitful strategy in seeking particle design solutions to challenges in biomedical engineering. I am confident that Ms. Saxena, Dr. McDevitt, and their co-workers will be able to tackle these challenges and develop innovative new technologies.

7.5. Self-Healing Films

7.5.1. Introduction

Self-healing materials will remain a key subject of study, and the field is full of many examples of clever designs and strategies to incorporate this attribute into a plethora of materials. The key challenges will be translating these demonstrations into

functional applications. In this regard, microgel films have some advantages, in that the healing response is autonomic in the presence of high humidity environments, meaning that virtually any conceivable application of a microgel-film-coated device should also be an environment that will promote healing of any damage. However, there are numerous opportunities for fundamental studies on microgel films. The group's previous studies on the subject,^{19,20} as well as the work in **Chapter 5**, are all very phenomenological in their analysis – that is, the primary observables have been whether or not a particular film composition undergoes reversible damage or healing, with little in the way of quantitative analysis possible. Consequently, exploring both the design space to ascertain the key factors governing self-healing, as well as additional characterization of the mechanical properties of the films will be major areas of interest going forward.

To take one example, the stiffness of individual microgels would be expected to affect the overall mechanical properties of a film. In particular, the film's modulus should be reflected in the strain necessary to bring about the onset of the wrinkling, plastic deformation.²¹ The disulfide-co-AAc particles described above in **Chapter 7.3** provide an opportunity to assemble films wherein the stiffness of individual particles can be altered before and after assembly. These may allow analysis of the buckling properties of the films to provide additional characterization of their overall mechanical properties.

7.5.2. Experimental

7.5.2.1. Film Assembly

Films were assembled onto amine-functionalized PDMS substrates in a manner similar to that described in **Chapters 5 & 6**. Films were assembled from particles that were in the co-cross-linked form (disulfide – SS) as well as particles that had been reduced by addition of dithiothreitol to reveal thiols (SH). Particles were deposited from 0.1 mg/mL solutions in PBS buffer via centrifugal deposition, and 400-500 kDa

PDADMAC was used to assemble the particles into multilayers. Film buildup proceeded until eight microgel layers had been added. Films were characterized using AFM imaging to observe buildup. Films that were reduced post assembly were exposed to 5 mM TCEP in PBS at room temperature for a minimum of two hours.

7.5.2.2. Film Damage & Healing

Films were stretched and damaged using the apparatus described in **Chapter 5**. Healing was attempted by immersion of the films in deionized water for a period of fifteen seconds. Assessment of the damage and healing of films was conducted using brightfield microscopy, consistent with methods in **Chapter 5**.

7.5.3. Results and Discussion

The disulfide-co-AAc microgels were able to assemble into multilayer films, regardless of their oxidation state, as shown in **Figure 7.7**. The SH particles did seem to form smoother gels, which is likely due to their reduced cross-linking following disulfide cleavage. The SS particles also seemed to be prone to forming films with irregular cracks. It is possible that the greater cross-link density in this case is both limiting PDADMAC's ability to penetrate the particles and strengthen particle – particle interactions, and limiting the ability of the particles to deform in order to maximize interactions.

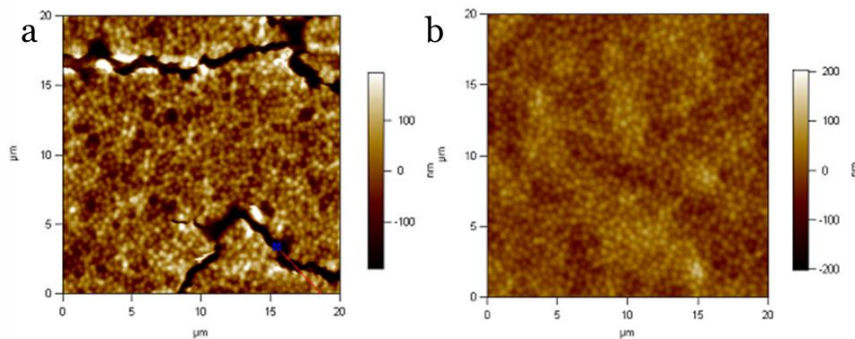


Figure 7.7. 8-layer films assembled from pNIPMAm-BIS-BAC-AAc microgels in the a) oxidized (SS) state and b) reduced (SH) state. Images are 20 μm x 20 μm .

The film response to damage is also dependent upon the oxidation state of the microgels during assembly. The SS films undergo additional cracking when stretched and relaxed. These cracks are not of the same type observed with PEI films cross-linked with glutaraldehyde, but do seem to generally be perpendicular to the axis of strain. Though difficult to quantify, it also appears that these cracks may undergo limited healing upon hydration, as shown in **Figure 7.8a-c**. In contrast, the SH films show the characteristic wrinkling damage and healing as microgels lacking thiols or disulfides (**Figure 7.8d-f**). Modification of the oxidation state of the microgels following assembly can still lead to changes in their healing properties. SS films exposed to TCEP convert to SH films, as in **Figure 7.8g-i**. While wrinkling patterns do appear that disappear on healing, they are distinct from the patterns formed from SH particles initially, which suggests that there may be some differences in film structure that are retained from the assembly condition.

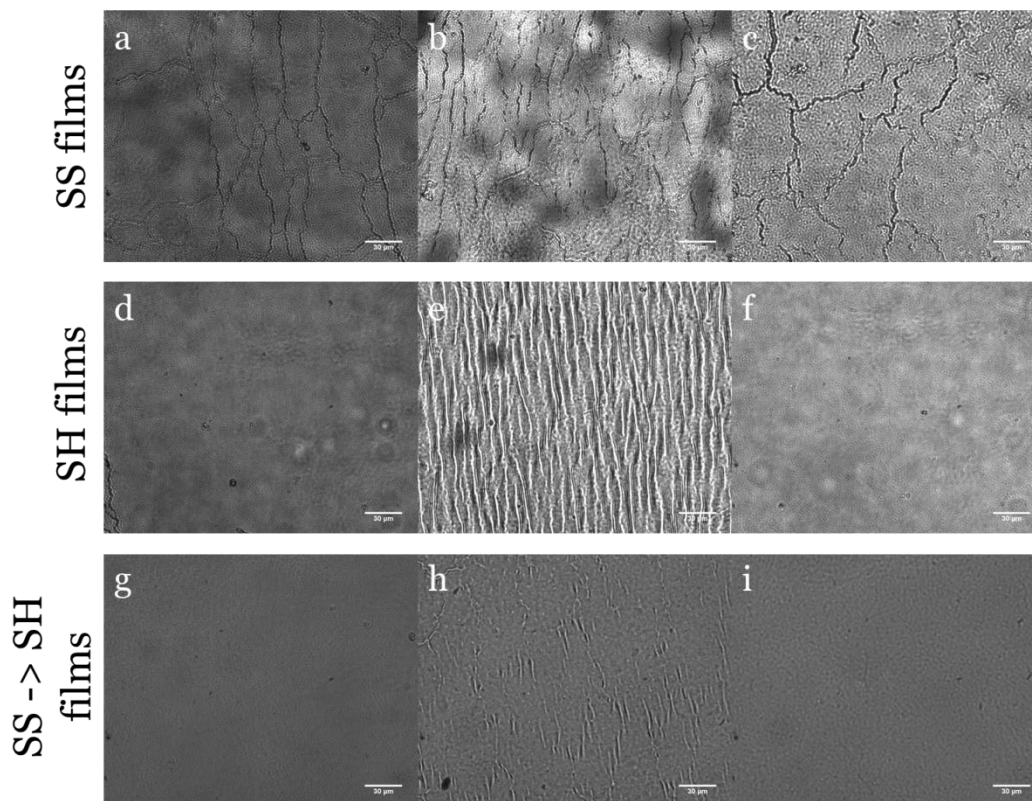


Figure 7.8. 8-layer films assembled from pNIPMAm-BIS-BAC-AAc microgels in the a-c) oxidized (SS) state, d-f) reduced (SH) state, and g-i) assembled in the oxidized state then reduced following film assembly. The films undergo damage when exposed to b) 80% strain, e) 20% strain, or h) 10% strain. The SS films show increases in irregular cracking following stretching, some of which seems to be reversible (c). Wrinkling damage to the SH films (e, h) in contrast, is completely reversible (f, i). Scale bar in all images is 30 μm .

7.5.4. Future Perspectives

As referenced in the introduction to this section, self-healing is ripe for additional exploration with regard to microgel multilayers. While **Chapter 5** serves to illustrate the damage mode for the initial demonstrations of self-healing and establishes the minimal conditions necessary for healing, there are numerous questions regarding particle and film design and how these effects may impact self-healing. For example, PDADMAC and (in **Chapter 6**) PEI have been demonstrated to confer self-healing onto microgel multilayers, and the insensitivity of the response to polycation length in **Chapter 5**

suggests that this may be a fairly general phenomenon. Therefore, substitution of polycations in order to enable analysis of the films in a more quantitative manner should be considered a viable approach.

Both my predecessor Dr. Toni South and myself attempted to investigate film properties using FRAP on fluorescently-labeled microgels. Our efforts suggested that the mobility of individual microgels in the film is rather low, but instrumental limitations prevented robust measurements of particle diffusion in the films. Future investigations utilizing fluorescently-labeled polycation, however, should yield much greater rates of diffusion. Thus, carefully designed experiments could use this strategy to directly probe the internal environment of the films and their connectivity. Such measurements could also be conducted under varying conditions, like controlled humidity or *in situ* buffered conditions to observe the effects on mobility of at least that component of the film. Changes in film mobility might also be expected as a function of microgel composition – for example, the charge content of the particles or particle stiffness, which as evidenced above may affect the ability of films to damage and heal.

Finally, such quantitative measurements may dovetail nicely with qualitative assays of the self-healing response, allowing for greater predictive power for more exotic films. Additional exploration of the design space with regard to the self-healing response is warranted. A simple example that may be of interest for a variety of applications would be the healing response of a composite film; that is a film containing multiple types of microgels. This case may be especially interesting for inquiry, such as whether the mobility associated with damage and healing leads to de-mixing or other effects on the microgels' distribution. Furthermore, assessing the self-healing characteristics of pNIPMAm microgels, cationic microgels assembled with polyanions, and/or core-shell particles can lead to a broader perspective on the key factors at the heart of self-healing microgel films.

7.6. Film Mobility and Cell Adhesion

As discussed in **Chapter 6**, our interests in film mobility arose from efforts to reconcile some seemingly disconnected observations about microgel multilayers – namely that they strongly resist cell attachment despite high levels of protein loading and that hydrated films exhibit rapid reorganization from non-equilibrium states. While the efforts described in that chapter present some promising efforts to make connections between these two characteristics, this is a topic that merits more expansive studies. To ascertain the importance of film mobility in cell adhesion, more direct methods of cell observation and manipulation would enable us to go beyond correlative observations.

Efforts are already underway within the group to introduce photo-patterning into multilayer films. There are a few different ways that this strategy can enable direct observation of the cellular response to the films. One example would be similar to FRAP studies previously described, however rather than observing passive mobility, the activity of cells attempting to adhere could serve to disrupt a patterned framework of fluorescently-labeled microgels or polycation. Such disruptions suggest that the forces exerted by the cells suffice to move individual particles or film elements. Alternatively, photo-cross-linking reactions can allow spatial control over the local mobility of the films, allowing a single film to exhibit both regions of cell attachment and repulsion. Cell motility in response to the two regimes would therefore represent a direct observable.

Introducing a switchable or reversible chemistry into these films would provide a powerful method to probe cell adhesion. Disulfides are highly attractive for this purpose – a cross-linked film rigidified by disulfide bonds could be made analogous to the cross-linked films in **Chapter 6**, followed by physiologically-suitable reduction to convert the films back to a mobile state. Disulfides can be incorporated in a variety of ways:

- The commercially available cross-linker bis[2-(4-azidosalicylamido)ethyl] disulfide (BASED) features homobifunctional photo-reactive moieties with an internal disulfide, suitable for cross-linking any combination of polycation and

microgel. However, this molecule has poor aqueous solubility and its lack of specificity may consign it to many “unproductive” reactions with respect to altering film mobility.

- Incorporation of thiols within particles in films, as has been described previously within this chapter, allows a secondary network to be formed that limits microgel mobility. This network could also be supplemented with extrinsic bis-thiolated polymers to improve or otherwise tune the connectivity, and any polycation could be used during assembly. Incorporation of sufficient levels of disulfide without altering the mechanical properties of the film may make this a challenging strategy, however.
- Also commercially available is the homobifunctional amine-reactive crosslinker dimethyl 3,3'-dithiobispropionimidate (DTBP), which features an internal disulfide. Though it requires reactive amines in the polycation, this should serve to create a double-network that restricts the mobility of both microgels and polycation. Preliminary work with this cross-linker and its analogue lacking disulfides, dimethyl suberimidate (DMS), has suggested that while it is suitable for rigidifying a film to promote cell attachment, the reversibility has yet to be demonstrated.

As we continue to build our understanding of microgel multilayers, particularly with regard to the key factors that govern their mobility revealed from self-healing analyses, our designs to understand their cell adhesive properties can benefit. The cells currently serve both to test for a desired application outcome, and also as biological probes to sample the mechanical properties of the film surface. Replacing the cells' latter role with more readily controllable experimental techniques can only serve to facilitate a better understanding of microgel multilayered films as a whole.

7.7. Concluding Remarks

There are many challenges facing the future of healthcare, and microgels are poised to provide material-based solutions to some of the major obstacles. Their synthetic versatility, stimuli-responsivity, and biocompatibility make them attractive for applications as diverse as particulate nanocarriers for drug delivery and bio-contacting surface modification. Much of the work presented in this thesis has sought to expand the capabilities of thermo-responsive microgels as platforms for biological applications, through incorporation of physiologically degradable modalities or the generation of microparticulate-based films, or to study the fundamental basis of phenomena of applied interest, such as cell adhesion resistance and self-healing. As some of the perspectives in this chapter reveal, it is clear that the great potential of hydrogel nanoparticles and their assemblies is only beginning to be fully realized within the realm of biomaterials.

7.8. References

- [1] Ulbrich, K.; Subr, V.; Seymour, L. W.; Duncan, R., Novel Biodegradable Hydrogels Prepared Using the Divinylic Crosslinking Agent N,O-Dimethacryloylhydroxylamine. 1. Synthesis and Characterization of Rates of Gel Degradation, and Rate of Release of Model-Drugs, In vitro and In vivo. *Journal of Controlled Release* **1993**, *24*, 181-190.
- [2] Das, M.; Kumacheva, E., From polyelectrolyte to polyampholyte microgels: comparison of swelling properties. *Colloid and Polymer Science* **2006**, *284*, 1073-1084.
- [3] Smith, M. H.; South, A. B.; Gaulding, J. C.; Lyon, L. A., Monitoring the Erosion of Hydrolytically-Degradable Nanogels via Multiangle Light Scattering Coupled to Asymmetrical Flow Field-Flow Fractionation. *Analytical Chemistry* **2010**, *82*, 523-530.
- [4] South, A. B.; Lyon, L. A., Direct Observation of Microgel Erosion via in-Liquid Atomic Force Microscopy. *Chemistry of Materials* **2010**, *22*, 3300-3306.
- [5] Gaulding, J. C.; South, A. B.; Lyon, L. A., Hydrolytically degradable shells on thermoresponsive microgels. *Colloid and Polymer Science* **2013**, *291*, 99-107.

- [6] Yin, W. S.; Akala, E. O.; Taylor, R. E., Design of naltrexone-loaded hydrolyzable crosslinked nanoparticles. *International Journal of Pharmaceutics* **2002**, *244*, 9-19.
- [7] Scheler, S.; Kitzan, M.; Fahr, A., Cellular uptake and degradation behaviour of biodegradable poly(ethylene glycol-graft-methyl methacrylate) nanoparticles crosslinked with dimethacryloyl hydroxylamine. *International Journal of Pharmaceutics* **2011**, *403*, 207-218.
- [8] Bartlett, R. L.; Panitch, A., Thermosensitive Nanoparticles with pH-Triggered Degradation and Release of Anti-inflammatory Cell-Penetrating Peptides. *Biomacromolecules* **2012**, *13*, 2578-2584.
- [9] Smith, M. H.; Lyon, L. A., Multifunctional Nanogels for siRNA Delivery. *Accounts of Chemical Research* **2012**, *45*, 985-993.
- [10] Meng, Z. Y.; Hendrickson, G. R.; Lyon, L. A., Simultaneous Orthogonal Chemoligations on Multiresponsive Microgels. *Macromolecules* **2009**, *42*, 7664-7669.
- [11] Hu, X. B.; Tong, Z.; Lyon, L. A., Synthesis and physicochemical properties of cationic microgels based on poly(N-isopropylmethacrylamide). *Colloid and Polymer Science* **2011**, *289*, 333-339.
- [12] Liu, R. X.; Milani, A. H.; Freemont, T. J.; Saunders, B. R., Doubly crosslinked pH-responsive microgels prepared by particle inter-penetration: swelling and mechanical properties. *Soft Matter* **2011**, *7*, 4696-4704.
- [13] Liu, R. X.; Milani, A. H.; Saunders, J. M.; Freemont, T. J.; Saunders, B. R., Tuning the swelling and mechanical properties of pH-responsive doubly crosslinked microgels using particle composition. *Soft Matter* **2011**, *7*, 9297-9306.
- [14] Bird, R.; Freemont, T.; Saunders, B. R., Tuning the properties of pH-responsive and redox sensitive hollow particles and gels using copolymer composition. *Soft Matter* **2012**, *8*, 1047-1057.
- [15] Bird, R.; Freemont, T. J.; Saunders, B. R., Hollow polymer particles that are pH-responsive and redox sensitive: two simple steps to triggered particle swelling, gelation and disassembly. *Chemical Communications* **2011**, *47*, 1443-1445.
- [16] Milani, A. H.; Freemont, A. J.; Hoyland, J. A.; Adlam, D. J.; Saunders, B. R., Injectable Doubly Cross-Linked Microgels for Improving the Mechanical Properties of Degenerated Intervertebral Discs. *Biomacromolecules* **2012**, *13*, 2793-2801.

- [17] Bratt-Leal, A. M.; Carpenedo, R. L.; McDevitt, T. C., Engineering the Embryoid Body Microenvironment to Direct Embryonic Stem Cell Differentiation. *Biotechnology Progress* **2009**, *25*, 43-51.
- [18] Carpenedo, R. L.; Bratt-Leal, A. M.; Marklein, R. A.; Seaman, S. A.; Bowen, N. J.; McDonald, J. F.; McDevitt, T. C., Homogeneous and organized differentiation within embryoid bodies induced by microsphere-mediated delivery of small molecules. *Biomaterials* **2009**, *30*, 2507-2515.
- [19] Park, C. W.; South, A. B.; Hu, X. B.; Verdes, C.; Kim, J. D.; Lyon, L. A., Gold nanoparticles reinforce self-healing microgel multilayers. *Colloid and Polymer Science* **2011**, *289*, 583-590.
- [20] South, A. B.; Lyon, L. A., Autonomic Self-Healing of Hydrogel Thin Films. *Angewandte Chemie-International Edition* **2010**, *49*, 767-771.
- [21] Yang, S.; Khare, K.; Lin, P. C., Harnessing Surface Wrinkle Patterns in Soft Matter. *Advanced Functional Materials* **2010**, *20*, 2550-2564.

VITA

JEFFREY CLINTON GAULDING

Jeffrey was born in Opelika, Alabama and grew up outside of Hogansville, Georgia, where he attended LaGrange High School. He attended Emory University in Atlanta, Georgia and graduated with highest honors with a B.S. in Chemistry and a minor in Mathematics. He worked for GlaxoSmithKline in Research Triangle Park, North Carolina for two years before beginning his doctoral program in Chemistry at Georgia Tech. When he is not working on his research, Jeffrey's interests include reading, games, playing with his dog Lexi, and spending time with his beloved wife, Jennifer.